NOTE TO USERS

This reproduction is the best copy available.

UMI®

UNIVERSITY OF ALBERTA

Optimum Deposition For Sub-Aerial Tailings Disposal

by

Yunxin Qiu ©

A thesis submitted to the Faculty of Graduate Studies and Research in partial fulfillment
of the requirements for the degree of **Doctor of Philosophy**

in

Geotechnical Engineering

Department of Civil and Environmental Engineering

EDMONTON, ALBERTA

Fall 2000

National Library
of Canada

Acquisitions and
Bibliographic Services

395 Wellington Street
Ottawa ON K1A 0N4
Canada

Bibliothèque nationale
du Canada

Acquisitions et
services bibliographiques

395, rue Wellington
Ottawa ON K1A 0N4
Canada

Your file Votre référence

Our file Notre référence

The author has granted a non-exclusive licence allowing the National Library of Canada to reproduce, loan, distribute or sell copies of this thesis in microform, paper or electronic formats.

L'auteur a accordé une licence non exclusive permettant à la Bibliothèque nationale du Canada de reproduire, prêter, distribuer ou vendre des copies de cette thèse sous la forme de microfiche/film, de reproduction sur papier ou sur format électronique.

The author retains ownership of the copyright in this thesis. Neither the thesis nor substantial extracts from it may be printed or otherwise reproduced without the author's permission.

L'auteur conserve la propriété du droit d'auteur qui protège cette thèse. Ni la thèse ni des extraits substantiels de celle-ci ne doivent être imprimés ou autrement reproduits sans son autorisation.

0-612-59656-7

Canadä

UNIVERSITY OF ALBERTA

Library Release Form

Name of Author: Yunxin Qiu

Title of Thesis: Optimum Deposition For Sub-Aerial Tailings Disposal

Degree: Doctor of Philosophy

Year this Degree Granted: 2000

Permission is hereby granted to the University of Alberta Library to reproduce single copies of this thesis and to lend or sell such copies for private, scholarly or scientific research purposes only.

The author reserves all other publication and other rights in association with the copyright in the thesis, and except as herein before provided, neither the thesis nor any substantial portion thereof may be printed or otherwise reproduced in any material form whatever without the author's prior written permission.

10815-83AVE, #204
EDMONTON, ALBERTA
Canada, T6E 2E6

August 15, 2000

ABSTRACT

A vast amount of mining waste is produced around the world every day. The wastes are generally in the form of slurry, which is transported for deposition hydraulically. With the increasing size of these mining operations, tailings facilities become larger and larger. These huge earth structures have the potential of liquefaction failure due to the sandy nature of most mineral tailings. In addition, the need for the optimal use of water resources, especially in arid regions, is a critical issue. Stability enhancement, storage volume reduction, and water recycling have become major issues facing mine designers and operators. The sub-aerial technique is a promising disposal method for dealing with these challenges. The principle objective of this study was to provide an approach to improve the efficiency of sub-aerial tailings deposition.

A series of laboratory experiments were carried out to investigate the engineering properties and desiccation behavior of the tailings. These experiments included basic physical property tests, consolidation and permeability tests, shrinkage tests, and desiccation tests. Four tailings, copper, gold, coal, and oil sand CT tailings, were tested. Some special techniques for the consolidation and desiccation behavior tests were developed.

A theory for modeling the sedimentation, consolidation and desiccation of the tailings was developed. A numerical solution for the highly nonlinear partial differential equations was presented. In addition, the factors affecting the optimum deposition design for the sub-aerial tailings deposition in arid regions are discussed and a theoretical model for optimum sub-aerial tailings deposition was developed. The model, referred to as DOSTAR is capable of predicting sedimentation, consolidation and desiccation, as well as crack initiation, propagation, crack dimensions (spacing, depth, and width), tailings volume, and amount of recyclable water.

The validity of the model was tested through comparing the modeled results with the laboratory test results. A detailed procedure for using DOSTAR to perform the optimum depositional parameter design is described. Finally, some case studies as examples are presented. DOSTAR has been shown to be able to accurately predict the deposited properties of the mine tailings and to be useful for optimum deposition design.

UNIVERSITY OF ALBERTA

Faculty of Graduate Studies and Research

The undersigned certify that they have read, and recommend to the Faculty of Graduate Studies and Research for acceptance, a thesis entitled **Optimum Deposition For Sub-Aerial Tailings Disposal** submitted by **Yunxin Qiu** in partial fulfillment of the requirements for the degree of **Doctor of Philosophy** in **Geotechnical Engineering**.

D C Sego
Dr. D.C. Sego (Supervisor)

J. D. Scott
Dr. J. D. Scott

Dwayne Tannant
Dr. D. Tannant

Yongsheng Feng
Dr. Y. Feng

D Pufahl
Dr. D. E. Pufahl (External Examiner)

August 14, 2000
Date of Approval by Committee

to

my dear wife, Yanping and daughter, Sishuang
for your support, love and understanding along the way

and to

my parents
who always support me with love

ACKNOWLEDGEMENTS

I would like to express my deepest gratitude to my supervisor, Dr. David C. Sego, for his guidance, supervision, patience, enthusiasm, encouragement, and continual technical and financial support throughout this endeavor. His support throughout the research and writing of this thesis will never be forgotten. Special thanks are extended to Dr. Norbert R. Morgenstern for leading me into this exciting research area, for his leadership, and for his professional inspiration.

Gratitude is extended to each of the professors within the geotechnical group, particularly Dr. K. Biggar, Dr. J. D. Scott, Dr. R. J. Chalaturnyk, and Dr. P. K. Robertson, who contributed to both my personnel and professional development during these studies. Thanks to Sally Petaske for always being helpful. I would also like to thank the rest of staff of the Department of Civil and Environmental Engineering, particularly Dr. T.Y. Gan.

I am also very grateful to Christine Hereygers for all her help in the laboratory. I also wish to thank Gerry Cyre for his help, humor, and ingenuity in the laboratory and Steve Gamble for his help in the laboratory.

I would like to thank Dr. Y. Feng of the Department of Renewable Resources for his help and encouragement and Ms. K. Ostermann of the Department of Renewable Resources for her help in the laboratory.

I thank Dr. G. Ward Wilson (University of Saskatchewan), Dr. G. E. Swarbrick (University of New South Wales, Australia), and Dr. G. E. Blight (University of the Witwatersrand, South Africa) for their advice on this project.

I would also like to thank Knight Piesold LLC in Denver, particularly Mr. Bryan Ulrich for kindly providing valuable data. Mr. Ulrich, thank-you for all your help.

Thanks to D. T. Jensen (Utah Climate Centre), D. Hohnstein (Echo Bay Mines Ltd.), and R. N. Kostaschuk (Knight Piesold Ltd.) for their valuable help.

This research would not have been possible without the financial support provided by several organizations. My sincere gratitude is extended to The Natural Sciences and Engineering Research Council (NSERC), University of Alberta, Luscar Ltd., and the Department of Civil and Environmental Engineering at the University of Alberta.

Special acknowledgement is extended to Mr. D. Clyburn of the Academic Support Centre at University of Alberta for his help in editing.

The love and support of my family were important to the success of these studies. I would like to express my deepest gratitude to my wife for her love, support, and encouragement throughout these studies. Despite her young age, my daughter knew how to be supportive and understanding.

TABLE OF CONTENTS

CHAPTER 1 INTRODUCTION 1

1.1 INTRODUCTION 1
1.2 RESEARCH SCOPE AND OBJECTIVE 2
1.3 THESIS OUTLINE 3

CHAPTER 2 LITERATURE REVIEW 5

2.1 INTRODUCTION 5
2.2 THE SUB-AERIAL TAILINGS DEPOSITION TECHNIQUE 5
2.3 SEGREGATION BEHAVIOR AND GEOMETRY OF A TAILINGS BEACH. 7
2.4 SEDIMENTATION 10
2.5 CONSOLIDATION 12
2.6 DESICCATION OF TAILINGS 19
  2.6.1 Water retention characteristics 20
  2.6.2 Evaporation 22
  2.6.3 Shrinkage of soils 25
  2.6.4 Cracking of Soils due to Desiccation 26
    2.6.4.1 Initiation of tension cracks 27
    2.6.4.2 Propagation, depth and spacing of tension cracks 28
    2.6.4.3 Width of tension cracks 32
2.7 HYDRAULIC CONDUCTIVITY OF TAILINGS 32
  2.7.1 Saturated Hydraulic Conductivity 33
  2.7.2 Unsaturated Hydraulic Conductivity 34
  2.7.3 Effect of Tension Cracks 37
2.8 STRENGTH OF AN UNSATURATED SOIL 38
  2.8.1 Shear Strength 38
  2.8.2 Tensile Strength 39
2.9 REVIEW OF EXISTING MODEL ON SOIL DESICCATION 40
2.10 SUMMARY AND CONCLUSIONS 48

CHAPTER 3 LABORATORY TEST PROGRAM 59

3.1 INTRODUCTION 59
3.2 CONSOLIDATION AND HYDRAULIC CONDUCTIVITY TESTS 60
  3.2.1 Test Equipment 60
  3.2.2 Tailings Saturation 61
  3.2.3 Consolidation Tests 62
  3.2.4 Hydraulic Conductivity Test 63
3.3 COLUMN DRYING TEST 64
  3.3.1 Test Environment 64
  3.3.2 Drying Column 64
  3.3.3 Layout of the Test Apparatus 65
  3.3.4 Sample Preparation and Drying Test 66
3.4 WATER RETENTION CHARACTERISTICS TEST 66
  3.4.1 Pressure-Plate Extractor Method 67
    3.4.1.1 Test apparatus 67
    3.4.1.2 Sample preparation 68
    3.4.1.3 Test 69
  3.4.2 Saturated Salt Solution Method 69
    3.4.2.1 Sample preparation and test 71
3.5 STRENGTH TEST 72
3.6 SHRINKAGE LIMITS AND SHRINKAGE CURVE TESTS 73
  3.6.1 Test Apparatus 73
  3.6.2 Sample Preparation 73
  3.6.3 Test 74
3.7 SUMMARY AND CONCLUSIONS 75

CHAPTER 4 PRESENTATION AND ANALYSES OF TEST RESULTS 92

4.1 INTRODUCTION 92
4.2 BASIC PHYSICAL PROPERTIES 92
4.3 CONSOLIDATION AND PERMEABILITY BEHAVIOR 93
4.4 SOIL-WATER RETENTION CHARACTERISTICS OF TAILINGS 95

4.5 DESICCATION BEHAVIOR 98
4.5.1 Shrinkage Limits and Shrinkage Curve 98
4.5.2 Evaporation of Tailings 98
4.5.3 Moisture Content of tailings 99
4.5.4 Shrinkage and Cracking of tailings 101
4.6 SHEAR STRENGTH 102
4.7 SUMMARY AND CONCLUSIONS 103

CHAPTER 5 THEORIES OF SEDIMENTATION, CONSOLIDATION, AND DESICCATION 123

5.1 INTRODUCTION 123
5.2 BACKGROUND AND COORDINATE SYSTEMS 123
5.3 GOVERNING EQUATIONS 125
5.4 SATURATED CONDITION 127
5.5 SEDIMENTATION 129
5.6 UNSATURATED CONDITION 130
5.7 DEFINITION OF AUXILIARY CONDITIONS 133
5.7.1 System Geometry 134
5.7.2 Hydraulic Conductivity of the Tailings 134
5.7.2.1 Saturated hydraulic conductivity 134
5.7.2.2 Unsaturated hydraulic conductivity 134
5.7.2.3 Hydraulic conductivity in the cracked layer 135
5.7.3 Compressibility of the Tailings 136
5.7.4 Tailings-Water Retention Curve 136
5.7.5 Evaporation of the tailings 137
5.7.5.1 Potential evaporation rate (E_p) 137
5.7.5.2 Actual evaporation rate of tailings (E_A) 138
5.7.6 Effective Stress and Bishop Parameters 138
5.7.7 Unsaturated Coefficient of Compressibility 139
5.7.8 Upper Boundary Conditions 141
5.7.8.1 Sedimentation 141

5.7.8.2 Consolidation 141
5.7.8.3 Desiccation 142
5.7.9 Lower Boundary Conditions 143
5.7.9.1 The impermeable boundary 143
5.7.9.2 The permeable boundary 144
5.7.10 Initial Conditions 145
5.8 NUMERICAL SOLUTION 145
5.9 SUMMARY AND CONCLUSIONS 149

CHAPTER 6 MODELING SUB-AERIAL TAILINGS DEPOSITION 157

6.1 INTRODUCTION 157
6.2 WATER BALANCE EVALUATION 157
6.3 FACTORS INFLUENCING THE OPTIMUM DESIGN 159
6.3.1 Hydraulic Conductivity Versus Matric Suction 159
6.3.2 Crack Width and Crack Location 160
6.3.3 Drying Time and Evaporation 161
6.3.4 Layer Thickness 162
6.4 DESIGN CRITERION AND SCHEMES 162
6.4.1 Optimum Design Scheme 1: Maintaining Full Saturation 163
6.4.2 Optimum Design Scheme 2: Cracking Through a Deposited Layer 163
6.5 ESTABLISHMENT OF THE DESIGN MODEL 164
6.5.1 Prediction of Crack Initiation 164
6.5.2 Prediction of Crack Propagation and Depth 166
6.5.3 Prediction of Crack Spacing 169
6.5.4 Prediction of Crack Width 170
6.5.5 Calculation of Tailings Volume and Amount of Recyclable Water 172
6.5.6 Slow Deposition 172
6.5.7 Instantaneous Layered Deposition 174
6.5.8 Cycle Deposition Parameters 175
6.6 IMPLEMENTATION OF MODEL 177
6.7 SUMMARY AND CONCLUSIONS 178

CHAPTER 7 VALIDATION AND APPLICATION OF THE MODEL 189

7.1 INTRODUCTION 189
7.2 VALIDATION OF THE MODEL 190
  7.2.1 Ten Meter High Standpipe Test 190
  7.2.2 Column Drying Test 190
7.3 APPLICATION ON OPTIMUM DESIGN FOR ARID REGIONS 191
  7.3.1 Optimum design scheme 191
  7.3.2 Modeling Results for Single Layer Deposition 194
    7.3.2.1 Variation of initial condition (depositional layer thickness) 194
    7.3.2.2 Variation of environmental condition (potential evaporation rate) 196
    7.3.2.3 Desiccation cracks 198
    7.3.2.4 Settlement 198
    7.3.2.5 Degree of saturation 200
    7.3.2.6 Tailings volume 201
    7.3.2.7 Recyclable water 202
    7.3.2.8 Hydraulic conductivity change 203
  7.3.3 Modeling Results for Multiple Layer Deposition 204
  7.3.4 Optimum Deposition Design for Arid Regions 204
7.4 CASE STUDIES AS EXAMPLES 207
  7.4.1 Introduction 207
  7.4.2 Optimum deposition design 210
    7.4.2.1 Optimum design for the case history #1 210
    7.4.2.2 Optimum design for case history #2 212
    7.4.2.3 Optimum design for the case history #3 213
    7.4.2.4 Summary of the optimum design for the case histories 214
  7.4.3 Modeling current operations 216
    7.4.3.1 Case history #1 216
    7.4.3.2 Case history #2 217
  7.4.4 Comparison between current and optimum operation 218
    7.4.4.1 Comparison of the case history #1 218
    7.4.4.2 Comparison of case history #2 219

7.5 SUMMARY AND CONCLUSIONS 221

CHAPTER 8 SUMMARY, CONCLUSIONS, AND RECOMMENDATIONS... 256

8.1 SUMMARY AND CONCLUSIONS 256
  8.1.1 Phase 1: theoretical background investigation 257
  8.1.2 Phase 2: establishment of the unified theoretical framework 258
  8.1.3 Phase 3: Validation and application of the model 260
8.2 RECOMMENDATIONS FOR FUTURE STUDIES 261

REFERENCES 263

APPENDIX A ENGINEERING BEHAVIOR OF TAILINGS 274

APPENDIX B LABORATORY TEST RESULTS 291

APPENDIX C DERIVATION OF EQUATIONS 313

LIST OF TABLES

Table 2.1 Normalized crack-edge stress-intensity factor λ (modified from Lachenbruch 1962) 50
Table 2.2 Empirical equations for the unsaturated hydraulic conductivity (modified from Fredlund et al. 1994) 50
Table 3.1 Properties of the selected saturated salt solution 77
Table 4.1 Basic properties of mine tailings 105
Table 4.2 Consolidation parameters and saturated hydraulic conductivity 106
Table 4.3 Regression parameters of void ratio versus effective stress relation 107
Table 4.4 Regression parameters of hydraulic conductivity versus void ratio 107
Table 4.5 Soil-water retention characteristic data of tailings 108
Table 4.6 Fitting parameters for soil-water retention curves of the tailings 109
Table 4.7 Fitting parameters for the shrinkage curves 109
Table 4.8 Time ranges and residual values for normalized evaporation rate 110
Table 4.9 Regression parameters of relative evaporation change 110
Table 4.10 Shear strength parameters of tailings 110
Table 6.1 Surface tensile stress relief (modified from Lachenbruch 1961) 179
Table 7.1 Properties of oil sand mature fine tailings (MFT) (modifiec from Suthaker 1995) 223
Table 7.2 Parameters for MFT used in the model (modified from Suthaker 1995) 223
Table 7.3 Main input data used in model (modified from Qiu and Sego 1998b) 224
Table 7.4 Comparison between scheme 1 and scheme 2 225
Table 7.5 Comparison of modeling results for variation of a layer thickness 226
Table 7.6 Comparison of modeling results for different potential evaporation rate 227
Table 7.7 D_{100} and predicted tensile crack dimensions and time of the tailings 228
Table 7.8 Predicted final volume and recyclable water after cracking 228
Table 7.9 Predicted surface hydraulic conductivity before and after cracking 229
Table 7.10 Comparison of modeling results for multiple layer deposition 230
Table 7.11 Original conditions and existing deposition parameters 231
Table 7.12 Measured properties and in situ conditions of tailings for Case 1 231
Table 7.13 Regression parameters for case 1 232

Table 7.14 Basic properties of the tailings in case 2 232
Table 7.15 Modeling results under optimum conditions 233
Table 7.16 Summary of the optimum depositional parameters 234
Table 7.17 Modeling results for the existing operation in case history #1 235
Table 7.18 Modeling results for the existing operation in case history #2 236
Table 7.19 Comparison of the modeling results for case history #1 237
Table 7.20 Comparison of the modeling results for case history #2 238

Table A. 1 Specific gravity and plasticity of tailings (modified from Vick, 1983) 279
Table A. 2 Slime sedimentation rates (modified from Vick 1983) 280
Table A. 3 Typical in-place density and void ratios (modified from Vick 1983) 281
Table A. 4 Minimum and maximum densities of tailings (modified from Vick 1983) 282
Table A. 5 Average in-place relative density of tailings (modified from Vick 1983) .. 282
Table A. 6 Typical hydraulic conductivity of tailings (modified from Vick 1983) 282
Table A. 7 Typical values of compression index, C_c (modified from Vick 1983) 283
Table A. 8 Typical values of coefficient of consolidation, c_v 284
Table A. 9 Typical values of drained friction angle ϕ' (modified from Vick 1983) 285
Table A. 10 Typical total-stress strength parameters (modified from Vick 1983) 286
Table A. 11 Dimensions of in situ desiccation cracks 287

Table B. 1 Consolidation and hydraulic conductivity test results for copper tailings .. 291
Table B. 2 Consolidation and hydraulic conductivity test results for gold tailings 292
Table B. 3 Consolidation and hydraulic conductivity test results for coal tailings 293
Table B. 4 Consolidation and hydraulic conductivity test results for oil sand CT 294
Table B. 5 Triaxial test results for tailings 307
Table B. 6 Shrinkage limits of tailings 308
Table B. 7 Shrinkage curve test results for copper tailings 309
Table B. 8 Shrinkage curve test results for gold tailings 310
Table B. 9 Shrinkage curve test results for coal tailings 311
Table B. 10 Shrinkage curve test results for CT 312

LIST OF FIGURES

Figure 2.1 Sketch of the sub-aerial tailings disposal method (after Qiu and Sego 1998a) 51
Figure 2.2 Beach profiles for dams of various types of tailings (modified from Blight 1987) 52
Figure 2.3 The Eulerian and Lagrangian coordinate systems (modified from Swarbrick 1992) 53
Figure 2.4 Solids coordinate z and relations with Eulerian and Lagrangian coordinates (modified from Gibson et al. 1981; Schiffman et al. 1988) 53
Figure 2.5 Typical water-soil characteristic curves (modified from Fredlund et al. 1994) 54
Figure 2.6 Typical shrinkage curve of soils 55
Figure 2.7 Opening crack mode 55
Figure 2.8 Theoretical values of elastic stress relief due to a vertical crack (modified from Lachenbruch 1962) 56
Figure 2.9 Comparison between the cracked and intact saturated hydraulic conductivity 57
Figure 2.10 Stress intensity functions for uniform and linear stress distribution (modified from Konrad et al. 1997) 58
Figure 3.1 Large strain consolidation apparatus (modified from Qiu and Sego 1998b) 78
Figure 3.2 Data acquisition system 79
Figure 3.3 De-airing cylinder 80
Figure 3.4 Tailings placement technique 81
Figure 3.5 Consolidation test apparatus 82
Figure 3.6 De-humidifier 83
Figure 3.7 Drying column (modified from Wilson 1990) 84
Figure 3.8 Layout of the drying test apparatus 85
Figure 3.9 Beam system used to accurately weigh 20 kg sample 85
Figure 3.10 Pressure-plate extractor test assembly 86
Figure 3.11 Sample retainer ring and porous ceramic plate 87

Figure 3.12 Saturated salt solution desiccator 88
Figure 3.13 Triaxial test apparatus 89
Figure 3.14 Shrinkage test apparatus 90
Figure 3.15 Shrinkage test specimens and dishes 91
Figure 4.1 Tailings grain size distribution 111
Figure 4.2 Compressibility of tailings 112
Figure 4.3 Void ratio versus hydraulic conductivity plots of tailings 112
Figure 4.4 Soil-water retention curves of tailings 113
Figure 4.5 Measured and predicted soil-water retention curves of tailings 114
Figure 4.6 Measured and fitted water retention curves for tailings 115
Figure 4.7 Shrinkage curves for mine tailings 116
Figure 4.8 Normalized evaporation rate of mine tailings 117
Figure 4.9 Comparison of measured and predicted evaporation of tailings 118
Figure 4.10 Moisture changes on the surface of the tailings 119
Figure 4.11 Moisture profile changes of copper tailings 119
Figure 4.12 Moisture profile changes of gold tailings 120
Figure 4.13 Moisture profile changes of coal tailings 120
Figure 4.14 Moisture profile changes of CT 121
Figure 4.15 Specimen height changes of different tailings 121
Figure 4.16 Deviator stress versus strain plot after 50 kPa consolidation 122
Figure 4.17 Pore pressure change versus strain plot after 50 kPa consolidation 122
Figure 5.1 The Eulerian and Lagrangian coordinate systems (modified from Swarbrick 1992) 150
Figure 5.2 Lagrangian and convective coordinates (modified from Gibson et al. 1967, 1981) 151
Figure 5.3 Coordinate relationships and void ratio change (modified from Gibson et al. 1981; Schiffman et al. 1988) 151
Figure 5.4 Consideration of an element 152
Figure 5.5 Solids weight 152
Figure 5.6 A comparison between the measured soil-water retention curves and those predicted by Fredlund's model 153

Figure 5.7 Constitutive surfaces for an unsaturated soil (modified from Fredlund and Rahardjo 1993) 154
Figure 5.8 Typical shrinking and swelling curves for a soil (modified from Fredlund and Rahardjo 1993) 155
Figure 5.9 Finite difference mesh 156
Figure 5.10 Boundary condition of the tailings deposition 156
Figure 6.1 Water balance components during the tailings pond operation 180
Figure 6.2 Location of new cracks 181
Figure 6.3 Optional design scheme 1 182
Figure 6.4 Optional design scheme 2 183
Figure 6.5 Stress path and critical suction for desiccating tailings (modified from Konrad and Ayad 1997) 184
Figure 6.6 Critical lateral tensile stress distribution 184
Figure 6.7 Assumptions of the tensile stress distributions 185
Figure 6.8 Use fictitious stress principle to determine tensile stress reduction (modified from Konrad and Ayad 1997) 185
Figure 6.9 Calculation of crack width 186
Figure 6.10 Constitutive relationship for soils (modified from Fredlund and Rahardjo 1993) 187
Figure 6.11 Flow chart of the optimum design model "DOSTAR" 188
Figure 7.1 Measured and predicted settlement in a Ten Meter Standpipe 239
Figure 7.2 Measured and predicted solids content profile in a Ten Meter Standpipe after 20400 hours 239
Figure 7.3 Measured and predicted settlement of copper tailings in drying test 240
Figure 7.4 Measured and predicted moisture content profile of copper tailings in drying test 240
Figure 7.5 Measured and predicted settlement of gold tailings in drying test 241
Figure 7.6 Measured and predicted moisture content profile of gold tailings in drying test 241
Figure 7.7 Measured and predicted settlement of coal tailings in drying test 242

Figure 7.8 Measured and predicted moisture content profile of coal tailings in drying test 242
Figure 7.9 Measured and predicted settlement of CT in drying test 243
Figure 7.10 Measured and predicted moisture content profile of CT in drying test 243
Figure 7.11 Relationship between crack width and layer thickness 244
Figure 7.12 Predicted single layer settlement of the copper tailings at cracking 244
Figure 7.13 Predicted single layer settlement of the gold tailings at cracking 245
Figure 7.14 Predicted single layer settlement of the coal tailings at cracking 245
Figure 7.15 Predicted single layer settlement of CT at cracking 246
Figure 7.16 Degree of saturation change in copper tailings 246
Figure 7.17 Degree of saturation change in gold tailings 247
Figure 7.18 Degree of saturation change in coal tailings 247
Figure 7.19 Degree of saturation change in CT 248
Figure 7.20 Normalized recyclable water in copper tailings 248
Figure 7.21 Normalized recyclable water in gold tailings 249
Figure 7.22 Normalized recyclable water in coal tailings 249
Figure 7.23 Normalized recyclable water in CT 250
Figure 7.24 Optimum design curve for case history #1 251
Figure 7.25 Deposition area versus cell number plot for case history #1 251
Figure 7.26 Optimum design curve for case history #2 252
Figure 7.27 Deposition area versus cell number plot for case history #2 252
Figure 7.28 Optimum design curve for case history #3 253
Figure 7.29 Deposition area versus cell number plot for case history #3 253
Figure 7.30 Degree of saturation in one-day operation for case history #1 254
Figure 7.31 Measured and predicted degree of saturation in case history #1 254
Figure 7.32 Primary and secondary cracks within the tailings in the field for case history #2 255

Figure A. 1 Grain size distribution of copper tailings (modified from Vick 1983) 288
Figure A. 2 Grain size distribution of gold-silver tailings (modified from Vick 1983) 289
Figure A. 3 Grain size distribution of fine coal refuse (modified from Vick 1983) 290

Figure A. 4 Grain size distribution of oil sand tailings (modified from Vick 1983) 290

Figure B. 1 Compressibility of copper tailings 295
Figure B. 2 Void ratio versus hydraulic conductivity curve for copper tailings 295
Figure B. 3 Compressibility of gold tailings 296
Figure B. 4 Void ratio versus hydraulic conductivity curve for gold tailings 296
Figure B. 5 Compressibility of coal tailings 297
Figure B. 6 Void ratio versus hydraulic conductivity curve for coal tailings 297
Figure B. 7 Compressibility of CT 298
Figure B. 8 Void ratio versus hydraulic conductivity curve for oil sand CT 298
Figure B. 9 Specimen height changes in column drying test for copper tailings 299
Figure B. 10 Evaporation changes in column drying tests for copper tailings 300
Figure B. 11 Specimen height changes in column drying tests for gold tailings 300
Figure B. 12 Evaporation changes in column drying tests for gold tailings 301
Figure B. 13 Specimen height changes in column drying tests for coal tailings 301
Figure B. 14 Evaporation changes in column drying tests for coal tailings 302
Figure B. 15 Specimen height changes in column drying tests for CT 302
Figure B. 16 Evaporation changes in column drying tests for CT 303
Figure B. 17 Soil-water retention curve test results for copper tailings 304
Figure B. 18 Soil-water retention curve test results for gold tailings 305
Figure B. 19 Soil-water retention curve test results for coal tailings 305
Figure B. 20 Soil-water retention curve test results for CT 306

LIST OF SYMBOLS

A	cross-sectional area in Equation [2-1]
A_r	constant related to the shape of evaporation curves
A_t	total available deposition area of the facility in m^2
a	initial thickness in the Lagrangian coordinate system
a_0	soil parameter that is related to the air-entry value of the soil
a_1	material constant in the compressibility formula, $e = a_1 (\sigma')^{b_1}$
a_2	material constant in the hydraulic conductivity formula, $k = a_2 e^{b_2}$
a_3	material constant in the compressibility formula, $e = a_3 \ln(\sigma') + b_3$
a_4	parameter in shrinkage curve, $e = a_4 w^2 + b_4 w + c_4$
a_5	parameter in $e = a_5 + b_5 \log(k)$
a_i	parameter in the Thomas Algorithm at any computational point, i
a_m	coefficient of compressibility with respect to a change in matric suction
a_s	characteristic constants of the beach in Equation [2-43]
a_t	coefficient of compressibility with respect to a change in net normal stress
a_v	coefficient of compressibility
a_w	activity of a solvent
B	crack spacing
B_0	parameter in Equation [2-4]
B_a	parameter in Equation [2-28]
B_r	constants related to the residual evaporation rate
b	crack depth
b_0	constant in Equation [2-20]
b_1	material constant in the compressibility formula, $e = a_1 (\sigma')^{b_1}$
b_2	material constant in the hydraulic conductivity formula, $k = a_2 e^{b_2}$
b_3	material constant in the compressibility formula, $e = a_3 \ln(\sigma') + b_3$
b_4	parameters in shrinkage curve, $e = a_4 w^2 + b_4 w + c_4$
b_5	parameters in $e = a_5 + b_5 \log(k)$

b_i	parameter in the Thomas Algorithm at any computational point, i
b_m	e coefficient of water content change with respect to a change in matric suction
b_s	characteristic constants of the beach in Equation [2-43]
b_t	coefficient of water content change with respect to a change in net normal stress
C	soil parameter
C_0	unconfined compressive strength
C_c	compression index
C_k	coefficient in Equation [2-46]
CT	oil sand composite/consolidated tailings
C_U	coefficient of uniformity
C_w	slurry concentration by weight
c'	effective cohesion
c_1	concentration of particles in Equation [2-6]
c_4	parameters in shrinkage curve, $e = a_4 w^2 + b_4 w + c_4$
c_i	parameter in the Thomas Algorithm at any computational point, i
c_m	mobilized cohesion
c_T	undrained shear strength parameter: total cohesion
c_v	coefficient of consolidation
D	soil parameter
D_0	initial layer thickness before desaturation
D_{10}	grain size for which 10% of tailings particle pass by weight
D_{50}	mean grain size of the tailings in Equation [2-1]
D_{50H}	mean particle size at a distance H along deposition
D_{50T}	mean particle size of total tailings deposited
D_{100}	grain size for which 100% of the particles pass by weight
D^*_a	coefficient of transmission for the air phase
D_r	relative density
D_w	depth from the ground surface to the water table
d	depth
E_A	actual evaporation rate of the tailings
E_m	Young's modulus

E_n	normalized evaporation rate
E_P	potential evaporation rate
e	void ratio
e	the natural number (e = 2.71828)
e_0	initial void ratio
e_0	initial void ratio
e_0^{avg}	average initial void ratio
$e_{s\text{-}c}$	changeover void ratio from sedimentation and consolidation on the upper surface
F	factor of safety
F_l	material parameter in Equation [2-55]
F_t	ratio of tensile strength and unconfined compressive strength
F_w	matric suction profile factor
f(u)	parameter in Equation [2-25a]
f_w	ratio of pore water pressure to the hydrostatic pressure
G	shear modulus
G_E	rate of release of strain energy with crack extension, i.e. "crack extension force"
G_s	the specific gravity
g	the acceleration of gravity
H	distance along beach from the deposition point in Equation [2-3]
H_m	elastic modulus with respect to matric suction $(u_a - u_w)$
H(t)	total height of the tailings at time t
H_z	total height of solids
H_ξ	deposition layer thickness
$H_{\xi o}$	optimum deposition layer thickness
h	pore pressure head
h_b	air-entry value in terms of the water pressure head
h_i^n	numerical solution for h at point z_i and time t_n
h_{ra}	relative humidity of the air
h_{rs}	relative humidity at the soil surface
h_w	elevation from the pond water level in Equation [2-3]
$h_z(t)$	total height of the solids at time t

$h_\xi(z,t)$	actual tailings thickness of the accumulating layer
i_{ov}	overall beach slope
K_0	coefficient of earth pressure at rest
K_{onc}	coefficient of earth pressure at rest for normally consolidated soils
k	hydraulic conductivity
k_0	hydraulic conductivity of the fresh tailings which infill the cracks
k_c	coefficient of the hydraulic conductivity of the cracked layer
k_d	hydraulic conductivity of the non-cracked portion of the dried tailings
$k_r(\theta)$	relative hydraulic conductivity at any water content
k_s	saturated hydraulic conductivity
k_w	coefficient of permeability with respect to water as a function of matric suction Equation [2-17]
k_x	saturated hydraulic conductivity in x direction
k_y	saturated hydraulic conductivity in y direction
k_z	saturated hydraulic conductivity in z direction
$k(\theta)$	hydraulic conductivity at any water content
M_c	number of full cycles per year
M_d	dry mass of a soil/tailings pad
MFT	oil sand mature fine tailings
M_s	mass of the solids
M_w	mass of the water
m	parameter related to the residual water content
m_1	constants in Equation [4-5]
m_3	material parameter
m_2^a	coefficient of air volume change with respect to a change in matric suction
m_2^w	coefficient of water volume change with respect to a change in matric suction
m_{1k}^w	coefficient of water volume change with respect to a change in the net normal stress
m_t	slope of the linear portion of the t/δ versus t plot
m_v	coefficient of volume compressibility

N	total time intervals
N_c	total number of deposition cells
n	porosity
n_0	dimensionless constant dependent on the tailings' characteristics in Equation [2-3]
n_1	constants in Equation [4-5]
n_2	soil/material parameters
n_3	soil/material parameters
n/N	ratio of actual to possible sunshine hours
P	parameter that is related to the residual water content in soil-water retention curve
P_{sa}	saturation vapor pressure of the mean air temperature
P_t	tailings production rate in tons per day (tpd)
P_{va}	actual vapor pressure of the air above the evaporation surface
P_{vs}	saturated vapor pressure
p	positive material constants in equation [4-7]
p'	an empirical parameter in Equation [2-1]
p_s	total weight of solids per unit area lying between the surface of the tailings and z co-ordinate
p_t	total pore pressure in Equation [2-66]
p_w	total weight of water per unit area lying between the surface of the tailings and the z co-ordinate
Q	parameter in the soil-water characteristic curve
Q_0	heat budget in Equation [2-25]
Q_1	initial input water during tailings discharge
Q_2	evaporation loss of water
Q_3	drainage through the free drainage zone of the dike
Q_4	drainage through the bottom sand filter blanket
Q_5	discharge due to consolidation of the tailings
Q_6	recyclable water from the drainage collection toe ditch
Q_7	precipitation (rain or snow)
Q_8	storage of water in the consolidated tailings layers
Q_d	the total flow rate in Equation [2-1]

Q_n	all net radiation
q	positive material constants in Equation [4-7]
R	total spatial intervals
R_a	solar radiation for a completely transparent atmosphere
R_c	shortwave radiation measured at the site
R_h	relative humidity
R_u	universal (molar) gas constant ($R_u = 8.31432$ J/(mol·K))
r	geometry factor which determines the partition of total volume change over change in layer thickness and change in crack volume
r_f	reflectance coefficient
S	degree of saturation
S_a	parameter in soil-water retention curve proposed by Aubertin et al. (1998)
S_c	parameter in soil-water retention curve proposed by Aubertin et al. (1998)
SL	shrinkage limit
S_r	residual degree of saturation
s_0	original solids content
T	absolute temperature in Kelvin ($T=273 + t$)
T_1	material parameter in Equation [2-55]
T_2	material parameter in Equation [2-55]
T_a	air temperature (°C)
T_c	cycle time in hours
T_d	discharge time in hours
T_s	drying time in hours
t	time
t_n	accumulated time in n steps
t_s	drying time in days in Equation [4-7]
t_d	exposure time at the surface of the tailings facility
U	value of suction in Equation [2-29]
U_a	wind speed
u	excess pore pressure
u_2	wind velocity

u_a	pore-air pressure
u_{ab}	absolute pore-air pressure
u_{atm}	atmospheric pressure
u_{cr}	suction required to reduce the horizontal stress to zero
u_w	pore water pressure
V	volume of soil matrix at saturation
V_0	initial volume of the tailings matrix before desaturation
V_i	initial volume in Equation [3-5]
V_d	volume of dry soils/tailings in Equation [3-5]
V_A	partial molar volume of a solvent
V_{cr}	crack volume
v^*	displacements in the y direction
v_s	velocity of the particles in Equation [2-5]
v_w	velocities of water
w	gravimetric water content
w^*	displacements in the z direction
w_i	inintial gravimetric water content
w_s	saturated moisture content
w_x	displacements in the directions x
w_y	displacements in the directions y
w_z	displacements in the directions z
X	length of the beach from discharge point to edge of pond in Equation [2-3]
X_k	material parameter in Equation [2-46]
x	dummy variable of integration representing water content
x_1	height above the bottom of the column of dispersed particles in Equation [2-6]
Y	elevation between the point of deposition and the liquid pool in Equation [2-3]
y	dummy variable of integration representing the logarithm of suction
Z	layer thickness of soil matrix at saturation
z	solids coordinate
z_0	roughness height of the surface
z_2	height in Equation [2-28a]

α	constant related to the air-entry value
α_1	solids parameter ($\alpha = 2.5$ for hard spheres)
α_2	soil parameter in Equqtion [2-21]
$\beta(e)$	interaction coefficient
Γ	slope of the saturation vapor pressure versus temperature curve
Γ_1	parameter related to wind velocity
γ	unit weight of the soil/tailings
γ_s	unit weight of the tailings particles
γ_w	unit weight of the water
ΔA	expansion area of a tailings facility
ΔD	decrease in layer thickness due to shrinkage from a fully saturated state to when the crack propagates
ΔV	decrease in volume of soil matrix as a result of shrinkage (positive)
ΔZ	decrease in layer thickness as a result of shrinkage (positive)
Δt	time interval for finite difference mesh
Δz	spatial interval for finite difference mesh
$\Delta \upsilon_c$	additional crack width
δ_{100}	deformation corresponding to 100% consolidation
ε_{ml}	mechanical lateral tensile strain
ε_t	tensile strain at failure
ζ	specific surface energy of a soil
$\zeta(t)$	total height of solids at time t
η	viscosity of water (10^{-6} kPa·sec at 20°C)
Θ	normalized volumetric water content
θ	volumetric water content
θ'	derivative of θ function
θ_r	residual volumetric water content
θ_s	saturated volumetric water content
κ	crack-edge stress-intensity-factor

κ_0	crack-edge stress-intensity-factor at crack arresting
κ_1	fitting parameter in Equation [2-52b]
κ_c	critical stress intensity factor or fracture toughness in $kN/m^{1.5}$
$\kappa_g(b)$	contribution to $\kappa(b)$ of the weight of the column of height
κ_{trap}	stress intensity factor corresponding to a trapezoidal tensile stress distribution
κ_{tria}	stress intensity factor corresponding to a uniform tensile stress distribution
$\kappa_U(b)$	contribution of the uniform tension to the intensity factor
κ_{unif}	stress intensity factor corresponding to a triangular tensile stress distribution
λ	coefficient in the calculation of the stress intensity factor κ (Equation [2-37])
λ_1	coefficients for the uniform stress distribution
λ_2	coefficients for the triangular distribution
μ	fluid viscosity
μ_1	Stokes' velocity in Equation [2-5]
ν	Poisson's ratio
ν_0	psychrometric constant in Equation [2-25]
ν_1	kinematic viscosity of water
ξ	convective coordinate (the Eulerian coordinate)
Π	osmotic pressure or suction
ρ	total density of the soil
ρ_0	original placement bulk density
ρ_1	volume concentration in Equation [2-5]
ρ_d	dry density of a soil
ρ_w	density of water
σ	total stress
σ'	effective stress
σ_3	total horizontal stress acting on the soil surface
$\sigma_3(b)$	tensile stress at the depth of b at the initiation of the crack
σ_{3a}	tensile stress at the bottom of the trapezoidal distribution
σ_h	lateral total tensile stress

σ_n	total normal stress on the plane of failure
σ_t	tensile strength
σ_v	total vertical stress
σ_v'	effective vertical stress
σ_x^*	normal stress in the x direction
σ_y^*	normal stress in the y direction
τ	shear strength
τ_{SB}	Stefan-Boltzman constant
τ_{us}	shear strength contribution due to suction
τ_{xy}^*	shear stress in the xy plane
υ	crack width
υ_c	crack width at the time of crack initiation
υ'_c	crack width at the time of the failure
ϕ'	effective friction angle of the material
ϕ^b	friction angle with respect to the matric suction
ϕ_m	mobilized friction angle
ϕ_T	undrained shear strength parameter: total friction angle
χ	Bishop parameter
χ_1	tensile strength parameter proposed by Snyder and Miller (1985)
ψ	soil suction
ψ_0	10^7 cm water
ψ_{aev}	air-entry value of a soil
ψ_b	the air-entry value
ψ_{cr}	critical value of suction at the initiation of a crack
ψ_r	residual matric suction of a soil
ω_a	molecular mass of air (kg/kmol)
Ω_c	critical crack tip opening
∇^2	Laplace operator

CHAPTER 1 INTRODUCTION

1.1 INTRODUCTION

The mining industry throughout the world has long been challenged by the problem of the disposal of tailings. The term "tailings" is mainly used to refer to the vast quantity of finely ground mill or mineral processing wastes remaining after extraction of minerals. Tremendous volumes and many types of mine tailings are produced worldwide every day. Most have to be treated and disposed of on the earth's surface. Generally, the following problems are encountered in tailings disposal: environmental impact and concerns with tailings dam stability, land use and reclamation, and water loss. For example, the two oil sands surface mining operations in northern Alberta, Syncrude Canada Ltd. and Suncor Inc., produce about 333,800 barrels per day of synthetic crude oil (Syncrude Web online in May 20, 1998 and Suncor Newsletter, April 23, 1998). Each 1 m^3 (6.3 barrels) of synthetic oil produced requires 16 m^3 of water and results in about 21 m^3 of tailings with a solids content of 45 to 50% by mass (Dawson 1994). Hence, the two companies produce about 121.8 million barrels of synthetic crude oil annually, requiring 309.4 million m^3 of water and resulting in 406.1 million m^3 tailings annually. At Syncrude, the tailings pond is designed to cover 22 km^2 area (Suthaker 1995). These tremendous quantities are striking and demonstrative of the very large scale of the operations. As previously mentioned, mineral processing requires large amounts of water. Hence, the demand on water resources is becoming a critical issue, especially in arid regions. The processing water needs to be recycled as completely as possible.

Most tailings are sandy soils from mineral extraction plants. These huge sandy earth structures have a potential of liquefaction failure due to the sandy nature of the tailings, especially in a high risk earthquake zone. Tailings disposal is a major environmental and safety issue that has become more serious as a result of more and tighter environmental regulations on the part of governments. How to treat tailings effectively and economically has become an important issue facing mining operations. The sub-aerial technique is a promising tailings treatment method. Knight and Haile (1983) defined the sub-aerial technique as the systematic deposition of tailings in a thin layer, which is then allowed to settle, drain and partially air dry prior to covering it with the next layer. Although this technique has existed for decades, its use still involves many technical challenges. Among these, an important concern is the selection of the optimum depositional parameters for achieving the best desiccation results. A rational method for predicting the response and behavior of the sub-aerial deposited tailings to aid in developing design criteria for the long-term performance of these facilities was not available. Therefore, the topic of the proposed research is to evaluate the optimum depositional parameter design for sub-aerial tailings disposal to recycle the optimum amount of process affected water.

1.2 RESEARCH SCOPE AND OBJECTIVE

The main objective of the research is to minimize the environmental impact of the tailings, to reduce the volume which must be stored in the tailings pond, and to maximize the recycling of the processing water back to the extraction plant.

The subsidiary objectives are as follows:

- To identify engineering properties of tailings;
- To demonstrate the physical process of tailings desiccation;
- To identify the factors affecting tailings desiccation;
- To formulate a theoretical (or empirical) framework for evaluation of the sedimentation, consolidation, and desiccation of tailings in the sub-aerial deposition method;

- To establish a model for carrying out the optimum sub-aerial depositional design;
- To verify the theoretical approach;
- To demonstrate the application of the theoretical model.

1.3 THESIS OUTLINE

The research carried out in this thesis can be divided into three phases. The first involved theoretical background and material characteristic investigations (Chapter 2, 3, and 4). Chapter 2 contains a literature review of previous work on sub-aerial tailings deposition, hydraulic fill, and modeling the sedimentation, consolidation, and desiccation of soils. In this study, copper, gold, coal and oil sand composite/consolidated (CT) tailings were selected to represent a wide range of tailings from different types of mines. A series of experiments were carried out to investigate the basic engineering properties and the desiccation behavior of the tailings. A detailed laboratory test program is described in Chapter 3. The experimental findings and results obtained from the laboratory tests are presented in Chapter 4.

The second phase of the research was to establish a unified theoretical framework for the evaluation of sedimentation, consolidation and desiccation, and a model to simulate the process of the sub-aerial tailings deposition for the optimum deposition design (Chapter 5 and 6). Chapter 5 presents a one-dimensional theory of sedimentation and consolidation that simulates the physical interaction of soil and fluid particles within the deformable soil skeleton. The numerical method for solving the partial differential equations is also described in Chapter 5. Chapter 6 discusses the factors affecting the optimum deposition design in arid regions and presents a theoretical model for optimum sub-aerial tailings depositional parameter design. The model, referred to as DOSTAR, was coded in the Visual Basic and is capable of predicting sedimentation, consolidation, desiccation, crack initiation, crack propagation, crack dimensions (spacing, depth, and width), tailings volume, and water available for recycling.

The final phase of the research was validation and application of the design model (Chapter 7). The validity of the model, obtained by comparing the modeled results with the laboratory test results, is presented in Chapter 7. Three field case studies as examples of the application of the model are also provided in Chapter 7.

A summary of the findings of this research and the recommendations for future research are presented in Chapter 8.

CHAPTER 2 LITERATURE REVIEW

2.1 INTRODUCTION

In sub-aerial tailings disposal, tailings from an extraction plant are hydraulically transported to and deposited in the tailings pond. The deposited tailings are then allowed to settle and consolidate. Gradually, the tailings, if exposed, are also allowed to air dry. There are many factors that affect this disposal process, e.g. segregation, sedimentation, consolidation, and desiccation behaviors.

This study focuses on the evaluation of the optimum design for sub-aerial tailings deposition in arid regions with the intent of optimizing the amount of water available for recycling to the process plant. A great deal of research work has been carried out to investigate the engineering properties of various tailings. As well, some physically based models have been established to handle the sedimentation, consolidation, and desiccation for both soils and tailings.

2.2 THE SUB-AERIAL TAILINGS DEPOSITION TECHNIQUE

Tailings are commonly deposited as a slurry into an impoundment formed by embankments or dykes. Based on the classification of the tailing deposition proposed by Morgenstern and Küpper (1988), any method which allows for deposition of tailings "under air" may be called sub-aerial deposition. Some literature also describes sub-aerial deposition as a special tailings deposition technique, e.g., Knight and Haile, (1983). The technique, which has also been referred to as the "thin-layer managed tailings deposition method" (Van Zyl 1993), the "semi-dry sub-aerial method" (Ritcey 1989), and the "semi-dry process" (Blight 1988) involves systematic deposition of tailings in a thin layer by discharging slurry from one or more points along the perimeter of the impoundment area. As slurry flows toward the low point in the impoundment, the tailings settle, drain, partially air dry, and increase in density in thin layers. The free water released to the surface drains to a central location or low point where it can be recycled into the processing system, decanted to a separate containment facility for reuse or evaporation, or allowed to evaporate in place. Subsequent layers are then deposited, and the cycle is repeated.

The concept of sub-aerial tailings disposal can be seen in Figure 2.1 (Qiu and Sego 1998a). The tailings from a mill are pumped to the disposal site through a tailings pipeline. The tailings impoundment area is divided into several deposition cells where the tailings are discharged through a spray bar or spigot to provide flow over a beach in a given cell (e.g. Cell #2). After the cell has been covered with a thin layer, the discharge point is moved to the next cell (e.g. Cell #3), and the previously deposited layer is allowed to settle and dry prior to covering it with a fresh layer. During deposition, the different fractions of the segregating tailings settle along the beach, while non-segregating tailings settle along the beach with no segregation, and the supernatant flows to the pond area. Except for limited horizontal movement after deposition, the water in the tailings moves predominately vertically, i.e. the water moves upward under the influence of sedimentation, self-weight consolidation, and evaporative-flux and downward as seepage to any under-drainage system. At the low point, the seepage and supernatant runoff are collected and pumped back for recycling or drained to a pond for treatment prior to release into the environment.

The physical processes of the sub-aerial tailings disposal method are sedimentation, consolidation, and desiccation. Sedimentation takes place only during deposition and for a short period immediately after. Consolidation occurs throughout the entire deposition process. Desiccation is mainly due to evaporation from the exposed tailings surface.

Blight (1988) concluded that surface drying has the effect of considerably reducing the void ratio of the deposited slurry material and increasing the solid storage capacity of the impoundment. The technique has been practiced by the South African gold mining industry since the early part of this century and is currently used in all hydraulic fill gold tailings impoundment in South Africa (Blight 1988). The technique was also used at the Key Lake Uranium mine and the base metal mine of Westmin Resources Ltd. in Canada (Knight and Haile 1983). Ridlen et al. (1997) reported the usage of the sub-aerial deposition at the Kennecott Utah Copper Corporation.

2.3 SEGREGATION BEHAVIOR AND GEOMETRY OF A TAILINGS BEACH

Küpper et al. (1992) and Küpper (1991) conducted an experimental study of hydraulic fill to examine the deposition process, the characteristics of the fill and the relationship between the mechanisms of fill placement and resulting physical properties. Laboratory flume deposition tests with three types of sands and field deposition tests were conducted. They used both segregating and non-segregating slurries in their tests and found that these two types of slurry generated distinct depositional conditions, with significant impact on the fill geometry, density and grain size distribution along the beach. Segregating slurry deposits are flatter and have denser beaches with mean grain sizes varying with distance from the discharge point, while non-segregating slurries do not permit hydraulic sorting and produce a steeper beach with approximately constant granulometric characteristics and a relatively low depositional density.

Density is a key factor affecting stability of hydraulic structure under both static and dynamic conditions. The results of flume tests showed a decrease in density with increasing slurry concentration, flow rate, and mean grain diameter. But the trend in the variation of density with slurry concentration for field tests was less clear.

Beach geometry is a main issue in the design of hydraulic fills for containment. Beach geometry controls several factors such as fill volume, duration of construction, position and size of the pond, location of decant facilities, lay-out and area of the structure, storm water storage capacity, and costs.

To estimate the average slope, Küpper (1991) proposed an empirical dimensionless parameter (p′):

$$[2\text{-}1] \quad p' = \frac{A}{Q_d}\sqrt{g(G_s - 1)D_{50}C_w}$$

where G_s is the specific gravity of the tailings particles, Q_d is the total flow rate at the discharge point, g is the acceleration of gravity, D_{50} is the mean grain size of the tailings, C_w is the slurry concentration by weight, and A is the cross-sectional area of the discharge pipe.

The following empirical relationship was proposed to calculate the overall beach slope i_{ov}:

$$[2\text{-}2] \quad i_{ov} = 5\sqrt{p'}$$

Küpper (1991) also concluded that the overall beach slope of hydraulic fills increases for larger slurry concentrations and for coarser materials and decreases as the slurry flow rate increases.

Both the beach profile and segregation of particles along the beach are functions of the specific gravity of the tailings (solids), solids content within the slurry, and discharge rate of the slurry. Blight (1987) realized that the profile appears to be generated by gravitational sorting of particle sizes as the tailings slurry flows down the beach. A master profile of the beach was proposed as shown in Figure 2.2, and the following empirical equation was proposed (Blight 1987):

[2-3] $$\frac{h_w}{Y} = \left(1 - \frac{H}{X}\right)^{n_0}$$

where h_w is the elevation from the pond water level, Y is the elevation between the point of deposition and the liquid pool, H is the distance along beach from the deposition point, X is the length of the beach from discharge point to edge of pond, and n_0 is the dimensionless constant dependent on the tailings' characteristics.

Each type of tailings can be characterized by a different n_0, as illustrated in Figure 2.2. n_0 equals 1.4, 1.5, 2.0, and 4.0 for the copper, diamond, platinum and gold tailings, respectively. The exponent is also affected by the solids concentration of the slurry and the fine particle size of the tailings material. The concept of a master profile enables the designer to predict the position of the pool relative to the deposition point, to assess the storm-water capacity of the constructed impoundment, and to more accurately assess the tailings' storage capacity.

As a result of sorting by particle size, the coarser particles deposit near the discharge point while the finer particles deposit farther along the beach. Blight (1987) proposed a relationship to predict the size of particles at a distance H along a hydraulic fill beach:

[2-4] $$\frac{D_{50H}}{D_{50T}} = e^{-B_0 H/X}$$

where D_{50H} is the mean particle size at a distance H along deposition, D_{50T} is the mean particle size of total tailings deposited, e is the natural number, i.e. e = 2.718 28, B_0 is a parameter dependent on the characteristics of the tailings (a sample showed that B_0 has a value of 2.5), H is the distance along the beach from the deposition point, and X is the total length of the beach.

In summary, segregating slurry deposits are flatter and have denser beaches with mean grain sizes varying with distance from the discharge point, while non-segregating slurries do not permit hydraulic sorting and produce a steeper beach with approximately constant granulometric characteristics and a relatively low density. The results of flume tests showed a decrease in density with increasing slurry concentration, flow rate, and mean grain diameter. The overall beach slope of hydraulic fills increases for larger slurry concentrations and for coarser materials and decreases as the slurry flow rate increases. The concept of a master profile proposed by Blight (1987) enables the designer to predict the position of the pool relative to the deposition point, to assess the storm-water capacity of the constructed impoundment, and to more accurately assess the tailings' storage capacity.

2.4 SEDIMENTATION

Particles dispersed in a fluid tend to settle under gravity. The process of sedimentation of the solids particles is very common in tailings disposal using hydraulic placement. The solids (fines) concentration by weight, in a solids-suspension tailings discharge from many mineral extraction process industries, is generally very low (as low as 1 to 3%) (Yong 1984). If the solids are non surface-active, and if they are silt-sized or larger, it is likely that they will settle in accord with the general predictions advanced by the simple Stokesian model. It can be formulated as follows when the concentration of particles is very small and their particle-particle distance is much greater than their size (Kynch 1952)

$$[2\text{-}5] \quad v_s = \mu_1(1-\alpha_1\rho_1)$$

where v_s is the speed of fall of the particle, α_1 is the solids parameter, $\alpha_1 = 2.5$ for hard spheres, μ_1 is the Stokes' velocity, and ρ_1 is the volume concentration.

However, if the particles are clay-sized or smaller, and if they are surface-active, the simple Stokesian model cannot accurately predict the settling of the solids. The theoretical background for sedimentation was developed by Kynch (1952). The downward motion of this particle system was referred as "hindered settling." In his theory of hindered sedimentation, Kynch considered only the continuity of the solid phase and ignored the effective stress in the sediment which is formed at the bottom of the dispersion. Kynch assumed that the velocity (v_s) of any particle is a function only of the local concentration (c_l) of particles in its immediate neighborhood. The concentration here means the number of particles per unit volume of the dispersion. The settling process was formulated as follows (Kynch 1952):

$$[2\text{-}6] \quad \frac{\partial c_l}{\partial t} + \frac{d}{dc_l}\left[c_l v_s(c_l)\right]\frac{\partial c_l}{\partial x_l} = 0$$

where c_l is the concentration of particles, $v_s(c_l)$ is the velocity of the particles, t is the time, and x_l is the height above the bottom of the column of dispersed particles.

The Kynch theory has been commonly applied in chemical engineering but seldom in geotechnical engineering analysis (McRoberts and Nixon 1976; Chan and Masala 1998). Some experimental studies related to geotechnical engineering have been carried out by McRoberts and Nixon (1976), Been (1980), and Imai (1980, 1981). Through experimental studies using soft clay, Imai (1981) concluded that the genesis of developing soil deposits could be divided into three stages. In the first stage, no settling takes place, but flocculation yields flocs. In the second stage, the flocs gradually settle and form a layer of sediment, which undergoes consolidation and reduction of water content. The boundary between the upper settling zone and the sediment is the birth place of new sediments. While the sediment grows, the settling zone becomes thinner and finally vanishes. In the last stage, all of the sediment thus formed undergoes self-weight consolidation and finally approaches an equilibrium state (Imai 1981).

Schiffman et al. (1988) noted that at the top of the settling zone, the total stress and the pore water pressure are equal. This indicates that the particles have not aggregated, and thus the effective stresses remain zero. However, he also recognized that sedimentation and consolidation occur simultaneously in a variety of industrial operations including hydraulic mine waste disposal. Hence, there is also a thin transition zone separating the setting and consolidating zones where the effective stresses are non-zero but do not control the consolidation process as assumed in geotechnical engineering. This phenomenon has led to a modified effective stress equation to build a link between sedimentation and consolidation process as follows (Schiffman et al. 1984; Pane and Schiffman 1985):

$$[2\text{-}7] \quad \sigma = \beta(e)\sigma' + u_w \qquad (0 \leq \beta(e) \geq 1)$$

where σ is the total stress, $\beta(e)$ is the interaction coefficient, which is a monotonic function of the void ratio (in a dispersion β is zero while in a mature soil β becomes unity), σ' is the effective stress, and u_w is the pore water pressure.

Based on the Kynch's theory of "hindered sedimentation," Chan and Masala (1998) proposed a model for the analysis of the sedimentation of suspensions of fine grained soils. The model was used to calculate the increase of the solids content with time in the suspension zone by relating both the suspension settlement rate and the sediment growth rate to the particle settling velocity, which is in turn taken as a unique function of the solids concentration. The model was applied to the sedimentation analysis of the oil sand fine tailings, and close agreement was found between predictions of suspension settlement, solids content profile, excess pore pressure profile, and experimental data.

2.5 CONSOLIDATION

The application of a load to a soil will result in the generation of excess pore water pressure within a saturated soil or both pore-water and pore-air pressures within an unsaturated soil. The excess pore pressures will dissipate with time. The dissipation process of the pore pressures is called consolidation, and the process results in a volume decrease or settlement (Fredlund and Rahardjo 1993). According to Schiffman et al. (1984), modern geotechnical engineering was founded by the initial publication of the theory of consolidation. This theory first defined the fundamental relationships governing the response of a soil system to imposed loads, and on this basis predictions of the stresses and displacements of a loaded soil as functions of space and time could be made.

The conventional theory of consolidation was first established by Terzaghi (Schiffman et al. 1969). The one-dimensional theory of primary consolidation is based on the following constitutive assumptions: (1) the soil is completely saturated with water, (2) the soil particles and the pore water are incompressible, (3) the pore fluid flow is governed by Darcy's law, (4) the strains of the soil skeleton are controlled exclusively via a linear time-independent relation between void ratio and effective stress, (5) the strains, velocities, and stress increments are small and the theory is quasi-static, (6) the soil is homogeneous, and (7) the soil properties do not vary with stress and strain. Terzaghi (1936) proposed the effective stress, $(\sigma\text{-}u_w)$, as the stress variable to describe the behavior of a saturated soil. The governing equation for one-dimensional consolidation is as follows (Terzaghi 1943):

$$[2\text{-}8] \quad \frac{\partial u}{\partial t} = c_v \frac{\partial^2 u}{\partial z^2}$$

and

$$[2\text{-}9] \quad c_v = \frac{k}{m_v \gamma_w}$$

where u is the excess pore pressure, t is the time, c_v is the coefficient of consolidation, z is the depth, k is the saturated hydraulic conductivity, m_v is the coefficient of volume compressibility, and γ_w is the unit weight of the water.

The one-dimensional consolidation theory has been widely applied to the analysis of field situations. However, it has been found to produce results which generally overestimate the time required for consolidation (Skempton and Bjerrum 1957; Darragh 1964), especially for overconsolidated clays (Schiffman et al. 1969).

Rendulic (1936) proposed another interpretation of the conventional theory that the time behavior of the internal total stresses is strictly equivalent to the applied total stresses. This interpretation led to the Terzaghi-Rendulic pseudo three-dimensional consolidation theory. For a time-independent loading, the excess pore pressures are governed by (Schiffman et al. 1969):

$$[2\text{-}10] \quad c_v \nabla^2 u = \frac{\partial u}{\partial t}$$

which c_v is a coefficient of consolidation and ∇^2 is the Laplace operator. The total stress components are treated independently from the excess pore pressure.

Biot (1941) proposed a three-dimensional consolidation theory, which consists of two equations, i.e. continuity and equilibrium equations. Biot's three-dimensional consolidation theory provides a coupling between magnitude and progress of displacement. In fact, there are four variables, i.e. three displacement components and the excess pore pressure in the equation. To solve the two equations both the following continuity equation [2-11] and the equilibrium equation [2-12] have to be used. Therefore, the governing equations for three-dimensional consolidation are as follows with $k_x = k_y = k_z = k$:

$$[2\text{-}11] \quad -\frac{\partial}{\partial t}\left(\frac{\partial w_x}{\partial x} + \frac{\partial w_y}{\partial y} + \frac{\partial w_z}{\partial z}\right) + \frac{k}{\gamma_w}\nabla^2 u = 0$$

and

$$
[2\text{-}12] \quad \begin{cases}
-\nabla^2 w_x - \dfrac{G}{1-2v}\dfrac{\partial}{\partial x}\left(\dfrac{\partial w_x}{\partial x}+\dfrac{\partial w_y}{\partial y}+\dfrac{\partial w_z}{\partial z}\right)+\dfrac{k}{\gamma_w}\dfrac{\partial u}{\partial x}=0 \\
-\nabla^2 w_y - \dfrac{G}{1-2v}\dfrac{\partial}{\partial y}\left(\dfrac{\partial w_x}{\partial x}+\dfrac{\partial w_y}{\partial y}+\dfrac{\partial w_z}{\partial z}\right)+\dfrac{k}{\gamma_w}\dfrac{\partial u}{\partial y}=0 \\
-\nabla^2 w_z - \dfrac{G}{1-2v}\dfrac{\partial}{\partial z}\left(\dfrac{\partial w_x}{\partial x}+\dfrac{\partial w_y}{\partial y}+\dfrac{\partial w_z}{\partial z}\right)+\dfrac{k}{\gamma_w}\dfrac{\partial u}{\partial z}=-\gamma
\end{cases}
$$

where w_x, w_y, and w_z are the displacements in the directions x, y, and z respectively, ∇^2 is the Laplace operator, G is the shear modulus, v is Poisson's ratio, k is the coefficient of hydraulic conductivity, γ and γ_w are the unit weights of the soil and water, respectively, and u is the excess pore water pressure.

Gibson et al. (1967) presented a one-dimensional nonlinear finite strain theory for thin, homogeneous clay layers. In this theory, the influence of the self-weight of the consolidation layer, an important factor which was neglected in conventional consolidation analysis, was considered. The usual coordinate system used in geotechnical engineering is the Eulerian system. As shown in Figure 2.3, in the Eulerian system, the material deformation is related to planes fixed in space. It is worth noting that both the solids and liquids change within the fixed box; thus, the excess pore pressure in a consolidating clay layer is measured at a point which is specifically related to a fixed physical datum. Therefore, the distance from the datum to the piezometer is always supposed to remain the same. Since the deformations are large compared with the thickness of the consolidating soil layer, the use of the Eulerian system can be very inconvenient (Gibson et al. 1981). The governing relationship of the nonlinear finite large strain consolidation theory is best accomplished using Lagrangian coordinates (a, t) (Schiffman et al. 1988). As illustrated in Figure 2.3, in the Lagrangian coordinate system, the vertical coordinate is fixed relative to the soil skeleton, i.e. only fluids change within the fixed box. The governing equation of the nonlinear finite large strain consolidation theory (Gibson et al. 1967) can be expressed as follows in the Lagrangian system (Schiffman et al. 1988):

[2-13] $$\frac{\partial}{\partial a}\left[\frac{k(e)}{\gamma_w}\frac{1+e_0}{(1+e)}\frac{\partial u}{\partial a}\right]=\frac{a_v(e)}{1+e_0}\left[\frac{\partial u}{\partial t}-\frac{\partial \sigma}{\partial t}\right]$$

where e_0 is the initial void ratio, which is generally a function of the initial thickness, a, and k is the hydraulic conductivity.

Schiffman, et al. (1984) reviewed the theory of nonlinear finite strain consolidation and presented a modification of the effective stress equation (Equation [2-7]) to account for settling and consolidation as a unified phenomenon of saturated clays. Since the saturated thick clay layer has large displacements during consolidation, the usual use of Eulerian coordinates will lead to difficulties since the location of the surface of the layer (upon which certain boundary conditions must be imposed) is not given and is part of the solution. However, the volume of solids in a clay layer never changes. Thus, a special coordinate, the reduced/solids coordinate z, was introduced. The solids coordinate z is defined as the volume of tailings particles per unit area lying between the datum plane and the point being analyzed, or the height of solids particles lying between the datum plane and the point being analyzed. Once a solution is developed in terms of z and t, the instantaneous Eulerian coordinate ξ can be found from (Figure 2.4):

[2-14] $$\xi(z,t)=\int_0^z\left[1+e(z,t)\right]dz$$

where e(z, t) is the void ratio in terms of the solid coordinate at that time, t.

In the solids coordinate system, the governing equation of the nonlinear finite large strain consolidation theory is as follows (Gibson et al. 1967):

[2-15] $$\frac{\partial e}{\partial t}=\frac{\partial}{\partial z}\left\{\frac{k}{(1+e)}\left[\left(-\frac{1}{\gamma_w}\frac{d\sigma'}{de}\right)\frac{\partial e}{\partial z}+(1-G_s)\right]\right\}$$

The governing equation of the modified nonlinear finite strain consolidation that accounts for settling and consolidation as a unified phenomenon for saturated clays was presented as (Schiffman et al. 1984):

$$[2\text{-}16] \quad \frac{\partial}{\partial z}\left\{a(e)\left[\beta\frac{\partial\sigma'}{\partial z}+\sigma'\frac{\partial\beta}{\partial z}\right]\right\}+f(e)\frac{\partial e}{\partial z}+\frac{\partial e}{\partial t}=0$$

with

$$[2\text{-}16a] \quad a(e)=\frac{k}{\gamma_w(1+e)}$$

and

$$[2\text{-}16b] \quad f(e)=\left(\frac{\gamma_s}{\gamma_w}-1\right)\frac{d}{de}\left[\frac{k(e)}{(1+e)}\right]$$

where e is the void ratio, k(e) is the saturated hydraulic conductivity, as a function of void ratio, and σ' is the vertical effective stress.

This relationship would then govern the process of sediment formation and consolidation for saturated clays. The theory was applied to a 15 m thick loaded clay layer with the instantaneous application of a 200 kPa surcharge. The index properties of the clay were as follows: liquid limit = 137% and plastic limit = 40%. The natural water content at the surface of the sediment was 140%. Results were compared to the results from the other three consolidation theories, i.e. the finite strain theory with a single average value for compressibility and hydraulic conductivity, the infinitesimal strain theory using nonlinear consolidation properties, and the conventional theory with 3.62 m^2/s of the coefficient of compressibility. The comparisons led to the conclusions that conventional consolidation theory is an over-predictor of the settlement times and nonlinear finite strain theory offers a consistent, potentially more accurate alternative. The results also show that the rate of settlement is substantially faster than the rate of dissipation of excess porewater pressure.

In general, the consideration of the consolidation of deposited tailings is based on the assumption that the consolidating medium is fully saturated with an incompressible viscous fluid (Schiffman et al. 1988). Most consolidation models applied to tailings are based on the one-dimensional nonlinear finite strain theory (Gibson et al. 1967).

Fredlund and Hasan (1979) presented two partial differential equations that could be solved for the pore-air and pore-water pressures during the consolidation process of an unsaturated soil. The water flow was governed by Darcy's law, while the air flow was governed by Fick's law. The coefficients of permeability with respect to both the water and air phases were considered to be a function of matric suction or one of the volume-mass properties of the soil. The two partial differential governing equations for consolidation of the unsaturated soil are as follows (Fredlund and Rahardjo 1993):

For the water phase:

$$[2\text{-}17]\quad m_2^w \frac{\partial u_w}{\partial t} = -\left(m_{1k}^w - m_2^w\right)\frac{\partial u_a}{\partial t} + \frac{k_w}{\gamma_w}\frac{\partial^2 u_w}{\partial y^2} + \frac{1}{\gamma_w}\frac{\partial k_w}{\partial y}\frac{\partial u_w}{\partial y} + \frac{\partial k_w}{\partial y}$$

where m_2^w is the coefficient of water volume change with respect to a change in matric suction, $d(u_a\text{-}u_w)$, during K_0-loading, u_w is the pore-water pressure, t is the time, m_{1k}^w is the coefficient of water volume change with respect to a change in the net normal stress, $d(\sigma_y\text{-}u_a)$, during K_0-loading, u_a is the pore-air pressure, k_w is the coefficient of permeability with respect to water as a function of matric suction, which varies with location in the y-direction, and y is the vertical coordinate (height).

For the air phase:

[2-18]

$$-\left[m_{1k}^{a}-m_{2}^{a}-\frac{(1-S)n}{u_{ab}}\right]\frac{\partial u_{a}}{\partial t}=m_{2}^{a}\frac{\partial u_{w}}{\partial t}-\frac{D_{a}^{*}}{(\omega_{a}/RT)u_{ab}}\frac{\partial^{2}u_{a}}{\partial y^{2}}-\frac{1}{(\omega_{a}/RT)u_{ab}}\frac{\partial D_{a}^{*}}{\partial y}\frac{\partial u_{a}}{\partial y}$$

where m_2^a is the coefficient of air volume change with respect to a change in matric suction, $d(u_a-u_w)$, during K_0-loading, m_{1k}^w is the coefficient of air volume change with respect to a change in the net normal stress, $d(\sigma_y-u_a)$, during K_0-loading, S is the degree of saturation, n is the porosity, u_{ab} is the absolute pore-air pressure, i.e. $u_{ab} = u_a + u_{atm}$, u_a is the gauge pore-air pressure, u_{atm} is the atmospheric pressure, i.e. u_{atm} = 101 kPa, D_a^* is the coefficient of transmission for the air phase, which is a function of the volume-mass properties or matric suction of the soil. Therefore, it can vary with location in the y-direction, ω_a is the molecular mass of air (kg/kmol), R is the universal (molar) gas constant, i.e. R = 8.31432 J/(mol·K), and T is the absolute temperature, i.e. T = t + 273.16 (K).

2.6 DESICCATION OF TAILINGS

Desiccation due to surface drying and lowering of the groundwater level is an important phase in sub-aerial tailings deposition. Desiccation may considerably reduce the void ratio of the deposited slurry materials and increase the solids storage capacity of the impoundment (Blight 1988).

An important property of the desiccated soil is the water retention characteristics. The main processes affecting desiccation are evaporation, shrinkage, and the formation of desiccation cracks at the surface of the tailings deposit.

2.6.1 Water retention characteristics

The water retention characteristic of a soil is a measure of the ability of a soil to hold water within its pores. The soil-water characteristic curve defines the relationship between the amount of water in the soil and suction applied to the soil. The amount of water can be either a gravimetric water content, *w*, a volumetric water content, θ, or degree of saturation, S. Typical soil-water characteristic curves for a drying and wetting cycle are shown in Figure 2.5.

When using the soil-water characteristic curve in a model, it is convenient to express the soil-water characteristic curve in mathematical form. Many empirical equations have been proposed to simulate the soil-water characteristic curve. Brooks and Corey (1964) proposed a power-law relationship as follows:

$$[2\text{-}19] \quad \frac{\theta-\theta_r}{\theta_s-\theta_r}=\left(\frac{\psi}{\psi_b}\right)^{\lambda}$$

where θ is the volumetric water content, θ_r is the residual volumetric water content, θ_s is the saturated volumetric water content, ψ is the suction, ψ_b is the air-entry value, and λ is the pore-size distribution index.

Campbell (1974) proposed a simpler form as follows:

$$[2\text{-}20] \quad \frac{\theta}{\theta_s}=\left(\frac{\psi_b}{\psi}\right)^{\frac{1}{b_0}}$$

where b_0 is a constant.

Van Genuchten (1980) proposed another frequently used form for the relationship between suction and water content:

[2-21] $$\frac{\theta-\theta_r}{\theta_s-\theta_r}=\left[\frac{1}{1+(\alpha_2\psi)^{n_2}}\right]^{m_2}$$

where α_2, m_2, and n_2 are soil parameters.

Fredlund and Xing (1994) proposed a general equation describing the soil-water characteristic curve over the entire range of matric suction as follows:

[2-22] $$\theta=\theta_s\left[1-\frac{\ln\left(1+\frac{\psi}{\psi_r}\right)}{\ln\left(1+\frac{10^6}{\psi_r}\right)}\right]\left\{\frac{1}{\ln\left[e+\left(\frac{\psi}{a_0}\right)^Q\right]}\right\}^P$$

where e is the natural number, 2.718 28, a_0 is a soil parameter that is related to the air-entry value of the soil, Q is a parameter that controls the slope at the inflection point in the soil-water characteristic curve, P is a parameter that is related to the residual water content, ψ is the matric suction of the soil, and ψ_r is the residual matric suction of the soil.

Equation [2-22] can be expressed in terms of the matric suction of the soil as:

[2-23] $$\theta=\theta_s\left\{1-\frac{\ln\left[1+\frac{(u_a-u_w)}{(u_a-u_w)_r}\right]}{\ln\left[1+\frac{10^6}{(u_a-u_w)_r}\right]}\right\}\left\{\frac{1}{\ln\left[e+\left(\frac{(u_a-u_w)}{a_0}\right)^Q\right]}\right\}^P$$

where $(u_a - u_w)_r$ is the matric suction corresponding to the residual water content, θ_r.

For mine tailings, Aubertin et al. (1998) proposed a modified Kovács Model (MK) to describe the tailings-water curve as follows:

$$[2\text{-}24]\quad \theta = \theta_s\left[S_c + S_a(1 - S_c)\right]$$

with

$$[2\text{-}24a]\quad S_c = 1 - \left[\left(\frac{0.4}{eD_{10}\Psi}\right)^2 + 1\right]\exp\left[-m\left(\frac{0.4}{eD_{10}\Psi}\right)^2\right]$$

with

$$[2\text{-}24b]\quad S_a = \frac{a}{e^{1/3}\Psi^{1/6}}\left(\frac{0.4}{eD_{10}}\right)^{2/3}\left[1 - \frac{\ln\left(1 + \frac{\Psi}{\Psi_r}\right)}{\ln\left(1 + \frac{\Psi_0}{\Psi_r}\right)}\right]$$

where e is the void ratio, D_{10} is the diameter for which 10% of the tailings by weight passed the sieve having an opening size D (in mm), ψ is the matric suction (in cm water), m and a are material parameters, ψ_0 equals to 10^7 cm water, and ψ_r is the suction corresponding to the residual water content of the tailings.

2.6.2 Evaporation

Surface drying of deposited tailings is caused by evaporation at a rate that depends on the varying climatic conditions at a site. Numerous empirical equations have been proposed to predict the evaporation rate. The most commonly used methods in engineering practice include the Thornthwaite Method, the Penman Method, the Priestley-Taylor Method, and the complementary relationship proposed by Wilson (1990).

Each method has advantages and disadvantages. Rosenberg et al. (1983) reported that the Penman Method has become the most popular and widely used combination model for estimating potential evaporation, ETp. The primary advantage of the Penman Method is that only weather parameters which are routinely measuring daily such as air temperature, relative humidity, and wind speed are required.

The equation presented by Penman (1948) for calculating potential evaporation rates is as follows:

$$[2\text{-}25] \quad E_P = \frac{\Gamma Q_0 + \nu_0 E_a}{\Gamma + \nu_0}$$

$$[2\text{-}25a] \quad E_a = f(u)(P_{sa} - P_{va})$$

$$[2\text{-}25b] \quad f(u) = 0.35(1 + U_a(9.8x10^{-3}))$$

where E is the potential evaporation per unit time in mm/day, P_{sa} is the saturation vapor pressure of the mean air temperature in mm·Hg, P_{va} is the vapor pressure of the air above the evaporation surface in mm of Hg, U_a is the wind speed, usually in miles/day, Q_0 is the heat budget or net radiation ('Q_n'), Γ is the slope of the saturation vapor pressure versus temperature curve at the mean temperature of the air, and ν_0 is a psychromatic constant.

A heat budget may be determined by an empirical formula given by Penman (1948):

$$[2\text{-}26] \quad Q = R_c(1-r_f) - \tau_{SB}T_a^4(0.56-0.092\sqrt{P_{va}})(0.10 + 0.9n/N)$$

$$[2\text{-}26a] \quad R_c = 0.95R_a(0.18 + 0.55n/N)$$

where R_c is the shortwave radiation measured at the site, R_a is the solar radiation (from charts) for a completely transparent atmosphere, r_f is the reflectance coefficient, τ_{SB} is the

Stefan-Boltzman constant, T_a is the air temperature, and n/N is the ratio of actual to possible sunshine hours.

Wilson (1990) proposed a modified Penman approach for calculating the potential evaporation on the basis of net radiation, wind speed, and the relative humidity of the air and the soil surface:

[2-27] $$E = \frac{\Gamma Q_0 + v_0 E_a}{(\Gamma + \frac{v_0}{h_{rs}})}$$

[2-27a] $$E_a = f(u) P_{va} (1/h_{ra} - 1/h_{rs})$$

where h_{rs} is the relative humidity at the soil surface and h_{ra} is the relative humidity of the air.

Chow et al. (1988) proposed an aerodynamic method to estimate the potential evaporation rate as:

[2-28] $$E_p = B_a (P_{vs} - P_{va}) \qquad \text{(mm/day)}$$

where

[2-28a] $$B_a = \frac{0.102 U_a}{\left[\ln\left(\frac{z_2}{z_0}\right)\right]^2} \qquad \text{(mm/day.Pa)}$$

and

[2-28b] $$P_{vs} = 611 \exp\left(\frac{17.27 T_a}{237.3 + T_a}\right) \qquad \text{(Pa)}$$

and

[2-28c] $P_{va} = R_h P_{vs}$ (Pa)

where P_{vs} is the saturated vapor pressure, P_{va} is the actual vapor pressure, R_h is the relative humidity, T_a is the air temperature (°C), U_a is wind velocity (m/s) measured at height z_2 (cm), and z_0 is the roughness height of the surface, i.e. $z_0 = 0.01\text{-}0.06$ for a water surface, $z_0 = 0.001$ for an ice and a mud flat surface.

2.6.3 Shrinkage of soils

Clays consist of minerals such as kaolinite, illite, and montmorillonite. Clay minerals exist in crystals that are built up of small platelets that are surrounded by water films. Upon desiccation, the water escapes, and hence the platelets approach one another. This process causes shrinkage of soil aggregates. Therefore, some tailings also exhibit shrinkage behavior as they desiccate due to the presence of clay minerals.

The three main phases of soil shrinkage as a soil desiccates are normal, residual, and zero shrinkage (Bronswijk 1988) as illustrated in Figure 2.6. Haines (1923) and Keen (1931) presented definitions of these shrinkage phases in the following terms:

> *When the decrease in volume of the clay aggregates equals the loss of water, "normal shrinkage" takes place and the soil aggregates remain fully saturated.*
>
> *When the loss of water is greater than the decrease in volume of soil in drying, the "residual shrinkage" occurs and air enters the pore spaces within the aggregates.*

Finally, when the soil aggregates have reached their densest configuration, even continuously drying, the volume of aggregates remains constant, the loss of water equals the increase in air volume in the aggregates. This is called "zero shrinkage."

A shrinkage curve is usually used to describe the relationship between shrinkage and water content. In general, soils with high clay content show normal shrinkage over a wide range of moisture content while soils with low clay content show mostly residual shrinkage (Bronswijk 1988).

The amount of shrinkage depends on many factors such as the type and amount of clay minerals, the soil fabric arrangements, the initial water content, and the confining pressure (Mitchell 1976). The more plastic the soil, the larger the amount of shrinkage. The amount of shrinkage of illite is larger than that of kaolinite, but less than that of montmorillonite. A dispersed structure in a clay soil may experience more shrinkage than that of a flocculated structure (Mitchell 1976; Abu-Hejleh 1993).

2.6.4 Cracking of Soils due to Desiccation

Tension cracks are often observed in soils that undergo drying. In general, tension cracks in soils can be assumed to be the opening mode (Meguid 1989), i.e. the crack surfaces move directly apart as showing in Figure 2.7.

It is common to assume that desiccation cracking results from excessive tensile stresses that exceed the tensile strength of the soil. The shrinkage of soil results in the development of tensile stresses as it undergoes volume decrease.

Shrinkage cracks can be characterized by their depth, spacing, and aerial distribution. Lachenbruch (1961,1962) studied the development of shrinkage cracks in permafrost regions and presented a mathematical solution for crack depth and spacing. He identified the types of shrinkage crack polygons, namely orthogonal and non-orthogonal systems. To estimate the depth and spacing of tension cracks, we must give some thought to the entire problem of the initiation, propagation, and arresting of a tension crack in an extended medium (Irwin 1958; Lachenbruch 1961). Raats (1984) presented the deformation gradient tensor of the solid phase to describe the swelling and shrinkage of soils and reviewed two crack-slip failure criteria, i.e. the Coulomb's and Griffith's failure criterion and Irwin's and Lachenbruch's fracture theories.

2.6.4.1 Initiation of tension cracks

Tension cracks initiate where stresses exceed the tensile strength locally (Lachenbruch 1962). Abu-Hejleh (1993) studied the desiccation theory for soft cohesive soils and described two criteria for cracking initiation at any depth as follows:

Cracking Criterion I: as a condition for a crack to initiate at any depth, the suction developed due to desiccation, which applies tension at the crack tip, must exceed the lateral compressive stress under K_0 conditions due to the vertical stress on the soil at the elevation of the crack tip. This condition is expressed as:

$$[2\text{-}29] \quad -U = K_0\sigma'_v = K_0(\sigma_v + U)$$

where U is the value of suction, K_0 is the coefficient of earth pressure at rest, σ_v is the total vertical stress, and σ_v' is the effective vertical stress.

In this situation, the suction required to reduce the horizontal stress to zero, u_{cs}, is:

$$[2\text{-}30] \quad u_{cs} = \frac{K_0\sigma_v}{K_0 - 1}$$

Cracking Criterion II: the crack at any depth in the soil initiates once the developed lateral total tensile stress (σ_h) reaches the tensile strength (σ_t) or once the developed mechanical lateral tensile strain (ε_{ml}) reaches the tensile strain at failure (ε_t). This criterion is expressed by:

[2-31] $-\sigma_h = \sigma_t$

or

[2-32] $-\varepsilon_{ml}(e_{vc}, e_{cs}) = \varepsilon_t$

2.6.4.2 Propagation, depth and spacing of tension cracks

To describe the propagation of an extension crack, a special parameter, κ, called crack-edge stress-intensity-factor, was presented by Irwin (1958). The parameter κ depends on the length of the crack and the stress distribution within the material. For a long tension crack in an ideally elastic material, κ can be calculated as follows (Irwin 1958):

[2-33] $$\kappa = \left[\frac{E_m G_E}{\pi(1-\nu^2)}\right]^{\frac{1}{2}}$$

where κ is the crack-edge intensity factor, E_m is Young's modulus in MPa, G_E is the rate of release of strain energy with crack extension or the so called "crack extension force," and ν is Poisson's ratio.

Under applied tension, small flaws grow slowly as a result of plastic deformation. The crack-extension force G generally increases with the length of the flaw so that ultimately a critical value, G_c (characteristic of the material), is reached at which the rate of release of strain energy with crack extension exceeds the rate of plastic dissipation. At this point, unstable fast propagating fractures begin. The value G_c is, therefore, a measure of fracture resistance: it is large for ductile and small for brittle materials (Irwin 1958; Lachenbruch 1962). Therefore, Irwin's criterion for initiation of a fast fracture, i.e. propagation of a crack, can be expressed as:

[2-34] $\kappa = \kappa_c > 0$

where κ_c is the critical stress intensity factor or fracture toughness in $kN/m^{1.5}$. It can be obtained from equation [2-33] with G_c (Lachenbruch 1961).

The critical stress intensity factor can also be determined using the following formula (Lawn and Wilshaw 1975; Morris et al. 1992):

[2-35] $$\kappa_c = -\frac{2\zeta E_m}{1-\nu^2}$$

where ζ is the specific surface energy of the soil (Lee and Ingles (1968) suggested that ζ lies between 0.1 and 1.0 J/m^2), E_m is Young's modulus in MPa and ν is Poisson's ratio.

κ_c is considered to be independent of crack geometry and loading and may be regarded as an intrinsic material constant (Sih 1973).

Corresponding to G_c, Lachenbruch (1962) assumed that there exists a critical value, G_0, for "crack arresting". Thus, a tension crack continues to propagate until the crack-extension force falls below G_0. Therefore, the criterion for crack arresting can be expressed as:

[2-36] $\kappa = \kappa_0 < 0$

Consider a simple case of a semi-infinite solid in which the stress is represented by a uniform tension A to some depth a, the crack depth b and a superimposed gravitational compression $-\gamma gz$, (here γ and g represent density and gravitational acceleration, respectively and z is depth). When a is not larger than b, the stress-intensity-factor κ can be expressed as (Lachenbruch 1961; Konrad et al. 1997):

[2-37] $\kappa = \lambda\sigma(b)^{0.5}$

where σ is the maximum value of the tensile stress, b is the crack depth, and λ is a coefficient depending on the tensile stress distribution and the ratio (a/b) (Table 2.1).

Lachenbruch (1961) stated that the crack depth (b) could be calculated implicitly by

[2-38] $\kappa_U(b) + \kappa_g(b) = \kappa_c$

where $\kappa_U(b)$ represents the contribution of the uniform tension to the intensity factor and $\kappa_g(b)$ represents the contribution to $\kappa(b)$ of the weight of the column of height, b:

[2-39] $\kappa_U(b) = \lambda A\sqrt{b}$

[2-40] $\kappa_g(b) = -0.68\gamma g\sqrt{b^3}$

Based on the assumption that the coefficient of earth pressure at rest, K_0, is zero at the bottom of a crack, Fredlund and Rahardjo (1993) proposed an expression for the depth of cracking, b:

[2-41] $$b = \frac{D_w}{1 + \frac{\nu \rho H_m}{f_w \rho_w E_m}}$$

where D_w is the distance from the ground surface to the water table, ν is Poisson's ratio of the soil, ρ is the total density of the soil, ρ_w is the density of water, H_m is the elastic modulus with respect to a change in $(u_a\text{-}u_w)$, E_m is the elastic modulus with respect to a change in $(\sigma - u_a)$, and f_w is the ratio of pore water pressure to the hydrostatic pressure.

In slope stability analysis, based on Rankine's theory of earth pressure in an infinite half space, Chowdhury (1978) proposed the following formula for estimating the depth of the tension crack, b:

[2-42] $$b = \frac{2c_m}{\gamma} \tan(45 + \frac{\phi_m}{2})$$

where $c_m = c/F$ is the mobilized cohesion, $\phi_m = \arctan(\tan\phi/F)$ is the mobilized friction angle, F is the factor of safety, and γ is the unit weight of the soil.

After a crack has reached its ultimate depth b, the tensile stresses in its vicinity will be reduced. In other words, when the crack forms, the horizontal stresses on the crack walls vanish. Hence, this creates a stress relief zone that extends to a certain distance from the crack. Within the stress relief zone, stresses are reduced below the tensile strength of the soil (σ_t), and no further cracking can occur at the time of the crack initiation. Beyond this zone, the tensile stress near the surface is close to σ_t, allowing other cracks to open and propagate. Therefore, the spacing of the cracks is controlled by the horizontal stress relief at the surface. Lachenbruch (1961, 1962) proposed that the spacing of the cracks can be estimated from the theoretical stress relief field by assuming that another crack may exist at points between about 5% and 10% of the stress relief. Lachenbruch's theoretical stress relief zones are presented in Figure 2.8.

2.6.4.3 Width of tension cracks

Little has been published in the literature about the estimation of the width of desiccation cracks. Penev and Kawamura (1993) have described a simplified method to estimate the width of cracks caused by restrained shrinkage in a pavement slab made with cement-treated materials. Shrinkage cracking was considered as a time-dependent process that was divided into three stages: the initiation of a crack, its slow growth and final failure. Consequently, the width of the crack at the time of the failure (υ'_c) is determined by the width of crack at the time of crack initiation (υ_c), which was equal to the difference between the contraction of the slab due to free shrinkage and the elongation caused by the stress $\sigma(x,t)$ including creep strain, the critical crack tip opening (Ω_c), and the additional crack width ($\Delta\upsilon_c$) that is equal to the difference between the free shrinkage displacement and the elongation of uncracked portions of the slab. The calculated final crack widths (0.74 and 1.33 mm) were found to be in good agreement with the in-situ measured results (0.5 to 2.5 mm).

2.7 HYDRAULIC CONDUCTIVITY OF TAILINGS

Hydraulic conductivity is one of the most intriguing properties of soils that soil scientists and geotechnical engineers must understand. The change in the hydraulic conductivity can vary over a range of several orders of magnitude (Cedergren 1989). Hydraulic conductivity depends on the characteristics of both the water and the soil. Viscosity, unit weight, and polarity are the major water characteristics that influence hydraulic conductivity, while particle size, void ratio, composition, fabric, and degree of saturation are among the major soil characteristics that affect hydraulic conductivity (Lambe and Whitman 1968).

2.7.1 Saturated Hydraulic Conductivity

Abadjiev (1976, 1985) and Blight (1987) proposed the following formula to calculate the change of the saturated hydraulic conductivity of the tailings along the beach of a tailings impoundment:

[2-43] $k = a_s e^{b_s H}$

where a_s and b_s are characteristic constants of the beach, H is the distance along the beach from the deposition point, and *e* is the natural number, i.e. *e* = 2.718 28.

A segregating deposition produces a particle size variation along the beach, i.e. due to the segregating deposition, the larger particles settle near the discharge point and the smaller particles settle farther along the beach. Thus, the hydraulic conductivity is higher near the discharge point and decreases with distance from the discharge point. Equation [2-43] expresses this trend.

Since void ratio e versus log k is close to a straight line (Lambe and Whitman 1968), the following empirical equation was used to express the relationship between void ratio and hydraulic conductivity (Swarbrick 1992):

[2-44] $e = a_5 + b_5 \log(k)$

where e is the void ratio, k is the hydraulic conductivity, and a_5 and b_5 are the parameters.

Somogyi (1979), Abu-Hejleh (1993) and Qiu and Sego (1998c) proposed an exponential relationship between void ratio and hydraulic conductivity

[2-45] $k = a_2 e^{b_2}$

where k is the saturated hydraulic conductivity, e is the void ratio, and a_2 and b_2 are soil parameters. Abu-Hejleh (1993) used Equation [2-45] to calculate the hydraulic conductivity.

Aubertin et al. (1996) proposed a modified version of the Kozeny-Carman equation to predict the hydraulic conductivity of homogenized tailings from hard rock mines:

$$[2\text{-}46] \quad k = C_k \frac{\gamma_w}{\mu} D_{10}^2 C_U^{1/3} \frac{e^{3+X_k}}{(1+e)}$$

where C_k is a coefficient, γ_w is the unit weight of the water, μ is the fluid viscosity ($\mu \approx 9.8 \times 10^{-6}$ N·s/cm^2 for water at 20°C), D_{10} is the sieve of size that 10% of the tailings passes through, C_U is the coefficient of uniformity, e is the void ratio, and X_k is a material parameter.

2.7.2 Unsaturated Hydraulic Conductivity

During desiccation, the hydraulic conductivity of a soil decreases as the soil desaturates. The hydraulic conductivity, k, of an unsaturated soil depends not only on void ratio, but also on the volumetric water content, θ, which in turn depends upon the suction ψ within the soil. Numerous empirical or semi-empirical equations have been proposed to predict the unsaturated hydraulic conductivity as a function of matric suction within the soil.

Van Genuchten (1980) proposed a closed-form equation for predicting the hydraulic conductivity of unsaturated soils as follows:

$$[2\text{-}47] \quad k_r(\theta) = \frac{k(\theta)}{k_s} = \left(\frac{\theta - \theta_r}{\theta_s - \theta_r}\right)^{1/2} \left\{1 - \left[1 - \left(\frac{\theta - \theta_r}{\theta_s - \theta_r}\right)^{1/m_3}\right]^{m_3}\right\}^2$$

where $k_r(\theta)$ is the relative hydraulic conductivity at any water content, $k(\theta)$ is the hydraulic conductivity at any water content, k_s is the saturated hydraulic conductivity, θ is the volumetric water content, θ_s is the saturated volumetric water content, θ_r is the residual volumetric water content, and m_3 is a material parameter ($0 < m_3 < 1$).

Or

$$[2\text{-}48] \quad k_r(h) = \frac{k(h)}{k_s} = \frac{\left\{1-\left(\frac{h}{h_b}\right)^{n_3-1}\left[1+\left(\frac{h}{h_b}\right)^{n_3}\right]^{-m_3}\right\}^2}{\left[1+\left(\frac{h}{h_b}\right)^{n_3}\right]^{m_3/2}}$$

$$[2\text{-}48a] \quad m_3 = 1-\frac{1}{n_3}$$

where $k_r(h)$ is the relative hydraulic conductivity at any pressure head (h), $k(h)$ is the hydraulic conductivity at any pressure head, k_s is the saturated hydraulic conductivity, h is the pressure head, h_b is the air-entry value in terms of the water pressure head, and m_3 and n_3 are the material parameters.

Fredlund et al. (1994) reviewed the hydraulic conductivity functions of unsaturated soils and concluded that there are two approaches to obtain the functions: (i) empirical equations and (ii) statistical models. Table 2.2 shows the empirical equations for the unsaturated hydraulic conductivity $k(\theta)$ and $k(\psi)$ reported in the literature.

Based on the model proposed by Childs and Collis-George (1950) and modified by Marshall (1958) and Kunze et al. (1968), and combining Equation [2-22], Fredlund et al. (1994) proposed a hydraulic conductivity function for unsaturated soils. Its relative hydraulic conductivity form is expressed as follows:

$$[2\text{-}49] \qquad k_r(\theta) = \frac{k(\theta)}{k_s} = \int_{\theta_r}^{\theta} \frac{\theta - x}{\psi^2(x)} dx \bigg/ \int_{\theta_r}^{\theta_s} \frac{\theta_s - x}{\psi^2(x)} dx$$

where $k_r(\theta)$ is the relative hydraulic conductivity at any water content, $k(\theta)$ is the hydraulic conductivity at any water content, k_s is the saturated hydraulic conductivity, ψ is soil suction (kPa) given as a function of volumetric water content θ, x is a dummy variable of integration representing water content, θ_s is the saturated volumetric water content, and θ_r is the residual volumetric water content. Figure 2.5 aids in illustrating the values of θ from the typical water-soil characteristic curve.

The conventional procedure for predicting hydraulic conductivity using [2-49] consists of two steps (Fredlund et al. 1994). First, the residual water content of the soil under consideration is estimated from the experimental data. Then the measured soil-water characteristic data are fitted by a mathematical equation over the interval from θ_r to θ_s, and the integration is evaluated using the best-fitting curve. Since there is no generally accepted procedure for determining the residual water content, it would be meaningful to predict the hydraulic conductivity without having to first estimate the residual water content.

To perform the integration along the soil suction axis, Equation [2-49] can be transferred into the following form:

$$[2\text{-}50] \qquad k_r(\psi) = \int_{\ln(\psi)}^{b} \frac{\theta(e^y) - \theta(\psi)}{e^y} \theta'(e^y) dy \bigg/ \int_{\ln(\psi_{aev})}^{b} \frac{\theta(e^y) - \theta_s}{e^y} \theta'(e^y) dy$$

where b equals $\ln(10^6)$, y is a dummy variable of integration representing the logarithm of suction, and ψ_{aev} is the air-entry value of the soil under consideration, which can be estimated from the water-soil characteristic curve as shown in Figure 2.5.

Through the use of equation [2-48] and [2-50], the hydraulic conductivity can be predicted without requiring a prior evaluation of the residual water content of the material under consideration.

2.7.3 Effect of Tension Cracks

The network of tension cracks controls the hydraulic conductivity of the soil mass, and the hydraulic conductivity is much greater than that of the intact soil. Extensive research in the field of rock mechanics has concluded that the bulk hydraulic conductivity of any fractured medium depends strongly upon both the opening and spacing of the fractures (Konrad et al. 1997). If there is no infill of the cracks, the coefficient of the hydraulic conductivity of the cracked layer can be expressed as (Lee et al. 1983):

[2-51] $$k_c = \frac{\upsilon^3 g}{12 v_1 B}$$

where k_c is the coefficient of the hydraulic conductivity of the cracked layer (m/sec), υ is the width of the cracks (m), B is the spacing of the cracks (m), g is the gravitational constant (9.81 m/sec^2), v_l is the kinematic viscosity of water = η/ρ_w, η is the viscosity of water (10^{-6} kPa·sec at 20°C), and ρ_w is the density of water (Mg/m^3).

Figure 2.9 shows the comparisons between the cracked hydraulic conductivity and the intact hydraulic conductivity for the saturated coal tailings after 100 kPa consolidation. The plot indicates that the hydraulic conductivity of the coal tailings with a crack width larger than 0.02 mm and spacing smaller than 1000 mm will be larger than its saturated hydraulic conductivity after 100 kPa consolidation. In other words, with the desiccation cracks, the hydraulic conductivity of the tailings increases dramatically.

2.8 STRENGTH OF AN UNSATURATED SOIL

2.8.1 Shear Strength

A knowledge of the shear strength of tailings is required for analysis of the stability of tailings disposal facilities. Tailings deposited by the sub-aerial deposition technique are often unsaturated. Traditionally, the saturated shear strength is commonly used in engineering practice to evaluate the stability of partially saturated soils. However, this approach is conservative due to its neglect of the soil suction which enhances the resistance of a partially saturated material.

Fredlund et al. (1995) proposed a nonlinear model to predict the shear strength of an unsaturated soil using the soil-water characteristic curve and the saturated shear strength parameters. It is proposed that the shear strength for an unsaturated soil consists of two parts, i.e., the saturated shear strength and the shear strength contribution due to suction as follows:

[2-52] $\tau = c' + (\sigma_n - u_a)\tan\phi' + \tau_{us}$

[2-52a] $\Theta = \dfrac{\theta - \theta_r}{\theta_s - \theta_r}$

[2-52b] $\tau_{us} = (u_a - u_w)\Theta^{\kappa_1}\tan\phi'$

where Θ is the normalized volumetric water content, τ_{us} is the shear strength contribution due to suction, κ_1 is a fitting parameter which ranges from 1.0 to 4.8, σ_n is the total normal stress on the plane of failure, and u_a and u_w are the pore-air and pore-water pressure respectively.

The value of κ_1 generally increases with the plasticity of the soil. The first part of equation [2-52] represents the saturated shear strength, and c' and ϕ' are generally constant for a saturated soil. τ_{us} can be predicted using the soil-water characteristic curve for the material being studied.

2.8.2 Tensile Strength

Tensile strength is important in determining the initiation of a tensile crack that may form in soils. Cracking can be assumed to occur when the horizontal stress at the tip of a crack is greater than the tensile strength of the soil (Morris et al. 1992). Snyder and Miller (1985) proposed that a parameter, χ_1 used to estimate tensile strength as a function of pore water pressure can be expressed as a function of the degree of saturation. They also pointed out that once air intrusion has initiated desaturation, the maximum tensile strength which can be expected is about half the gauge pressure of the pore water. Nearing et al. (1988) suggested a linear relationship between tensile strength and suction. Lau (1987) suggested that tensile strength was related to the unconfined compressive strength by a factor F_t as follows:

$$[2\text{-}53] \quad \sigma_t = F_t \cdot C_0$$

where σ_t is the tensile strength and C_0 is the unconfined compressive strength. F_t varies from 1/13 to 1/3 for soils (Lau 1987).

Morris et al. (1992) used the following equation to calculate the tensile strength in their study on cracking in soils as they dried:

$$[2\text{-}54] \quad \sigma_t = 0.5\left[c' + (u_a - u_w)\tan\phi^b\right]$$

where σ_t is the tensile strength, c' is the effective cohesion, $(u_a\text{-}u_w)$ is the matric suction, ϕ^b is the friction angle with respect to the matric suction ($\phi^b = \phi' -5°$, a broad interpretation of data presented by Fredlund et al. (1978)), and ϕ' is the effective friction angle of the material obtained by testing the soil under saturated condition.

However, the usual range of angle ϕ^b is between 12 and 23 degree (Fredlund 1985; Lau 1987).

Based on the relationship between the tensile strength and unconfined compressive strength proposed by Lau (1987), and an empirical relationship between the undrained shear strength and void ratio, Abu-Hejleh (1993) adopted a linear relationship between the tensile strength and the undrained shear strength. Consequently, an exponential relationship between the tensile strength and the void ratio was obtained as follows:

[2-55] $$\sigma_t = F_1 \cdot 10^{(T_1 - e)/T_2}$$

where σ_t is the tensile strength and F_1, T_1, and T_2 are all material parameters. For a soft Speswhite China clay, T_1=1.945, T_2=0.435, and F_1 = 0 or 0.5 (Abu-Hejleh 1993).

2.9 REVIEW OF EXISTING MODEL ON SOIL DESICCATION

Several theoretical models have been published in the soil science and geotechnical literature for modeling soils as they undergo desiccation.

Lau (1987) studied desiccation cracking of soils. In order to quantify the matric suction at a given depth in any mathematical analysis, he proposed two idealized matric suction profiles. Profile "A" represents a linear matric suction relationship with depth, i.e. matric suction at depth d is

[2-56] $$(u_a - u_w)_d = F_w \gamma_w (D_w - d)$$

where $(u_a - u_w)_d$ is the matric suction at depth(d) above ground water table, F_w is a constant, γ_w is the unit weight of the water, D_w is the depth of the ground water table, and d is the depth of any point above ground water table.

Profile "B" represents constant matric suction with depth, i.e. matric suction at depth, d, is:

$$[2\text{-}57] \quad (u_a - u_b)_d = F_w \gamma_w D_w$$

A mathematical model for the prediction of desiccation crack depth was proposed. The model consists of two mathematical expressions which were derived using the volume change (i.e., elastic equilibrium analysis) and shear strength (i.e. plastic equilibrium analysis) behavior of unsaturated soils for the prediction of the crack depth.

Using elastic equilibrium analysis and assuming that the allowable tensile strain is equal to zero, the following expressions were obtained:

$$[2\text{-}58] \quad b = \frac{D_w}{1 + \frac{\nu}{F_w} \frac{\gamma}{\gamma_w} \frac{1}{(E_m / H_m)}} \qquad \text{(For the matric suction profile "A")}$$

and

$$[2\text{-}59] \quad b = \frac{D_w}{\frac{\nu}{F_w} \frac{\gamma}{\gamma_w} \frac{1}{(E_m / H_m)}} \qquad \text{(For the matric suction profile "B")}$$

where b is the crack depth, D_w is the depth of the ground water table, F_w is the matric suction profile factor, ν is Poisson's ratio (the normal range is between 0.2 and 0.5 for most soils), γ is the total unit weight of the soil, γ_w is the total unit weight of water, E_m is the elastic modulus with respect to total stress $(\sigma - u_a)$, and H_m is the elastic modulus with respect to matric suction (u_a - u_w). The theoretical E_m/H_m ratio has a range between 0 to 1/3.

Using plastic equilibrium analysis, the following expressions were obtained:

[2-60] $$b = \frac{\frac{c'}{\gamma_w} + F_w D_w \tan\phi^b}{X + F_w \tan\phi^b}$$ (For the matric suction profile"A")

with

[2-60a] $$X = \frac{\frac{\gamma}{\gamma_w}(1 - \sin\phi')^2}{2\cos\phi'[(1 - F_t) - (1 + F_t)\sin\phi']}$$

and

[2-61] $$b = \frac{2(c' + F_w D_w \gamma_w \tan\phi^b)Y}{\gamma}$$ (For the matric suction profile"B")

with

[2-61a] $$Y = \frac{\cos\phi'}{(1 - \sin\phi')}\left[1 - F_t - \frac{2F_t \sin\phi'}{(1 - \sin\phi')}\right]$$

where b is the depth of crack, c' is the cohesion intercept when total stress and matric suction are equal to zero, ϕ' is the friction angle with respect to (σ - u_a), ϕ^b is the friction angle with respect to (u_a - u_b), F_t is the ratio of tensile strength and unconfined compressive strength, F_w is the matric suction profile factor, γ is the total unit weight of soils, and γ_w is the total unit weight of water.

Lau (1987) concluded that the theoretical crack depth predicted by the elastic equilibrium analysis is a function of matric suction profile, the ratio of the elastic moduli E_m and H_m, Poisson's ratio, the tensile strain-at-failure, and the unit weight of the soils. The theoretical crack depth predicted by the plastic equilibrium analysis is a function of the matric suction profile, the tensile strength of soils, the effective cohesion intercept c', the effective friction angle ϕ' and ϕ^b, and the unit weight of soils. Based on laboratory test results, he found that the desiccation cracks are initiated at a matric suction of less than 10 kPa for most soil types. The matric suction at cracking for silty soils appears to be higher than that for clayey soils. He finally pointed out that the crack depth predicted by the plastic analysis was almost twice as deep as that predicted by the elastic analysis. Since desiccation cracks are formed as a result of soil volume reduction, the elastic analysis is expected to be more appropriate for the prediction of crack depth.

Bronswijk (1988, 1989, 1990, and 1991) studied shrinkage, displacement, and cracking of a clay under desiccation and developed theoretical relationships between the vertical soil movements and water-content changes in clays as they undergo desiccation. Bronswijk (1990) concluded that in-situ shrinkage occurring in Bruchem heavy clay soil could be isotropic. Therefore, the measured one-dimensional surface subsidence of the soil was converted into a three-dimensional decrease in soil matrix volume and into crack volume by using the following equations (Bronswijk 1989, 1991):

[2-62] $\Delta V = \{1-(1-\Delta Z/Z)^3\}V$

and

[2-63] $V_{cr} = \Delta V - Z^2\Delta Z$

where V is the volume of soil matrix at saturation (m^3), Z is the layer thickness of soil matrix at saturation (m), ΔV is the decrease in volume of soil matrix as a result of shrinkage (positive) (m^3), ΔZ is the decrease in layer thickness as a result of shrinkage (positive) (m), and V_{cr} is the change in the crack volume (m^3).

However, the conversion of the vertical settlement into a three-dimensional volume change and crack volume requires knowledge of the size of the soil element subjected to shrinkage. As pointed out by Browswijk (1988), choosing a dimension of the soil element that is too large causes an overestimation of the three-dimensional volume change and of crack volume. On the other hand, these equations are only valid if the crack spacing is known. Therefore, the model can not be used to predict the spacing of the cracks.

Lee et al. (1988) proposed a finite-element model of crack propagation in brittle soils that simulated the physical separation of a material on either side of the crack. In this model, a single node was split into two distinct nodes in the wake of an advancing crack tip to replicate separation of the material on either side of the crack, and the linear elastic fracture mechanics (LEFM) was used to predict the crack propagation. In their sample modeling, the tensile strength (σ_t) of 19 kN/m^2 and fracture toughness (κ_c) of 12.7 kN/m$^{3/2}$ were used for the stiff embankment material. The predicted crack length was in good agreement with the laboratory measured results.

Swarbrick (1992) studied the desiccating behavior of mine tailings. Based on equilibrium and continuity of the tailings and Darcy's Law, a uniform theoretical framework to account for sedimentation, consolidation and desiccation of the tailings was proposed. A semi-empirical model for predicting the desiccation behavior was developed. Both the laboratory and field experiments were carried out and used to validate the model. In his model, however, the effect of desiccation crack was not considered.

Morris et al. (1992) reviewed the occurrence and morphology of cracks in the dry-climate regions of Australia and Canada and developed theoretical relationships between the depth of cracks, the properties of the soil, and a given suction profile. Their solutions were developed based on: (I) linear elasticity, (II) linear elastic fracture mechanics (LEFM), and (III) cracking related to shearing failure. In their analyses, they assumed that the distributions of suction with the depth were either constant or decrease linearly with depth, and the effective cohesion c′ was set to zero.

Abu-Hejleh and Znidarcic (1995) studied the desiccation theory for soft cohesive soils. They developed a new desiccation theory which provide a framework for the consolidation and desiccation analysis of soft fine-grained waste soils. The overall consolidation and desiccation process of soft soils is modeled with four consecutive segments, which correspond chronologically to the phases that a soft soil layer undergoes in the field after deposition. These phases are consolidation under one-dimensional compression, desiccation under one-dimensional shrinkage, propagation of desiccation vertical cracks with tensile stress release, and desiccation under three-dimensional shrinkage. A key element in their model is to consider the principle of effective stress in the slurry to relate total stress induced by a condition of zero lateral strain during shrinkage to the suction and the effective stress path followed by any soil element during consolidation. It was assumed that the soil starts cracking during one-dimensional shrinkage when the total lateral tensile stress at any point reaches the tensile strength of the soil. Furthermore, the analysis of crack propagation was performed by using the cracking function approach, which considers that the soil starts cracking at a given depth only when the soil void ratio, e, at this depth has decreased enough to reach the cracking void ratio, e_{cr}. Finally, volume change during the three-dimensional desiccation is calculated for a soil element with a unit initial area and a unit solid volume. Therefore, this approach can not predict the spacing between primary cracks at the onset of their formation. On the other hand, the sedimentation, stress concentration, and LEFM were not considered in the model.

Recently, Konrad and Ayad (1997) presented an idealized framework for the prediction of the spacing between primary shrinkage cracks in cohesive soils undergoing desiccation. Their approach used interactively three distinct known models in close association with the principle of effective stress to describe stress partitioning within the soil.

First, a one-dimensional mass transfer model enabling the determination of the suction profile with time for a given surface evaporation flux provides the input to determine the condition of crack initiation by using total and effective stress paths during desiccation. A crack occurs at the soil surface only when the total horizontal stress acting on the soil surface (σ_3) reaches the tensile strength of the soil (σ_t). At crack initiation, the negative pore-pressure acting on a soil element adjacent to the surface has thus reached a critical value referred to as ψ_{cr}. In the slurried waste soil disposal, assuming that K_{0nc} can be approximated by (1-sinϕ'), ψ_{cr} can be calculated as:

$$[2\text{-}64] \quad \psi_{cr} = \frac{\sigma_t}{\sin\phi'}$$

where ψ_{cr} is the critical value of suction at the initiation of a crack, σ_t is the tensile strength of the soil, and ϕ' is the effective friction angle of the soil.

Second, the LEFM theory was used to determine the ultimate depth of a crack under a given lateral stress field. According to the theory of LEFM, the ultimate crack depth depends upon the tensile stress distribution applied on the side of the crack and the value of the stress intensity factor, which changes with crack length. Furthermore, the lateral tensile stress profile at crack initiation depends on the initial state of stresses, the tensile strength of the soil, and suction profile at crack initiation. To estimate the depth of crack propagation at the time of initiation, it is necessary to calculate the stress intensity factor, κ, as a function of different crack lengths and determine the value of the crack length, b, for which κ is equal to the soil 's fracture toughness, κ_c. The crack length b was determined with a trapezoidal distribution of the total horizontal tensile stress as derived from the material constitutive equations in the following formula:

$$[2\text{-}65] \quad \lambda_1\sigma_t\sqrt{b} - \lambda_2\left[\sigma_t - \sigma_{3a}\right]\sqrt{b} = \kappa_c$$

where λ_1 and λ_2 are the coefficients for the uniform stress distribution and the triangular distribution respectively ($\lambda_1 = 1.12$ and $\lambda_2 = 0.68$ for $b \leq a$, when $b > a$, the values of λ can be found in Figure 2.10), b is the crack depth, a is the depth of the tensile stress zone, σ_t is the tensile strength of the soil, σ_{3a} is the tensile stress at the bottom of the trapezoidal distribution, and κ_c is the soil's fracture toughness.

Finally, the theory of linear elasticity was used to compute the stress redistribution around the crack for determining the extent of the stress relief zone, which, in turn, relates directly to the spacing of these primary cracks. In this stage, a fictitious stress superposition concept was used and stress reduction was calculated using the finite-element method by considering a linear elastic material. However, it was considered that another crack could exist when the predicted total horizontal stress on the surface reaches 95% of the tensile strength value.

Seneviratne et al. (1996) conducted numerical modeling of consolidation and evaporation of slurried mine tailings. Based on Gibson's large-strain consolidation theory, the following governing equation of self-weight consolidation in terms of the total pore pressure was obtained:

$$[2\text{-}66] \quad \frac{\partial}{\partial z}\left[\frac{k}{\gamma_w(1+e)}\frac{\partial p_t}{\partial z}\right]+\frac{\partial k}{\partial z}=\frac{de}{d\sigma'_v}\left[\frac{\partial \sigma_v}{\partial t}-\frac{\partial p_t}{\partial t}\right]$$

where z is the solids coordinate, k is the hydraulic conductivity, γ_w is the unit weight of the water, e is the void ratio, p_t is the total pore pressure, σ'_v is the effective vertical stress of the soil, and σ_v is the total vertical stress of the soil.

In this model, three types of bottom boundary conditions, i.e. completely permeable, completely impermeable, and partially permeable conditions were used. The pore pressure at the base was specified under the permeable conditions. Two top boundary conditions were adopted. First, the top boundary condition was a 'no evaporation' condition. It was assumed that the top boundary was free draining initially; in turn, a particular total pore pressure value was specified for the top boundary. Secondly, the top boundary condition was set as 'with evaporation.' Evaporation was modeled by specifying an evaporation potential (E_P), i.e. the evaporation rate measured using a Class A evaporation pan. When the air-entry value was reached, the boundary condition was then specified as a constant suction boundary until a new layer was deposited.

The model proposed by Seneviratne et al. (1996) was used to simulate the one-dimensional saturated consolidation of slurried gold mine tailings under a high evaporation rate. In this model, the sedimentation of slurried mine tailings was not modeled. The sedimentation void ratio was specified, and it was assumed that all freshly deposited layers reached the sedimentation void ratio instantaneously. Furthermore, the desiccation or unsaturated consolidation of the tailings was not considered. Consequently, the desiccation cracking of the tailings was not simulated.

2.10 SUMMARY AND CONCLUSIONS

The literature has been reviewed to investigate the previous work related to this thesis research. The information obtained from the review indicates that a comprehensive model for the evaluation of design of optimum deposition for sub-aerial tailings disposal in arid region with the intent of maximizing the amount of water available for recycling is not currently available. The following conclusions are also drawn from this review:

1. Surface drying has the effect of considerably reducing the void ratio of the deposited slurry materials and increasing the solids storage capacity of the impoundment in sub-aerial tailings disposal. Therefore, sub-aerial tailings deposition is a promising tailings disposal method;
2. At the top of the settling zone, the effective stress equals zero;
3. Most tailings consolidation models are based on the one-dimensional nonlinear finite strain theory (Gibson et al. 1967);
4. An important property of the desiccated soil is the soil-water retention characteristics; any analysis of soil undergoing desiccation should consider this characteristic;

5. Surface drying of deposited tailings is caused by evaporation at a rate that depends on the varying climatic conditions at a site; therefore, if the evaporation data are not available in the local climatic station, a climatic based equation should be used to calculate the evaporation rate;
6. Hydraulic conductivity is an important parameter in modeling consolidation and desiccation of soils, and the unsaturated hydraulic conductivity decreases dramatically with the increase in the matric suction;
7. Both shear and tensile strength of the soil can be related to the effective cohesion, friction angle, and the soil suction;
8. A tension crack initiates when the total lateral tensile stress reaches the tensile strength of the soil. Linear elastic fracture mechanics is usually used to analyze crack propagation, and it is commonly proposed that the spacing of the cracks can be estimated from the theoretical stress relief field by assuming that another crack may exist at points between about 5% and 10% stress relief.

Table 2.1 Normalized crack-edge stress-intensity factor λ (modified from Lachenbruch 1962)

a/b	$\lambda(a/b) = \kappa(a/b)/A\sqrt{b}$
0.05	0.04
0.1	0.08
0.2	0.16
0.3	0.24
0.5	0.41
0.75	0.64
1.0	1.1

Table 2.2 Empirical equations for the unsaturated hydraulic conductivity (modified from Fredlund et al. 1994)

Function	Published Year
$k_r = \Theta^n$, where $\Theta = (\theta - \theta_r)/(\theta_s - \theta_r)$ and $n = 3.5$	1950
$k = k_s(\theta/\theta_s)^n$	1973
$k = k_s \exp[\alpha(\theta - \theta_s)]$	1969
$k = k_s$ for $\psi \leq \psi_{aev}$ $k = (\psi/\psi_{aev})^{-n}$ for $\psi \geq \psi_{aev}$	1964
$k_r = \exp(-\alpha\psi)$ $k = k_s/(a\psi^n + 1)$	1958
$k = a\psi + b$	1931
$k = k_s$ for $\psi \leq \psi_{aev}$ $k_r = \exp[-\alpha(\psi - \psi_{aev})]$ for $\psi_{aev} \leq \psi \leq \psi_r$ $k = k_r(\psi/\psi_r)^{-n}$ for $\psi > \psi_r$, where k_r is k at $\psi = \psi_r$	1965
$k = a\psi^{-n}$	1955

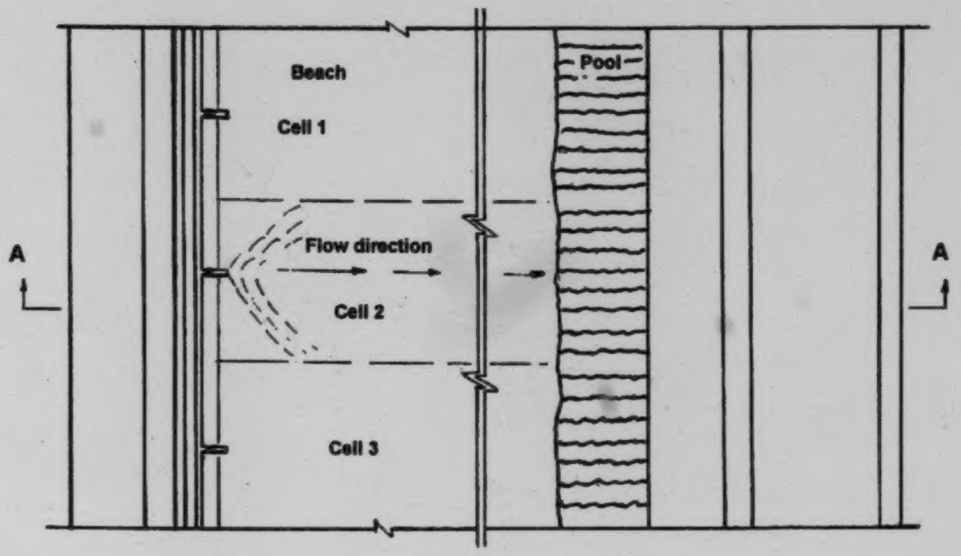
Beach
Pool
Cell 1
A
Flow direction
A
Cell 2
Cell 3

A-A Section

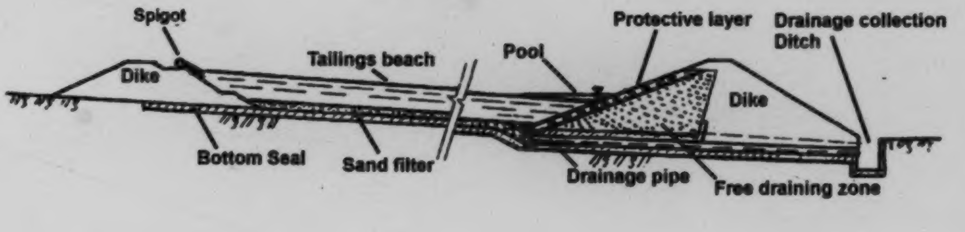
Spigot
Protective layer
Drainage collection Ditch
Tailings beach
Pool
Dike
Dike
Bottom Seal
Sand filter
Drainage pipe
Free draining zone

Figure 2.1 Sketch of the sub-aerial tailings disposal method (after Qiu and Sego 1998a)

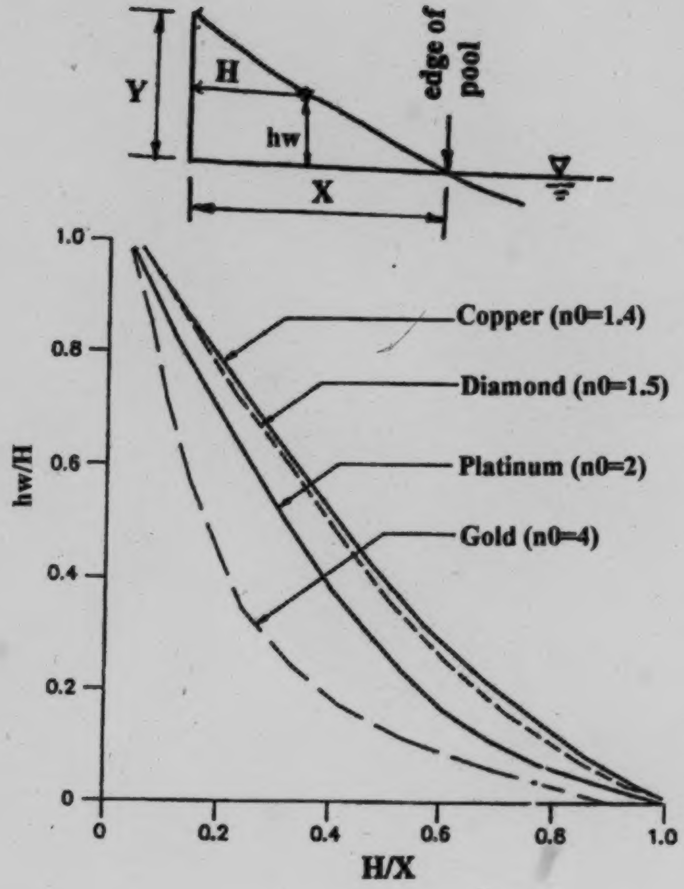

Figure 2.2 **Beach profiles for dams of various types of tailings (modified from Blight 1987)**

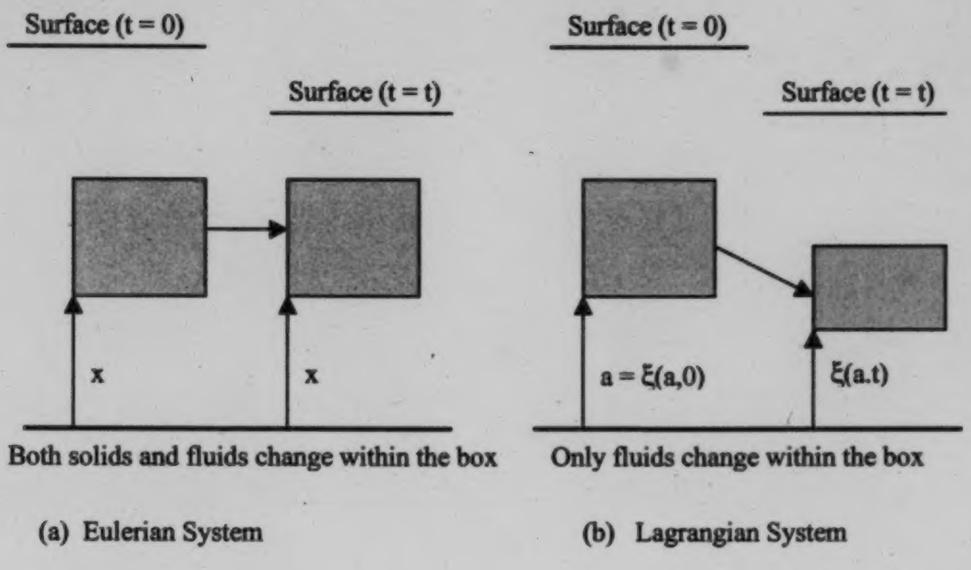
Surface (t = 0)
Surface (t = t)
x
x
Both solids and fluids change within the box
(a) Eulerian System
Surface (t = 0)
Surface (t = t)
a = ξ(a,0)
ξ(a.t)
Only fluids change within the box
(b) Lagrangian System

Figure 2.3 The Eulerian and Lagrangian coordinate systems (modified from Swarbrick 1992)

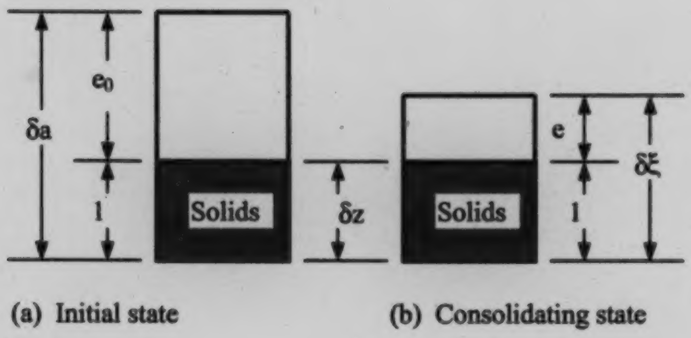
e0
δa
1
Solids
δz
Solids
e
δξ
1
(a) Initial state
(b) Consolidating state

Figure 2.4 Solids coordinate z and relations with Eulerian and Lagrangian coordinates (modified from Gibson et al. 1981; Schiffman et al. 1988)

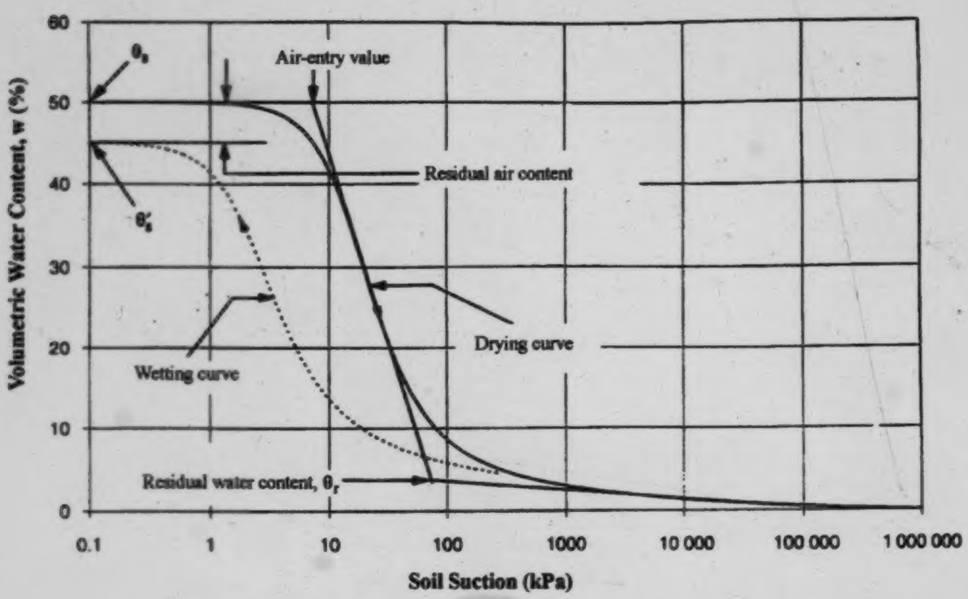

Figure 2.5 Typical water-soil characteristic curves (modified from Fredlund et al. 1994)

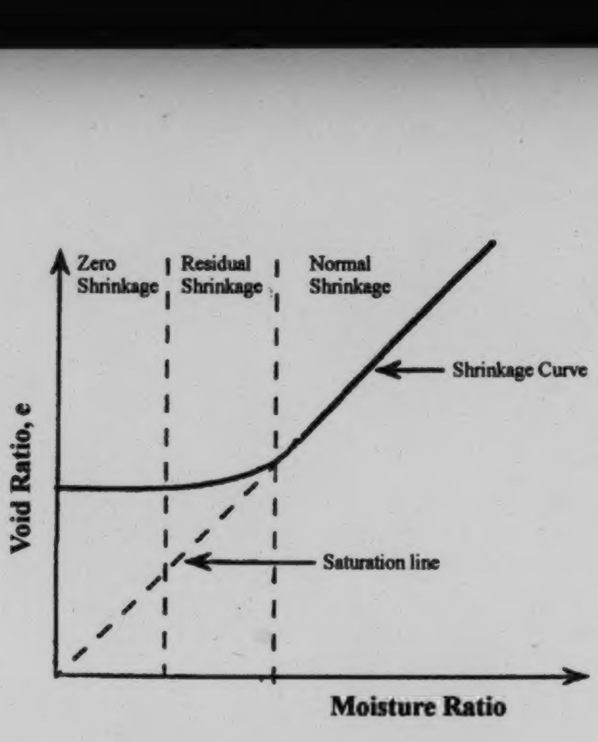

Figure 2.6 Typical shrinkage curve of soils

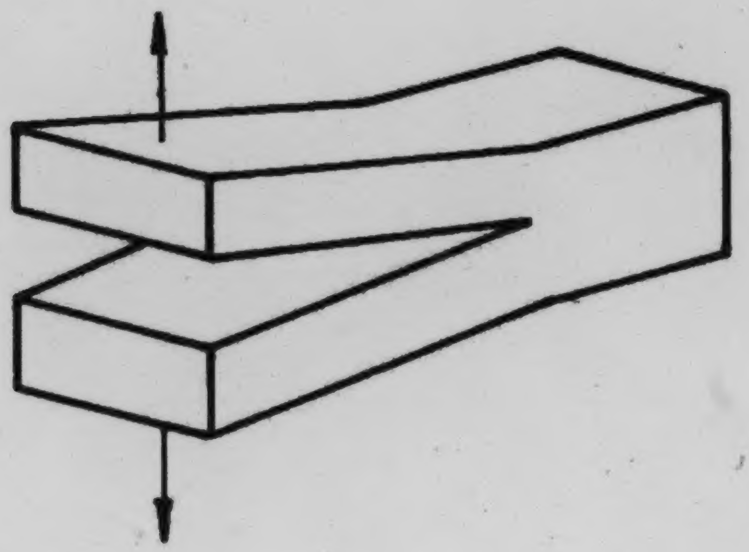

Figure 2.7 Opening crack mode

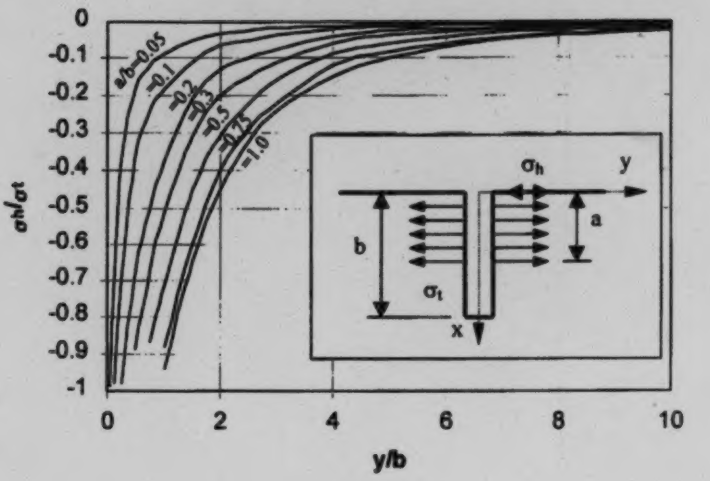

Figure 2.8 Theoretical values of elastic stress relief due to a vertical crack (modified from Lachenbruch 1962)

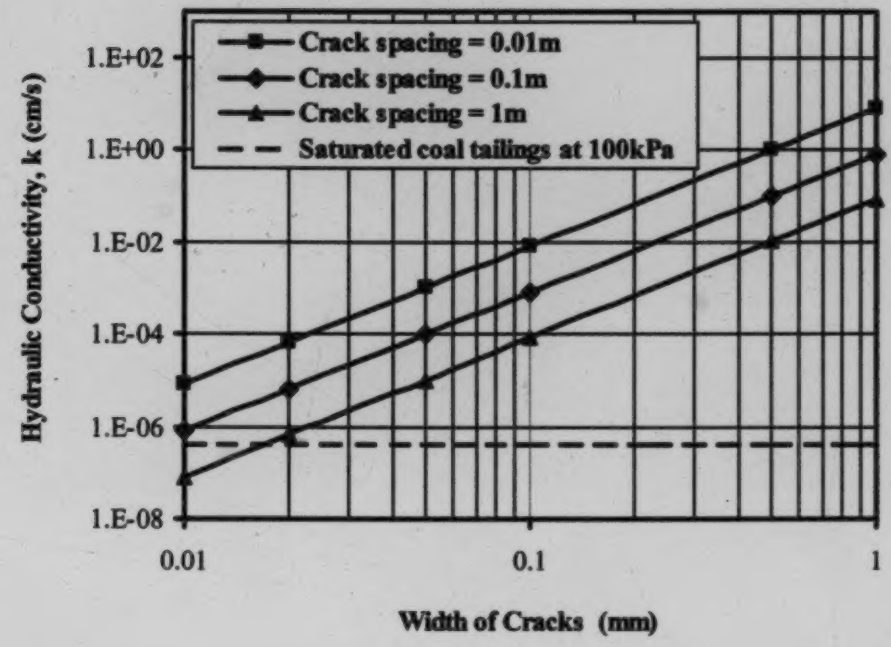

Figure 2.9 **Comparison between the cracked and intact saturated hydraulic conductivity**

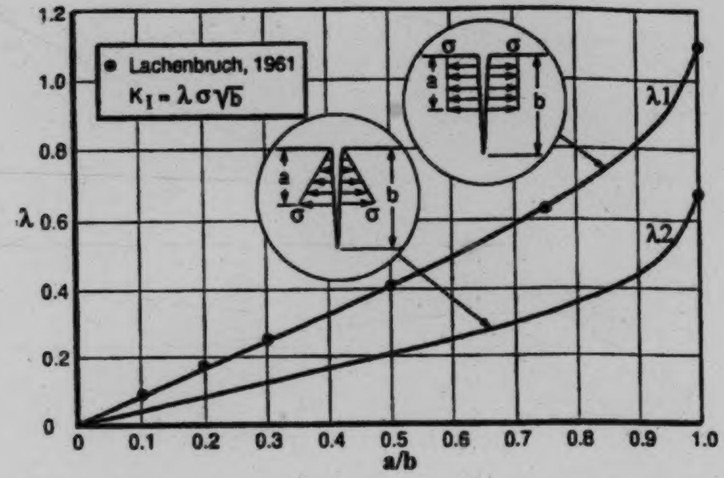

Figure 2.10 Stress intensity functions for uniform and linear stress distribution (modified from Konrad et al. 1997)

CHAPTER 3 LABORATORY TEST PROGRAM

3.1 INTRODUCTION

In the mining industry, most fine grained wastes (tailings) are produced in mineral processing plants. The wastes are generally in the form of a slurry, which is transported for deposition hydraulically. A vast amount of mining wastes is produced around the world each day. How to treat the wastes effectively and economically has become a major issue facing mining operations. The sub-aerial technique is a promising tailings disposal method (Qiu and Sego 1998a).

Although the sub-aerial tailings disposal technique has existed for more than a decade, there is little information related to the optimum design of the disposal scheme in arid regions. Obviously, the physical processes of the sub-aerial tailings disposal method are sedimentation, consolidation, and desiccation. A knowledge of the basic physical properties of the mine tailings, and their consolidation and desiccation behaviors is required to understand the tailings material behavior and to further improve the efficiency of the disposal method (Qiu and Sego 1998b). The objective of this laboratory study is to ascertain basic properties of various mine tailings related to the sub-aerial deposition. Most laboratory tests were carried out using standard ASTM test procedures. However, due to the complexity of the tailings and the technical requirement for deposition, some special testing techniques were needed and developed. Special experimental methods that were used to carry out the consolidation and desiccation behavior tests are described.

In this study, copper, gold, coal, and oil sand composite/consolidated (CT) tailings were selected to represent a wide range of tailings from different types of mines. The tailings samples were provided by Kennecott Mining, Echo Bay's Lupin Mines, the Coal Valley

Mine of Luscar Sterco (1977) Ltd. and Syncrude Canada Ltd. for the copper, gold, coal, and oil sand composite/consolidated tailings (CT) tailings respectively. Laboratory tests on these tailings were carried out (Qiu and Sego 1998c), and the measured engineering properties of the tailings are presented and compared in Chapter 4.

3.2 CONSOLIDATION AND HYDRAULIC CONDUCTIVITY TESTS

The purpose of the consolidation and hydraulic conductivity tests is to determine the behavior of the various tailings over the effective stress range of 0.5 to 100 kPa. This low range in stresses is appropriate as it is operative in the majority of tailings management facilities. The saturated hydraulic conductivity at the end of each consolidation stress increment was also determined by direct measurement by applying a constant water head difference across the sample to measure the flow through the sample.

3.2.1 Test Equipment

Most mine tailings are processed as slurry to allow them to be deposited hydraulically because of the economics of slurry transport. Due to the large initial void ratio associated with the low solids content in the original tailings, a large strain consolidation apparatus was used to carry out the test. Figure 3.1 shows a sketch of the apparatus. The loading system consists of a diaphragm and PVC piston. The unit has an inside diameter of 100 mm and can accommodate a 100 to 130 mm high sample. Air pressure is applied to the load chamber to provide uniform stress increments to the sample. To collect and record the test data, a data logging system consisting of a signal controller, a data logger (model: FLUKE Helios Plus 2287A), and a micro computer were attached to the deformation measuring system, as shown in Figure 3.2.

3.2.2 Tailings Saturation

Most tailings samples taken from mine sites are unsaturated. To saturate the tailings, tailings pond water was added to the tailings in a pail, using an internal vibrator to agitate the sample for 5 minutes. The sample was then covered and left for at least 12 hours to release entrapped air. Then the sample was mixed for 2 to 5 minutes before taking test samples from the pail. Immediately the required amount of sample was taken after mixing and placed into a de-airing cylinder (Figure 3.3). The de-airing cylinder was then placed on a vibrating table while applying a vacuum of 60 kPa for at least 2 hours to the cylinder to draw off any remaining gas trapped in the sample. To avoid segregation of the tailings, the tailings were stirred in the cylinder occasionally.

Before placing the sample in the test apparatus, the base of the consolidation cell was saturated. First, the porous stone and filter paper was boiled for at least 15 minutes, and then the stone and filter paper were carefully placed on the base of the cell. Distilled water was added to the cell so that the filter remained submerged. Next, the cylinder was assembled and placed on the vibrating table. Suction was applied to the cell until no air bubbles flow from the base. Finally, the cell was weighed and recorded for future use.

It is easy to trap air in a sample when it is being placed into the consolidation apparatus. To eliminate entrapping air, a special placement technique was used as illustrated in Figure 3.4. The de-airing cylinder and the consolidation cell were connected via a rubber filling tube. Suction was applied on both the de-airing cylinder and the cell simultaneously to remove air from the cell and connections. Then, with a continuous suction, the bottom valve of the de-airing cylinder was opened to allow the saturated sample to gradually flow into the consolidation cell.

To check the degree of saturation of the sample, the sample weight, sample dimensions, supernatant volume, water temperature, and sample unit weight were measured. Then the degree of saturation was calculated using:

[3-1] $S = \frac{wG_s\gamma}{G_s\gamma_w(1+w)-\gamma}$

where S is the degree of saturation, G_s is the specific gravity of the sample solids, and γ_w is the unit weight of the water.

For CT, due to the presence of bitumen, saturation is difficult to maintain throughout the test as gases are released from the tailings due to biological processes. To eliminate this problem, the tests on CT were carried out in a cold room maintained at an average temperature of +3 °C to suppress biological activity.

3.2.3 Consolidation Tests

Consolidation tests were conducted by applying incremental loads to the samples. The samples were loaded one-dimensionally in compression under condition of no lateral yield in the large strain test apparatus. The excess pore pressures generated under each stress were allowed to dissipate before the next load increment was applied. Therefore, a unique relationship between void ratio and effective stress was obtained. Using the test data, the consolidation parameters were then calculated. Load increments that applied stresses of 0.5, 2, 4, 10, 20, 50 and 100 kPa were used. A pressure transducer and LVDT (linear variable displacement transducer) were used to monitor the applied load and the deformation of the sample. Figure 3.5 shows a photograph of the consolidation test apparatus.

The rectangular hyperbola method was used to analyze the consolidation test (Sridharan et al. 1987). The following equation was used to predict the deformation corresponding to 100% primary consolidation at the end of each load increment:

[3-2] $\delta_{100} = \frac{0.859}{m_t}$

where δ_{100} is the deformation corresponding to 100% consolidation and m_t is the slope of the linear portion of the t/δ versus t plot obtained during each load increment, and t is the elapsed time.

3.2.4 Hydraulic Conductivity Test

Hydraulic conductivity has an important influence on both the consolidation and desiccation behavior of the tailings as it controls their water flow characteristics. Because of the complicated factors that influence hydraulic conductivity, it is difficult to accurately measure the hydraulic conductivity of tailings, especially the unsaturated hydraulic conductivity. In this study, only the saturated hydraulic conductivity was measured directly. The unsaturated hydraulic conductivity was predicted based on the measured saturated value and the tailings-water retention curve using the procedure outlined by Fredlund et al. (1994). Generally, there are two different methods to determine the saturated hydraulic conductivity (the direct and indirect method). The direct method uses a constant or a falling head permeameter along with Darcy's law to directly measure values of hydraulic conductivity.

In this study, the constant head hydraulic conductivity tests were carried out at the end of each consolidation stress increment to measure the hydraulic conductivity. Both distilled water and tailings pond water were used in two separate tests to evaluate whether any fluid chemistry effect existed. During the tests, water from the constant head reservoir flowed upward through the samples under a low constant gradient. The outflow volume was measured as it flowed through a graduated glass tube. The sample height and the applied head were measured so that the hydraulic gradient could be calculated (Figure 3.5).

The consolidation parameters-- the coefficient of consolidation, the coefficient of volume compressibility and the hydraulic conductivity --were then calculated from the test results from each load increment using techniques outlined by Head (1992).

3.3 COLUMN DRYING TEST

To measure the desiccation behavior of the various mine tailings, laboratory column drying tests were conducted in a controlled environment. In the tests, the potential evaporation rate, the actual evaporation rate, the water content and the temperature profile, as well as the settlement of the tailings, were measured.

3.3.1 Test Environment

The column drying tests were performed in a controlled environment in the Geotechnical Engineering Laboratory at the University of Alberta. The temperature and humidity of the room were controlled using a de-humidifier (Figure 3.6). The room temperature was maintained in the range of 30 to 35°C, and the relative humidity of the room was maintained within a range of 9 to 13%. These conditions resulted in a potential evaporation of between 5.0 to 8.0 mm/day, which are similar to the summer potential evaporation rates of the oil sand site in Fort McMurray, Alberta, Canada.

3.3.2 Drying Column

A drying column or a lysimeter is commonly used to measure the evaporation behavior of a soil under laboratory conditions. Most columns or lysimeters used in the laboratory are PVC or Perspex cylinders 100 to 300 mm in diameter (Wilson 1990; Swarbrick 1992). In this study, a 153 mm outside diameter PVC tube with a wall thickness of 10 mm was selected as the test columns. Two drying columns, A and B, with a height of 500 mm (Figure 3.7) were used for the tailings drying tests and a water evaporation pan (column C) with a height of 200 mm was selected (Figure 3.8). Column A was used to allow sampling and temperature profile measurement, while Column B was for monitoring the actual evaporation rate from the surface, the suction at bottom of the column and settlement of the tailings sample. A schematic of column A is shown in Figure 3.7. It had four series of vertically spaced sampling ports each 10 mm in diameter and spaced 20 mm center to center along the length of the column. The sampling ports were located at 90° intervals around the perimeter of the column as shown in Figure 3.7. Soft rubber stoppers were used to seal the ports. A drain port 20 mm in diameter was drilled at the bottom for drainage and cleaning. A tensiometer port for monitoring the suction change at the bottom of the sample was also installed in each test column.

Seven thermocouples were installed along the central axis of the column. They were located at depths of 0, 25, 50, 100, 150, 300 and 450 mm. Column B had the same dimensions as column A but without the sampling ports. The water evaporation pan (column C) also did not have any sampling ports.

3.3.3 Layout of the Test Apparatus

The layout of the column drying test apparatus is shown in Figure 3.8. Column B and the water evaporation pan were placed on scales which could be read electronically and were connected to a data logging system.

To minimize lateral heat flow through the test cylinder, all columns were wrapped with fiberglass insulation. To avoid elevation differences, the surface elevations of the top of each column were the same. The scales had a precision of 0.01g to provide accurate measurement of the evaporation losses. However, it was difficult to find a reasonably priced scale with a capacity of 20 kg and a precision of 0.01 g. Therefore, a beam system with a counter weight and a lower capacity high precision scale were used (Wilson 1997). A sketch of the beam measuring system is shown in Figure 3.9. To measure the room temperature and relative humidity, a hygrometer-thermometer was used. Its probe was mounted in the center of the room, and the data were recorded via the data logging system.

3.3.4 Sample Preparation and Drying Test

The process of saturating the tailings was the same as was used to prepare the consolidation samples. After the tailings were saturated, column A and B were filled carefully. Once the columns were filled, the tailings surfaces of each column were leveled and sealed with aluminum foil until the start of the test. The rest of the tailings were stored in the controlled- environment room for future use. The samples were left in the room for about 3 days to allow them to reach temperature equilibrium. Before beginning the evaporation test, the supernatant released from the tailings was removed and additional tailings were added to level off the sample height.

Once all columns were filled and at test temperature, the transducers were connected to the data logger and the samples were uncovered to begin the evaporation tests. All data were recorded automatically at 15 minute intervals, while the water content samples were taken from column A at 0, 1, 2, 3, 5, 7, 14, 21, 28, and 35 days after beginning the evaporation test. The samples were all taken using a 5mm I.D. glass tube pushed through the sampling ports into the tailings. The water evaporation pan was refilled with additional water stored in the room each day. The settlement measurement was carried out daily. The column drying tests took between 4 and 6 weeks to complete.

3.4 WATER RETENTION CHARACTERISTICS TEST

The soil-water retention characteristics indicate the relationship between soil suction and water contained in the soil. This is an important property of unsaturated soils. In the sub-aerial tailings disposal method, the tailings are deposited in a thin layer and allowed to desiccate under climatic influences. Thus, the tailings desaturate. As mentioned previously, the unsaturated hydraulic conductivity can be derived using the data from saturated samples and the tailings-water retention curve. Therefore, to study sub-aerial deposition, it is necessary to understand the water retention characteristics of the tailings being deposited.

In this study, pressure plate extractors were used to measure the soil-water retention curve of the tailings from 0 to 1500 kPa suction, and glass desiccators containing saturated salt solution were used to measure the retention characteristics from 1500 to 296 000 kPa suction.

3.4.1 Pressure-Plate Extractor Method

The pressure-plate extractor test method is described in ASTM D2325 (1997). The procedure of the test was as follows: saturated tailings samples were placed on a saturated porous ceramic plate installed in a steel pressure chamber; the bottom of the plate was wrapped using a rubber membrane and maintained at atmospheric pressure. When a desired air pressure was applied to the pressure chamber and, consequently to the top surface of the plate, a pressure drop across the porous plate was generated. The tailings placed on the plate established equilibrium with the water within the porous plate. Only the pore water held at a matric suction less than the pressure drop across the porous plate flow out of the soil to pass through the plate. Once no more water flowed from the sample, equilibrium was established for the suction level applied to the sample. Then the water content of each sample could be determined. For a complete tailings-water retention curve from 0 to 1500 kPa suction, different pressures and different porous plates were used in a series of tests using the same tailings samples.

3.4.1.1 Test apparatus

The test equipment used in the pressure-plate extractor method is shown in Figure 3.10. The extractors were connected to the manifold using rubber tubes. The air pressure was generated by an air-compressor and applied to the pressure chamber of the pressure-plate extractor via the manifold. The applied pressure was controlled with a pressure regulator. Two types of the pressure-plate extractors are commercially available (500 and 1500 kPa extractors). There are various commercial porous plates with different air-entry values. One hundred and 1500 kPa ceramic plates were used in this study. The saturated tailings samples were held in individual sample rings which were placed directly on the porous plates in the pressure chamber. The rings made of PVC tube were 15 mm high by 50 mm in inside diameter and had a wall thickness of 3 mm. To prevent loss of the fines portion of the tailings, the bottom of each ring was covered using a 50 mm diameter filter paper. Figure 3.11 shows the sample rings and the porous plate.

The porous plates were saturated before each test. The method for saturating was as follows: all plates were installed in the extractor (usually up to 3 plates for the 500 kPa extractor and 2 for 1500 kPa extractor). The extractor was filled with distilled water to submerge the plates. The extractor was covered with its lid and locked firmly. Then 1 atm pressure was applied to the pressure chamber. When the rate of water outflow from the plate reached at least 10 ml/min, the plate was considered saturated (ASTM D2325 1997). Then the pressure was released and the excess water was removed before placing the tailings sample holders on the plate.

3.4.1.2 Sample preparation

The tailings were saturated with process water under a suction of 60 kPa in a vacuum jar. The degree of saturation was checked using equation [3-1]. Then the saturated tailings were transferred into the sample rings that were placed on the saturated plates. Two samples of each type of the tailings were located at diameterically opposite positions on the porous plate. A reference ring filled with saturated standard loam was placed in the center of each plate for comparison to the data obtained for the tailings. Furthermore, two filter papers of the same type as those used at the base of each ring were placed on each plate. Next, the plates with the samples were placed in the extractor, and the plate outlet was connected to the atmosphere with a small tube. Finally, the extractor was covered and the lid was locked in position.

3.4.1.3 Test

Once the extractor was locked, the air pressure was slowly applied to the pressure chamber via a connection tube. The pressure was maintained at the desired value by the pressure regulator, and the test started. The outflow was collected and measured using a graduated cylinder. It took several days for some tailings to reach moisture equilibrium. No water outflow for a period of one day indicated that equilibrium had been established. The drainage tube was closed to avoid the water flowing back into the plate and samples when the pressure was released slowly. Each plate was lifted out, and the samples were quickly transferred into sample containers. The samples with containers were weighed. At the same time, the reference filter papers were weighed. Furthermore, the sample volumes were obtained by measuring the settlement of the surface of each tailings sample.

Several pressure intervals, (2, 4, 5, 7, 10, 30, 50, 75, 100, 300, 500, and 1500 kPa) were used so a smooth soil-water retention curve was obtained. For suctions less than 100 kPa, the samples were placed on the 1 bar plate, which was tested in the 5 bar extractor cell. The rest of the test was carried out using the 15 bar plate placed in the 15 bar extractor cell.

Finally, the samples were dried in an oven at 110 ± 5 °C for at least 24 hours. Then their final moisture content and dry densities were obtained.

3.4.2 Saturated Salt Solution Method

The soil-water retention curve for higher values of suction can be determined using osmotic pressures generated by salt solutions (Wilson et al. 1997). The basic principle of the method is described as follows. At constant temperature, any salt solution at a certain chemical concentration is in equilibrium with a fixed partial vapor pressure of water and, consequently, defines a fixed relative humidity (Young 1967). Robinson and Stokes (1955) proposed a formula to calculate the osmotic pressure (or suction) as:

$$[3\text{-}3] \quad \Pi = \frac{R_u T}{V_A} \ln a_w$$

where Π is osmotic pressure or suction (kPa), R_u is the universal gas constant, R_u=8.31439 J/mol·K, T is the absolute temperature in degree Kelvin, i.e. T=273 + t, t is the temperature in °C, V_A is the partial molar volume of the solvent, V_A=18.0545x10^{-3} m^3/mol for water at 22°C, and a_w is activity of the solvent, in this case equal to the relative humidity R_h.

As a result, various salt solutions can be selected to establish different suctions. In this research program, four saturated salt solutions were chosen from Young's (1967) recommendation for the best control of humidity, (potassium sulfate [K_2SO_4], sodium chloride [NaCl], magnesium nitrate [$Mg(NO_3)_2.6H_2O$] and lithium chloride [$LiCl.H_2O$]). A laboratory room temperature of 22°C was established as the control temperature. Thus, the osmotic pressure induced by the solutions could be calculated using Equation 3-3, and the results are summarized in Table 3.1.

To carry out this test, a leak-proof container was needed as a humidity chamber. A vacuum glass desiccator is an ideal container. Furthermore, a rigid plastic ring was needed to hold the sample. In this test, the PVC rings of 10 mm in height by 40 mm in inside diameter were used. To avoid loss of any tailings solids, a filter paper was glued on the bottom of the ring with silicone glue.

3.4.2.1 Sample preparation and test

The tailings were saturated using the same technique as was used to prepare the pressure-plate extractor samples. The saturated salt solutions were prepared at the desired temperature (22°C). Then the solutions were placed into the separate desiccators with the solution level at least 25 mm beneath the porcelain desiccator plate. The tailings were carefully filled to the level of the marked rings that were placed on top of the desiccator plate. Two samples of each tailings were placed diameterically opposite from each other on the plate. The desiccators were sealed using vacuum grease applied on the lid. Finally suction was applied to the desiccator to remove all the air to avoid contamination by atmospheric gases.

The desiccators were stored in an insulated chamber to maintain a constant temperature (22°C) and the test started. Figure 3.12 shows the saturated salt solution desiccator.

Each sample was removed from the desiccator and weighed once a week until no change in the sample weight over a week was observed. No reduction in the sample weight for one week indicated that the sample moisture content had reached equilibrium under the osmotic suction within the desiccator. After each sample was weighed, the sample volume was immediately measured. Then the sample was dried in an oven at 110 ± 5 °C for at least 24 hours to determine the actual moisture content.

Once the water content, the dry density and the temperature in the chamber were measured, one could convert the gravimetric water content to the volumetric water content based on the following relationship:

$$[3\text{-}4] \quad \theta = \frac{\rho_d}{\rho_w} w$$

where θ is volumetric water content, w is gravimetric water content, ρ_d is dry density of the tailings and ρ_w is the density of the water at temperature (t).

3.5 STRENGTH TEST

To determine the effective shear strength parameters of the tailings, consolidated undrained compression triaxial tests (CU) (ASTM D 4767 1997) were carried out.

The specimen preparation methods were the same except for the coal wash tailings. For copper, gold, and CT tailings, the compaction method (ASTM D 4767 1997) was used to prepare the specimens. The compacted specimens were prepared by compacting material in 7 equal-mass layers using a 63 mm diameter split mold to achieve the required densities. For coal wash tailings, specimens with a diameter of 37.5 mm were directly trimmed from a large compacted sample.

The standard test procedure (ASTM D 4767; Bishop and Henkel 1957; Head 1992) was followed. Once the triaxial apparatus was set up, the de-aired water was allowed to flow through the specimen to exclude the air. Then the rest of the test was finished in four stages. In the first stage, under conditions of no drainage, the all around cell pressure and the back pressure were increased in increments of 50 kPa up to an applied cell pressure of 400 kPa and a back pressure of 390 kPa. During this stage, a 10 kPa difference between the cell pressure and back pressure was always maintained. These final pressures were maintained for at least 24 hours to allow the excessive air to dissolve into the pore fluid. In the second stage, a "B" test was carried out. The cell pressure was increased in increments of 25 kPa until the pore pressure parameter B was measured to be equal to 1. In the third stage, the saturated specimen was consolidated to effective stresses of 25, 50 and 100 kPa. After the consolidation was complete, the fourth stage, shearing of the sample, was carried out under the conditions of no drainage. The shearing strain rate was determined based on the estimated failure time using the recommendation of Bishop and Henkel (1957). Figure 3.13 shows the triaxial test apparatus.

3.6 SHRINKAGE LIMITS AND SHRINKAGE CURVE TESTS

When moisture content changes, volume expansion and/or contraction occur over a period of time. These changes depend both on soil type and changes in water content. To obtain a quantitative indication of how much volume changes in sub-aerial tailings disposal, a shrinkage limit test and a shrinkage curve test are required. The shrinkage limit was defined as the water content at which the volume of the soil reaches its lowest value as it dries out (Craig 1992). A shrinkage curve indicates the void ratio change behavior with moisture content. The shrinkage tests on copper, gold, coal, and CT tailings were carried out in the soil mechanics laboratory from October to December 1999. In these tests, an ASTM standard test method for shrinkage factors of soils by the mercury method, i.e. ASTM D 427-93 (ASTM 1999), was used.

3.6.1 Test Apparatus

A standard test apparatus was used. It consisted of a spatula, copper shrinkage dishes, a porcelain evaporation dish, a glass cup with a diameter of 57 mm and a height of 31 mm, a glass plate with 3 metal prongs, a plastic cup for delivering displaced mercury to weigh, a flat bottomed glass dish with a diameter of 95 mm and a height 22 mm, a straightedge and a balance with a precision of 0.01g. Figure 3.14 shows the test apparatus.

3.6.2 Sample Preparation

Tailings samples with a moisture content exceeding the liquid limit were prepared. The sample was first de-aired on a vibrating table while applying a vacuum of 60 kPa for at least 2 hours to the sample to draw off any remaining gas entrapped in the sample. The volume of the shrinkage dish was calibrated with water before use in the tests. The inside of the shrinkage dishes was coated with a thin layer of vacuum grease and the weights of the empty dishes were recorded. Then the de-aired sample was placed in the dish in three layers while the dish was tapped on a firm surface. The excess soils were struck off with a straight edge, the mass of the dish and wet sample was determined and recorded. The specimens were placed in a moisture control room to dry slowly to be ready for future measurements. Figure 3.15 illustrates the shrinkage test specimens and the shrinkage dishes.

3.6.3 Test

During the shrinkage limit test, the tailings pad was allowed to dry in the moisture control room for two days. Then the specimen with the shrinkage dish was placed in an oven for oven-drying to constant mass at 110 ± 5 °C. The mass of the dish and dry tailings was determined and recorded. Next, the volume of the dry soil pat was determined by immersing the tailings pad in a glass cup full of mercury. The detailed mercury test procedure can be found in ASTM D 427-93. The shrinkage limit can be calculated by using:

$$[3\text{-}5]\quad SL = w_i - \frac{(V_i - V_d)\rho_w}{M_d} \times 100$$

where SL is the shrinkage limit, w_i is the initial water content, V_i is the initial volume of the wet tailings, V_d is the volume of the dry tailings, ρ_w is the density of water, and M_d is the dry mass of the tailings pad.

For the shrinkage curve test, a different procedure from the shrinkage limit test was used. The specimens were allowed to dry in the moisture control room for different durations, thus achieving different water content changes. Figure 3.15 shows the drying specimens in the shrinkage dishes. Once the specimens were dried to the expected state based on the experience, at least two specimens were taken to test for moisture content and volume determination. First, the mass of the shrinkage dish and drying tailings pad was determined and recorded. Then the specimen was carefully moved from the dish to an aluminum tray, and the mass of the specimen in the tray was determined and recorded.

Next the volume of the drying tailings pad was determined by immersing it in the glass cup full of mercury. When the tailings pad was immersed in the mercury, extreme caution was required due to the weakness of the drying specimen. Finally, the specimen was placed in an oven under a hood for oven-drying to a constant mass at 110 ± 5 °C. The mass of the dry tailings pad was determined and recorded.

The void ratio and moisture content of the drying tailings pad were back calculated using the following equations:

$$[3\text{-}6] \quad \rho_d = \frac{Ms}{V_d}$$

$$[3\text{-}7] \quad e = \frac{G_s\rho_w}{\rho_d} - 1$$

$$[3\text{-}8] \quad w = \frac{M_w}{M_s}$$

where ρ_d is the dry density of the drying tailings pad, M_s is the mass of the solids in the pad, V_d is the volume of the drying tailings pad, e is the void ratio of the tailings pad, G_s is the specific gravity of the tailings, ρ_w is the density of water, w is the moisture content, and M_w is the mass of the water in the pad.

3.7 SUMMARY AND CONCLUSIONS

Laboratory tests are widely used to determine the engineering properties of tailings. The large strain consolidation and hydraulic conductivity tests for the saturated tailings were discussed. The techniques for saturating and placing the tailings sample prior to the consolidation tests were summarized. A method to eliminate the volatilization of the bitumen from within the sample during the test was introduced. The column drying test was used for investigating the desiccation behavior of various mine tailings. The tailings-water retention characteristic was measured using both the pressure-plate extractor test method and the saturated salt solution desiccator test method to determine the tailings-water retention curve over the entire suction range for the material. As a result of this study, the following conclusions were made:

1. A large strain consolidation apparatus can be used to conduct the consolidation and hydraulic conductivity tests on mine tailings.

2. Through the control of the temperature and the relative humidity, the potential evaporation rate could be controlled in an environmentally controlled room. The desiccation behavior of the mine tailings could be measured in this facility.

3. It is important to understand the tailings-water retention characteristics to incorporate them into sub-aerial tailings deposition. With the pressure-plate extractor test and saturated salt solution desiccator test, the tailings-water retention curve over the entire suction range could be measured.

4. To calculate the volume change with the moisture content, knowledge of the shrinkage limit and the relationship between void ratio and moisture content of the tailings is required.

Table 3.1 Properties of the selected saturated salt solution

Saturated salt solution	$\frac{d(R_h)}{dt}$ (%/°C)	R_h @25°C (%)	t (°C)	R_h @ t (%)	Osmotic suction (kPa)
K_2SO_4	-0.05	97.0	22	97.15	3928
NaCl	-0.02	75.1	22	75.16	38793
$Mg(NO_3)_2.6H_2O$	-0.29	52.8	22	53.67	84543
$LiCl.H_2O$	-0.01	11.3	22	11.33	295848

Note: R_h is relative humidity.

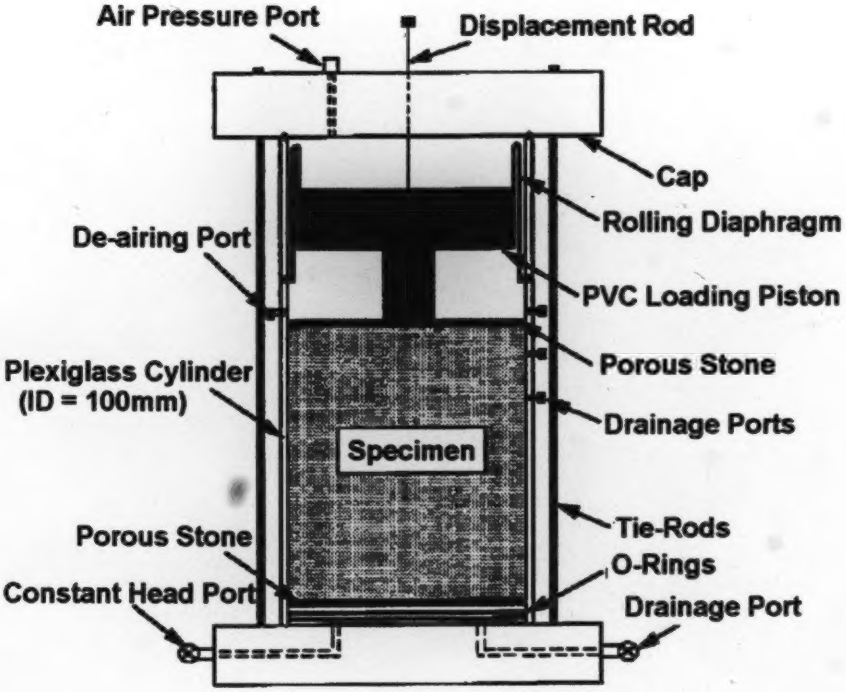
Air Pressure Port
Displacement Rod
Cap
Rolling Diaphragm
De-airing Port
PVC Loading Piston
Porous Stone
Plexiglass Cylinder
(ID = 100mm)
Drainage Ports
Specimen
Tie-Rods
Porous Stone
O-Rings
Constant Head Port
Drainage Port

Figure 3.1 Large strain consolidation apparatus (modified from Qiu and Sego 1998b)

Figure 3.2 Data acquisition system

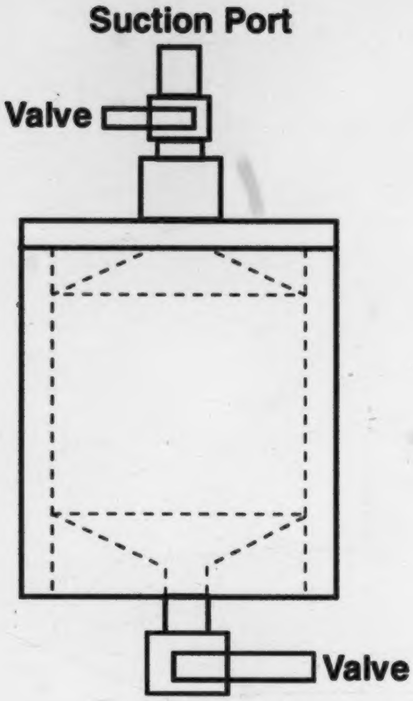
Suction Port
Valve
Valve

Figure 3.3 De-airing cylinder

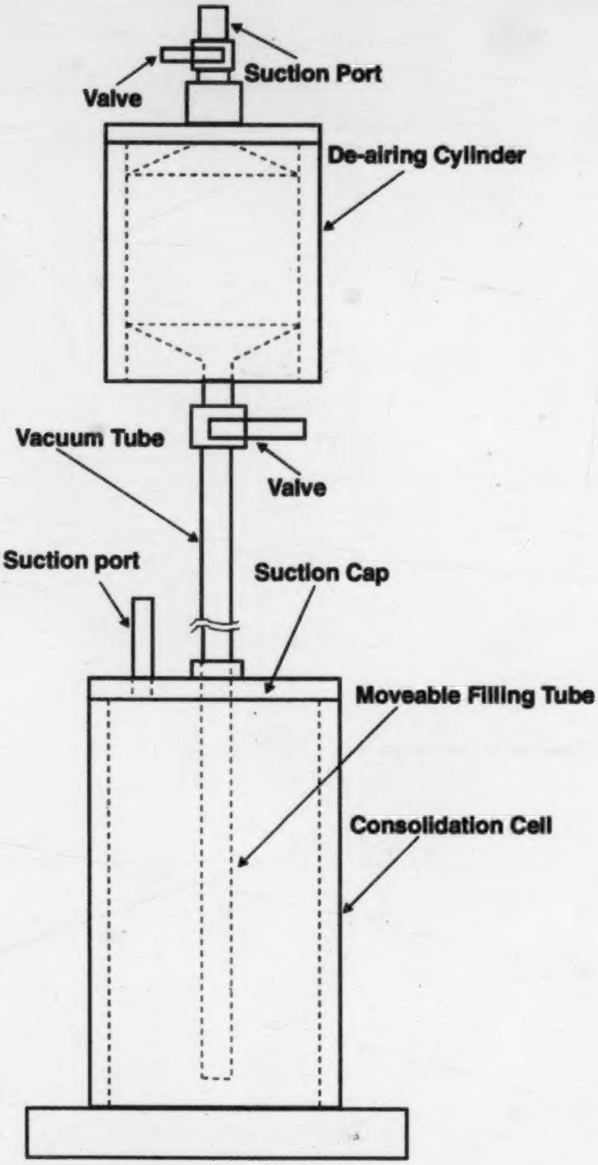
Suction Port
Valve
De-airing Cylinder
Vacuum Tube
Valve
Suction port
Suction Cap
Moveable Filling Tube
Consolidation Cell

Figure 3.4 Tailings placement technique

Coal
Tailings

Figure 3.5 Consolidation test apparatus

Figure 3.6 De-humidifier

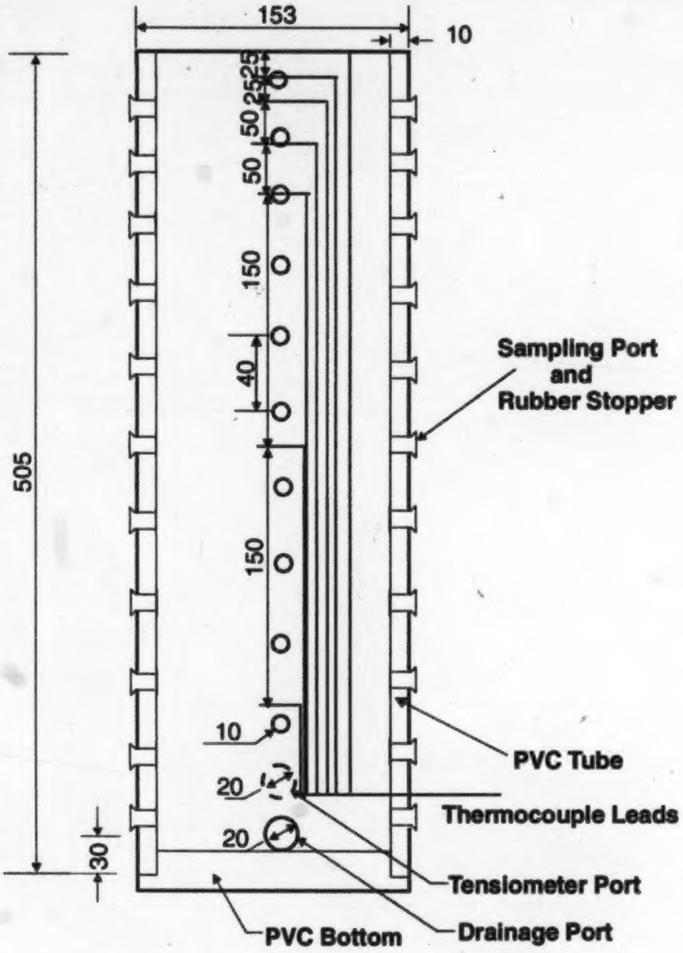
153
10
25
25
25
50
50
150
40
505
150
10
20
20
30
Sampling Port and Rubber Stopper
PVC Tube
Thermocouple Leads
Tensiometer Port
Drainage Port
PVC Bottom

Figure 3.7 Drying column (modified from Wilson 1990)

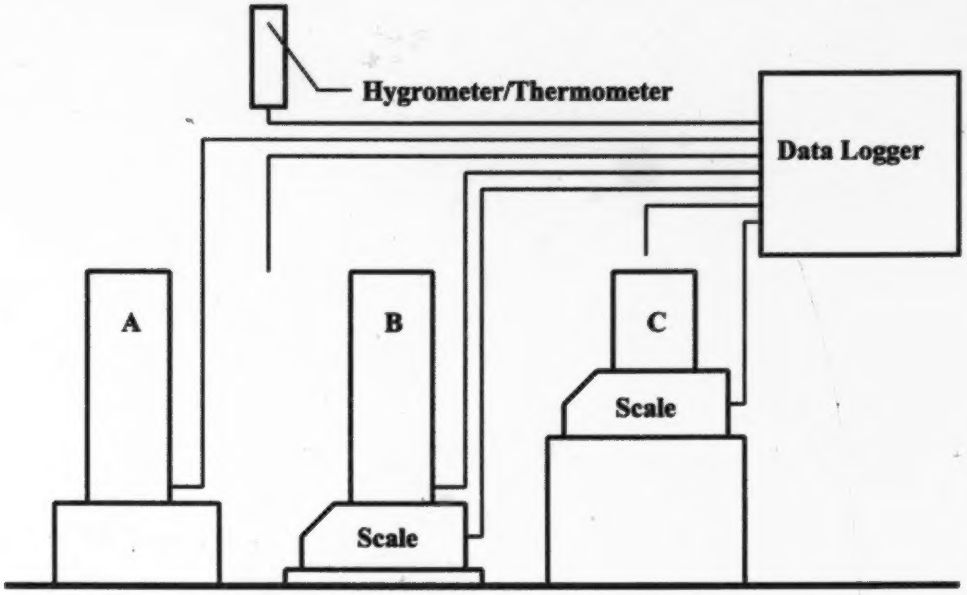
Hygrometer/Thermometer
Data Logger
A
B
C
Scale
Scale

Figure 3.8 Layout of the drying test apparatus

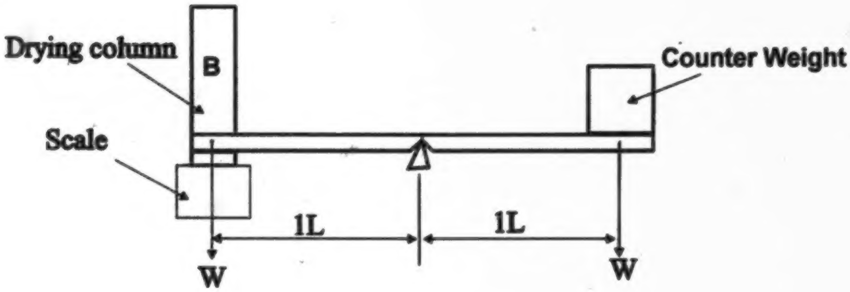
Drying column
B
Counter Weight
Scale
1L
1L
W
W

Figure 3.9 Beam system used to accurately weigh 20 kg sample

Figure 3.10 Pressure-plate extractor test assembly

Figure 3.11 Sample retainer ring and porous ceramic plate

Figure 3.12 Saturated salt solution desiccator

Figure 3.13 Triaxial test apparatus

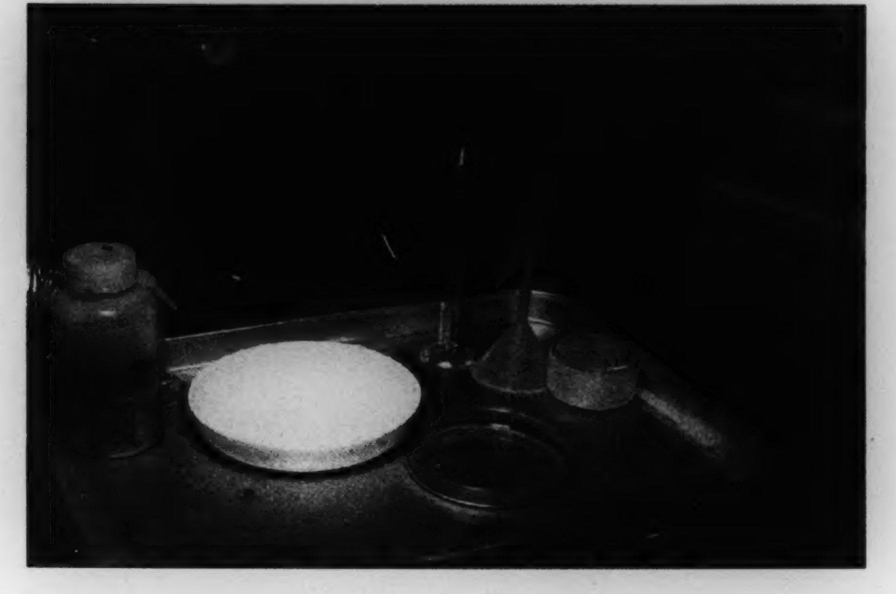

Figure 3.14 Shrinkage test apparatus

Figure 3.15 Shrinkage test specimens and dishes

CHAPTER 4 PRESENTATION AND ANALYSES OF TEST RESULTS

4.1 INTRODUCTION

To understand the sub-aerial tailings deposition technique and carry out the design for optimum deposition in arid regions, properties of mine tailings related to the sub-aerial deposition in arid regions must be ascertained. These include not only the basic physical properties but also their consolidation, hydraulic conductivity, and desiccation behavior and strength parameters. Four different mine tailings were selected to represent a wide range of the tailings for this study: copper mine tailings from Kennecott Mining, gold mine tailings from Echo Bay's Lupin Mines, coal wash plant tailings from the Coal Valley Mine of Luscar Sterco (1977) Ltd. and oil sand composite/consolidated tailings (CT) from Syncrude Canada Ltd.. Laboratory tests on these tailings were carried out (Qiu and Sego 1998b). The appropriate engineering properties of the tailings have been investigated and are presented in this chapter.

4.2 BASIC PHYSICAL PROPERTIES

The soil index tests for the tailings were carried out in the Soil Mechanics Laboratory of the University of Alberta. The basic physical index properties of the as tested mine tailings are shown in Table 4.1, and the grain size distributions are presented in Figure 4.1.

Based on the grain size distribution (Figure 4.1) and the basic physical properties summarized in Table 4.1, the tailings are non-plastic except for the coal wash tailings. The copper tailings' specific gravity and liquid and plastic limits are within the range presented by Mittal and Morgenstern (1975) and Volpe (1979). The copper tailings and oil sand CT are sandy soils and are classified as SM according to the Unified Soil Classification System (USCS). The gold tailings are silty and are classified as ML, while the coal wash tailings are clayey silts and are classified as CL.

4.3 CONSOLIDATION AND PERMEABILITY BEHAVIOR

To determine the compressibility of the tailings and the water flow characteristic in the tailings, the consolidation and constant head permeability tests were carried out in the Soil Mechanics Laboratory of the University of Alberta. The change in saturated hydraulic conductivity as a function of void ratio, the consolidation behavior, and the change in void ratio with effective stress were measured. The consolidation and constant head permeability tests were conducted over an effective stress range of 0.5 to 100 kPa. The tests were carried out in a large strain consolidation apparatus. The test samples had a diameter of 100 mm and a height between 100 and 130 mm. The coefficient of consolidation (c_v) was determined using Casagrande's method, Taylor's method (Head 1992) and the Rectangular Hyperbola method (Sridharan et al. 1987). The coefficient of volume compressibility (m_v) was calculated based on the relationship between applied pressure and void ratio (Head 1992).

Table 4.2 summarizes the coefficient of consolidations (c_v) for the tailings. The c_v values for both copper and gold tailings are smaller than the data (473 m^2/y for pond area and 1167 m^2/y for dam area) for copper tailings provided by Volpe (1979) and the mean value (200 m^2/y) for gold slime outlined by Blight and Steffen (1979). These differences may be caused by the different tailings in the test samples. The c_v values for coal and CT tailings are similar to the data (15-60 m^2/y) for coal wash tailings presented by Williams and Morris (1990) and the data (0.25-11.3 m^2/y) for CT provided by Liu et al. (1994).

The relationships between effective stress and void ratio for various tailings are illustrated in Figure 4.2. The figure shows a near linear relationship on a semi log plot.

The compression index (C_c) for the copper, gold, coal wash tailings and CT are 0.09, 0.16, 0.38 and 0.27 respectively.

The compression index for copper is the same as has been summarized in the collected data of Vick (1983) and Volpe (1979). The C_c for gold tailings is smaller than in Vick's data (0.35), while the data for coal wash tailings is larger than in Vick's data (0.06-0.27) and Williams and Morris (1990) data (0.2). These differences may be due to the differences in the material tested. For the coal wash tailings, this may be because the samples in Vick's collections had smaller initial void ratios (0.6-1.0) and lower clay contents (15%).

The best fitting line through the void ratio versus effective stress data of the mine tailings can be also expressed as:

[4-1] $e = a_1(\sigma')^{b_1}$

or

[4-2] $e = a_3 \ln(\sigma') + b_3$

where e is the void ratio, σ' is the vertical effective stress (kPa), and a_1, a_3, b_1, and b_3 are fitting parameters (constants). The parameters for the best fitting lines are summarized in Table 4.3. Data indicate that the coefficients of determination for equation [4-1] for gold tailings and the oil sand CT are larger than in equation [4-2]. The coefficients of determination for the copper tailings indicate that Equation [4-2] is better than [4-1] to represent the compressibility of the copper tailings. This implies that Equation [4-1] is better than [4-2] to express the relationship between void ratio and effective stresses. For the coal tailings, both expressions are good for representing the compressibility of the coal tailings. In summary, since all coefficients of determination are larger than 93%, both expressions should be good enough to represent the relationships between the void ratio and effective stress.

Table 4.2 also summarizes the saturated hydraulic conductivity of the various tailings. The measured values of the hydraulic conductivity are 4.5 to 9.8 x 10^{-5}, 2.7 to 6.7 x 10^{-5}, 0.04 to 1.1 x 10^{-5} and 2.2 to 6.3 x 10^{-7} cm/s for the saturated copper, gold, coal wash and CT tailings respectively. The data for the copper tailings are within the range (9 x 10^{-6} to 1 x 10^{-4} cm/s) for undisturbed samples presented by Volpe (1979). The values for the gold tailings are larger than in the undisturbed sample (3.6 x 10^{-6} cm/s) presented by Blight and Steffen (1979). The hydraulic conductivity of the coal wash tailings is similar to the average result (3 x 10^{-7} cm/s) presented by Williams and Morris (1990). The results for CT coincide with the results (2.5 to 8.5x10^{-7} cm/s) presented by Liu et al. (1994).

A plot of void ratio versus the measured hydraulic conductivity of the tailings is presented in Figure 4.3. It indicates that the hydraulic conductivity is proportional to the void ratio of the tailings. The best fitting line, the relationship between the hydraulic conductivity and void ratio of the mine tailings, can be expressed as:

[4-3] $k = a_2 e^{b_2}$

where k is the saturated hydraulic conductivity (cm/s), e is the void ratio, and a_2 and b_2 are constants. This expression is similar to the one for the coal wash tailings presented by Williams and Morris (1990). The parameters for the best fitting lines are shown in Table 4.4.

4.4 SOIL-WATER RETENTION CHARACTERISTICS OF TAILINGS

To obtain the tailings-water retention curve over the entire suction range, both a pressure plate extractor test and a glass desiccator test were carried out. The pressure plate extractor test was conducted in the Soil Science Laboratory of the University of Alberta, while the glass desiccator test was carried out in the Soil Mechanics Laboratory of the same university. The pressure plate extractors were used to build up the tailings-water retention curve from 0 to 1500 kPa suction, while the glass desiccators with saturated salt solutions were used to measure the retention characteristics higher up to 296,000 kPa suction. The continuous feature of water content versus suction relationship is illustrated in Figure 4.4. Using a graphical analysis method, the soil-water retention characteristic parameters, such as the air-entry value and residual moisture content, were obtained from the semilog plot of the soil-water retention curve (Figure 4.4), and the results are summarized in Table 4.5. The desaturation process of the tailings can be divided into three stages: the boundary effect, the transition and the residual stages of desaturation (Vanapalli et al. 1996). The suction ranges for each stage are included in Table 4.5.

In the boundary effect stage, all the pores in the tailings are water filled. Therefore, the soil is essentially saturated. With an increase in the suction, the tailings start to desaturate in the transition stage, and the water content in the tailings decreases significantly with increasing suction. Eventually, a large increase in suction results in a small decrease in water content (or degree of saturation). This stage is referred to as the residual stage of desaturation (Vanapalli et al. 1996). The residual volumetric water contents of the tailings are presented in Table 4.5.

Fredlund and Xing (1994) proposed a general equation for the soil-water retention curve as follows:

$$[4\text{-}4] \quad \theta(\psi) = C(\psi)\frac{\theta_s}{\left\{\ln\left[e + (\psi / a_0)^n\right]\right\}^m}$$

where C(ψ) is a correction function defined as

$$[4\text{-}4a] \quad C(\psi) = 1 - \frac{\ln(1 + \psi / \psi_r)}{\ln[1 + 1000000 / \psi_r]}$$

where θ_s is the saturated volumetric water content, *e* is the natural number, i.e. $e = 2.718\ 28$, ψ is the matric suction (kPa), a_0 is a soil parameter that is related to the air-entry value of the soil, *Q* is a parameter that controls the slope at the inflection point in the soil-water retention curve, *P* is a parameter related to the residual water content, and ψ_r is the suction corresponding to the residual water content within the tailings.

Based on the laboratory test results, the four parameters a_0, *P*, *Q*, and ψ_r were graphically estimated using the graphical analysis procedure proposed by Fredlund and Xing (1994) for the four types of tailings as summarizing in Table 4.6. Equation [4-4] predicted results in good agreement with the measured data. Figure 4.5 shows the comparison between the measured and predicted tailings-water data for the various mine tailings.

The water retention characteristics of the tailings can also be expressed as the relationship between gravimetric moisture content and suction head in terms of water. Based on best curve fitting, the relationship between the gravimetric moisture content and suction head can be expressed as:

$$[4\text{-}5] \quad w = \frac{w_s}{\left\{\ln\left[e + \left(\frac{h}{h_b}\right)^{n_1}\right]\right\}^{m_1}}$$

where *w* is the gravimetric moisture content, w_s is the saturated moisture content, *e* is the natural number ($e = 2.71828$), *h* is the suction head in m· H_2O, h_b is the air entry value (in terms of water pressure head), and m_1 and n_1 are the constants.

Using the regression technique, all the parameters were estimated and presented in Table 4.6. The regression results are also shown in Figure 4.6.

4.5 DESICCATION BEHAVIOR

To examine the desiccation behavior of the tailings, column drying tests were conducted in a controlled environment, and the shrinkage tests were carried out in the soil mechanics laboratory. The test results are presented and discussed in the following subsections.

4.5.1 Shrinkage Limits and Shrinkage Curve

Shrinkage limits of the mine tailings are presented in Table 4.1. The shrinkage curves of the mine tailings are shown in Figure 4.7. Based on the regression result, the shrinkage curves can be expressed as

$$[4\text{-}6] \quad e = a_4 w^2 + b_4 w + c_4$$

where e is the void ratio of the tailings, w is the gravimetric moisture content, and a_4, b_4 and c_4 are the fitting parameters. The regression parameters for the copper, gold, and coal tailings and CT are presented in Table 4.7. The fitting curves are shown in Figure 4.7.

4.5.2 Evaporation of Tailings

Figure 4.8 presents the normalized evaporation rate of the mine tailings. The normalized evaporation rate is the ratio of the actual evaporation rate of the tailings to the potential evaporation rate of the environment.

Figure 4.8 shows that the drying processes of the tailings can be identified as involving three stages: the rapid decrease stage, the transition stage, and the residual stage. In the rapid decrease stage, the normalized evaporation rate drops quickly to around 0.6 (0.64

for coal wash tailings and CT). Since the tailings surface desaturates as drying continues, the hydraulic conductivity of the surface decreases significantly, and, consequently, the actual evaporation rate of the tailings drops dramatically. In the transition stage, although the surface drying continues, the hydraulic conductivity of the surface layer decreases slowly, and, therefore, the evaporation rate eventually drops from around 0.6 to 0.2 for copper tailings, from 0.6 to 0.15 for gold tailings, from 0.64 to 0.52 for coal tailings, and from 0.64 to 0.6 for CT. In the residual stage, the surface layer is at the residual water content. The evaporation rate remains about 0.2 for copper tailings, 0.15 for gold tailings, 0.52 for coal wash tailings, and 0.6 for CT. The time ranges and residual values of the normalized evaporation rate are summarized in Table 4.8.

Based on the column drying test results, the normalized evaporation rate can be expressed as (Qiu and Sego 1998c):

$$[4\text{-}7] \quad E_n = \frac{E_A}{E_P} = A_r\left[\frac{1}{1+(\alpha t_s)^p}\right]^q + B_r$$

where E_n is the normalized evaporation rate, E_A is the actual evaporation rate of the tailings (cm/day), E_P is the potential evaporation rate of the environment (cm/day), A_r and B_r are positive constants related to the residual evaporation rate, α is a constant related to the air-entry value, p and q are positive constants related to the material properties, and t_s is drying time (day), $t_s \geq 1$. The regression parameters for the various tailings are shown in Table 4.9. Figure 4.9 shows the fitting curves of evaporation rate versus drying time.

4.5.3 Moisture Content of tailings

As a result of evaporation, the moisture content of the tailings changes with the drying time. Figure 4.10 shows the moisture content (*w*) of the upper 5 mm of the tailings surface changes with time. The figure indicates that the surfaces of the copper and gold tailings dried more rapidly than those of the coal tailings and CT, although the coal tailings dried rapidly at the beginning of the tests. This was mainly due to lower hydraulic conductivity in coal tailings and CT. The surface moisture content of the copper tailings decreased from 67 % to 40% within 5 days, and then gradually reduced to about 19% after 2 weeks of drying. The gold tailings dried even faster than the copper tailings, their surface moisture content dropped from 46.6% to 28.8% during the first drying day, and then gradually decreased to about 19% after 2 weeks. After 3 weeks, their moisture content remained around 13%. The coal tailings dried more slowly than the copper and gold tailings, as illustrated by the moisture content slowly decreasing to 26.9% after 5 weeks. After 6 weeks of drying, their surface moisture content remained about 15%. The CT dried the slowest of all the tailings samples. This was due to the presence of bitumen on the surface of the CT. The surface moisture content of the CT slowly decreased from 69.2% to 57% during the first 3 weeks. After the third week, their moisture content decreased rapidly from 57% to 22.9% over the next week. Finally, the moisture content stabilized at around 1% after 8 weeks of drying. The increase in the surface moisture content for the CT during the first week was due to measurement errors.

Figures 4.11 to 4.14 show the moisture profiles of various tailings during the different drying stages. For comparison, normalized depth, i.e. the depth of measurement divided by the total height of the specimen was used. The plots indicate that before drying, the moisture profiles of the different tailings had a similar shape, i.e., due to self-weight consolidation, the lower 2/3 portion of the specimen had a roughly consistent moisture content and a lower value than the top 1/3 portion. After drying for one week, the moisture contents of the upper 1/3 of all tailings but CT were lower than those of the rest of the portions due to drying effects. The moisture contents at the bottom of the copper and gold tailings decreased significantly after one week of drying. However, no large changes occurred in the moisture content at the bottom of the coal and CT tailings. After 21 days of drying, the moisture content in the copper tailings along the whole depth was the same. The gold tailings showed the same trend as the copper tailings. After 35 days of drying, the specimen had a uniform moisture content. After 37 days of drying, the coal tailings had a uniform moisture content with a value of about 30%, and they had a uniform moisture content after 65 day drying with a value of about 22%.

The CT had a different drying behavior from the other tailings. During 21 days of drying, the upper 1/3 portion of the specimen had a higher moisture content than the rest of the samples. After 35 days of drying, the situation was reversed, i.e. the upper 1/3 portion of the specimen had lower moisture contents. Finally, after 71 days of drying, the moisture content of the CT was at 1% near the surface and 28% at the bottom of the sample.

4.5.4 Shrinkage and Cracking of tailings

The volume decrease of each specimen was due to consolidation and desiccation. Figure 4.15 shows the specimen height change with drying time for the different tailings. The plots indicate that the copper and gold tailings had similar changes in height, while the coal tailings and CT had similar change in height. The height changes of the copper and gold tailings were small and mainly caused by consolidation. The final heights of both the copper and gold tailings stabilized at a value of about 46.6cm. However, the height changes of the coal tailings and CT were much greater than those of the copper and gold tailings and the decrease continued over a longer time. The main reason was the presence of the clay mineral in the coal tailings and CT. After extended drying, the heights of the specimens remained at 38 cm for the coal tailings and 35 cm for the CT.

With the specimen surface drying out, shrinkage of the tailings surface occurs, and, consequently cracks appear on the surfaces of the specimens. Based on the observation, almost all cracks were along the perimeters of the surfaces. The cracks on the surfaces of the tailings appeared after 3 days of drying for the copper tailings, 5 days of drying for the gold tailings, 7 days of drying for the coal tailings, and 10 days of drying for the CT.

4.6 SHEAR STRENGTH

To determine the effective shear strength parameters of the tailings, consolidated undrained compression triaxial tests were carried out in the soil mechanics laboratory of the University of Alberta.

Figure 4.16 shows the deviator stress versus strain relationships, while the corresponding relationship between the pore water pressure and strain is presented in Figure 4.17. The effective stress strength parameters were determined based on the Mohr circles. The interpreted results are presented in Table 4.10.

The values of shear strength parameters c' and ϕ' and Atterberg limits indicate that the copper, gold, and oil sand CT tailings behaved as cohesionless soils, while the coal tailings are characterized as cohesive soils. Furthermore, Figure 4.16 shows that the copper and gold tailings both have slight strain weakening characteristics and behave like dense sandy soils, while the coal tailings and CT have strain hardening characteristics. From the pore pressure change (Figure 4.17), the deviator stress changes can be explained. For the copper and gold tailings, their pore pressures increase continuously, thus resulting in the effective stresses decreasing, and consequently causing the deviator stresses to decrease after peak. For CT, however, the pore pressure change has a peak value, and the decrease of the pore pressure in the sample causes an increase in the effective stress and thus the increase in the deviator stress. The CT are different from the other cohesionless tailings such as the copper and gold tailings. This is due to the presence of the clay mineral and bitumen. For coal wash tailings, the pore pressure drops slowly from the peak, and therefore, the deviator stress increases slowly.

Based on the above discussion, it can be clearly seen that the sandy tailings can totally lose their effective stresses due to their pore pressure increases. In other words, the sandy tailings have the potential for both static and cyclic liquefaction failures. Most mineral mine tailings are sandy tailings. Therefore, methods to reduce pore pressure should be addressed in the design of the tailings facility or a good drainage system should be provided in the design to enhance the stability of the facility.

4.7 SUMMARY AND CONCLUSIONS

A series of laboratory tests were carried out to study the properties of mine tailings for sub-aerial deposition in arid regions. The basic physical and engineering properties related to the sub-aerial tailings disposal in arid regions were obtained. The information obtained from the tests can be used in the design of optimum deposition for sub-aerial tailings disposal in arid regions. The following conclusions are drawn from this study:

1. A linear relationship exists between the void ratio and the logarithmic scale of the effective stress for these tailings. The compression indexes are 0.09, 0.16, 0.38 and 0.27 for copper, gold, coal and CT tailings respectively. The saturated hydraulic conductivity of the tailings is related to their void ratio.
2. The desiccation behavior of the mine tailings can be observed in a controlled environment. The copper tailings and gold tailings dried more quickly than the coal tailings and CT. And the height change due to desiccation in the coal tailings and CT were greater than in the copper and gold tailings.
3. A shrinkage curve indicates the void ratio change behavior with moisture content. A non-linear relationship exists between the void ratio and moisture content. The relationship can be expressed in the form of a polynomial.
4. It is important to understand the tailings-water retention characteristics and to incorporate them into sub-aerial tailings deposition. With the pressure-plate extractor test and saturated salt solution desiccator test, the tailings-water retention curve over the entire suction range was measured.
5. The copper, gold and oil sand CT tailings are non-plastic cohesionless soils. They behave like sandy soils, except for the CT, which behaves unusually due to the presence of the bitumen. However, the coal wash tailings are plastic cohesive soils.

6. The copper and gold tailings behave as strain softening soils in undrained loading, while the coal tailings and CT exhibit strain hardening behavior.
7. It is important to address the pore pressure reduction in the design of a tailings facility.

Table 4.1 Basic properties of mine tailings

Tailings	Copper	Gold	Coal	CT
Specific Gravity, Gs	2.75	3.17	1.94	2.60
pH value in process water	7.8	9.7	7.2	7.7
Liquid limit (%)	----	----	40	----
Plasticity index (%)	----	----	16	----
Shrinkage limit (%)	24.4	21.6	21.1	25.2
Clay size particles(< 2μm), (%)	1.3	5.3	22.5	8.9
Sand content (>0.06mm), (%)	74.5	33.3	40	77
Fines content (<74 μm), (%)*	31.3	81.3	66.4	21.2
D_{10} (μm)	16.28	5.0	1.31	2.7
D_{30} (μm)	72.25	19.0	4.13	11.2
D_{50} (μm)	120.6	44.8	29.2	182
D_{60} (μm)	153.5	54.0	60.0	204
D_{100} (μm)	2000	840	2000	2000
Unified Soil Classification	SM	ML	CL	SM

Note: fines are referred to the particle size less than 45 μm for CT.

Table 4.2 Consolidation parameters and saturated hydraulic conductivity

Consolidation Stress, σ' (kPa)		0.5	2	4	10	20	50	100
Copper Tailings	e	0.95	0.89	0.86	0.83	0.81	0.77	0.72
	c_v		22	70	104	99	85	58
	m_v	18.6	19.8	6.4	2.9	1.2	0.7	0.6
	k ($\times 10^{-5}$)	9.8	8.9	8.6	7.2	6.0	5.3	4.5
Gold Tailings	e	1.03	0.99	0.84	0.79	0.76	0.72	0.69
	c_v		80	14	43	33	49	45
	m_v	162.5	13.4	36.8	4.8	1.6	0.8	0.3
	k ($\times 10^{-5}$)	6.7	5.5	4.1	3.5	3.3	2.9	2.7
Coal Wash Tailings	e	1.57	1.31	1.19	1.02	0.92	0.79	0.70
	c_v	2	3	5	5	9	11	17
	m_v	188.2	67.1	27.7	12.7	4.8	2.3	1.1
	k ($\times 10^{-6}$)	11.0	5.3	3.4	1.9	1.2	0.7	0.4
CT	e	1.14	0.84	0.75	0.65	0.59	0.53	0.48
	c_v		1	0.3	1	1	5	9
	m_v	379.9	92.9	25.3	9.7	3.3	1.3	0.6
	k ($\times 10^{-7}$)	6.3	5.0	4.6	2.6	2.5	2.4	2.2

Note: c_v is in m^2/year, m_v is in m^2/MN and k is in cm/s.

Table 4.3 Regression parameters of void ratio versus effective stress relation

Tailings	$e = a_1(\sigma')^{b_1}$			$e = a_3 \ln(\sigma') + b_3$		
	a_1	b_1	R^2	a_3	b_3	R^2
Copper	0.9233	-0.0491	0.98	-0.0409	0.9217	0.99
Gold	0.9803	-0.0806	0.95	-0.0684	0.9799	0.93
Coal	1.4444	-0.1536	0.99	-0.1646	1.4288	0.99
CT	0.9651	-0.1585	0.99	-0.1179	0.9674	0.94

Note: σ' is in kPa.

Table 4.4 Regression parameters of hydraulic conductivity versus void ratio

Tailings	$k = a_2 e^{b_2}$		
	a_2 (cm/s)	b_2	R^2
Copper	0.0001	3.0892	0.95
Gold	0.00006	2.172	0.99
Coal	0.000002	4.0686	0.99
CT	0.0000006	1.3754	0.91

Table 4.5 Soil-water retention characteristic data of tailings

Tailings Type	Air-Entry Value (kPa)	θ_r (%)	Boundary Effect Stage (kPa)	Transition Stage (kPa)	Residual Stage (kPa)
Copper	5	3.4	< 5	>5 and <1500	> 1500
Gold	6	2.2	<6	>6 and <1500	> 1500
Coal	18	18	<18	>18 and <3900	> 3900
CT	6	6.2	< 6	>6 and <3900	> 3900

Note: θ_r is the residual volumetric water content.

Table 4.6 Fitting parameters for soil-water retention curves of the tailings

Tailings	$\theta(\psi)=C(\psi)\frac{\theta_s}{\left\{\ln\left[e+(\psi/a_0)^Q\right]\right\}^P}$				$w=\frac{w_s}{\left\{\ln\left[e+\left(\frac{h}{h_b}\right)^{n_1}\right]\right\}^{m_1}}$				
	a_0	P	Q	ψ_r	w_s	h_b	m_1	n_1	R^2
Copper	8.18	0.643	4.176	2203	0.332	0.510	0.94	1.587	0.98
Gold	18.87	0.943	1.489	2212	0.340	0.612	1.32	0.699	0.93
Coal	113.78	1.379	0.637	38793	0.543	1.835	1.041	0.643	0.98
CT	7	0.851	1.531	10000	0.287	0.612	1.035	1.055	0.98

Note: *e* is the natural number, i.e. *e*=2.71828, *h* and h_b is in m· H_2O.

Table 4.7 Fitting parameters for the shrinkage curves

Tailings	$e = a_4w^2 + b_4w + c_4$			
	a_4	b_4	c_4	R^2
Copper	4.726	-1.094	0.746	0.89
Gold	5.052	-0.787	0.734	0.96
Coal	2.560	-0.553	0.540	0.99
CT	2.782	-0.269	0.682	0.99

Table 4.8 Time ranges and residual values for normalized evaporation rate

Tailings	Fast-drop stage (day)	Transition stage (day)	Residual stage (day)	Residual rate (E_A/E_P)
Copper tailings	< 6	> 6 and < 20	> 20	0.16
Gold tailings	< 8	> 8 and < 17	>17	0.12
Coal tailings	< 4	> 5 and < 12	> 12	0.52
Oilsand CT	< 10	>10 and < 9	> 9	0.6

Table 4.9 Regression parameters of relative evaporation change

Tailings Type	$E_n = \frac{E_A}{E_P} = A_r\left[\frac{1}{1+(\alpha T)^p}\right]^q + B_r$					
	A_r	B_r	α	p	q	R^2
Copper	1.046	-0.03914	0.2	1.7834	0.48748	0.98
Gold	0.9717	-0.0517	0.167	2.7738	0.3945	0.98
Coal	0.4524	0.5542	0.056	3.2617	526.7815	0.94
CT	0.4614	0.5369	0.167	0.7137	1.4597	0.88

Table 4.10 Shear strength parameters of tailings

Tailings Type	Copper	Gold	Coal	CT
c' (kPa)	0	0	10	3
ϕ'	34°	33°	32°	30°

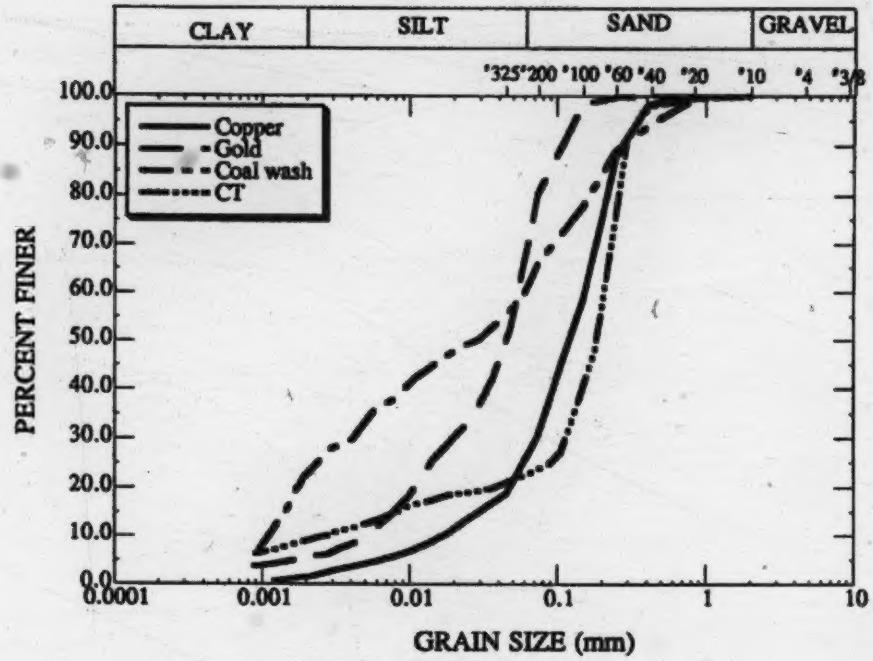

Figure 4.1 Tailings grain size distribution

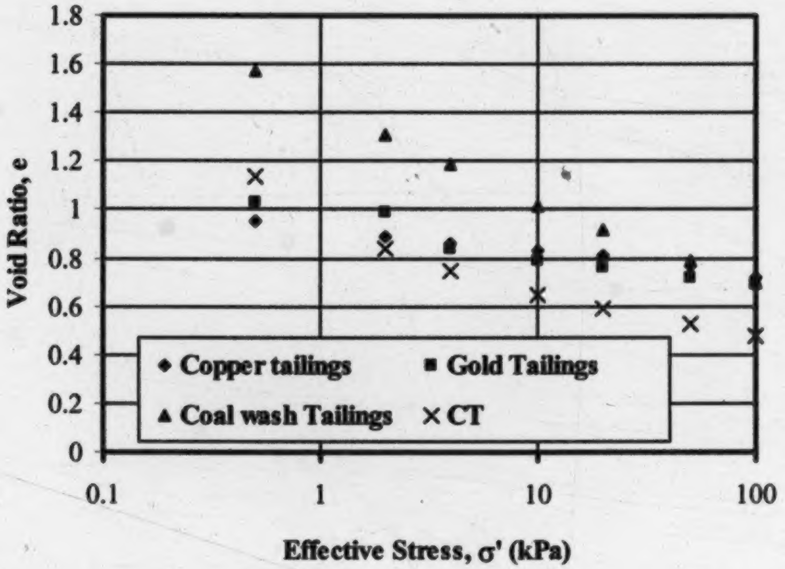

Figure 4.2 Compressibility of tailings

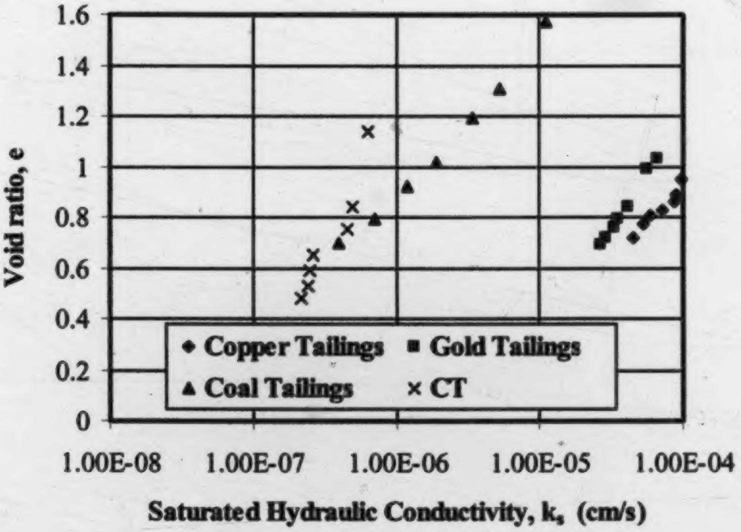

Figure 4.3 Void ratio versus hydraulic conductivity plots of tailings

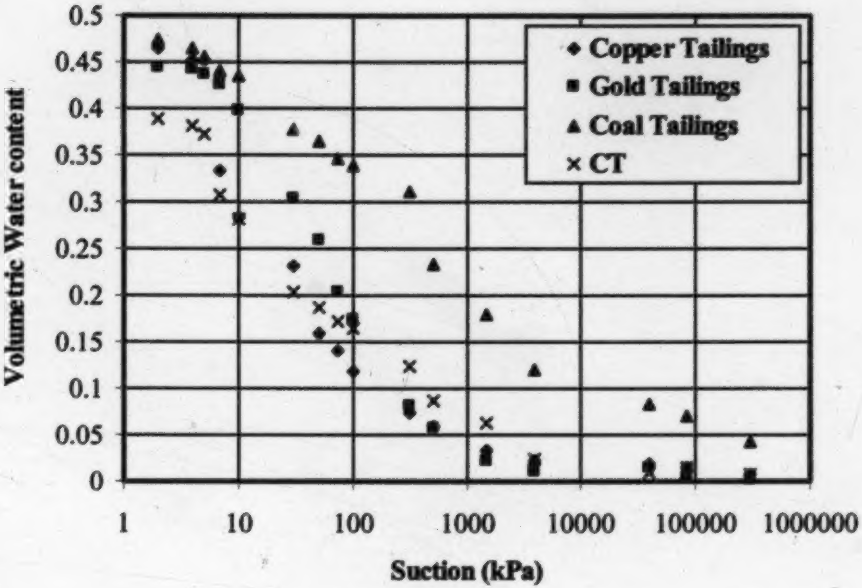

Figure 4.4 Soil-water retention curves of tailings

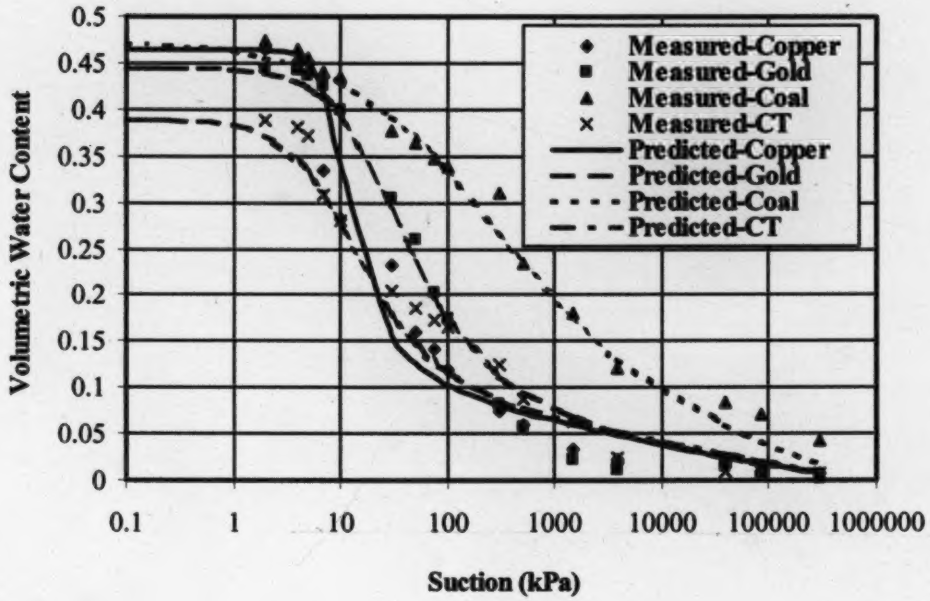

Figure 4.5 Measured and predicted soil-water retention curves of tailings

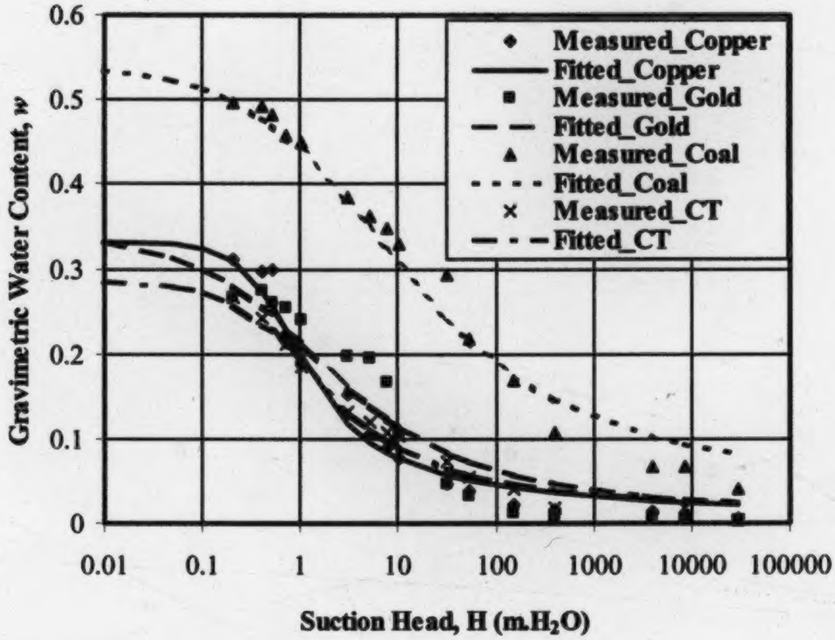

Figure 4.6 Measured and fitted water retention curves for tailings

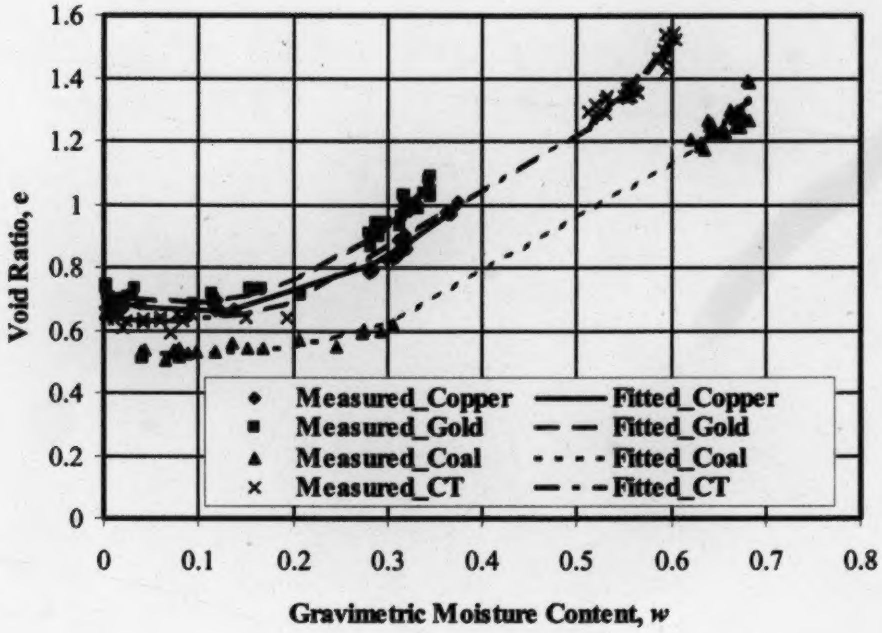

Figure 4.7 Shrinkage curves for mine tailings

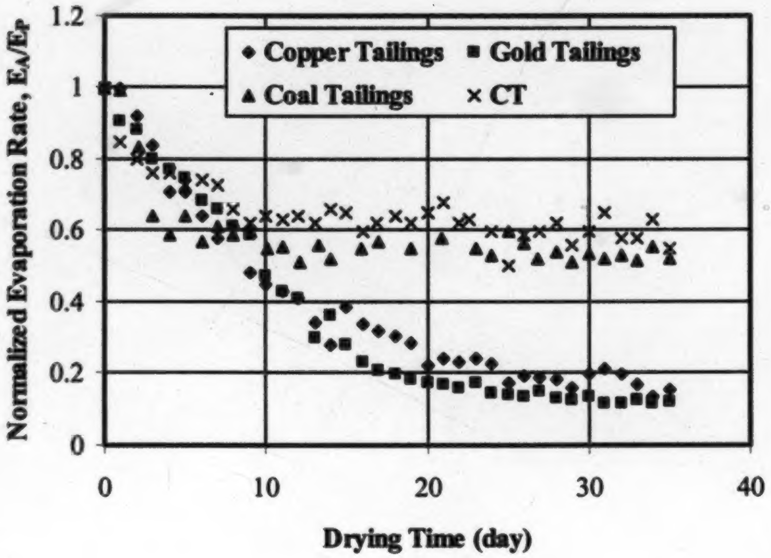

Figure 4.8 Normalized evaporation rate of mine tailings

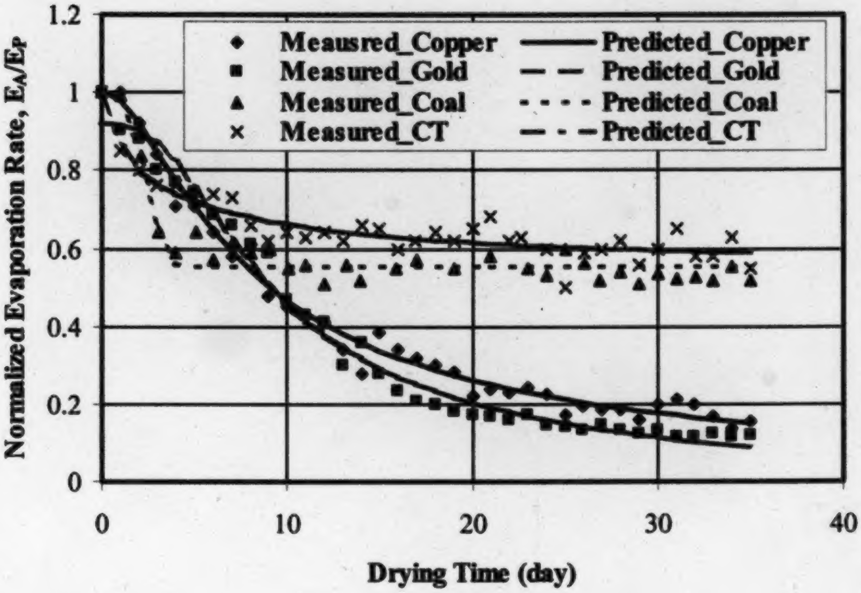

Figure 4.9 Comparison of measured and predicted evaporation of tailings

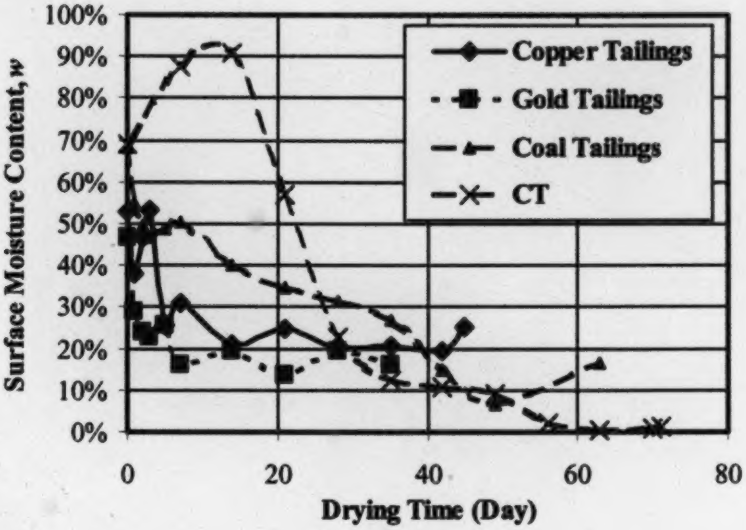

Figure 4.10 Moisture changes on the surface of the tailings

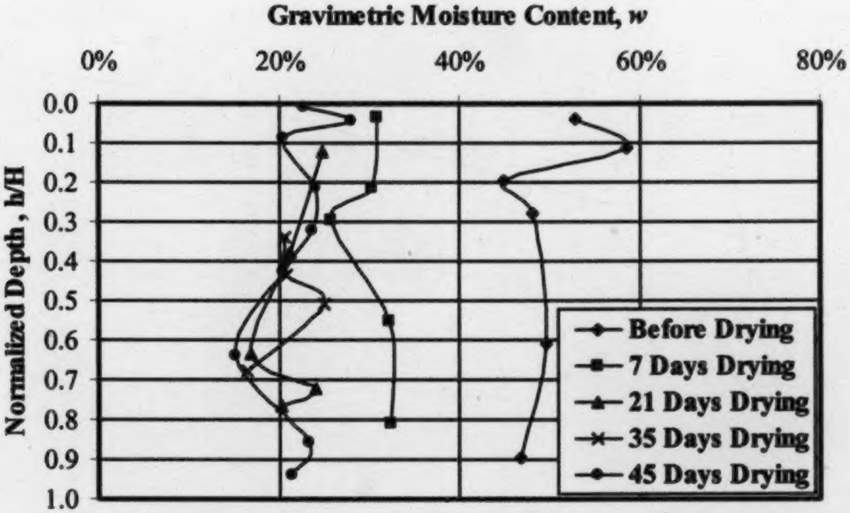

Figure 4.11 Moisture profile changes of copper tailings

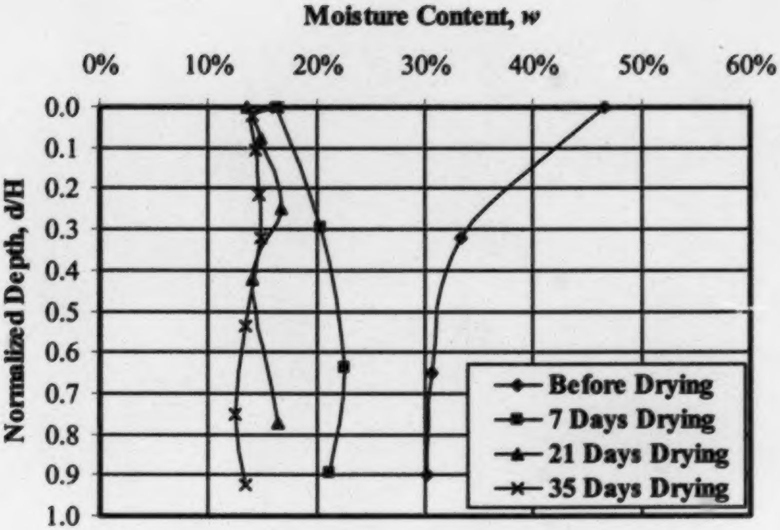

Figure 4.12 Moisture profile changes of gold tailings

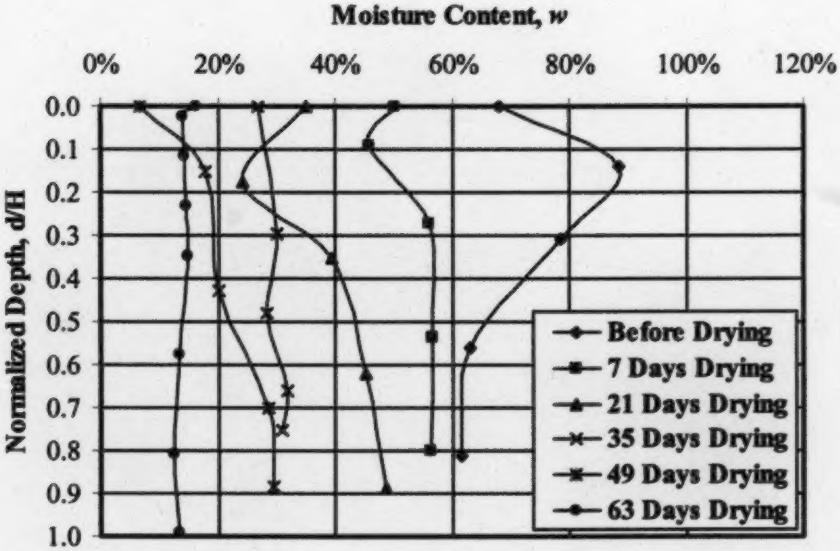

Figure 4.13 Moisture profile changes of coal tailings

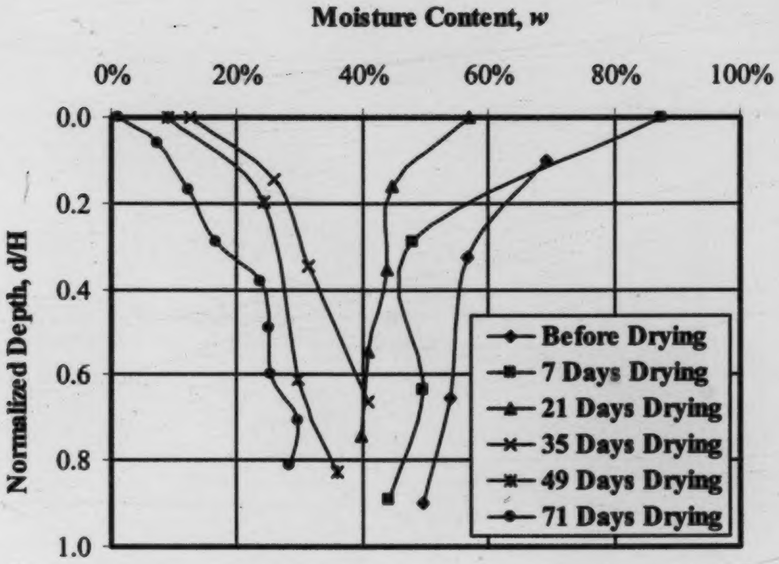

Figure 4.14 Moisture profile changes of CT

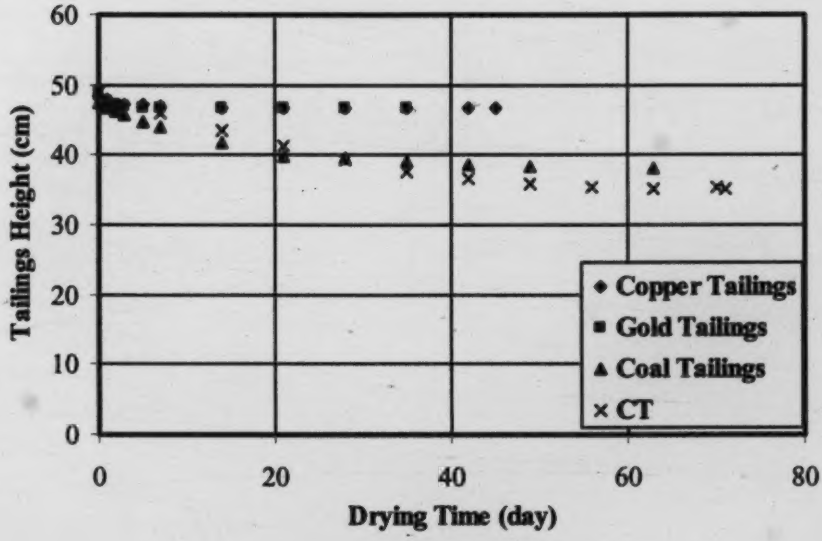

Figure 4.15 Specimen height changes of different tailings

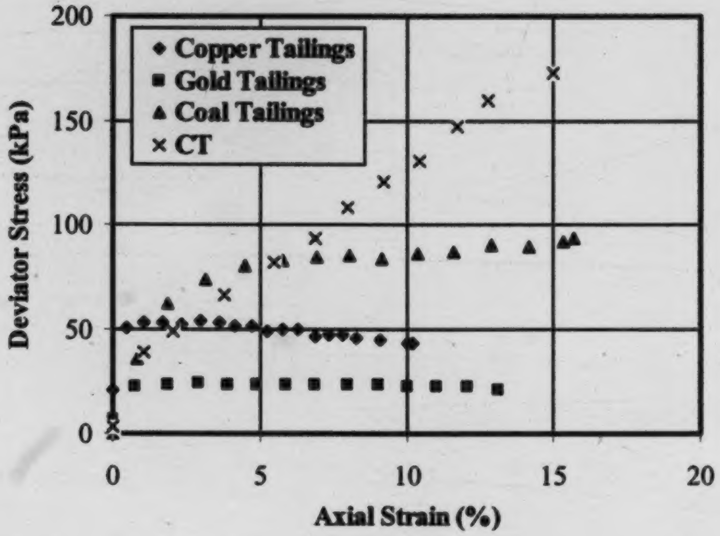

Figure 4.16 Deviator stress versus strain plot after 50 kPa consolidation

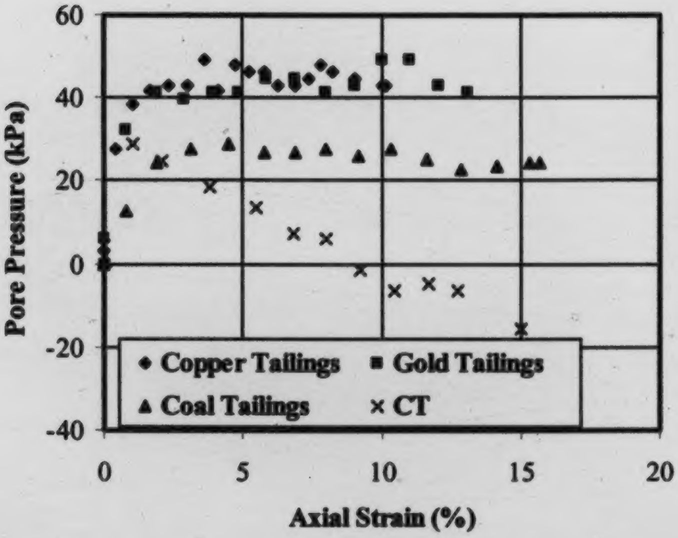

Figure 4.17 Pore pressure change versus strain plot after 50 kPa consolidation

CHAPTER 5 THEORIES OF SEDIMENTATION, CONSOLIDATION, AND DESICCATION

5.1 INTRODUCTION

As discussed in previous chapters, most mine tailings are transported to the impoundment in the form of a slurry. When the tailings are deposited hydraulically into the tailings pond, sedimentation and consolidation occur. The physical processes of sub-aerial tailings disposal after hydraulic deposition are sedimentation, consolidation, and desiccation. Therefore, to model the process of the sub-aerial tailings disposal, a unified theory is required. This chapter presents the development of the theoretical approach that links the three interrelated physical processes.

5.2 BACKGROUND AND COORDINATE SYSTEMS

Soil mechanics deals with both solid particles and fluids (air and water) which are moving with respect to each other. To describe the movement of the soil particles and fluids, two types of coordinate systems, the Eulerian system and the Lagrangian system, are useful. As shown in Figure 5.1, in the Eulerian system there is a box fixed in space through which both solids and fluids flow. Thus, the excess pore pressure in a consolidating soil layer is measured at a point which is specifically related to a fixed physical datum. Therefore, the distance from the datum to the piezometer is always supposed to remain the same. In the Lagrangian system (Figure 5.1(b)), there is also an elementary box, which in this case always contains the same amount of solids. If the solids are in motion, this box moves and only the fluid flows through the moving box.

Since the deformations in the sub-aerial tailings deposition are large compared with its layer thickness, the use of the Eulerian system can be inconvenient (Gibson et al. 1981). Developing the governing relationship of the nonlinear finite large strain consolidation theory is best accomplished using Lagrangian coordinates (Schiffman et al. 1988).

As shown in Figure 5.2, a layer of tailings has an initial configuration (Figure 5.2a). A tailings element with a unit area and a thickness of δa is considered ($A_0B_0C_0D_0$). The element has a Lagrangian coordinate a from the datum. After sedimentation or consolidation, the element has moved and deformed to a new element (ABCD), as shown in Figure 5.2b, while the datum plane remains fixed. The new element is at a new distance ξ from the datum plane. The distance ξ is a function of a and time t and is called the convective coordinate.

The sub-aerial deposited tailings layer has large displacements during consolidation. The usual use of Eulerian coordinates will lead to difficulties since the location of the surface of the tailings is not given and is part of the required solution. However, the volume of solids in the layer never changes. Thus, the special coordinate, named the solids coordinate z, has been introduced (McNabb 1960; Gibson et al. 1981; Swarbrick 1992). The solids coordinate z is defined as the volume of tailings particles per unit area lying between the datum plane and the point being analyzed, or height of solids particles lying between the datum plane and the point being analyzed.

The relationship between these coordinates is shown in Figure 5.3 and is expressed as:

$$[5\text{-}1] \quad z(a) = \int_0^a \frac{da}{1+e(a,0)}$$

or

$$[5\text{-}2] \quad \frac{dz}{da} = \frac{1}{1+e_0}$$

where e_0 is the void ratio at time t = 0.

And

[5-3] $$\xi(z,t)=\int_0^z[1+e(z,t)]dz$$

or

[5-4] $$\frac{\partial\xi}{\partial z}=1+e$$

The actual height of the tailings can be obtained from (Schiffman et al. 1988):

[5-5] $$h_\xi(z,t)=\int_0^{h_z(t)}[1+e(z,t)]dz$$

where $h_\xi(z,t)$ is the actual tailings thickness of the accumulating layer in terms of the momentary volume of solids, $h_z(t)$ at time t and e(z, t) is the void ratio of the tailings at a given time t.

5.3 GOVERNING EQUATIONS

To establish the theoretical formula for modelling sedimentation and consolidation, some assumptions are required: (1) the relationship between void ratio and effective stress is unique; (2) the relationship between pore pressure and saturation is unique; (3) the soil particles are incompressible; (4) the water flow is one dimensional.

Considering a tailings element ABCD with a thickness of $\partial\xi$ at some point in time t as shown in Figure 5.4, the governing equations can be derived based on the equilibrium and continuity of the mass of the tailings. (See Appendix C for details)

- The equilibrium of the tailings (solids and water) can be expressed as:

$$[5\text{-}6] \qquad \frac{\partial\sigma}{\partial a}+\frac{\partial\xi}{\partial a}\left(\theta\gamma_w+\frac{\gamma_s}{1+e}\right)=0$$

where σ is total stress, θ is the volumetric water content, γ_w is the unit weight of water, γ_s is the unit weight of the tailings particles, and e is the void ratio of the tailings.

- Continuity of the fluid phase can be expressed as:

$$[5\text{-}7] \qquad \frac{\partial}{\partial a}\left[\theta\gamma_w\left(v_w-v_s\right)\right]+\frac{\partial}{\partial t}\left[\frac{\partial\xi}{\partial a}\theta\gamma_w\right]=0$$

where v_w and v_s are the velocities of water and solids, respectively, and t is time.

- Continuity of the solids phase can be expressed as:

$$[5\text{-}8] \qquad \frac{\partial\xi}{\partial a}=\frac{(1+e)}{(1+e_0)}$$

where e_0 is initial slurry void ratio profile.

- Darcy's Law can be expressed as:

$$[5\text{-}9] \qquad \theta\left(v_w-v_s\right)=-k\left[\frac{\partial h}{\partial\xi}+1\right]$$

where h is the pore pressure head and k is the hydraulic conductivity.

Using equation [5-2], [5-4] and [5-8] to convert to the z coordinate leads to the following two governing equations as derived in Appendix C:

[5-10] $$\frac{\partial \sigma}{\partial z} + \gamma_w \left[\theta(1+e) + G_s\right] = 0$$

where G_s is the specific gravity of the tailings particles.

and

[5-11] $$\frac{\partial}{\partial z}\left\{\frac{k}{(1+e)}\left[\frac{\partial h}{\partial z} + (1+e)\right]\right\} = \frac{\partial\left[(1+e)\theta\right]}{\partial t}$$

The above theoretical formulas are similar to those presented by Swarbrick (1992).

These equations can be solved by numerical methods, e.g. the finite difference method, and can be programmed to model the sedimentation and saturated and unsaturated consolidation when different boundary conditions are applied.

5.4 SATURATED CONDITION

When the tailings are in a saturated condition, the principle of effective stress can be expressed as follows:

[5-12] $$\sigma' = \sigma - u_w$$

or

[5-13] $\sigma' = \sigma - \gamma_w h$

Differentiating equation [5-13] with respect to the reduced coordinate z,

[5-14] $$\frac{\partial \sigma'}{\partial z} = \frac{\partial \sigma}{\partial z} - \gamma_w \frac{\partial h}{\partial z}$$

Substituting equation [5-14] into equation [5-10],

[5-15] $$\frac{\partial \sigma'}{\partial z} + \gamma_w \frac{\partial h}{\partial z} + \gamma_w [\theta(1+e) + G_s] = 0$$

For the saturated condition, the following relation exists:

[5-16] $$\theta = \frac{e}{1+e}$$

Substituting [5-16] into [5-15] and rearranging gives

[5-17] $$\frac{\partial h}{\partial z} = -\frac{1}{\gamma_w} \frac{\partial \sigma'}{\partial z} - [e + G_s]$$

Substituting equation [5-16] into [5-11],

[5-18] $$\frac{\partial e}{\partial t} = \frac{\partial}{\partial z}\left[\frac{k}{1+e}\left\{\frac{\partial h}{\partial z} + (1+e)\right\}\right]$$

Substituting equation [5-17] into [5-18] results in the following expression:

[5-19] $$\frac{\partial e}{\partial t}=\frac{\partial}{\partial z}\left\{\frac{k}{(1+e)}\left[\left(-\frac{1}{\gamma_w}\frac{d\sigma'}{de}\right)\frac{\partial e}{\partial z}+(1-G_s)\right]\right\}$$

Equation [5-19] is the governing equation of the non-linear large strain consolidation theory first proposed by Gibson et al. (1967).

5.5 SEDIMENTATION

Solids particles in tailings slurry tend to settle under gravity due to the inability of the water to sustain shear stress. Over time, an initially uniform flocculation/suspension zone changes into three zones, i.e. supernatant, sedimentation and consolidation zones. In the sub-aerial deposition, the supernatant zone does not exist since the supernatant flows down to the pool area in the tailings area.

During sedimentation, the effective stress is zero:

[5-20] $$\frac{d\sigma'}{de}\approx 0$$

Equation [5-19], then, is reduced to:

[5-21] $$\frac{\partial e}{\partial t}=\frac{\partial}{\partial z}\left[\frac{k(1-G_s)}{1+e}\right]$$

5.6 UNSATURATED CONDITION

When tailings are in an unsaturated state, the two governing equations [5-10] and [5-11] have to be combined together and based on a single dependent variable, h. To do so, the total stress expression formula needs to be established.

In the reduced co-ordinate, z, the total weight of solids per unit area lying between the surface of the tailings and the z co-ordinate is (Figure 5.5):

[5-22] $$p_s = \gamma_s (H_z - z)$$

where p_s is the total weight of solids per unit area lying between the surface of the tailings and z co-ordinate, γ_s is the unit weight of the tailings particles, and H_z is the total height of the solids.

The total weight of water per unit area lying between the z co-ordinate and the surface is

[5-23] $$p_w = \gamma_w \int_z^{H_z} dV_w = \gamma_w \int_z^{H_z} \theta(1+e)dz$$

where p_w is the total weight of water per unit area lying between the surface of the tailings and the z co-ordinate.

Therefore, the total stress at any point z can be expressed as:

[5-24] $$\sigma(z) = p_s + p_w = \gamma_s (H_z - z) + \gamma_w \int_z^{H_z} \theta(1+e)dz$$

Bishop (1960) proposed an effective stress equation for unsaturated conditions as follows:

[5-25] $$\sigma' = \sigma - u_a - \chi(u_w - u_a)$$

where u_a is air pore pressure, u_w is water pore pressure, and χ is a parameter which equals unity for saturated soils and decreases with the degree of saturation.

If the air pore pressure, u_a, throughout the soil is assumed to be constant and at atmospheric pressure, u_a may be expressed relative to atmospheric pressure, i.e. $u_a = 0$. Thus, equation [5-25] becomes

[5-26] $$\sigma' = \sigma - \chi u_w = \sigma - \chi\gamma_w h$$

Substituting equation [5-24] into [5-26] gives:

[5-27] $$\sigma'(z) = \gamma_s(H_z - z) + \gamma_w \int_z^{H_z} \theta(1+e)dz - \chi\gamma_w h$$

Differentiating equation [5-27] with respect to time, t results in:

[5-28] $$\frac{\partial\sigma'}{\partial t} = \frac{\partial}{\partial t}[\gamma_s(H_z - z)] + \frac{\partial}{\partial t}\left[\gamma_w \int_z^{H_z} \theta(1+e)dz\right] - \frac{\partial}{\partial t}(\chi\gamma_w h)$$

In equation [5-28], because the volume of solids does not change over time:

[5-29] $$\frac{\partial}{\partial t}[\gamma_s(H_z - z)] = 0$$

Assuming that the total stress remains constant, the change in fluid volume may be neglected:

[5-30] $$\frac{\partial}{\partial t}\left[\gamma_w \int_z^{H_z} \theta(1+e)dz\right] \approx 0$$

Therefore, equation [5-28] is reduced to:

$$[5\text{-}31] \qquad \frac{\partial \sigma'}{\partial t} = -\frac{\partial}{\partial t}\{\chi \gamma_w h\} = -\gamma_w \left\{ h\frac{\partial \chi}{\partial t} + \chi \frac{\partial h}{\partial t} \right\}$$

Assuming $\frac{de}{d\sigma'}$ is a unique function, equation [5-31] multiplied by $\frac{de}{d\sigma'}$ gives:

$$[5\text{-}32] \qquad \frac{\partial \sigma'}{\partial t} \cdot \frac{de}{d\sigma'} = -\gamma_w \frac{de}{d\sigma'} \left\{ h\frac{\partial \chi}{\partial t} + \chi \frac{\partial h}{\partial t} \right\}$$

Rearranging [5-32] gives

$$[5\text{-}33] \qquad \frac{\partial e}{\partial t} = -\gamma_w \frac{de}{d\sigma'} \left[h\frac{d\chi}{dS}\frac{dS}{dh} + \chi \right] \frac{\partial h}{\partial t}$$

Equation [5-11] can be rewritten as

$$[5\text{-}34] \qquad e\frac{\partial S}{\partial t} + S\frac{\partial e}{\partial t} = \frac{\partial}{\partial z}\left[\frac{k}{1+e}\left\{ \frac{\partial h}{\partial z} + (1+e) \right\} \right]$$

Combining equation [5-34] and [5-33] results in the final governing relationship for unsaturated conditions:

$$[5\text{-}35] \qquad e\frac{dS}{dh}\frac{\partial h}{\partial t} - S\gamma_w \frac{de}{d\sigma'}\left[h\frac{d\chi}{dS}\frac{dS}{dh} + \chi \right]\frac{\partial h}{\partial t} = \frac{\partial}{\partial z}\left[\frac{k}{1+e}\left\{ \frac{\partial h}{\partial z} + (1+e) \right\} \right]$$

then

$$[5\text{-}36] \qquad \left[e\frac{dS}{dh} - S\gamma_w \frac{de}{d\sigma'}\left\{ h\frac{d\chi}{dS}\frac{dS}{dh} + \chi \right\} \right]\frac{\partial h}{\partial t} = \frac{\partial}{\partial z}\left[\frac{k}{1+e}\left\{ \frac{\partial h}{\partial z} + (1+e) \right\} \right]$$

Equation [5-36] can be rewritten as:

[5-37] $$f\frac{\partial h}{\partial t}=\frac{\partial}{\partial z}\left[g\left\{\frac{\partial h}{\partial z}+(1+e)\right\}\right]$$

or,

[5-38] $$f\frac{\partial h}{\partial t}=\frac{\partial g}{\partial z}\left\{\frac{\partial h}{\partial z}+(1+e)\right\}+g\left(\frac{\partial^2 h}{\partial z^2}+\frac{\partial e}{\partial z}\right)$$

with

[5-38a] $$f=f(h,e)=e\frac{dS}{dh}+S\cdot f_e$$

and

[5-38b] $$f_e=f_e(h,e)=-\gamma_w\frac{de}{d\sigma'}\left\{h\frac{d\chi}{dS}\frac{dS}{dh}+\chi\right\}\approx\frac{de}{dh}$$

and,

[5-38c] $$g=g(h,e)=\frac{k(S(h),e)}{1+e}$$

5.7 DEFINITION OF AUXILIARY CONDITIONS

In modelling the tailings deposition process, in addition to the governing equations, some auxiliary conditions are also required. There are three types of auxiliary conditions (Remson et al. 1971): (a) the system geometry, (b) the hydraulic characteristics of the system matrix, or system parameters, and (c) the initial and boundary conditions through out the depositional process.

5.7.1 System Geometry

The system geometry for this model is the whole tailings impoundment area. It can be divided into several deposition cells. In most situations, only a column of tailings with a unit area is considered in the model since all the water flows and deformation occurs in one dimension.

5.7.2 Hydraulic Conductivity of the Tailings

Hydraulic conductivity is one of the most important parameters which affects the behavior of the sub-aerial tailings disposal. During the disposal process, the tailings first undergo sedimentation, then they undergo self-weight consolidation, and, finally, they dry due to desiccation. They change from a saturated to an unsaturated state. Therefore, the hydraulic conductivity changes dramatically, and these changes must be incorporated into the model.

5.7.2.1 Saturated hydraulic conductivity

Based upon the laboratory results, the saturated hydraulic conductivity of the tailings can be expressed using an exponential relationship with the void ratio (Qiu and Sego 1998c):

$$[5\text{-}39] \quad k = a_2 e^{b_2}$$

where a_2 and b_2 are constants and e is the void ratio (Table 4.4).

5.7.2.2 Unsaturated hydraulic conductivity

Due to desiccation and drying at the surface, the tailings will desaturate, and therefore the hydraulic conductivity decreases from the saturated value. Fredlund et al. (1994)

proposed a relationship for the hydraulic conductivity which depends on the suction versus moisture content curve for the tailings (i.e. the water retention curve):

$$[5\text{-}40] \qquad k(\psi) = k_s \frac{\int_{\ln(\psi)}^{b} \frac{\theta(e^y) - \theta(\psi)}{e^y} \theta'(e^y) dy}{\int_{\ln(\psi_{aev})}^{b} \frac{\theta(e^y) - \theta_s}{e^y} \theta'(e^y) dy}$$

where $k(\psi)$ is the hydraulic conductivity of the unsaturated soil, k_s is the saturated hydraulic conductivity of the soil, b equals $\ln(10^6)$, e is the natural number (2.71828), y is a dummy variable of integration representing the logarithm of suction, θ is the volumetric water content of the soil, θ_s is the saturated water content , θ' is the derivative of θ function, and ψ_{aev} is the air-entry value of the tailings under consideration.

5.7.2.3 Hydraulic conductivity in the cracked layer

Once the desiccation cracks progress through the tailings layer, the hydraulic conductivity is dominated by the cracks. Assuming that there is no fill in the cracks, i.e. a crack width $\upsilon \leq D_{100}$, D_{100} is the grain size for which 100% of the particles pass by weight, then the coefficient of the hydraulic conductivity of the cracked layer can be expressed as (Lee et al. 1983):

$$[5\text{-}41] \qquad k_c = \frac{\upsilon^3 g}{12 \nu_1 B}$$

where k_c is the coefficient of the hydraulic conductivity of the cracked layer (m/sec), υ is the width of the cracks (m), B is the spacing of the cracks (m), g is the gravitational constant (9.81 m/sec^2), ν_1 is the kinematic viscosity of water = η/ρ_w, η is the viscosity of water (10^{-6} kPa.sec at 20°C) and ρ_w is the density of water (Mg/m^3).

If $\upsilon > D_{100}$, the freshly placed tailings will infill the cracks and the hydraulic conductivity of the cracked layer changes to (Lee et al. 1983)

$$[5\text{-}42] \quad k_e = k_d\left(1-\frac{\upsilon}{B}\right)+k_0\left(\frac{\upsilon}{B}\right)$$

where k_d is the hydraulic conductivity of the non-cracked portion of the dried tailings and k_0 is the hydraulic conductivity of the fresh tailings which infill the cracks.

5.7.3 Compressibility of the Tailings

The consolidation characteristics of the tailings can be evaluated from the laboratory tests carried out on them. It is necessary to obtain data such as compressibility for purposes of consolidation analysis. Furthermore, for modelling consolidation, the relationship between void ratio and effective stress is important. Based on the tests carried out in this study, the relationship can be expressed as (Qiu and Sego 1998c):

$$[5\text{-}43] \quad e = a_1(\sigma')^{b_1}$$

where e is void ratio, σ_v' is the vertical effective stress, and a_1 and b_1 are constants (Table 4.3).

5.7.4 Tailings-Water Retention Curve

The tailings-water retention curve is the relation between suction within the tailings and volumetric water content of the tailings. Fredlund and Xing (1994) proposed a general equation to describe the tailings-water curve as follows:

$$[5\text{-}44] \quad \theta(\psi) = C(\psi)\frac{\theta_s}{\left\{\ln\left[e + (\psi / a_0)^Q\right]\right\}^P}$$

with

$$[5\text{-}44a] \quad C(\psi) = 1 - \frac{\ln(1 + \psi / \psi_r)}{\ln[1 + 1000000 / \psi_r]}$$

where θ_s is the saturated volumetric water content, e is the natural number ($e = 2.718\ 28$), Ψ is the matric suction (kPa), a_0 is a soil parameter that is related to the air-entry value of a soil, Q is a parameter that controls the slope at the inflection point in the soil-water retention curve, P is a parameter that is related to the residual water content, and ψ_r is the suction corresponding to the residual water content. Figure 5.6 shows the comparison between measured and predicted data using Fredlund and Xing's model.

5.7.5 Evaporation of the tailings

Surface drying of deposited tailings is mainly due to evaporation in the absence of a vegetative cover. To evaluate the water balance in the sub-aerial tailings disposal, equations for estimating both the potential and actual evaporation rates are required.

5.7.5.1 Potential evaporation rate (E_p)

Chow et al. (1988) proposed an aerodynamic method to estimate the potential evaporation rate from a surface as:

$$[5\text{-}45] \quad E_p = \Gamma_1(P_{vs} - P_{va}) \qquad \text{(mm/day)}$$

where P_{vs} and P_{va} are the saturated and the actual vapour pressure respectively and Γ_1 is a parameter related to wind velocity.

5.7.5.2 Actual evaporation rate of tailings (E_A)

The actual evaporation rate of the deposited tailings decreases with time after a layer of tailings begins to dry from the surface downward. Qiu and Sego (1998c) proposed the following equation to account for the normalized evaporation rate (E_n) of the laboratory measured drying rate or the ratio of the actual evaporation rate to the potential evaporation rate (E_A/E_P):

$$[5\text{-}46] \quad E_n = \frac{E_A}{E_P} = A_r\left[\frac{1}{1+(\alpha t_s)^p}\right]^q + B_r$$

where A_r and B_r are positive constants related to the residual evaporation rate, α is a constant related to the air-entry value, p and q are the positive constants related to the material properties, and t_s is the drying time (day) (Table 4.6).

5.7.6 Effective Stress and Bishop Parameters

As defined in equation [5-25], Bishop's parameter χ equals 1 when the soil is fully saturated, and when it is in an unsaturated state, $0 \le \chi < 1$. Since χ is related to the degree of saturation, the parameter may be expressed as:

$$[5\text{-}47] \quad \chi = \frac{S - S_r}{1 - S_r}$$

where S_r is the residual degree of saturation of the tailings.

When tailings are fully saturated, based on equation [5-28], the effective stress at any time is

[5-48] $$\sigma'(z,t)=\gamma_s(H_z-z)+\gamma_w\int_z^{H_z}e(z,t)dz-\gamma_w h(z,t)$$

Once consolidation has finished, the pore pressure becomes purely hydrostatic, hence

[5-49] $$h(z,\infty)=\int_z^{H_z}[1+e(z,\infty)]dz$$

The effective stress then becomes

[5-50] $$\sigma'(z,\infty)=\gamma_w(G_s-1)(H_z-z)$$

5.7.7 Unsaturated Coefficient of Compressibility

Fredlund and Rahardjo (1993) proposed that void ratio and gravimetric water content can be used as the deformation state variables for the unsaturated soil structure and water phase respectively. The constitutive equations can be expressed as:

[5-51] $$de=a_t d(\sigma_{mean}-u_a)+a_m d(u_a-u_w)$$

where a_t is the coefficient of compressibility with respect to a change in net normal stress, $d(\sigma_{mean}-u_a)$, and a_m is the coefficient of compressibility with respect to a change in matric suction, $d(u_a-u_w)$.

[5-52] $$dw=b_t d(\sigma_{mean}-u_a)+b_m d(u_a-u_w)$$

where b_t is the coefficient of water content change with respect to a change in net normal stress, $d(\sigma_{mean} - u_a)$, and b_m is the coefficient of water content change with respect to a change in matric suction, $d(u_a - u_w)$.

Figure 5.7 visualizes the above equations as constitutive surfaces in three-dimensional space.

To solve the governing equation [5-38], the unsaturated coefficient of compressibility, $a_m = de/dh$, must be evaluated. Fredlund and Rahardjo (1993) pointed out that the a_m coefficient can be evaluated with the b_m coefficient and the shrinkage curve as shown in Figure 5.8. The slope of the shrinkage curve can be expressed as:

$$[5\text{-}53] \quad \frac{de}{dw} = \frac{\dfrac{\partial e}{\partial(u_a - u_w)}}{\dfrac{\partial w}{\partial(u_a - u_w)}} = \frac{a_m}{b_m}$$

Therefore, parameter f_e in equation [5-38] can be calculated as follows:

$$[5\text{-}54] \quad f_e \approx \frac{de}{dh} = \frac{de}{dw} \cdot \frac{dw}{dh} = b_m \frac{de}{dw}$$

where b_m is the slope of gravimetric water content versus suction and de/dw is the slope of the shrinkage curve.

5.7.8 Upper Boundary Conditions

5.7.8.1 Sedimentation

During sedimentation, the effective stress is assumed to be zero. Hence, from equation [5-21], a prescribed surface flux ($q_{z=H_z}$) condition is applied at the upper surface as follows:

$$[5\text{-}55] \qquad q_{z=H_z} = -\frac{k(1-G_s)}{1+e}$$

5.7.8.2 Consolidation

In the deposition analyses, it is required to determine when the consolidation begins, i.e. when the change from sedimentation to consolidation occurs. It is common that sedimentation is assumed to occur prior to the commencement of consolidation. Swarbrick (1992) assumed that the change from sedimentation to consolidation takes place when the upper surface void ratio no long changes with time, i.e. at the upper surface of the tailings, the following equation exists:

$$[5\text{-}56] \qquad \left.\frac{\partial e}{\partial t}\right|_{z=H_z} = 0$$

To determine the beginning of the consolidation, the changeover void ratio $e_{s\text{-}c}$ on the upper surface must be known. Before consolidation, the tailings remain saturated, so equation [5-19] is the governing equation.

Substituting [5-56] into [5-19] and rearranging yields:

$$[5\text{-}57] \quad \frac{d\sigma'}{de_{s-c}} \cdot \frac{\partial e_{s-c}}{\partial z} = \gamma_w (1 - G_s)$$

where e_{s-c} is the changeover void ratio on the upper surface.

Using numerical techniques, the changeover void ratio e_{s-c} can be obtained. The details of the numerical solution will be described in the section on numerical solutions. Once the surface void ratio reaches e_{s-c} it is held at this value until evaporation becomes the dominate boundary condition, i.e. the surface flux due to self-weight consolidation is less than the potential evaporation rate.

5.7.8.3 Desiccation

Tailings in the disposal facility desiccate due to evaporation. There are two stages of evaporation. During the first stage, the velocity of the water flowing out because of sedimentation and self-weight consolidation is larger than the potential evaporation rate. Therefore, during the first stage, the upper boundary flux is larger than or equal to the potential evaporation rate:

$$[5\text{-}58] \quad \text{Flux}_{z=Hz} = -\frac{k}{1+e}\left\{\frac{\partial h}{\partial z} + (1+e)\right\} \geq E_p$$

The second stage of evaporation occurs when the surface flux due to self-weight consolidation is less than the potential evaporation rate. In this stage, the evaporation rate is equal to actual evaporation rate, E_A:

$$[5\text{-}59] \quad -\frac{k}{1+e}\left\{\frac{\partial h}{\partial z} + (1+e)\right\} = E_A$$

Based on the test results, the actual evaporation rate can be expressed as equation [4-5]; hence, equation [5-55] becomes

$$[5\text{-}60] \qquad -\frac{k}{1+e}\left\{\frac{\partial h}{\partial z}+(1+e)\right\}=E_p\left\{A_r\left[\frac{1}{1+(\alpha t_s)^p}\right]^q+B_r\right\}$$

5.7.9 Lower Boundary Conditions

Generally, there are two types of lower boundary conditions. One is the impermeable boundary; the other is the permeable one.

5.7.9.1 The impermeable boundary

The impermeable boundary condition requires:

$$[5\text{-}61] \quad v_w = v_s$$

Substituting [5-61] into Darcy's law equation [5-9] gives

$$[5\text{-}62] \qquad -k\left[\frac{\partial h}{\partial \xi}+1\right]=0$$

Rearranging and substituting [5-4] gives

$$[5\text{-}63] \qquad \frac{\partial h}{\partial z}=-(1+e)$$

5.7.9.2 The permeable boundary

There is generally a bottom drainage system in the sub-aerial tailings disposal facility. Therefore, the boundary condition in the facility is a permeable one. If it is assumed that the lower boundary is not hindered by the foundation material, drained conditions apply, and the effective stress and void ratio are known. From equation [5-48], the effective stress at the lower boundary is

$$[5\text{-}64] \quad \sigma'(z=0,t)=\gamma_w(G_s-1)H_s$$

This condition applies during both sedimentation and saturated consolidation.

Under Equation [5-64], the lower boundary never desaturates. In reality, Because of the desiccation of the tailings due to gravity, the lower boundary may desaturate to the point that an equilibrium exists between gravitational forces and water retention forces resulting from suction within the tailings.

Since the bottom drainage can be considered as "free drainage," the lower boundary condition in this situation can be expressed as (Swarbrick 1992):

$$[5\text{-}65] \quad \frac{\partial h}{\partial z}\Big|_{z=0}=0$$

Based on Equation [5-58], the above equation implies that the lower boundary flux is

$$[5\text{-}66] \quad \mathrm{Flux}_{z=0}=-k$$

where k is the hydraulic of conductivity at the bottom.

5.7.10 Initial Conditions

The initial conditions within the tailings being deposited are needed. These conditions are the average initial void ratio e_0^{avg}, the initial placement height of tailings, H_0, and the initial unit weight of the tailings, γ_0.

5.8 NUMERICAL SOLUTION

Because it is difficult to find analytical solutions for the governing equations, a numerical method is used to find the solutions for the governing equations.

Numerical methods are among the most powerful tools for solving partial differential equations. Due to their simplicity and flexibility for non-linear problems, finite difference techniques have been traditionally used for solving problems of fluid flow in unsaturated porous media. Therefore, for the sub-aerial tailings deposition modelling, using the finite difference techniques to solve problems under one-dimensional conditions are adequate.

It has been stated that the best method for solving one-dimensional problems is probably the Douglas-Jones predictor-corrector method (Gilding 1983). It is assumed that the total solids height is H_z and total time is T. To apply the Douglas-Jones method (Douglas and Jones 1963) to equation [5-38], the solids height z ($0 \leq z \leq H_z$) is discretized into n portions of equal length, $\Delta z = H_z/R$. The point $z_i = i\Delta z$ denotes computational points for $i = 1, 2, 3 \ldots R$. The time t is discretized into N portions of equal length, $\Delta t = T/N$, $t_n = n\Delta t$. The numerical solution for h at point z_i and time t_n is denoted by h_i^n. The finite difference mesh for this case is shown in Figure 5.9.

The finite difference equation for the predictor step takes the form:

[5-67]

$$f_i^n \frac{h_i^{n+\frac{1}{2}} - h_i^n}{\frac{1}{2}\Delta t} = \left(\frac{g_{i+1}^n - g_{i-1}^n}{2\Delta z}\right)\left\{\frac{h_{i+1}^n - h_{i-1}^n}{2\Delta z} + \left(1 + e_i^n\right)\right\} + g_i^n\left[\frac{h_{i+1}^{n+\frac{1}{2}} - 2h_i^{n+\frac{1}{2}} + h_{i-1}^{n+\frac{1}{2}}}{(\Delta z)^2} + \frac{e_{i+1}^n - e_{i-1}^n}{2\Delta z}\right]$$

with

[5-67a] $f_i^n = f\left(h_i^n, e_i^n\right)$

and

[5-67b] $g_{i+1}^n = g(h_{i+1}^n, e_{i+1}^n)$

and

[5-67c] $g_{i-1}^n = g\left(h_{i-1}^n, e_{i-1}^n\right)$

The corrector equation follows the predictor with the form:

[5-68]
$$f_i^{n+\frac{1}{2}} \frac{h_i^{n+1} - h_i^n}{\Delta t} = \frac{g_{i+1}^{n+\frac{1}{2}} - g_{i-1}^{n+\frac{1}{2}}}{2\Delta z}\left\{\frac{h_{i+1}^{n+\frac{1}{2}} - h_{i-1}^{n+\frac{1}{2}}}{2\Delta z} + 1 + e_i^{n+\frac{1}{2}}\right\} +$$
$$+ g_i^{n+\frac{1}{2}}\left[\left(\frac{h_{i+1}^{n+1} - 2h_i^{n+1} + h_{i-1}^{n+1}}{2(\Delta z)^2} + \frac{h_{i+1}^n - 2h_i^n + h_{i-1}^n}{2(\Delta z)^2}\right) + \frac{e_{i+1}^{n+\frac{1}{2}} - e_{i-1}^{n+\frac{1}{2}}}{2\Delta z}\right]$$

with

[5-68a] $f_i^{n+\frac{1}{2}} = f\left(h_i^{n+\frac{1}{2}}, e_i^{n+\frac{1}{2}}\right)$

and

[5-68b] $$g_{i+1}^{n+\frac{1}{2}} = \frac{1}{2}\left[g\left(h_{i+1}^{n+1}, e_{i+1}^{n+1}\right) + g\left(h_{i+1}^{n}, e_{i+1}^{n}\right)\right]$$

[5-68c] $$g_{i}^{n+\frac{1}{2}} = \frac{1}{2}\left[g\left(h_{i}^{n+1}, e_{i}^{n+1}\right) + g\left(h_{i}^{n}, e_{i}^{n}\right)\right]$$

[5-68d] $$g_{i-1}^{n+\frac{1}{2}} = \frac{1}{2}\left[g\left(h_{i-1}^{n+1}, e_{i-1}^{n+1}\right) + g\left(h_{i-1}^{n}, e_{i-1}^{n}\right)\right]$$

From equation [5-38b], the $e_i^{n+\frac{1}{2}}$ can be calculated from:

[5-69] $$e_i^{n+\frac{1}{2}} = e_i^n + f_{ei}^n \cdot \left[h_i^{n+\frac{1}{2}} - h_i^n\right]$$

To determine e_{s-c} numerically, Equation [5-57] was expressed in the backward finite difference form:

[5-70] $$e_{s-c} = \frac{\Delta z \cdot \gamma_w \left(-G_s\right)}{\dfrac{d\sigma'}{de_{s-c}}} + e_{n-1}$$

where e_{s-c} and e_{n-1} are the void ratios at the upper surface node n and n-1 respectively.

This relationship should rapidly converge to a single value of e_{s-c} in the numerical modelling.

In the Douglas-Jones method, first, the predictor estimates the values of h at each spatial node i at the time step n + 1/2. The known values of h_i at the time n are adopted in all non-linear terms. Then the predicted values of $h_i^{n+1/2}$ and $e_i^{n+1/2}$ are used in the subsequent corrector to predict the values of h_i^{n+1}.

Equations [5-67] and [5-68] are general equations for internal nodal points, and can be reduced to the general form:

$$[5\text{-}71] \quad a_i h_{i-1} + b_i h_i + c_i h_{i+1} = d_i$$

Applying Equation [5-71] to each node in both the predictor and corrector results in the following systems of equations:

for the predictor:

$$[5\text{-}72] \quad a_i h_{i-1}^{n+\frac{1}{2}} + b_i h_i^{n+\frac{1}{2}} + c_i h_{i+1}^{n+\frac{1}{2}} = d_i \qquad i = 1, 2, \ldots R$$

for the corrector:

$$[5\text{-}73] \quad a_i h_{i-1}^{n+1} + b_i h_i^{n+1} + c_i h_{i+1}^{n+1} = d_i \qquad i = 1, 2, \ldots R\,.$$

Both equations [5-72] and [5-73] produce a tridiagonal matrix that is diagonally dominant and that can be solved efficiently by the Thomas algorithm (Gilding 1983; Von Rosenberg 1969).

From equation [5-38b], the e_i^{n+1} can be calculated from:

$$[5\text{-}74] \quad e_i^{n+1} = e_i^{n+\frac{1}{2}} + f_{ei}^{n+\frac{1}{2}} \cdot \left[h_i^{n+1} - h_i^{n+\frac{1}{2}} \right]$$

To solve the system of equations, the appropriate boundary conditions must be in the finite difference form, and imaginary nodes are introduced at $i = 0$ and $i = R+1$, as shown in Figure 5.10. With the imaginary boundary node terms a_0h_0 and $c_{n+1}h_{n+1}$ and the boundary conditions, one or both of the real boundary node terms a_1h_1 and c_nh_n can be eliminated. Then the Thomas algorithm is used to solve the remaining system of equations. Details about using the Douglas-Jones method can be found in Appendix C.

5.9 SUMMARY AND CONCLUSIONS

A unified theory was established to describe the sedimentation, consolidation, and desiccation of the sub-aerial deposited tailings. The boundary conditions were presented.

With the numerical method, i.e. the Douglas-Jones method adapted here, the governing equations can be solved. Therefore, the processes of the sub-aerial tailings deposition can be modelled.

The unsaturated coefficient of compressibility, $a_m = de/dh$ can be calculated using slopes of the shrinkage curve and tailings-water retention curve.

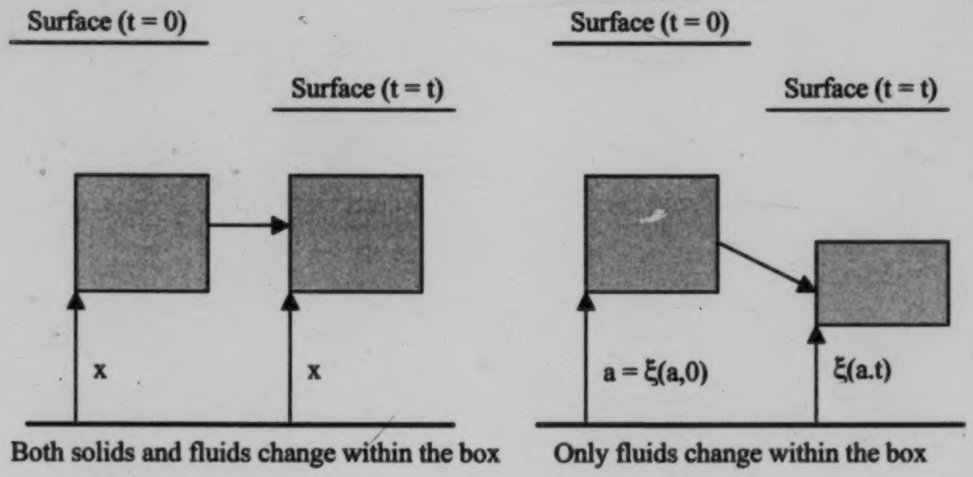
Surface (t = 0)
Surface (t = t)
x
x
Both solids and fluids change within the box
Surface (t = 0)
Surface (t = t)
a = ξ(a,0)
ξ(a.t)
Only fluids change within the box

(a) Eulerian system

(b) Lagrangian system

Figure 5.1 The Eulerian and Lagrangian coordinate systems (modified from Swarbrick 1992)

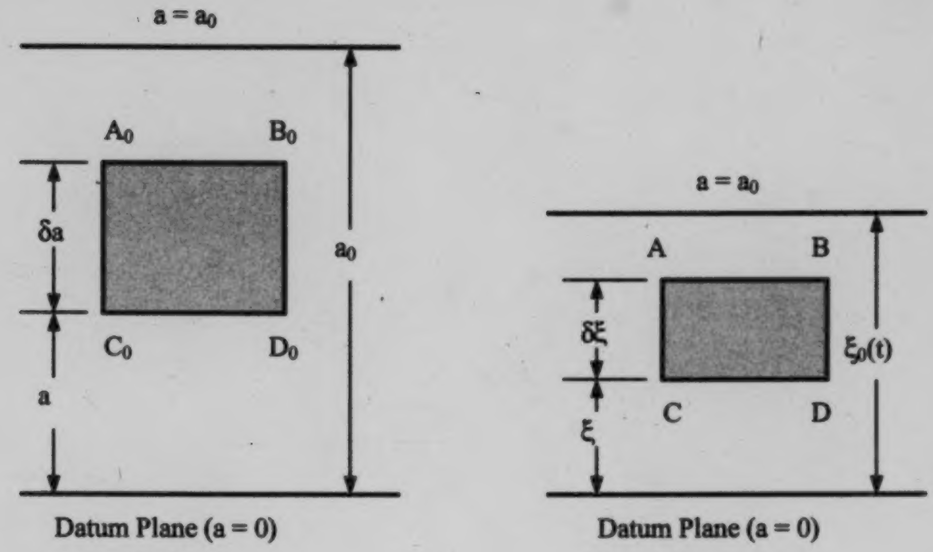
a = a_0
A_0
B_0
δa
a_0
C_0
D_0
a
Datum Plane (a = 0)
a = a_0
A
B
δξ
$\xi_0(t)$
C
D
ξ
Datum Plane (a = 0)

(a) Initial state (t = 0) (b) State at time t

Figure 5.2 Lagrangian and convective coordinates (modified from Gibson et al. 1967, 1981)

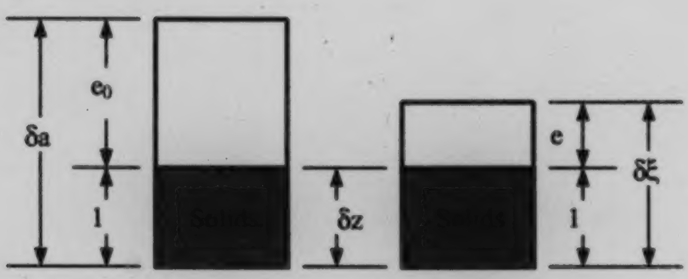
δa
e_0
1
Solids
δz
Solids
e
δξ
1

(a) Initial state (b) Consolidating state

Figure 5.3 Coordinate relationships and void ratio change (modified from Gibson et al. 1981; Schiffman et al. 1988)

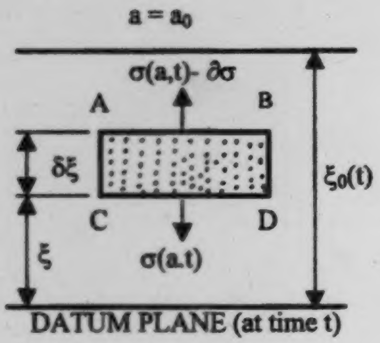
a = a_0
σ(a,t)- ∂σ
A
B
δξ
$\xi_0(t)$
C
D
ξ
σ(a.t)
DATUM PLANE (at time t)

Figure 5.4 Consideration of an element

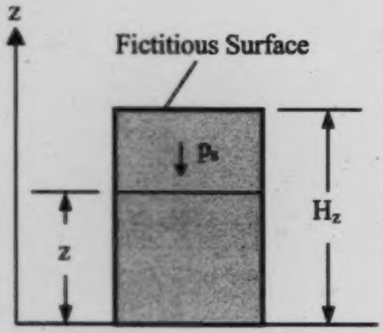
z
Fictitious Surface
p_s
H_z
z

Figure 5.5 Solids weight

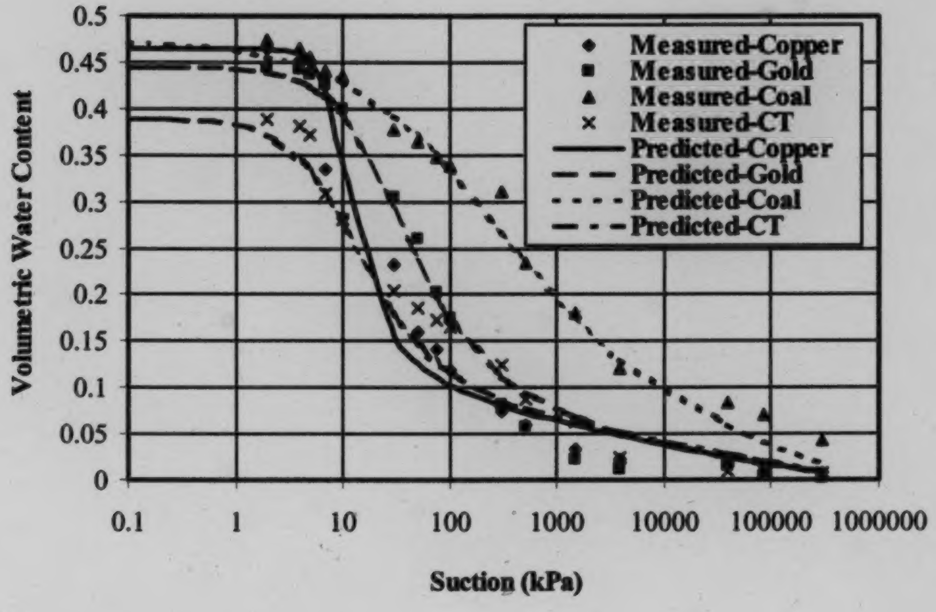

Figure 5.6 A comparison between the measured soil-water retention curves and those predicted by Fredlund's model

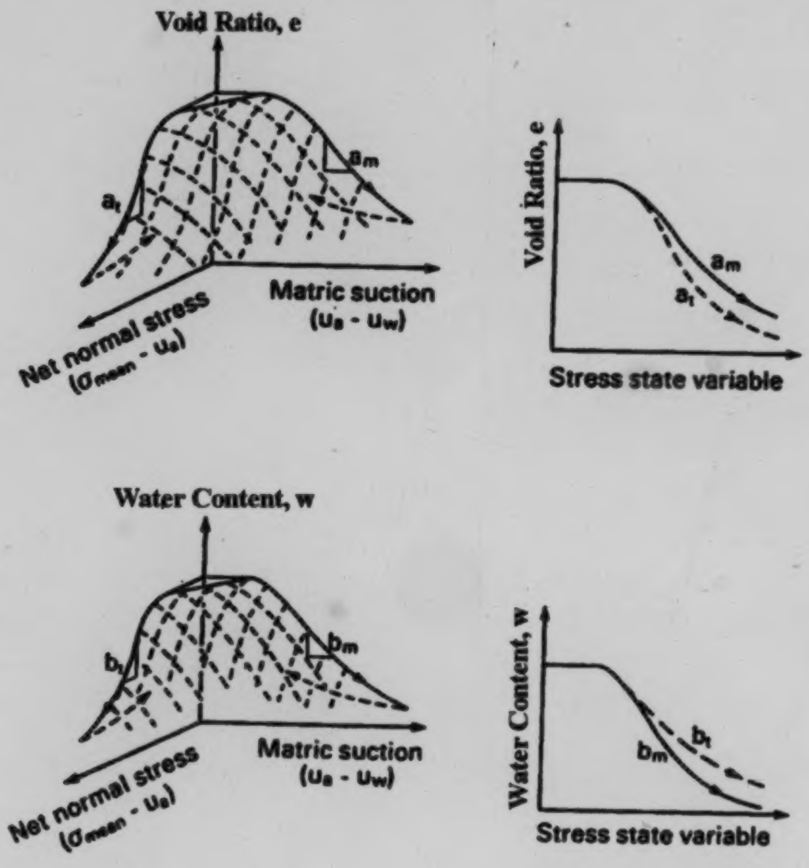
Void Ratio, e
a_t
a_m
Net normal stress
$(\sigma_{mean} - u_a)$
Matric suction
$(u_a - u_w)$
Void Ratio, e
a_m
a_t
Stress state variable
Water Content, w
b_t
b_m
Net normal stress
$(\sigma_{mean} - u_a)$
Matric suction
$(u_a - u_w)$
Water Content, w
b_t
b_m
Stress state variable

(a) Three-dimensional constitutive surfaces (b) Two-dimensional constitutive curve

Figure 5.7 Constitutive surfaces for an unsaturated soil (modified from Fredlund and Rahardjo 1993)

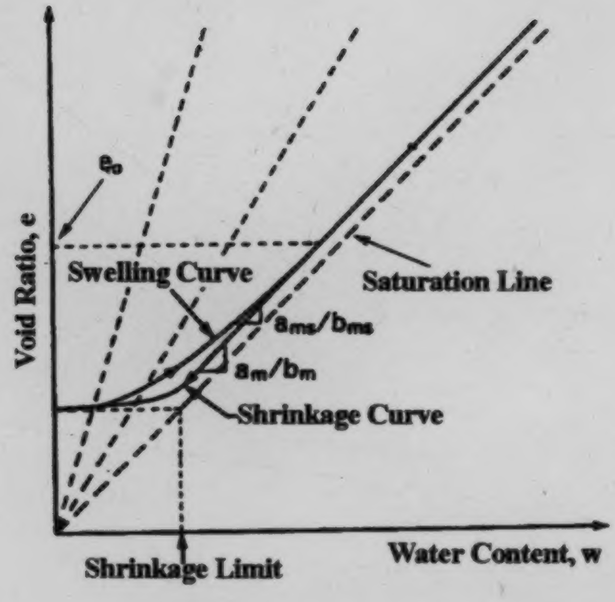

Figure 5.8 Typical shrinking and swelling curves for a soil (modified from Fredlund and Rahardjo 1993)

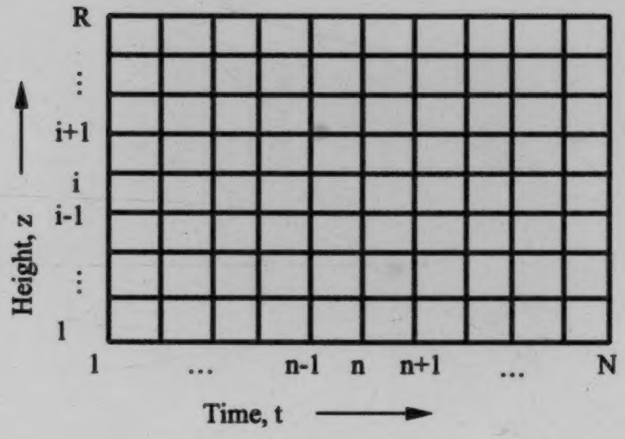
R
⋮
i+1
i
i-1
⋮
1
Height, z
1
...
n-1
n
n+1
...
N
Time, t

Figure 5.9 Finite difference mesh

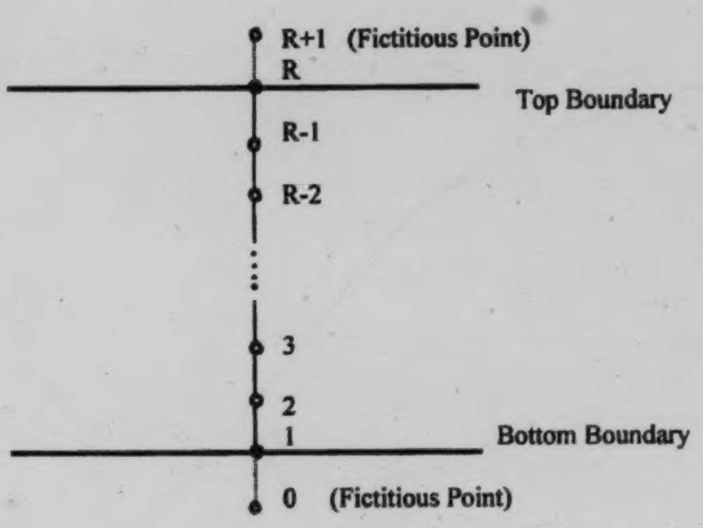
R+1 (Fictitious Point)
R
Top Boundary
R-1
R-2
3
2
1
Bottom Boundary
0 (Fictitious Point)

Figure 5.10 Boundary condition of the tailings deposition

CHAPTER 6 MODELING SUB-AERIAL TAILINGS DEPOSITION

6.1 INTRODUCTION

In the sub-aerial method, tailings are deposited cyclically at the same location in the tailings facilities. In general, mines produce tailings continuously and consequently generate a continuous discharge of tailings. To maintain continuous deposition using the sub-aerial method, the tailings impoundment is usually divided into several depositional cells to allow for continuous deposition of the tailings into different cells over time.

As described in Chapter 1, the objective of this research is to minimize the environmental impact, to reduce the volume of the tailings which must be stored, and to maximize the amount of the recyclable water for the extraction plant. This chapter will focus first on how to evaluate the water balance in sub-aerial tailings deposition and then analyze the factors influencing the optimum design of deposition. The criterion for the optimum deposition is presented along with the depositional schemes. The design model needed to evaluate these schemes is established and named "DOSTAR." Finally, the DOSTAR is coded in the Visual Basic computer language for implementation on a personal computer.

6.2 WATER BALANCE EVALUATION

In arid regions, the demand on the water resources is critical, and consequently, water recycling is an important issue faced by mine operators related to their tailings disposal. To evaluate the water balance in the sub-aerial deposition method, identification of all components of the water balance in the tailings facility are required. Some assumptions are made to simplify this identification: (1) the flow across the bottom seal beneath the tailings facility is negligible; (2) there is no surface runoff from outside of the facility onto the tailings surface; (3) there is no seepage through the containment dikes; (4) the infiltration into the dikes via the internal drain is negligible. The water balance components during the operation of the facility are as follows (Figure 6.1):

- Initial input water during tailings discharge (Q_1)
- Evaporation loss of water (Q_2)
- Drainage through the free drainage zone of the dike (Q_3)
- Drainage through the bottom sand filter blanket (Q_4)
- Discharge due to consolidation of the tailings (Q_5)
- Recyclable water from the drainage collection toe ditch (Q_6)
- Precipitation (rain or snow) (Q_7)
- Storage of water in the consolidated tailings layers (Q_8)

The amount of recyclable water per unit area can be determined using the following equation:

$$[6\text{-}1] \quad Q_6 = Q_3 + Q_4 = Q_1 + Q_7 - Q_2 - Q_8$$

The evaporation and the storage can be calculated using Equations [6-2] and [6-3] respectively:

$$[6\text{-}2] \quad Q_2 = \int_0^{t_d} E_A(t)dt$$

where $E_A(t)$ is the actual evaporation rate, it is a function of the time when the potential evaporation is constant, and t_d is the exposure time at the surface of the tailings facility.

$$[6\text{-}3] \quad Q_8 = \int_0^{H_f} \theta(1+e)dz$$

where H_z is the total height of the tailings solids at time t, $\theta(z, t)$ is the volumetric water content which can be obtained from the large strain consolidation model, and e is the void ratio.

6.3 FACTORS INFLUENCING THE OPTIMUM DESIGN

There are many factors affecting the optimum design of the sub-aerial method used to maximize the release water for recycling. The main factors are hydraulic conductivity (k), matric suction, drying (exposure) time, evaporation, and placement layer thickness.

6.3.1 Hydraulic Conductivity Versus Matric Suction

Hydraulic conductivity is very important to the successful application of the sub-aerial method. It affects not only drainage and consolidation but also the actual evaporation rate from the surface. The greater the hydraulic conductivity, the quicker that the consolidation of the tailings occurs. On the other hand, the higher the hydraulic conductivity, the greater the evaporation rate, and thus, the more water that is lost and the less that is available for recycling. This issue is critical for design in arid regions. As a result the larger the hydraulic conductivity, the better the disposal results from the consolidation point of view.

In the saturated state, the hydraulic conductivity of the tailings has an exponential relationship with its void ratio: the higher the void ratio, the higher the hydraulic conductivity.

In the unsaturated state, the matric suction created by the surface drying reduces the hydraulic conductivity dramatically once the air-entry value is reached. Therefore, limiting the suction that develops to a value smaller than the air-entry value can prevent a dramatic decrease in the hydraulic conductivity. However, when tension cracks propagate through the layer, the macro hydraulic conductivity due to cracking dominates the hydraulic conductivity of the layer and increases many orders of magnitude.

6.3.2 Crack Width and Crack Location

One of the features of sub-aerial tailings deposition is that there is a well designed downward drainage system. Therefore, the performance of the downward drainage directly influences the performance of the sub-aerial tailings disposal. To maintain good downward drainage performance, the vertical hydraulic conductivity within the layered tailings has to be as large as possible.

As discussed in the previous section, the hydraulic conductivity of the desiccating tailings decreases dramatically as they desaturate. Once the tailings crack, the macro hydraulic conductivity of the desiccating layer increases by many orders of magnitude. However, if the crack width is larger than D_{100} of the tailings, the cracks will be infilled by the fresh tailings. According to Equation [5-42], the hydraulic conductivity of the dried tailings with infilled cracks will be similar to the hydraulic conductivity of the non-cracked portion of the dried tailings. In other words, the hydraulic conductivity of the dried tailings with the infilled cracks is much smaller than the saturated hydraulic conductivity. Therefore, to take advantage of the macro hydraulic conductivity due to cracking, the crack width that develops must be properly managed during operation of the tailings disposal.

Since tailings are layered deposits, the location of the crack in the next layer is very important for the downward drainage system. As shown in Figure 6.2(a), when a fresh layer is deposited on the previously cracked layer, the downward drainage in the fresh layer takes place rapidly through the crack below. Hence, the portion right above the crack will consolidate and desiccate more quickly than anywhere else in the freshly deposited layer, and consequently, the suction in this part builds up more quickly. In addition, the tailings in the freshly deposited layer tend to contract due to their shrinkage during drying. The contraction is partially restrained by the friction between the upper layer and its sub-layer, and as a result tensile stresses are induced in the upper layer. Since the maximum friction force applies only on the contacted portion of the interface between the fresh layer and the previously cracked layer, this force tears the new layer apart at the non-contacted part, i.e. above the previous crack. Thus, a new crack is more likely to occur right above the previous crack as the dashed lines show in Figure 6.2 (a).

With the same deposition parameters and potential evaporation, the locations of the cracks within the upper layer should be directly above or close to those in the sub-layer. In this study, it was assumed that the cracks in the upper layer are located right above the cracks in its sub-layer, as shown in Figure 6.2(b).

6.3.3 Drying Time and Evaporation

The longer the exposure time, the more water that evaporates, and the greater the suction that develops, and consequently, the greater the decrease in the hydraulic conductivity. The dramatic decrease in the hydraulic conductivity due to development of high suction may result in horizontal flow channels being formed when the next fresh layer is deposited. However, once the suction increases sufficiently, tension cracks initiate and propagate through the layer. In this case, the macro hydraulic conductivity increases dramatically with little further decrease in void ratio.

Evaporation from the surface influences not only the amount of recyclable water available but also the magnitude of hydraulic conductivity within the deposit. The more water that evaporates from the surface, the more salt that is deposited on the tailings surface. This thin salt layer has the potential to block the upward water flow through it as the salt crust tends to seal the surface of the tailings deposit (Newson et al. 1996).

6.3.4 Layer Thickness

The thickness of each deposition layer is an important operating factor. The thinner the layer, the more rapid the desiccation of the tailings, and in turn, the more rapid the cracking of the tailings. This may cause wider cracks. Thus, a greater macro hydraulic conductivity is obtained if no infilling occurs. On the other hand, if the placement layer is too thick, it takes a long time to consolidate and then to desiccate and crack. The thick layer may cause smaller cracks, and cracks propagate through the layer with greater difficulty. Therefore, an optimum deposition layer thickness must exist under specific mine condition to achieve the best disposal results. This thickness will also change throughout the year as the climate varies with the seasons.

Combining all aspects discussed above, the optimum deposition parameters can be obtained for the particular criteria set by the mine owner or designer.

6.4 DESIGN CRITERION AND SCHEMES

In sub-aerial tailings deposition, since bottom drainage occurs, the best way to collect recyclable water is through downward drainage to the collection system. The design criterion for sub-aerial tailings deposition in arid regions is to maximize the amount of water available for recycling and tailings volume reduction combined with enhancing the stability of tailings facility, which in turn requires that a high hydraulic conductivity in each tailings layer be maintained.

As mentioned in the previous section, as tailings desiccation proceeds, the tailings desaturate. Therefore, the hydraulic conductivity decreases with a decrease in the saturation. Based on the design criterion, there are two optional design schemes. One is to keep the tailings fully saturated to maintain a higher saturated hydraulic conductivity. The other is to allow the tailings to desiccate to crack the layer and hence develop a macro hydraulic conductivity. Details about these two schemes are described in the following sections.

6.4.1 Optimum Design Scheme 1: Maintaining Full Saturation

In this scheme, all deposited layers should be placed to maintain full saturation. Thus, the hydraulic conductivity of the tailings is not affected by desaturation. As shown in Figure 6.3, the deposition procedure can be described as follows:

The first layer is deposited and allowed to dewater until the suction within the tailings at the surface reaches the air-entry value. Then the second layer is deposited and allowed to dewater until the suction within the tailings on its surface reaches the air-entry value, and then, the process of "the deposition and dewatering to the air-entry value mode of deposition" is repeated.

6.4.2 Optimum Design Scheme 2: Cracking Through a Deposited Layer

In this scheme, each new deposited layer is allowed to dewater and desiccate until tension cracks propagate through the layer. Based on knowledge of the hydraulic conductivity of cracks, the cracked tailings layer develops much higher hydraulic conductivity than the saturated layer. Consequently, it will enhance consolidation of the following deposited layer by facilitating downward drainage, and in turn, increase the recyclable amount of the processed water that flows downward to the subdrainage system. It is worth noting that the crack width at the surface should not be larger than about D_{100} of the tailings so that the crack will not become infilled by the next layer.

As illustrated in Figure 6.4, the deposition procedure in this scheme can be described as follows:

The first layer is deposited and allowed to dewater and desiccate until the primary tension cracks reach the bottom of the layer. Then the second layer is deposited on the first layer and allowed to dewater via downward flow and then to desiccate until the primary tension cracks reaches the bottom of the second layer. Next, the third layer is deposited on the second layer and the cycle is repeated. The cycle consists of "deposition-desiccation-cracking through the layer-deposition."

Schemes 1 and 2 were modeled and the predicted results are presented and compared to determine which scheme provides the greater amount of water for recycle and thus water conservation in Chapter 7.

6.5 ESTABLISHMENT OF THE DESIGN MODEL

The literature review indicates that a model for predicting the sub-aerial tailings disposal involving cracking in arid regions and finally leading to the optimum design is not presently available. In this section, a design model capable of predicting sedimentation, consolidation and desiccation, as well as crack initiation, propagation, tailings volume change and the amount of recyclable water is presented. Each component related to the desiccation cracks of this model is described in detail in the following sections.

6.5.1 Prediction of Crack Initiation

Lachenbruch (1962) pointed out that tension cracks initiate where the stresses exceed the material's tensile strength locally. Therefore, a crack initiates when the total lateral stress reaches the tensile strength of the tailings (Abu-Hedjleh 1993; Konrad and Ayad 1997):

$$[6\text{-}4] \quad \sigma_h = -\sigma_t$$

where σ_h is the lateral stress and σ_t is the tensile strength of the tailings.

With the progress of desiccation, the negative porewater pressure present in the tailings increases. The porewater pressure corresponding to the initiation of the tension crack, u_{cr}, depends on the tensile strength of the soil, its initial stress state, and the total and effective stress paths followed by a soil element at the surface during the consolidation-shrinkage process and the stress history of the soil (Abu-Hedjleh and Znidarcic 1995). In sub-aerial tailings deposition, the initial stresses at the surface equal zero. The total and effective stress paths of a surface element of the tailings are shown in Figure 6.5.

Initially, the stress state of a surface element of the tailings is at point "O". During desiccation, the water pressure becomes progressively negative, and the tailings consolidate under a condition of zero lateral strain. Under this situation, the total stress state moves along the $\sigma_1 = 0$ line while the effective stress state follows the K_{0nc} line. Surface cracks occur when the minor total stress $\sigma_3 = \sigma_h$ reaches the tensile strength of the tailings, σ_t (point F in Figure 6.5). Hence, the critical suction $\psi_{cr} = u_{cr}$ is given by the magnitute FF' in Figure 6.5. Equation [6-4] can be rewritten as:

[6-5] $$\left[\sigma'_h + u_{cr}\right] = -\sigma_t$$

then,

[6-6] $$\left[K_{0nc}\sigma'_v + \psi_{cr}\right] = -\sigma_t$$

then, equation [6-6] can be expressed as:

[6-7] $$K_{0nc}\sigma_v + \psi_{cr}\left(1 - K_{0nc}\right) = -\sigma_t$$

For normally consolidated soils, the coefficient of earth pressure at rest, K_{onc}, is usually related to the friction angle, ϕ', using the Jáky's equation (Jáky 1944; Hamouche et al. 1995):

[6-8] $K_{onc} = 1 - \sin\phi'$

Substituting it with $\sigma_v = 0$ into Equation [6-7] and reorganizing gives:

[6-9] $\psi_{cr} = -\dfrac{\sigma_t}{\sin\phi'}$

where, ψ_{cr} is the critical suction when the crack initiates, σ_t is the tensile strength of the tailings at that moment, and ϕ' the effective friction angle.

The tensile strength of the tailings under desiccation is hard to measure. The tensile strength σ_t could be evaluated using a relationship presented by Morris et al. (1992)

[6-10] $\sigma_t = 0.5\left[c' + (u_a - u_w)\tan\phi^b\right]$

where σ_t is the tensile strength of the tailings, c′ is the cohesion of the tailings, $(u_a - u_w)$ is the suction of the tailings and ϕ^b is the friction angle with respect to the matric suction, and $\phi^b = \phi' - 5°$ as recommended by Fredlund et al. (1978).

6.5.2 Prediction of Crack Propagation and Depth

After its initiation, the crack usually propagates downward. Assuming that the theory of the linear elastic fracture mechanics (LEFM) applies, then the ultimate length of the cracks can be calculated. According to the theory of LEFM, the ultimate crack depth, b, depends upon the tensile stress distribution applied on the sides of the crack and the value of the stress intensity factor, κ, which changes with crack length (Morris et al. 1992).

Lau (1987) and Morris et al. (1992) assumed that the distribution of suction with depth is either constant or decreases linearly with depth. But neither is true in most soils that undergo desiccation. It is more common to observe a transient nonlinear change of the suction profile. In sub-aerial tailings deposition, according to the suction profiles obtained from the model, the tensile stress distribution can be calculated. The lateral tensile stress σ_h at crack initiation at the tailings surface equals the tensile strength σ_t. Therefore, prior to crack initiation, the lateral total stress distribution in the tailings is characterized by a value of $\sigma_3 = -\sigma_t$ at the surface and $\sigma_3 = 0$ at a depth a as illustrated schematically in Figure 6.6. According to the LEFM, to calculate the depth of crack propagation at the time of initiation, it is necessary to calculate the stress intensity factor κ as a function of different crack lengths and further determine the value of the crack length b for which κ equals the soil's fracture toughness κ_c.

According to the theory of LEFM, the stress intensity factor κ corresponding to a crack in a semi-infinite medium can be expressed as:

$$[6\text{-}11] \quad \kappa = \lambda\sigma(b)^{0.5}$$

where λ is a coefficient depending upon the tensile stress distribution and on the ratio a/b, σ is the maximum value of the tensile stress, b is the crack length, and a is the depth of the tensile stress zone.

Assuming that the actual tensile stress distribution applied on the side of the crack can be approximated by a trapezoidal distribution as illustrated in Figure 6.7 (a), according to the superposition principle, this distribution can be considered as the superposition of a uniform distribution of σ_t (Figure 6.7(b)) and a triangular distribution with a maximum value of $(\sigma_t - \sigma_3(b))$ (Figure 6.7(c)). Thus, the stress intensity factor corresponding to the trapezoidal tensile stress distribution (κ_{trap}) can be obtained using:

$$[6\text{-}12] \quad \kappa_{trap} = \kappa_{unif} - \kappa_{tria}$$

where κ_{unif} and κ_{tria} are known stress intensity factors corresponding to a uniform and a triangular tensile stress distribution respectively.

The values of the stress intensity factor, κ, corresponding to various crack lengths are determined using the analytical solutions proposed by Lachenbruch (1961). The depth of crack propagation, b, at the time of crack initiation can be calculated using the following equation:

$$[6\text{-}13] \quad \kappa_{unif} - \kappa_{tria} = \kappa_c$$

where κ_c is the fracture toughness of tailings.

Based on Equation [6-11], Equation [6-13] can be expressed as

$$[6\text{-}14] \quad \lambda_1 \sigma_t \sqrt{b} - \lambda_2 [\sigma_t - \sigma_3(b)] \sqrt{b} = \kappa_c$$

For a tensile zone of given depth (a), two different cases must be considered in the determination of κ as a function of crack length (b). Case I corresponds to a crack length equal to or smaller than the extent of the tensile zone, i.e. $b \leq a$. In this case, according to Lachenbruch's (1961) solution, when $b = a$, $\lambda_1 = 1.12$ for the uniform tensile stress distribution, and $\lambda_2 = 0.68$ for the triangular distribution. Hence, equation [6-13] becomes

$$[6\text{-}15] \quad 1.12\sigma_t \sqrt{b} - 0.68[\sigma_t - \sigma_3(b)] \sqrt{b} = \kappa_c$$

where $\sigma_3(b)$ is the tensile stress at the depth of b at the initiation of the crack.
Rearranging [6-15] one obtains the expression for the crack depth (b) as:

$$[6\text{-}16] \quad b = \left[\frac{\kappa_c}{0.44\sigma_t + 0.68\sigma_3(b)} \right]^2 \qquad \text{(when } b = a\text{)}$$

Case II refers to a crack length larger than the depth of the tensile zone, i.e., $b > a$. The values of λ_1 and λ_2 can be obtained from Figure 2.12.

6.5.3 Prediction of Crack Spacing

When tailings are in the process of desiccation, the desiccation-induced suction increases to the critical suction level that leads to crack formation at various places on the tailings surface. After each crack reaches its ultimate depth (b), the tensile stress surrounding it will be reduced. Meanwhile, these cracks have to be distributed spatially so that the total lateral tensile stress over the entire tailings surface is reduced below the tensile strength of the tailings. Once the crack forms, the horizontal stress on the crack walls vanishes. This perturbation of the desiccation-induced stress field may be accounted for by superposition of a fictitious total normal stress with a value of $-\sigma_3$ distributed on the crack walls within the thickness of the tensile zone. When this perturbation stress is added to the existing stress field, the stress condition on the crack surfaces is satisfied (Lachenbruch 1961). The stress relief caused by the crack can be calculated using existing numerical methods, such as SIGMA/W and FLAC by considering the tailings as a linear elastic material. As shown in Figure 6.8, consider a vertical isolated crack in a semi-infinite medium for plane strain conditions with body condition (Konrad and Ayad 1997):

[6-17a] $\sigma_y^* = -\sigma_t \quad y = 0, x = 0$

[6-17b] $\sigma_y^* = 0 \quad y = 0, x = A$

[6-17c] $\sigma_x^*, \sigma_y^*, \tau_{xy}^* \rightarrow 0 \quad x, y \rightarrow \infty$

[6-17d] $\sigma_x^* = \tau_{xy}^* = 0 \quad x = 0$

[6-17e] $v^* = 0 \quad x = 0, y > b$

[6-17f] $w^* = 0 \quad \text{all } x, y$

where v^* and w^* are the displacements in the y and z direction, respectively.

Assuming that the second crack initiates at the point where the tensile stress equals 95% of the tensile strength, according to this assumption and the surface lateral stress relief, the crack spacing, B, can be determined as shown in Figure 6.8.

Based on the assumption for the tensile stress distribution, an alternative method can be used to calculate the crack spacing, i.e., Lachenbruch's calculated stress relief results for a semi-infinite medium (Lachenbruch 1961). Combining the results for both the step function and linear function, the relationships between surface tensile stress relief and distance from the crack (y) (Figure 6.8) under different ratios of the depth of the tensile stress zone (a) to the crack depth (b) are obtained, as shown in Table 6.1. Hence, the location of $0.95\sigma_t$ can be easily found, and in turn the spacing of the primary tensile cracks are obtained. Using Table 6.1 to determine the crack spacing is simple.

6.5.4 Prediction of Crack Width

Crack width must be evaluated to account for the effect of the cracks on the macro hydraulic conductivity. Consider an element with a width and length the same as the spacing of the crack as shown in Figure 6.9. Assuming that shrinkage of the tailings is isotropic, the total volume of the element at full saturation is

$$[6\text{-}18] \quad V_0 = B^2 D_0$$

where B is the spacing of cracks and D_0 is the layer thickness at full saturation.

Then the change in volume of this element is (Bronswijk 1989, 1991):

$$[6\text{-}19] \quad \Delta V = \left[1 - \left(1 - \frac{\Delta D}{D_0}\right)^r\right] \cdot V_0$$

where ΔV is the decrease in volume of the tailings matrix due to shrinkage, ΔD is the decrease in layer thickness due to shrinkage from the fully saturated state to when the crack propagates (the value can be obtained from the consolidation modeling), D_0 is the initial layer thickness before desaturation, V_0 is the initial volume of the tailings matrix before desaturation, and r is a geometry factor which determines the partition of total volume change over change in layer thickness and change in crack volume. The geometry factor, r, depends on sedimentation, moisture content and load, etc, for three-dimensional isotropic shrinkage: $r = 3$, for one-dimensional shrinkage: $r = 1$. In this research, it is assumed that the shrinkage of tailings is three-dimensionally isotropic, resulting in the use of $r = 3$.

The total crack volume is (Bronswijk 1989):

$$[6\text{-}20] \quad V_{cr} = \Delta V - \Delta D \cdot B^2$$

where V_{cr} is the total crack volume and B is the spacing of the cracks.

From Figure 6.9(b), the total crack volume can be expressed as

$$[6\text{-}21] \quad V_{cr} = 2b\upsilon B$$

where b is the crack depth and υ is the width of the crack.

Substituting [6-21] into [6-20] and rearranging yields:

$$[6\text{-}22] \quad \upsilon = \frac{\Delta V - \Delta D \cdot B^2}{2b \cdot B}$$

6.5.5 Calculation of Tailings Volume and Amount of Recyclable Water

Assuming the deposition area is constant, then the change in accumulated layer thickness represents the volume change of the tailings. Based on the definition of the solids coordinate z, the total height of the tailings, or the total volume of the tailings per unit area, can be calculated using the following equation (Shiffman et al. 1988):

$$[6\text{-}23] \quad H(t) = \int_{0}^{h_z(t)} [1 + e(z,t)]dz$$

where, H(t) is the total height of the tailings, or the total volume of the tailings per unit area, $h_z(t)$ is the total height of the solids at time t, or total volume of solids per unit area at time t, and e(z,t) is the void ratio at time t.

The amount of recyclable water can be calculated using equation [6-1]. In this model, the precipitation was ignored for simplification.

6.5.6 Slow Deposition

When the tailings are slowly deposited in the tailings facility, the effects of slow deposition should be considered in the model.

Since both pore pressure head h and void ratio e are functions of time t and solids coordinate z, and z is also a function of time t in the slow deposition, the partial derivative of the function h with respect to time t can be rewritten as:

$$[6\text{-}24] \quad \frac{\partial h(z,t)}{\partial t} = \frac{\partial h}{\partial z}\frac{\partial z}{\partial t} + \frac{\partial h}{\partial t}$$

To account for a moving boundary, a simple transformation to reduce the spatial coordinate to one that was independent of time and ranged from 0 to 1 was first introduced by Gibson

(1958). Hornberger and Remson (1970), Gilding (1983) and Swarbrick (1992) also used a similar approach to deal with the moving boundary. The principle of the approach is described as follows.

If it is assumed that the total height of solids at time t is given by ζ(t), then a new variable, x, can be defined as such x = z/ζ(t). Obviously, x is independent of time and it ranges from 0 to 1. Hence, equation [6-24] can be rewritten as:

$$[6\text{-}25] \quad \frac{\partial h(z,t)}{\partial t} = \frac{\partial h}{\partial x} \cdot \frac{x}{\zeta(t)} \cdot \frac{\partial \zeta}{\partial t} + \frac{\partial h}{\partial t}$$

Substituting equation [6-25] into the governing equation [5-37] yields:

$$[6\text{-}26] \quad f \cdot \zeta \frac{\partial h}{\partial t} = \frac{\partial}{\partial x}\left[\frac{g}{\zeta}\left\{\frac{\partial h}{\partial x} + \zeta(1+e)\right\}\right] - f \cdot x \cdot \frac{\partial h}{\partial x} \cdot \frac{d\zeta}{dt}$$

where f and g are the same as previously presented in section 5.6.

In the layered deposition, once the placement for the layer is finished, no deposition activity takes place until the next fresh layer is placed. Between depositions, the total solids height ζ is a constant; hence, $\frac{d\zeta}{dt} = 0$, therefore the governing equation [6-26] becomes

$$[6\text{-}27] \quad f \cdot \zeta \frac{\partial h}{\partial t} = \frac{\partial}{\partial x}\left[\frac{g}{\zeta}\left\{\frac{\partial h}{\partial x} + \zeta(1+e)\right\}\right]$$

Both equations [6-26] and [6-27] can be solved using numerical techniques which have been described in the Chapter 5.

6.5.7 Instantaneous Layered Deposition

When the time of tailings discharge is much shorter than the total elapsed time between each deposition cycle, the deposition process can be considered as an instantaneous deposition, i.e. the discharge time can be neglected. An expanding mesh was adopted to account for the newly deposited layer in the instantaneous layered deposition in the model. In other words, the same spatial interval as for the old layers was used to the discrete of the new layer, i.e. ΔZ is maintained at the same value, and the new spatial nodes were directly added into the model. The new layer undergoes the process from sedimentation to desiccation, while the older layers continue to consolidate.

In the optimum design scheme 2, the old layers desiccate and crack before a new layer is deposited. A high suction is thus built up at the surface of the tailings. When a new layer is deposited with the same layer thickness H_ξ, the maximum effective stress added to the previous layer is

$$[6\text{-}28] \quad \Delta\sigma' = \gamma' H_\xi$$

where γ' is the buoyant unit weight and H_ξ is the deposition layer thickness.

In the sub-aerial deposition, the tailings are hydraulically deposited as a thin layer. Based on Equation [6-28], $\Delta\sigma'$ is a small magnitude. On the other hand, the maximum pore pressure head, H_ξ, is much smaller than the suction head at the old layer surface (say, H_ξ= 0.1 m, suction head =2.4 m in the copper tailings). In addition, the drainage from the new layer goes through the cracks rather than through the desiccated parts of the old layer. Therefore, the suction is hard to eliminate, i.e. the suction change in the old layer due to the new deposition can be neglected. According to the constitutive relationship of the unsaturated soil as shown in Figure 6.10, after the new layer deposition, a small amount of matric suction $(u_a\text{-}u_w)$ decrease will not induce noticeable volume change. In addition, the volume change caused by a small change in net normal stress, $(\sigma\text{-}u_a)$, can also be neglected once the soil is highly desaturated. Therefore, the volumetric change of the old layer can be neglected.

In this study, it was assumed that there is no volume change in the old layer due to a new layer deposition and the resaturation of the old layer due to the fresh layer did not occur.

6.5.8 Cycle Deposition Parameters

As mentioned previously, continuous mining operation produces tailings continuously. To ensure that the sub-aerial tailings disposal facility operates properly, the impoundment facility has to be segmented and operated in a cyclical manner. In addition, parameters such as number of deposition cells, area, and deposition thickness and drying time should be carefully designed to optimize the deposition system.

Based on the chronological relationships, the required discharge time can be expressed as:

$$[6\text{-}29] \quad T_d = \frac{24H_\xi A_t \rho_0}{P_t N_c}$$

where, T_d is the discharge time in hours, H_ξ is the deposition layer thickness which can be obtained from the model in m, P_t is a given tailings production rate in tons per day (tpd), A_t is the total available deposition area of the facility in m^2, N_c is the total number of deposition cells, and ρ_0 is the original placement bulk density in Mg/m^3.

To maintain continuous deposition, the discharge time has to meet the following condition:

$$[6\text{-}30] \quad T_s = (N_c - 1)T_d$$

where T_s (in hours) is the drying time which can be obtained from the model.

If A_t, ρ_0, P_t, H_ξ and T_s are known, combining Equation [6-29] and [6-30], both T_d and N_c can be obtained as follows:

$$[6\text{-}31] \quad N_c = \frac{24H_\xi A_t \rho_0}{24H_\xi A_t \rho_0 - T_s P_t}$$

and

$$[6\text{-}32] \quad T_d = \frac{T_s}{N_c - 1}$$

Thus, the cycle time T_c is

$$[6\text{-}33] \quad T_c = T_d + T_s$$

If the total deposition area A_t is unknown, e.g. for a new design or for a design for a mine expansion, A_t can be obtained as follows:

$$[6\text{-}34] \quad A_t = \frac{T_s P_t N_c}{24H_\xi \rho_0 (N_c - 1)}$$

If M_c denotes the number of full cycles per year, then

$$[6\text{-}35] \quad M_c = \frac{365 \times 24}{T_c}$$

6.6 IMPLEMENTATION OF MODEL

The design model described in the previous sections is named "DOSTAR." It uses a unified sedimentation-unsaturated consolidation theory coupled with the linear elastic fracture mechanics (LEFM) theory and semi-empirical desiccation deformation theory to predict tailings behavior associated with the sub-aerial tailings disposal. DOSTAR not only can handle a variety of boundary and initial conditions but also can predict the initiation and the propagation of the desiccation crack and the dimensions of the crack formed.

The proposed model is illustrated in a simple flow chart presented in Figure 6.11. It consists of three main parts. The first contains a theoretical model of the one-dimensional transient fluid flow from the tailings under sedimentation, consolidation, and desiccation as described in the Chapter 5. The outputs from this part are the suction profile, water content profiles, and void ratio profiles with time. The flow chart for the first part can be found in Appendix C. The second part deals with prediction of the crack initiation, propagation, crack spacing as well as crack width. These are used to determine the macro hydraulic conductivity. The third part calculates the volume of the tailings and the amount of recyclable water available at the base of the facility.

To implement the model, it was coded using the Visual Basic language coupled with MS Excel spreadsheets. The outputs of the model include recyclable water amount, cracking dimensions, cracking time, void ratio, moisture content, degree of saturation and tailings height, and also graphical presentations of the profiles related to the output data.

6.7 SUMMARY AND CONCLUSIONS

There are eight identifiable components of the water balance in sub-aerial tailings deposition. The main factors that affect the design of a sub-aerial deposition to optimize the release water for recycling and volume reduction are hydraulic conductivity, suction, drying time, evaporation, and layer thickness.

The design criterion for sub-aerial tailings deposition in arid regions is to maximize the amount of water available for recycling and tailings volume reduction combined with enhancing the stability of tailings facility. There are two optional design schemes for sub-aerial tailings deposition. One is to keep the tailings fully saturated in order to maintain saturated hydraulic conductivity. The other is to allow the tailings to desiccate and crack through the layer and hence develop the macro hydraulic conductivity due to cracking.

A model capable of predicting sedimentation, consolidation and desiccation, crack initiation, crack propagation, crack dimensions (spacing, depth, and width), tailings volume, and amount of recyclable water is presented. It has been coded in a modern computer language for use on a personal computer.

Table 6.1 Surface tensile stress relief (modified from Lachenbruch 1961)

y/b	a/b			
	0.3	0.5	0.75	1.0
0.5	$-0.64\sigma_t - 0.25\sigma_3$			
0.75	$-0.37\sigma_t - 0.3\sigma_3$	$-0.57\sigma_t - 0.3\sigma_3$		
1	$-0.2\sigma_t - 0.31\sigma_3$	$-0.4\sigma_t - 0.31\sigma_3$	$-0.57\sigma_t - 0.31\sigma_3$	$-0.63\sigma_t - 0.31\sigma_3$
1.5	$-0.16\sigma_t - 0.25\sigma_3$	$-0.2\sigma_t - 0.25\sigma_3$	$-0.35\sigma_t - 0.25\sigma_3$	$-0.4\sigma_t - 0.25\sigma_3$
2.0	$-0.03\sigma_t - 0.17\sigma_3$	$-0.14\sigma_t - 0.17\sigma_3$	$-0.23\sigma_t - 0.17\sigma_3$	$-0.28\sigma_t - 0.17\sigma_3$
2.5	$-0.02\sigma_t - 0.13\sigma_3$	$-0.09\sigma_t - 0.13\sigma_3$	$-0.16\sigma_t - 0.13\sigma_3$	$-0.19\sigma_t - 0.13\sigma_3$
3.0	$-0.01\sigma_t - 0.1\sigma_3$	$-0.06\sigma_t - 0.1\sigma_3$	$-0.12\sigma_t - 0.1\sigma_3$	$-0.14\sigma_t - 0.1\sigma_3$
4.0	$-0.003\sigma_t - 0.056\sigma_3$	$-0.032\sigma_t - 0.056\sigma_3$	$-0.064\sigma_t - 0.056\sigma_3$	$-0.094\sigma_t - 0.056\sigma_3$
5.0	$0.004\sigma_t - 0.04\sigma_3$	$-0.021\sigma_t - 0.04\sigma_3$	$-0.042\sigma_t - 0.04\sigma_3$	$-0.057\sigma_t - 0.04\sigma_3$
7.0	$-0.003\sigma_t - 0.018\sigma_3$	$-0.011\sigma_t - 0.018\sigma_3$	$-0.024\sigma_t - 0.018\sigma_3$	$-0.031\sigma_t - 0.018\sigma_3$

Note: y is the horizontal distance from the crack, a is the depth of tensile stress zone, b is the crack depth (or length), and σ_3 is the tensile stress at the depth of b, i.e. $\sigma_3(b)$.

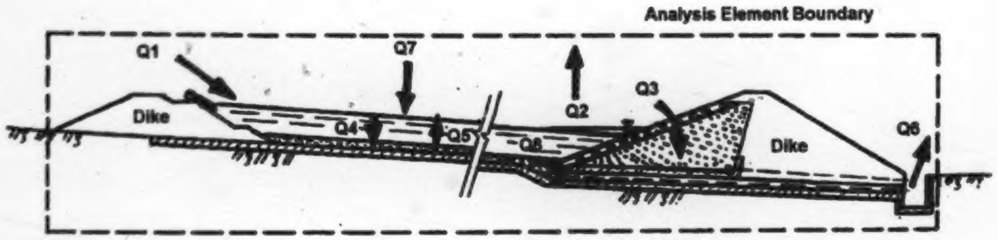
Analysis Element Boundary
Q1
Q7
Q2
Q3
Dike
Q4
Q5
Q8
Dike
Q6

Figure 6.1 Water balance components during the tailings pond operation

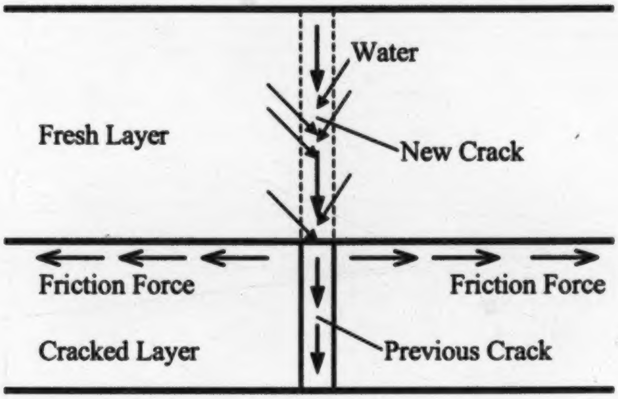
Water
Fresh Layer
New Crack
Friction Force
Friction Force
Cracked Layer
Previous Crack

(a) Genesis of the reflective crack in a fresh layer

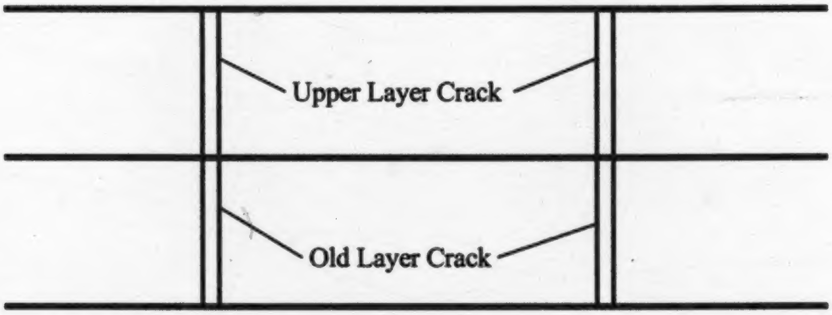
Upper Layer Crack
Old Layer Crack

(b) Reflective Cracks in the new layer

Figure 6.2 Location of new cracks

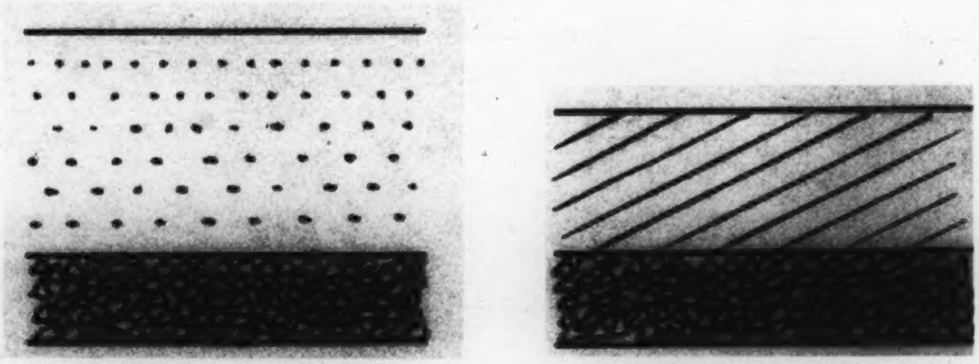

(a) First Layer Deposition

(b) First Layer Consolidation

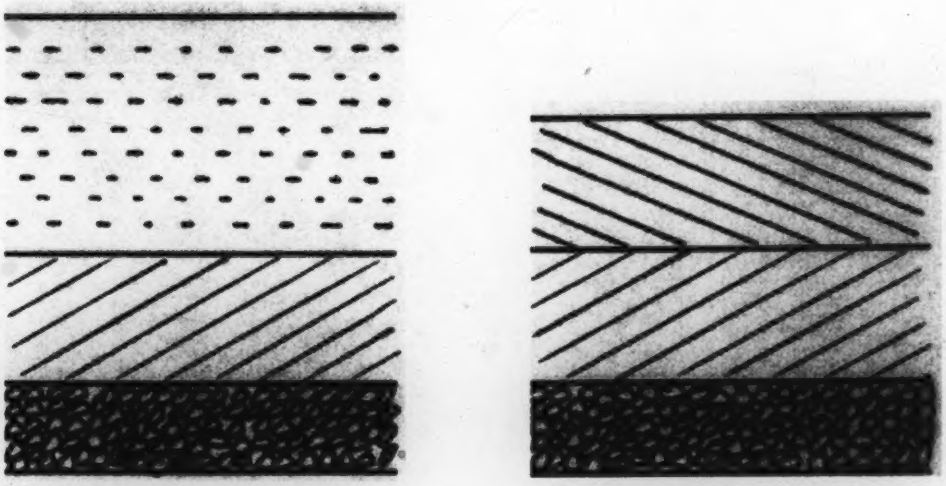

(c) Second Layer Deposition

(d) Second Layer Consolidation

Figure 6.3 Optional design scheme 1

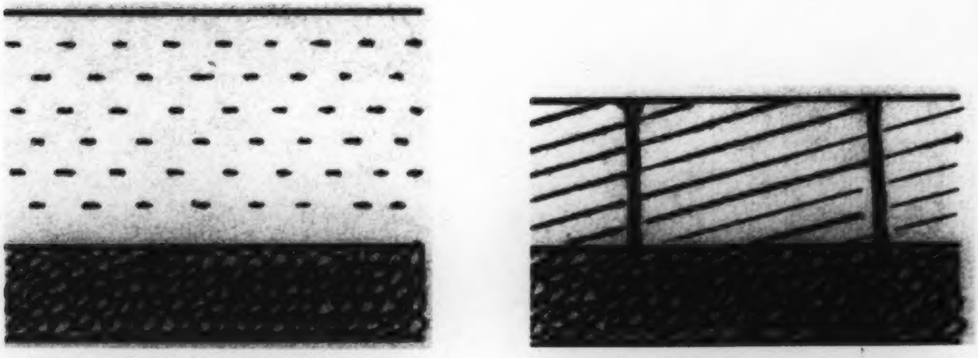

(a) First Layer Deposition (b) First Layer Cracks

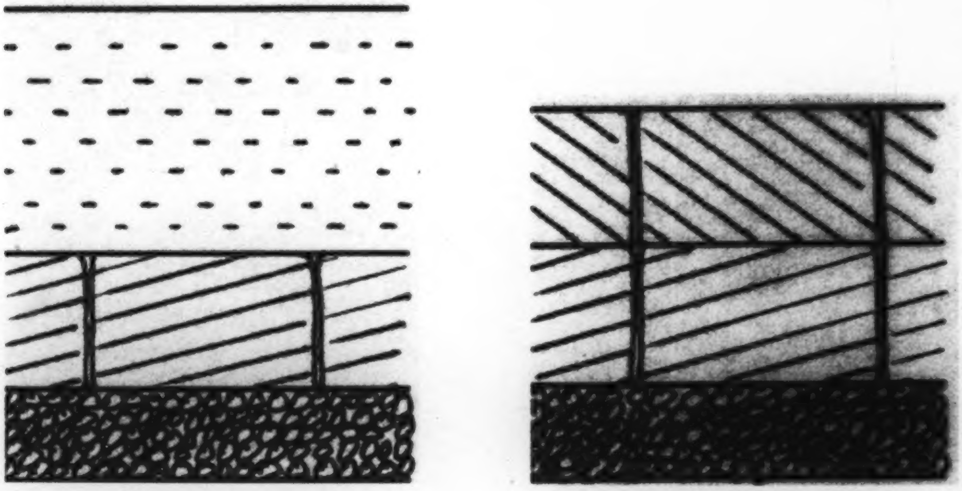

(c) Second Layer Deposition (d) Second Layer Cracks

Figure 6.4 Optional design scheme 2

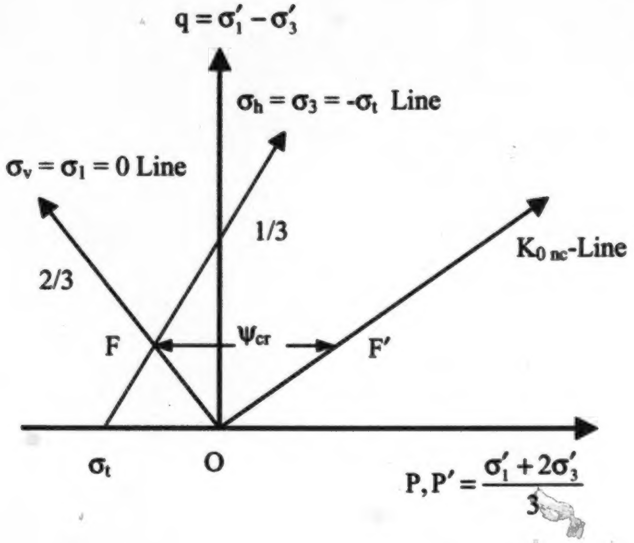
$q = \sigma_1' - \sigma_3'$
$\sigma_h = \sigma_3 = -\sigma_t$ Line
$\sigma_v = \sigma_1 = 0$ Line
1/3
2/3
$K_{0\,nc}$-Line
F
ψ_{cr}
F′
σ_t
O
$P, P' = \frac{\sigma_1' + 2\sigma_3'}{3}$

Figure 6.5 Stress path and critical suction for desiccating tailings (modified from Konrad and Ayad 1997)

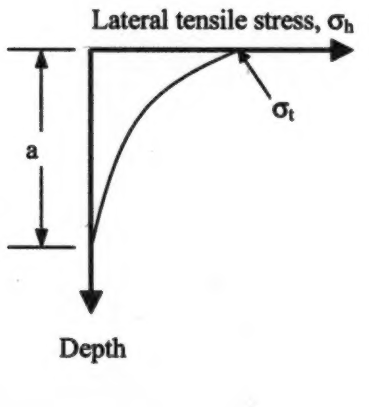
Lateral tensile stress, σ_h
σ_t
a
Depth

Figure 6.6 Critical lateral tensile stress distribution

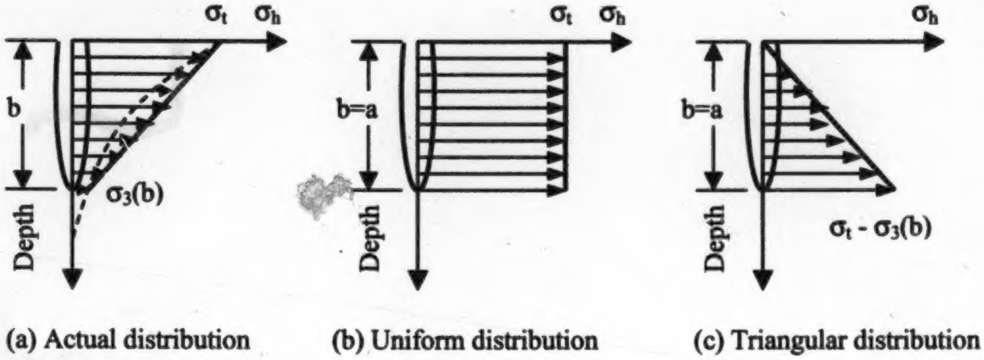
σ_t
σ_h
b
σ3(b)
Depth
b=a
σ_t - σ3(b)

(a) Actual distribution (b) Uniform distribution (c) Triangular distribution

Figure 6.7 Assumptions of the tensile stress distributions

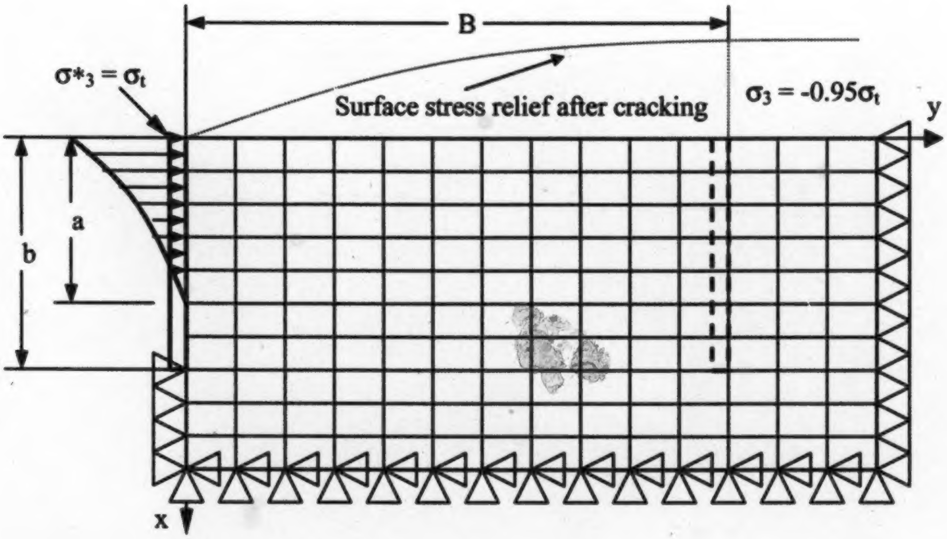
B
σ*3 = σt
Surface stress relief after cracking
σ3 = -0.95σt
y
a
b
x

Figure 6.8 Use fictitious stress principle to determine tensile stress reduction (modified from Konrad and Ayad 1997)

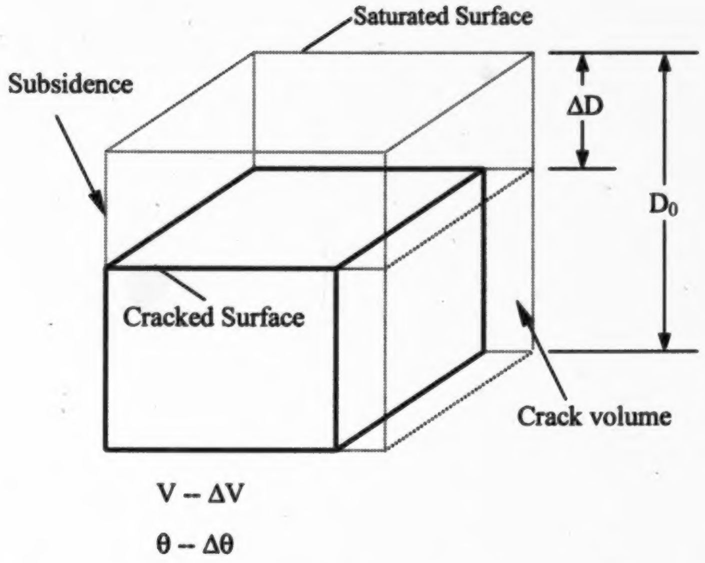
Saturated Surface
Subsidence
ΔD
D0
Cracked Surface
Crack volume
V -- ΔV
θ -- Δθ

(a) An element at the initiation of crack (modified from Bronswijk 1989)

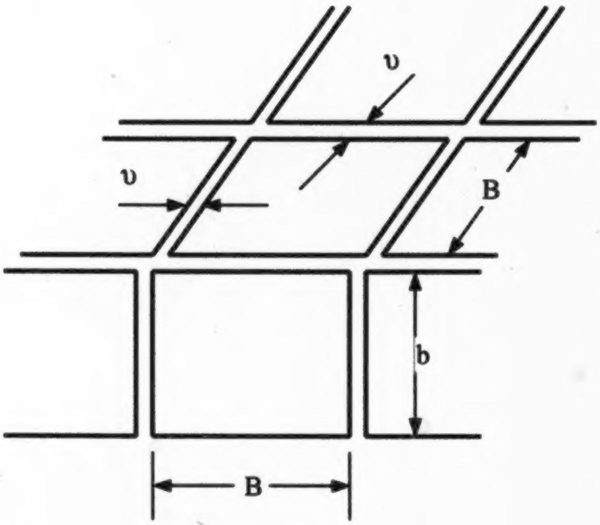

(b) Dimensions of the cracked element

Figure 6.9 Calculation of crack width

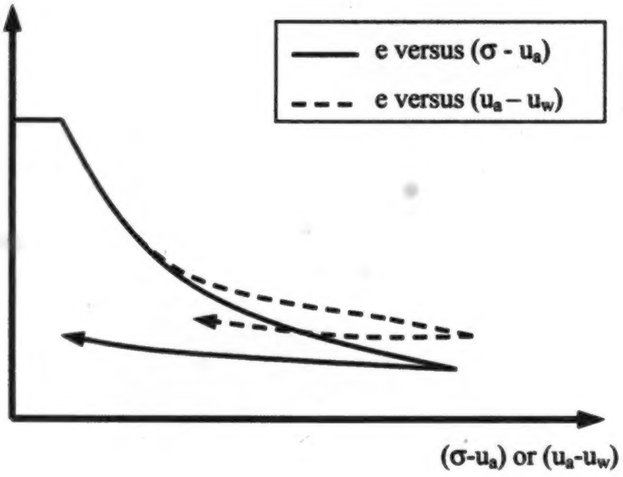

Figure 6.10 Constitutive relationship for soils (modified from Fredlund and Rahardjo 1993)

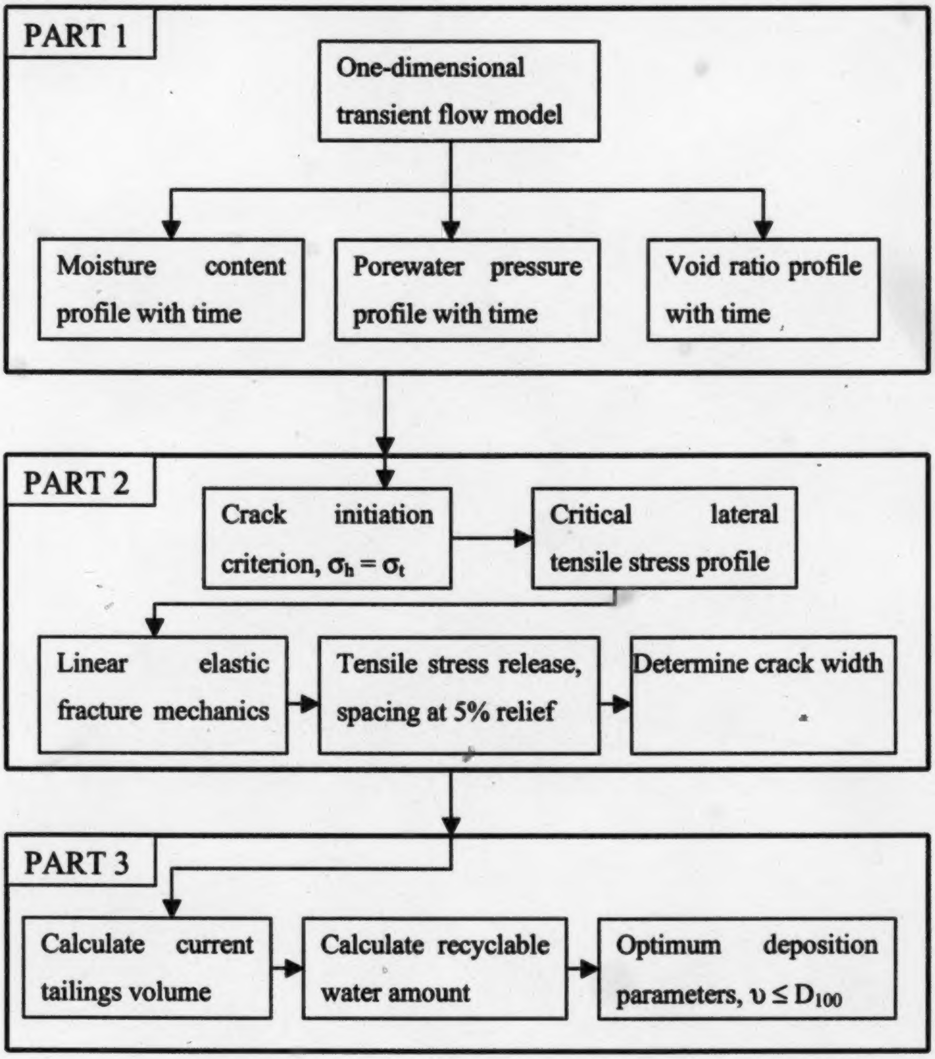
PART 1
One-dimensional transient flow model
Moisture content profile with time
Porewater pressure profile with time
Void ratio profile with time
PART 2
Crack initiation criterion, σh = σt
Critical lateral tensile stress profile
Linear elastic fracture mechanics
Tensile stress release, spacing at 5% relief
Determine crack width
PART 3
Calculate current tailings volume
Calculate recyclable water amount
Optimum deposition parameters, υ ≤ D100

Figure 6.11 Flow chart of the optimum design model "DOSTAR"

CHAPTER 7 VALIDATION AND APPLICATION OF THE MODEL

7.1 INTRODUCTION

As a result of shortcomings due to numerical schemes that may introduce instability, truncation, and round off errors, the performance of a numerical model should be evaluated to examine its validity in predicting physical results. A model is valid only if its approximate solutions are satisfactorily accurate or close to the exact solutions if they exist. The validity of a model can be tested by comparing its numerical solutions with either an analytical solutions or observed experimental data.

In this study, since an analytical solution is not available for the problem being studied, the validity of the model is tested by comparing the predicted results with laboratory test results. A ten meter high standpipe test and column drying test results were used to compare the predicted results from the model "DOSTAR." Then two optional design schemes were modeled using the model, and a comparison between the predicted results for the both schemes was made. The predicted results for both single layer and multiple layer deposition for different tailings are presented and discussed. Then a procedure for establishing the optimum depositional parameters using the model is also presented. Finally, three case studies as examples of the application of the model in practice are described.

7.2 VALIDATION OF THE MODEL

7.2.1 Ten Meter High Standpipe Test

A self-weight consolidation test of oil sand mature fine tailings with an initial solids content of 32% in a 10m high and 0.91m diameter standpipe has been conducted since 1982 (Pollock 1988; Suthaker 1995). The standpipe is equipped with pore pressure and sampling ports at 1m intervals. Additional ports at 0.5m intervals are used at the top and bottom to monitor rapid changes in solids content and pore pressure. The oil sand fine tailings were supplied by the Syncrude Canada Ltd. A summary of properties of the fine tailings is presented in Table 7.1.

The consolidation behavior of the fine tailings in the 10m standpipe was modeled using the measured compressibility and hydraulic conductivity parameters as shown in Table 7.2. Figure 7.1 shows the measured and predicted settlement for the 10m high standpipe test. The predicted values show an excellent agreement with measured values for a 6.3 years' duration (55200 hours). Figure 7.2 shows the measured and predicted solids content profile of the ten meter standpipe test after 20400 hours (850 days). The predicted data show good agreement with measured data after 20400 hours.

7.2.2 Column Drying Test

Column drying tests were carried out to investigate the desiccation behavior of various tailings evaluated in this research program. The detailed test methods and results are presented in Chapters 3 and 4. Comparisons between the predicted and measured settlements and moisture content profiles of tailings in the column drying tests are shown in Figure 7.3 to 7.10. The predicted values of the settlement show excellent agreement with the measured values. In addition, the predicted values of the moisture content have reasonable agreement with the measured values. The discrepant point (w = 0.39) in

Figure 7.4 may also be due to the measurement error. The comparisons show that DOSTAR supports the laboratory test results.

7.3 APPLICATION ON OPTIMUM DESIGN FOR ARID REGIONS

The sub-aerial tailings depositions for various tailings with different layer thicknesses (i.e. H_ξ= 0.1, 0.15, 0.2 and 0.25 m) and potential evaporation rates (i.e. E_P = 3.3E-8 and 6.6E-8 m/s) were simulated using DOSTAR. To match the in situ condition, the input solids contents for the model were the same as the field data, i.e. 35%, 37%, 42% and 58% for the copper, gold, coal and CT tailings, respectively. The main input data for the modeling are summarized in Table 7.3. The applications of DOSTAR on the sub-aerial tailings deposition are described in this section. Firstly, based on the modeling results, two optional designs are compared and the optimum design scheme is determined. Then, the effects of layer thickness during deposition and the influence of different potential evaporation rates on the sub-aerial tailings disposal are discussed. In addition, the modeling results for both single layer and multiple layers are presented and discussed. Finally, the optimum deposition design method is described.

7.3.1 Optimum design scheme

As described in Chapter 6, there are two optional design schemes in the sub-aerial tailings disposal. The layer has to always be kept at full saturation to maintain the saturated hydraulic conductivity in scheme 1. However, in scheme 2, the layer is allowed to dry and crack through a given layer so that the high macro hydraulic conductivity could be utilized.

Table 7.4 presents a comparison of the modeling results between schemes 1 and 2 for all tested tailings. For the sake of comparison, the inputs for the model for scheme 1 and 2 were the same. The potential evaporation rate of 3.3E-8 m/s was used for evaluations. It is worth noting that different layer thicknesses were used to ensure that no crack was infilled by fresh tailings in scheme 2. The layer thickness was 0.2, 0.25, 0.25 and 0.2 m for the copper, gold, coal, and CT tailings respectively. Data comparison indicates that scheme 2 has the following advantages over scheme 1:

1) **Hydraulic conductivity**: The minimum hydraulic conductivity of the tailings within a given layer before deposition of the next layer is listed in Table 7.4. It is worth noting that the listed hydraulic conductivity for scheme 1 is the saturated hydraulic conductivity after sedimentation and consolidation, while the data for scheme 2 are the macro hydraulic conductivity due to cracking. The data show that scheme 2 offers 3 to 7 orders of magnitude greater hydraulic conductivity for the deposited layer compared to scheme 1. This is due to the desiccation cracks offering high macro hydraulic conductivity. The higher the hydraulic conductivity, the quicker the consolidation and desiccation of the next deposited layer.

2) **Volume reduction**: Table 7.4 shows that the operation of scheme 2 results in a higher volume reduction compared to scheme 1. Although the saturated tailings in scheme 1 can be consolidated further after the next layer deposition, it is hard to reach the same volume reduction as occurs in scheme 2, since the effective stress increase due to the next layer is quite small. This implies that using scheme 2 can minimize the volume of the tailings in the facility, and consequently, the holding capacity of the tailings facility can be increased.

3) **Stability of a facility**: Liquefaction is a major cause of failure in a tailings facility, especially in high risk zones associated with earthquakes. The degree of saturation has a great effect on the potential liquefaction in sandy soils. Since most tailings are about the size of sand, the degree of saturation is of great

concern for the stability of the tailings dam. Grozic (1999) concluded that if the initial degree of saturation drops below about 88%, either static or cyclic liquefaction was only possible in extremely loose materials, and if the initial degree of saturation drops below 80%, flow liquefaction was not possible. In addition, the lower the degree of saturation, the higher the resistance to cyclic induced liquefaction.

Table 7.4 indicates that the final degrees of saturation of the tailings in scheme 2 are lower than 80% (except for the clayey coal tailings at 85%), while the degree of saturation in scheme 1 is 100%. Therefore, scheme 2 offers the potential for deposition of a "liquefaction resistance" tailings facility, while scheme 1 offers a high risk of liquefaction failure. In addition, the greater the density of the tailings, the higher the shear strength. It worth noting that resaturation of the layer by moisture from freshly placed layer was neglected in the model. Grozic (1999) also pointed out that as the density increases, the potential for liquefaction decreases. The lower final volume in scheme 2 means higher overall density of the tailings compared to scheme 1. Therefore, scheme 2 offers higher shear strength and resistance against liquefaction than scheme 1. In conclusion, scheme 2 offers the potential for a much safer tailings facility than scheme 1.

4) **Volume of recyclable water**: Table 7.4 shows that in scheme 1, the amount of the recyclable water was 83% for the copper tailings, 82% for the gold tailings, and 47% and 44.3% for the coal tailings and CT respectively. However, in scheme 2, the recyclable water amount was 92%, 88%, 49% and 44.7% for the copper, gold, coal, and CT tailings respectively. The data indicate that scheme 2 offers more recyclable water than scheme 1.

Obviously, scheme 2 takes a longer time to achieve than scheme 1. However, Table 7.4 shows that the differences of the elapsed times for the coal tailings and CT between the two schemes are not significant. The only drawback of scheme 2 is that there is a potential of blowing dust associated with the non-clayey tailings due to the need to desiccate the surface. However, dust control is a common problem associated with drying surfaces in a mine operation and is beyond the scope of this study.

From the above discussion, it is easy to conclude that scheme 2 can achieve better results in terms of the safety, tailings volume, and amount of recyclable water; thus, scheme 2 is the optimum one for sub-aerial tailings disposal.

7.3.2 Modeling Results for Single Layer Deposition

7.3.2.1 Variation of initial condition (depositional layer thickness)

There are many factors affecting the final result of sub-aerial tailings disposal as outlined in Chapter 6. The factors can be divided into two categories: inherent ones such as engineering properties of the tailings, and external factors such as the initial deposition condition and the in situ environmental condition. This section and the following one discuss the effects of the deposition layer thickness and potential evaporation rate on sub-aerial tailings disposal.

Table 7.5 presents a comparison of the modeling results for different deposition layer thicknesses. The layer thickness effects are discussed as follows:

(1) **Effect on crack width**: The graphical relationship between the deposition layer thickness (H_ξ) and desiccation crack width (υ) is shown in Figure 7.11. The relationships between the deposition layer thickness (H_ξ) and crack width (υ) for the selected tailings are almost linear except for the CT. The nonlinear relationship between the deposition layer thickness and crack width is mainly due to the nature of the sand and clay mixture and the presence of the bitumen in the oil sands CT. The data and plots indicate that under the same environmental

conditions, the crack width decreases as the deposition layer thickness increases. Therefore, the optimum deposition layer thickness can be determined based on the requirement of the crack width, i.e., $\upsilon \leq D_{100}$. The detailed determination of the optimum deposition layer thickness will be described later. Figure 7.11 also shows that the copper and gold tailings have a gentle slope to their H_{ξ}-υ curves, while the coal and CT tailings have a much steeper slope. On the other hand, data in Table 7.5 indicates that under the same depositional and environmental conditions, the crack width of the various tailings increases sequentially with respect to the copper, gold, CT, and coal tailings. This is due to the differences in their clay contents and/or clay particle size content (Table 4.1). This implies that under the same depositional and environmental conditions the higher the clay content, the greater the crack width. This is due to the increased shrinkage associated with higher clay content.

(2) **Effect on crack spacing**: The data show that the thicker the deposited layer, the greater the crack spacing. Comparisons of the crack spacing between different tailings indicate that under the same depositional and environmental conditions, the higher the clay contents, the smaller the crack spacing.

(3) **Effect on crack depth**: Table 7.5 shows that a crack will propagate through the thicker layer.

(4) **Effect on tailings volume**: Table 7.5 also presents the volume which remains as a percentage of the original input volume. Data indicate that for the copper, gold, and coal tailings, the remaining volume decrease slightly as the deposition layer thickness increases, while for the CT, the remaining volume increases slightly as the deposition layer thickness increases. However, both changes are small. The decrease in the volume is due partially to the longer drying time associated with the thick layer.

(5) **Effect on drying time**: The elapsed time for drying to cause cracks to propagate through the layer of tailings is shown in Table 7.5. The data indicate that the thicker the deposited layer, the longer the time for drying to cause cracks to propagate through the given layer. Also, the clayey tailings require a longer drying time than the sandy tailings.

(6) **Effect on recyclable water**: Data in Figure 7.4 show that if the tailings are allowed to dry and crack through the given layer in all cases, the available recyclable water for the sandy tailings is the same for all evaluated layer thicknesses, while the available recyclable water decreases as the layer thickness increases. This is because clay has a greater ability to hold water than sand.

7.3.2.2 Variation of environmental condition (potential evaporation rate)

Environmental conditions influence the consolidation and desiccation results of the sub-aerial deposited tailings. The potential evaporation rate (Ep) is usually used to represent the environmental effect in these circumstances, since Ep changes with the climatic conditions.

Table 7.6 presents a comparison of the modeling results for the different potential evaporation rates (E_p = 3.3E-8 and 6.6E-8 m/s). The effects on the sub-aerial tailings disposal of this change are discussed below:

(1) **Effect on crack spacing**: Table 7.6 shows that when the potential evaporation increases by 100%, the crack spacing decreases by about 5.3%, 8.4%, 20.5% and 26.1% in the copper, gold, CT, and coal tailings respectively. This indicates that the crack spacing decreases as the potential evaporation rate increases, and the more clay contents, the greater the decrease in crack spacing.

(2) **Effect on crack width**: Data in Table 7.6 show that the crack width increases with the potential evaporation rate. When the potential evaporation rate increases by 100%, the crack width increases by 1.9%, 5.5%, 27.5% and 59.5% in the copper, gold, CT, and coal tailings respectively. This is because a higher potential evaporation rate means a higher amount of energy involved, and consequently, a larger crack width occurs while releasing the higher amount of energy. In addition, the higher the clay contents in the tailings, the more significant the influence on the change in crack width.

(3) **Effect on tailings thickness**: Data in Table 7.6 indicate that when the potential evaporation rate increases from 3.3E-8 to 6.6E-8 m/s, the final tailings thickness decreases slightly for the copper and coal tailings and is almost the same for gold tailings. However, it increases for the CT. This is due to the higher potential evaporation rate resulting in earlier drying on the surface. Thus, it causes earlier hydraulic conductivity decrease, and consequently shutting off the upward flux earlier. Therefore, the shorter drying period which does not allow the low hydraulic conductivity CT tailings time to completely dry.

(4) **Effect on recyclable water**: The data in Table 7.6 imply that when the potential evaporation rate increases by 100%, the recyclable water decreases by about 1.7%, 1.8%, 10.4% and 19.1% in the copper, gold, CT and coal tailings respectively. This is mainly due to the higher evaporation loss associated with the higher potential surface evaporation rate.

(5) **Effect on drying time**: The predicted results show that the elapsed time for cracking through the layer decreases as the potential evaporation rate increases. This is because the high evaporation rate speeds up the surface desiccation, which in turn speeds up the tensile stress building up and crack initiation through the layer.

7.3.2.3 Desiccation cracks

With the progress of desiccation, internal horizontal tensile stresses build when the tailings are exposed to air. When the horizontal tensile stresses exceed the local tensile strength, a tensile crack occurs locally and may propagate through the layer. In this model, the whole process from deposition to desiccation is simulated until the desiccation crack extends through the given layer. The predicted desiccation crack dimensions and the time required to crack through the profile, under the conditions of E_P = 3.3E-8 m/s and H_ξ = 0.1m are listed in Table 7.7.

Table 7.7 indicates that copper tailings has the largest crack spacing (98 cm), while the coal tailings have the smallest crack spacing (56 cm). The gold tailings have a medium spacing (92 cm) which is greater than that of the CT (86 cm). However, the widths of the cracks differ. The coal tailings have the largest crack width (1.17 cm), while the copper tailings have the smallest crack width (0.31cm). In addition, the crack width of the CT (0.91cm) is greater than that of the gold tailings (0.48cm). These results imply that under the same environmental and depositional conditions, an increase in clay contents in the tailings results in larger crack width and smaller crack spacing. The time required to form cracks through the layer is about 13 and 16 hours for the copper and gold tailings respectively, while it is about 94 and 3414 hours for the coal tailings and CT respectively. The coal tailings and CT require a much longer time to crack through than the copper and gold tailings due to the contained clay which has a better water hold capacity than the copper and gold tailings. The bitumen also contributes to the drying behavior of the CT.

7.3.2.4 Settlement

The predicted settlement of the copper tailings is shown in Figure 7.12. During the early stage of sedimentation, the copper tailings settle quickly. Within two hours, the total settlement reaches 6 cm, i.e. the total volume of the copper tailings has decreased by 60%. Then the tailings continue to settle at a smaller rate. By the end of sedimentation, the accumulated settlement reaches about 6.6 cm. During the early stage of consolidation, the copper tailings still settle at an observable rate. Five hours after deposition, the copper tailings continue to settle but slowly. The figure indicates that 5 hours after deposition, the next layer of copper tailings can be deposited since the majority of the settlement is complete.

Figure 7.13 presents the predicted settlement of gold tailings. The settlement of the gold tailings has a shape similar to that of the copper tailings. Within 9 hours, the gold tailings settle quickly at a nearly constant rate, and the total settlement is about 6.9 cm. Then the tailings settle at a slow rate. Thirteen hours after deposition, the gold tailings settle at a much slower rate. This implies that 13 hours later, the next layer can be placed since the majority of the settlement has occurred.

Figure 7.14 presents the settlement of the coal tailings. Compared to the copper and gold tailings, the settlement of the coal tailings is much slower. During the early stage of sedimentation, the coal tailings settle at a slow, nearly constant rate. Then during the later stage of sedimentation and the early stage of consolidation, the coal tailings settle even more slowly. After 75 hours, the rate increases slightly as a result of the desiccation shrinkage which increases the settlement rate. Therefore, to reduce the final storage volume, the coal tailings should be allowed to dry until desiccation shrinkage begins to occur. This requires about 94 hours of drying time.

Figure 7.15 illustrates the predicted settlement of the CT. Among the selected tailings, the CT settles the most slowly. This is attributed to the presence of bitumen and its low hydraulic conductivity. The plot indicates that the CT settles at a constant rate during the sedimentation, and the first stage of consolidation takes 3250 hours after deposition. Then the CT settles quickly as it desiccates until tension cracks occur.

7.3.2.5 Degree of saturation

Figure 7.16 presents the degree of saturation changes in the copper tailings. The plots show that the copper tailings remained fully saturated for 4.8 hours after deposition. The results show that the desaturation started at both the surface and bottom with almost the same desaturation rate. When the degrees of saturation of the bottom and surface reached around 38%, desiccation cracks propagated through the layer.

Figure 7.17 shows the degree of saturation changes in the gold tailings. Similar to the copper tailings, the gold tailings remained fully saturated for 12 hours after deposition, and the desaturation began at the same time at both the bottom and surface. When the degree of saturation of the bottom and surface reached 69%, the tension cracks propagated through the layer. Comparing the degree of saturation changes in the copper and gold tailings, it is observed that the copper tailings desaturate faster than the gold tailings.

The changes in the degree of saturation in the coal tailings are presented in Figure 7.18. It is worth noting that the time scale in this figure is substantially different from those in Figure 7.16 and 7.17. The coal tailings remained fully saturated for 93 hours after deposition. Unlike the other tailings, desaturation in the coal tailings begins at the bottom, and the tension cracks initiate from the bottom. This is mainly due to its high air-entry value as shown in Table 4.5, i.e. the air-entry value of the coal tailings is 18 kPa, while it is 5 to 6 kPa for the other tailings. This high air-entry value indicates that even though suction builds up with desiccation at the surface, if the suction at the surface remains lower than 18 kPa, the surface of the coal tailings remains fully saturated. This result also indicates that the downward drainage at the bottom is faster than the upward surface flux. Once the degree of saturation at the bottom reaches 80%, even though the surface of the layer remains fully saturated, the desiccation cracks propagate upward to the surface. This phenomenon may lead one to presume that surface cracking in cohesive soils is initiated under saturated conditions as has been observed by Konrad and Ayad (1997).

Figure 7.19 shows the changes in the degree of saturation in the CT with an even greater difference in the time scale. The results show that the CT desaturates slowest among the four tailings. This is due to its low hydraulic conductivity. The CT remains fully saturated for 3389 hours after deposition. It also takes a long time to desaturate the profile. When the degree of saturation of the surface reduces to about 41%, the desiccation cracks initiate and propagate through the layer 3414 hours after deposition.

7.3.2.6 Tailings volume

One of the objectives of this research is to minimize the tailings volume in the containment facility. Following the process of sedimentation, consolidation, and desiccation, the tailings volume is dramatically reduced. Table 7.8 shows the normalized tailings volume and recyclable water after cracking through a single layer. The normalized tailings volume is the ratio of the final volume to the deposited original volume. The normalized recyclable water is the ratio of the recyclable amount of water to the amount of water contained in the tailings when deposited. It is worth noting that each tailings layer was deposited with a different initial solids content. The data indicate that the copper and gold tailings have smaller volumes, while the coal tailings and CT have larger volumes after desiccating sufficiently to crack through the layer. In other words, the volumes of the copper and gold tailings are reduced by about 70%, while the volumes of the coal tailings and CT decrease less than 50%. These results also indicate that sandy tailings are easier to consolidate and desiccate than the clayey tailings.

7.3.2.7 Recyclable water

Generally, mineral processing requires large amounts of water. Hence, the demand on water resources is becoming a critical issue, especially in arid climatic regions. The processing water needs to be recycled as completely as possible. The amount of normalized recyclable water changes in the copper tailings as is shown in Figure 7.20. The figure shows that during the first 3 hours, the recyclable water increases quickly to 78% of the initial input water. This is due to the rapid sedimentation of the copper tailings. Within the next two hours, it increases slowly. Five hours after deposition, the recyclable water increases at a constant rate. When the crack propagates through the layer, 92% of the water is available for recycling when the copper tailings are allowed to dry and crack through the deposited layer (Table 7.8).

The changes in the normalized recyclable water in the gold tailings are shown in Figure 7.21. Similar to the copper tailings, the recyclable water of the gold tailings increases quickly to 45% within the first 3 hours due to sedimentation. Then it increases slowly during the next 3 hours. After that, the recyclable water increases at a higher rate due to consolidation and desiccation. When the crack propagates through the layer, the maximum available amount of recyclable water is 89%.

Figure 7.22 presents the normalized recyclable water changes in the coal tailings. The plot shows that the amount of recyclable water of the coal tailings is quite different from that of the copper and gold tailings. The recyclable water increases slowly from 0 to 33% within the first 53 hours. Then the recyclable water remains at almost 33% for 17 hours. Seventy hours after deposition, it increases again at a similar rate as shortly after deposition. Ninety hours after deposition, it increases rapidly due to desiccation. When the crack propagates through the layer, the total amount of water available for recycling is 53%. This amount is smaller than that for the copper and gold tailings due to the presence of the large amount of clay minerals in the coal tailings which makes holding water easier.

Figure 7.23 shows the normalized recyclable water changes for the CT. It is worth noting that the time scale in this plot is quite different. Since the CT has very low hydraulic conductivity, the amount of recyclable water increases very slowly from 0 to 39% during the first 3306 hours. After that, the recyclable water increases much quicker due to consolidation and desiccation. When the tension cracks initiate and propagate through the layer 3414 hours after deposition, the amount of recyclable water has reached 56%. Although the CT contains less clay minerals than the coal tailings, the available recyclable water of the CT is only 3% greater than that for the coal tailings. This is due to the evaporation loss during the much long drying time.

7.3.2.8 Hydraulic conductivity change

While the consolidation progresses, the hydraulic conductivity of the tailings decreases. When the tailings are allowed to desiccate to an unsaturated state, the hydraulic conductivity then decreases dramatically. However, when the tension cracks initiate and propagate through the whole layer, the macro hydraulic conductivity caused by the open cracks will dominate the permeability of the layer. Hence, the cracks may dramatically increase the hydraulic conductivity of a given layer.

When the crack width is less than D_{100} of the tailings, there should be no infilling of the cracks. Then each crack increases the hydraulic conductivity within the tailings by several orders of magnitude. These increases are very important for the multiple layer deposition associated with sub-aerial tailings disposal since they enable the layer to act like a free drainage filter for the newly placed layer. However, if infilling occurs, the macro hydraulic conductivity will be limited by the infilling material. Table 7.9 presents a comparison of hydraulic conductivity of the tailings before and after cracking through the layer at different deposition layer thicknesses. The hydraulic conductivity when the deposition layer thickness (H_ξ) is 0.1 m is presented in column 1. Data in Table 7.9 show that the hydraulic conductivity in column 1 changes little. This is because the crack width in each type of tailings for this condition is larger than D_{100}, which results in fresh tailings infilling the cracks (Table 7.7). However, there are dramatic changes when the cracks remain open. Since the crack widths in column 2 are less than D_{100} of the tailings (Table 7.7 and 7.5), no infilling occurred. After cracking through the layer, the hydraulic conductivity in column 2 increased by 3 orders of magnitude for the copper and gold tailings, 4 orders of magnitude for the coal tailings, and 6 orders of magnitude for the CT. This indicates how important it is to optimize the deposition sequence (design) to produce the proper size of cracks to achieve the highest macro hydraulic conductivity in the layers while not allowing fresh tailings to infill newly formed cracks. Details about optimum deposition design will be discussed later.

7.3.3 Modeling Results for Multiple Layer Deposition

As described in Chapter 2, the sub-aerial tailings disposal technique involves the cyclic deposition of tailings in a thin layer by discharging slurry into one deposition cell at a time. Therefore, the multiple layered deposition process must be accounted for in the modeling. Table 7.10 shows the modeling results for the multiple deposition process for different tailings based on deposition scheme 2. The input potential evaporation rate was 3.3E-8 m/s for all cases, and the input for the following layer was the same as for the first layer. The optimum deposition layer thickness was used as input for each tailings. The data show that all the layers have almost the same crack dimension, especially crack spacing. The results for the third layer are essentially the same as for the second layer. This is due to the same input conditions including boundary and depositional conditions associated with the two layers.

7.3.4 Optimum Deposition Design for Arid Regions

Optimum sub-aerial deposition design for arid regions requires the optimum deposition parameters to meet the design criterion, i.e. to maximize the amount of water available for recycling combined with minimizing the volume in the tailings facility. In practice, a layer of 100 to 150 mm (Blight 1996) or 4 to 6 inches (Ulrich 1999) is deposited each time using the sub-aerial tailings disposal method. However, there is no design guide available for determining the optimum deposition layer thickness, deposition cycle time, and number of depositional cells at a particular mine. This study is intended to provide guidance. This section describes how to determine the optimum depositional parameters.

The optimum deposition parameters include, as described in Chapter 6, the deposition layer thickness (H_{ξ_0}), cycle time (T_c), number of deposition cells (N_c) and total deposition area (A_t). The method and procedure for determining the optimum deposition parameters are presented in this section.

The following parameters are assumed to be known:

(a) The in situ potential evaporation rate, E_p (m/s): This parameter can be obtained either directly from a local climatic station or indirectly calculated based on the local climatic data by using a climatic based formula such as Equation [2-27];

(b) The tailings production rate or discharge rate, P_t (Mg/h): This parameter can be obtained from the mill or the tailings office;

(c) Tailings particle size distribution, especially D_{100}: D_{100} is the size with 100% passing. It can be obtained through a grain size distribution test;

(d) Original tailings bulk density in the discharge pipeline, ρ_0 (Mg/m^3): This parameter can be also obtained from the mill or the tailings office;

(e) Related engineering properties of the tailings as described in Chapter 4, such as specific gravity, compressibility, hydraulic conductivity, shrinkage curve, and water retention curve: These parameters can be obtained from laboratory tests carried out using a particular tailings of interest.

The detailed optimum deposition design method is described as follows:

Step 1: determination of the optimum deposition layer thickness $H_{\xi o}$ and drying time T_s

Based on D_{100} and E_p, the "DOSTAR" model was used to predict the crack width versus deposition layer thickness curve. Then the optimum deposition layer thickness $H_{\xi o}$ could be obtained, i.e. a practicable deposition layer thickness which leads to the largest macro hydraulic conductivity (k_c) under the condition of crack width (υ) being smaller than D_{100}, i.e. $\upsilon \leq D_{100}$. Figure 7.11 shows the predicted relationships between crack with (υ) and depositional thickness (H_ξ) for the copper, gold, coal, and CT tailings studied in this project. For example, D_{100} was 2 mm for the copper tailings. A line at $\upsilon = D_{100} = 0.2$ cm was drawn to intercept the curve. Thus, the H_ξ coordinate corresponding to the cross point was the theoretical optimum deposition layer thickness for the copper tailings. In this case, the theoretical optimum deposition layer thickness based on the graphic result is 17 cm (Figure 7.11). Using the same method, the values of the optimum deposition layer thickness ($H_{\xi o}$) for the gold, coal and CT tailings were also obtained. They are 25 cm for the gold and coal tailings and 20 cm for the CT. These data indicate that under the condition of E_p = 3.3 E-8 m/s, the traditional deposition layer thickness range (0.1 to 0.15m) is not suitable for all tailings studied in this project.

Once the optimum layer thickness ($H_{\xi o}$) has been determined, the required drying time (T_s) for cracking to occur through the layer can be established using "DOSTAR."

Step 2: determination of the cell number (N_c) or the total deposition area (A_t)

If the total deposition area of the tailings facility is known, the deposition cell number (N_c) can be directly obtained from Equation [6-31]. It is worth noting that N_c is an integer that is larger than two or equal to two, and should not be too large to simplify the depositional procedure. If the calculated N_c is negative, the existing deposition area is too small. Consequently an expansion of the deposition area should be considered. The required total deposition area can be calculated using Equation [6-34] with a pre-assumed number of cells, and hence the expanded area of the facility is obtained.

If the calculated N_c is less than 2 but larger than 1, the existing deposition area of the facility is too large. Under this circumstance, a value of N_c has to be pre-assumed, and Equation [6-34] is used to determine the required total deposition area.

If the total deposition area of the tailings facility is unknown, a trial-and-error method has to be adopted to determine the optimum values of A_t and N_c. In general, a reasonable value of N_c is assumed to ensure smooth operations and then Equation [6-34] is used to calculate the total deposition area (A_t).

Step 3: determinations of the discharge time (T_d) and cycle time (T_c)

The discharge time (T_d) and cycle time (T_c) can be obtained directly from Equation [6-32] and [6-33].

Step 4: determination of the number of full cycles per year (M_c)

The number of full cycles per year (M_c) can be calculated from Equation [6-35].

7.4 CASE STUDIES AS EXAMPLES

7.4.1 Introduction

The sub-aerial tailings disposal technique has been adopted by two gold mining operations and by the Kennecott Utah Copper Corporation (Ridlen et al. 1997). These operations were chosen as case studies to demonstrate the optimum deposition design.

The existing operations were simulated using "DOSTAR" and then the optimum deposition design was performed. Finally, a comparison between the current operation and optimum deposition was carried out for case histories #1 and #2. All results are presented and discussed in the following sections.

Case History #1

The tailings facility was a gold mine tailings disposal facility. It is located in an area with an annual total lake evaporation of 42 inches (E_P = 3.3E-8 m/s). The facility had a deposition area of about 331,653 m^2 which was divided into 6 depositional cells along its perimeter. The sub-aerial tailings disposal method was used at this site. The sub-aerial technique basically consists of a fully under-drained tailings deposit with a managed spigotting operation. Tailings were spigotted over only one cell at any one time for one or two days (referred to as the one-day and two-day operation respectively) and allowed to flow onto the beach. The fresh tailings were allowed to settle, drain, and air dry for a period of 6 to 12 days. The cycle time was 7 and 14 days for the one-day and two-day operations respectively. The tailings production rate at this facility is about 11,430 tpd with a solids content of 35% by weight. The original conditions and the existing deposition parameters are summarized in Table 7.11.

Laboratory tests show that the tailings had an average specific gravity of 2.75. Tailings grain size distribution, consolidation, and hydraulic conductivity tests were carried out for the whole beach tailings. Based on the laboratory tests and in situ CPT tests, the effective friction angle of the tailings was typically in the range of 25 to 30°. The basic properties of the tailings from laboratory tests are presented in Table 7.12. Based on the available data, the tensile strength (σ_t) and fracture toughness (κ_c) were assumed to be 15 kPa and 3.6 $kN/m^{1.5}$ respectively. The relationships of void ratio (e) versus effective stress (σ') and hydraulic conductivity (k) versus void ratio (e) were similar to those described in Chapter 4, and the regression parameters based on the laboratory tests results for the compressibility and hydraulic conductivity relationships are shown in Table 7.13.

Case History #2

The tailings storage facility in case history #2 is located at a gold mining and milling complex in an area which is close to case history #1. The facility has a deposition area of about 696,355 m^2. It is divided into two separate storage areas, Cell 1 and 2. The sub-aerial tailings disposal method has been in use at this site since the beginning of its operation. In general, the tailings are sub-aerially deposited for 6 continuous months of the year into each cell, allowing 6 continuous months of "drying" time in each cell. The tailings production rate at this facility is 2500 tpd with a solids content of 48.6% by weight. The original conditions and the existing deposition parameters are summarized in Table 7.11.

Soil classification of the tailings range from very sandy silty (ML) to silt-clay (ML-CL), with an average specific gravity of 2.71. Laboratory tests on relatively undisturbed tailings samples showed that the average effective friction angle for the tailings was 35°. Basic properties of the tailings are presented in Table 7.14. Based on the available data, the tensile strength (σ_t) and fracture toughness (κ_c) were assumed to be 25 kPa and 3.5 $kN/m^{1.5}$ respectively.

Case History #3

The Magna Tailings Impoundment of the Kennecott Utah Copper Corporation was chosen as the third case study for demonstrating the optimum deposition design in this project. The tailings facility is located approximately 10 miles west of Salt Lake City, Utah, USA (Ridlen et. al. 1997). The existing facility has a depositional area of 23,067,900 m^2. Kennecott was planing to construct a new impoundment of 14,164,500 m^2 as an expansion to the north of the existing facility. Currently, the tailings production rate in this facility is 155,000 tons per day (tpd), and all the tailings are deposited by a peripheral spigotting system. The future tailings production rate may reach 213,000 tpd. All above data were provided by Ridlen et al. (1997). The whole beach tailings were tested in the soil mechanics laboratory at the University of Alberta, and the basic physical properties including desiccation properties were measured and presented in Chapter 4. As before, the tensile strength (σ_t) and fracture toughness (κ_c) were assumed to be 25 kPa and 3.5 kN/m$^{1.5}$ respectively. The annual lake evaporation in the region of Salt Lake City is 1168.4 mm (Jesen, 2000), equivalent to a potential evaporation rate (E_P) of 3.7E-8 m/s. The environmental and existing depositional parameters are listed in Table 7.11.

7.4.2 Optimum deposition design

Based on the original and environmental conditions of the tailings facilities, the optimum deposition design was performed using the model "DOSTAR" model. The design procedure and results are described in the following sections.

7.4.2.1 Optimum design for the case history #1

Step 1: determination of the optimum deposition layer thickness $H_{\xi o}$ and drying time T_s

The model was used to predict the crack dimensions under various deposition layer thicknesses (0.1, 0.15, 0.2, and 0.25m). The predicted relationship between the deposition layer thickness and crack dimensions is presented in Figure 7.24. A line at $\upsilon = D_{100} = 0.2$ cm is drawn to intercept the curve. Thus, the H_ξ coordinate corresponding to the cross point is the theoretical optimum deposition layer thickness. In this case, the theoretical optimum deposition layer thickness based on the graphic result is 13.6 cm. For the sake of convenience, 15 cm was selected as the optimum deposition layer thickness. The modeling results for the optimum deposition layer thickness at 15 cm are presented in Table 7.15. The data show that the drying time (T_s) is 155 hours. The predicted result shows that with the optimum design, the crack width is close to D_{100}, but not larger.

Step 2: determination of the cell number (N_c) or the total deposition area (A_t)

Substituting the known data into Equation [6-31] yields a negative value of N_c, which indicates that the depositional area of the existing facility is not large enough. To meet the optimum design, the facility has to be expanded. In this situation, the required total deposition area decreases as the cell number increases, as shown in Figure 7.25. For comparison, the figure also shows the existing area. Assuming that the cell number is 6, which is the same as the existing one, using Equation [6-34], the calculated total deposition area (A_t) is 457,791m^2. Hence, the expansion area (ΔA) is obtained from the difference between the calculated and existing area, i.e. $\Delta A = 457{,}791 - 331{,}653 = 126{,}138$m^2.

Step 3: determinations of the discharge time (T_d) and cycle time (T_c)

From Equation [6-32], the discharge time (T_d) can be obtained: $T_d = 31$ hours. Hence, the cycle time is the sum of the discharge time and drying time, $T_c = 31 + 155 = 186$ hours.

Step 4: determination of the number of full cycles per year (M_c)

From Equation [6-35], the annual cycle number is about 47.

The optimum depositional parameters are summarized in Table 7.16.

7.4.2.2 Optimum design for case history #2

Step 1: determination of the optimum deposition layer thickness $H_{\xi o}$ and drying time T_s

The sub-aerial tailings disposal was simulated using the "DOSTAR" model with different deposition layer thicknesses. The predicted relationship between the deposition layer thickness and crack dimensions is shown in Figure 7.26. A line at $\upsilon = D_{100} = 0.084$ cm is drawn to intercept the curve. Thus, the H_ξ coordinate corresponding to the cross point is the theoretical optimum deposition layer thickness. In this case, the theoretical optimum deposition layer thickness based on the graphic result is 24.1cm. For practical convenience, 25cm was selected as the optimum deposition layer thickness. The modeling results for the optimum deposition layer thickness of 25 cm are presented in Table 7.15. The data show that the drying time (T_s) is 321 hours.

Step 2: determination of the cell number (N_c) or the total deposition area (A_t)

Substituting the known data into Equation [6-31] yields $N_c = 1.15$, which indicates that the deposition area of the existing facility is too large for the optimum design. The relationship between the cell number and the required deposition area and the existing area is presented in Figure 7.27. The figure shows that the existing area for case history #2 is much larger than the required area in terms of the optimum design. Assuming that the cell number is equal to 6, using Equation [6-34], the required total deposition area (A_t) is equal to 111,458m^2.

Step 3: determinations of the discharge time (T_d) and cycle time (T_c)

From Equation [6-32], the discharge time (T_d) can be obtained: $T_d = 64.2$ hours. Hence, the cycle time is the sum of the discharge time and drying time, $T_c = 64.2 + 321 = 385.2$ hours.

Step 4: determination of the number of full cycles per year (M_c)

From Equation [6-35], the annual cycle number is obtained: $M_c = 22.7$.

The optimum depositional parameters are summarized in Table 7.16.

7.4.2.3 Optimum design for the case history #3

Step 1: determinations of the optimum deposition layer thickness $H_{\xi o}$ and drying time T_s

The sub-aerial tailings disposal for the Kennecott Utah Copper tailings was simulated using the "DOSTAR" model with different deposition layer thicknesses (H_ξ =0.1, 0.15, 0.2 and 0.25 m). The predicted relationship between the deposition layer thickness and crack dimensions is shown in Figure 7.28. A line at $\upsilon = D_{100} = 0.2$ cm is drawn to intercept the curve. Thus, the H_ξ coordinate corresponding to the cross point is the theoretical optimum deposition layer thickness. In this case, the theoretical optimum deposition layer thickness based on the graphic result is 16.8 cm. Hence, 17cm was chosen as the optimum deposition layer thickness. The modeling results for the optimum deposition layer thickness of 17 cm are presented in Table 7.15. The data show that the drying time (T_s) is 21 hours.

Step 2: determination of the cell number (N_c) or the total deposition area (A_t)

Substituting the known data into Equation [6-31] yields $N_c = 1.03$, which indicates that the deposition area of the existing facility is too large for the optimum design. The relationship between the cell number and the required depositional area is presented in

Figure 7.29. For comparison, the existing area and the future expanded area are also included in Figure 7.29. The figure shows that the existing area in the Kenncott Utah Copper Magna Tailings Impoundment is much larger than the required area in the optimum design. Assuming that the cell number is 4, i.e. the operation area is divided into 4 depositional cells. Based on Equation [6-34], the required total depositional area (A_t) is only 824,593 m^2. The calculated result indicates that the existing area is about 28 times larger than that required (it is worth noting that the total depositional data from Ridlen et al. (1997) may be not the exact deposition for the current operation). Even in the future, the expansion area (14,164,500 m^2) will still be 12 times larger than that required for the tailings production rate up to 213,000 tpd.

Step 3: determinations of the discharge time (T_d) and cycle time (T_c)

Substituting the above data into Equation [6-32] yields a discharge time (T_d) of 7 hours. Hence, the cycle time is the sum of the discharge time and drying time, $T_c = 21 + 7 = 28$ hours.

Step 4: determination of the number of full cycles per year (M_c)

From Equation [6-35], the annual cycle number, M_c, is about 313.

The optimum depositional parameters are summarized in Table 7.16.

7.4.2.4 Summary of the optimum design for the case histories

In summary, an expansion of 126,138 m^2 is required for optimum sub-aerial tailings deposition in case history #1. After expansion, the total facility should be divided into 6 depositional cells. The gold tailings should be continuously deposited into one cell at any one time for 31 hours, which results in a layer thickness of 15 cm. Then the tailings slurry should be deposited into an adjacent depositional cell. The freshly deposited layer should then be allowed to settle, drain, and air-dry for a period of 155 hours. The cycle time for the deposition is 186 hours.

In case history #2, since the existing depositional area (about 696,355 m^2) is much greater than the required area (111,458 m^2) for the optimum sub-aerial deposition, the facility should be divided into 6 sub-operational zones, each of which should then be further divided into 6 individual depositional cells. The sub-depositional zones should be operated sequentially to balance the elevation of the depositional area. The gold tailings should be continuously deposited into one depositional cell at any one time for 64 hours, which results in a layer thickness of 25 cm. Then the tailings should be deposited to an adjacent depositional cell and the freshly deposited layer should be allowed to settle, drain, and air-dry for a period of 321 hours. The cycle time for case history #2 is 385 hours.

The situation for case history #3 is similar to that of the second location, i.e. the existing depositional area (23,067,900 m^2) is larger than the required area for optimum sub-aerial deposition (824,593 m^2). The current facility should be divided into about 28 sub-depositional zones (the current total deposition area cited from the literature of Ridlen et al. (1997) may be not the true deposition area). All these zones should be deposited sequentially to maintain the balance of the deposition area. Each sub-depositional zone should be further divided into 4 individual depositional cells. Once the copper tailings have been deposited in one cell at any one time for 7 hours, or the layer thickness reaches 17 cm, the tailings deposition should be shifted to the adjacent cell. Then the fresh layer should be allowed to settle, drain, and desiccate for a period of 21 hours. The cycle time for case history #3 is about one day.

7.4.3 Modeling current operations

7.4.3.1 Case history #1

The existing operation in case history #1 was modeled using DOSTAR under the conditions of E_P=3.3E-8 m/s and H_ξ = 0.16 and 0.32 m. The input data for the model were mainly from the available data presented in Table 7.11 to 7.13. The other input data that were not available were assumed to be the same as for the gold tailings from the Lupin Mine as presented in Chapter 4.

Table 7.17 shows the modeling results for case history #1. When the tailings were deposited for only one day into each cell, i.e. the one-day operation, the deposition layer thickness was 0.16 m. The table shows that it takes 162 hours (i.e. 6.75 days) and 177 hours (i.e. 7.4 days) to desiccate the tailings to initiate and propagate the crack through the first layer and subsequent layers. In other words, the minimum cycle time for cracking through the layer is about 8 days. The predicted results for the third layer are the same as for the second layer. If the layers were allowed to desiccate and the cracking to occur through the layers, the amount of the recyclable water would be about 79% for the one-day operation.

When the tailings were continuously deposited for 2 days at each cell, i.e. the two-day operation, the deposition layer thickness was 0.32 m. The modeling results indicate that it takes 334 hours (i.e. 13.9 days) and 345 hours (i.e. 14.4 days) to dry the tailings to initiate and propagate the crack through the layers. Thus, the minimum cycle time for cracking through the layer to occur is 16 days for this operation. The predicted results for the third layer are the same as for the second layer. The predicted data show that there would be about 78% of the water available for recycling, if the layers were allowed to desiccate and cracking occurred through the layers.

However, the current cycle times are 7 and 14 days for the one-day and two-day operations respectively. A comparison of the predicted minimum cycle time and the current cycle time indicates that not enough time is presently allowed for drying to initiate and propagate cracks through the layers. Figure 7.30 presents the change in degree of saturation as the desiccation progress in the one-day operation. The figure shows that after 144 hours (6 days) of drying, the tailings only desaturated to a value of about 85%. In other words, the current one-day operation results in a degree of saturation of 85%, far from the value (71%) for drying to initiate and propagate cracks through the layer. This implies that the existing operations could not produce desiccation cracks. Field observation showed that the tailings in this facility did not typically exhibit tension cracks on the surface. Only a few cracks with a spacing of about three feet were observed. Figure 7.31 shows the comparison between the predicted and measured degree of saturation. The predicted results show good agreement with the observation made during the field operation.

7.4.3.2 Case history #2

The existing operation in case history #2 was modeled using DOSTAR under the conditions of E_P=3.3E-8 m/s and H_ξ = 0.91 m. The input data for the model were mainly from the available data presented in Table 7.11 and 7.14. Similarly, data which were not available were obtained from the gold tailings results presented in Chapter 4.

The modeling results for the second case are presented in Table 7.18. When the tailings were deposited for 6 continuous months of the year into one cell, the accumulated deposition layer thickness is about 0.91m. Table 7.18 shows that 2188 hours (3 months) after deposition finished, the tailings would desiccate and cracking would occur through the layer with a spacing of 88.3 cm and width of 2.8 cm. The tailings in this case were allowed to dry for 6 continuous months after deposition. Once the crack initiated and propagated through the layer, the crack width increases as moisture is continuously extracted by evaporation from the tailings for the rest of the drying period. On the other hand, the secondary crack may initiate as the desiccation continues for a long period. At the end of drying (6 months after deposition), the predicted crack dimensions are shown in Table 7.18. Data show that with the progress of desiccation, the spacing of primary cracks did not change essentially, while the crack width kept growing until after 2264 hours (94 days) they reached 7.5 cm. In other words, the desiccation crack is at its final width three days after it propagates through the layer.

Field observation revealed that cracks about 3 to 4 inches wide with 2 to 3 foot spacing and at least 3 feet deep occurred within the deposit. Figure 7.32 shows the primary and second cracks observed in the field. The comparison between the model prediction and in situ observed results shows remarkable agreement with crack spacing and width. This also supports the capability to predict cracking using "DOSTAR."

7.4.4 Comparison between current and optimum operation

7.4.4.1 Comparison of the case history #1

Since the optimum deposition layer thickness (H_{ξ_0}=15 cm) is close to that of the one-day operation (H_{ξ}=16 cm), the comparison in case history #1 was made between the one-day operation and the optimum operation. As mentioned previously, in the one-day operation, the tailings were deposited for one day into a cell and then the tailings were allowed to settle, drain, consolidate, and desiccate for only 6 days after deposition. Table 7.19 presents a comparison of the modeling results for the existing one-day operation and the optimum operation. Since there is not enough drying time for the one-day operation, the tailings only desiccated to a degree of saturation of 85% and cracking did not occur. Table 7.19 shows that the proposed optimum operation offers 5 orders of magnitude higher downward hydraulic conductivity for the new deposited layer than the existing one-day operation. The higher the downward hydraulic conductivity, the faster the consolidation of the next layer and the greater the amount of recyclable water available.

Data show that the optimum operation would have 79% recyclable water available, while the existing operation has 78% water available for recycling. Data indicate that the optimum operation has a larger volume reduction than the one-day operation. This figure is significant in that it saves the tailings facility volume and increases the life of the facility. After desiccation, the tailings in the optimum operation desaturate, and the minimum degree of saturation is 71% compared to 85% for the existing operation. Grozic (1999) concluded that if the degree of saturation decreases to below 80%, then the potential for flow liquefaction is greatly reduced. In addition, the lower the degree of saturation is, the higher the resistance to cyclic liquefaction. However, in the present one-day operation, the tailings only desaturate to 85% after drying for 144 hours, which raises a concern related to stability. In summary, the optimum operation has advantages over the existing one-day operation, including greater hydraulic conductivity, more recyclable water available, a lower storage volume and, potentially, increased stability of the tailings facility.

A comparison between Table 7.19 and 7.12 indicates that the predicted degrees of saturation after 144 hours of desiccation are in good agreement with the observed field data in case history #1.

One disadvantage of the optimum operation here is that it requires an expansion of the depositional area.

7.4.4.2 Comparison of case history #2

Table 7.20 presents a comparison between the current operation and the optimum operation in the first layer of deposition. Although data in the table indicate that the current operation has a slightly higher amount of recyclable water and volume reduction and a lower degree of saturation for the first single layer, the current operation has the following disadvantages over the optimum designed operation:

- **Lower hydraulic conductivity after the deposition of the second layer**. Due to the extremely long drying time of the existing operation, the desiccation cracks were well developed and the width of the cracks much larger than the maximum diameter of the tailings in the current operation. In this situation, the newly deposited tailings fill in the cracks and block the macro hydraulic conductivity associated with open cracks. This greatly reduces the macro hydraulic conductivity, which has a significant effect on the future consolidation and amount of recyclable water available. The predicted results show that the macro hydraulic conductivity in the current operation is only 7.5E-8 m/s, 3 orders of magnitude lower than in the optimum case. Obviously, a lower amount of recyclable water and a volume reduction will be experienced with placement of subsequent layers due to the lower hydraulic conductivity.
- **Higher potential of re-saturation of the dried layer**. As discussed above, due to the infilling of cracks, the downward overall hydraulic conductivity decreases; thus, the dried layer is more likely to become re-saturated by the fresh layer. Hence, the resistance to the liquefaction of the tailings could decrease dramatically.
- **Higher risk of blowing dust**. Due to the long drying time, the surface becomes extremely dry as indicated by the low degree of saturation. This dried surface will be much more likely to result in blowing dust. Special provisions have to be taken to control the dust blowing. Although the optimum operation has a similar problem, more frequent deposition decreases the problem.
- **A larger facility and higher construction costs**. Data show that only one sixth of the total current deposition area is sufficient for the optimum designed operation. This larger constructed facility means higher costs in terms of capital investment.

7.5 SUMMARY AND CONCLUSIONS

The "DOSTAR" model was tested using both laboratory measurements and field observations in this study. The optimum deposition design method for sub-aerial tailings disposal using the model was demonstrated. In addition, three case studies were carried out. The following conclusion are drawn from this chapter:

1. The numerical testing results show that DOSTAR can be used to model not only in situ sub-aerial tailings disposal but also laboratory sedimentation, consolidation, and desiccation tests. It works well for both sandy and clayey tailings. The model has the ability to predict the initiation and propagation of a desiccation crack.
2. In the sub-aerial tailings deposition design for arid regions, it is important to optimize the deposition parameters to minimize the storage volume of the tailings, maximize the recyclable water and to enhance the safety of the tailings facility. It was shown that DOSTAR is very useful for predicting the optimum depositional parameters.
3. In sub-aerial tailings deposition, the important deposition parameters are deposition layer thickness, crack dimensions, cycle time, total deposition area, and deposition cell number.
4. The crack width should be no greater than the maximum particle size of the tailings. The hydraulic conductivity of cracked tailings can increase dramatically by several orders of magnitude by keeping the cracks open. However, if infilling occurs in the cracked tailings, the hydraulic conductivity of the cracked tailings will show small increases beyond that of the consolidated tailings.
5. There are two optional deposition design schemes. One is to keep the layer fully saturated all the time. The other is allowing deposits to dry and crack to provide the macro hydraulic conductivity. It was concluded that the latter scheme is the best since it offers the following advantages over the former scheme: a higher

macro hydraulic conductivity and volume reduction, enhanced safety against liquefaction potential and a greater amount of recyclable water.

6. The deposition layer thickness directly influences the quality of the deposition. The thicker the layer, the larger the crack spacing and the smaller the crack width.
7. The clay contents have a great effect on the parameter of the cracks. The higher the clay contents, the greater the crack width and the smaller the crack spacing.
8. The traditional range of the deposition layer thickness in the sub-aerial tailings disposal (0.1 to 0.15m) is not suitable for most of the tailings studied in this project with a potential evaporation rate of 3.3E-8 m/s.
9. The potential evaporation rate also directly affects the deposition. The higher the potential evaporation rate, the larger the crack width, the smaller the crack spacing and the shorter time to dry and for cracks to propagate through the layer.
10. The most common safety risk of the sandy tailings facility is liquefaction failure. Desaturation of the tailings can enhance the resistance to liquefaction of the tailings. It is important to desaturate the sandy tailings to a degree of saturation of 80% to minimize the risk of liquefaction failure. Since the optimum sub-aerial tailings deposition offers a degree of saturation lower than 80%, these facilities may provide greater resistance against liquefaction.

Table 7.1 Properties of oil sand mature fine tailings (MFT) (modifiec from Suthaker 1995)

Initial solids content, S_0 (%)	Fine content (%)	Bitumen Content (%)	Specific Gravity, G_s	Unit Weight (kN/m^3)
32.4	89	8.6	2.35	12.2

Table 7.2 Parameters for MFT used in the model (modified from Suthaker 1995)

$e = A_1\sigma'^{B_1}$		$k = A_2 e^{B_2}$	
A_1	B_1	A_2 (m/s)	B_2
3.3697	-0.3118	6.16e-11	4.021

Note: σ' is in kPa.

Table 7.3 Main input data used in model (modified from Qiu and Sego 1998b)

Tailings Type		Copper	Gold	Coal	CT
Specific Gravity, Gs		2.75	3.17	1.94	2.6
Particle Size, D_{100} (mm)		2.00	0.84	2.00	2.00
Compression parameters ($e=a_1(\sigma')^{b1}$)	a_1	0.9233	0.9803	1.4444	0.9651
	b_1	-0.0491	-0.0806	-0.1536	-0.1585
Hydraulic conductivity parameters ($k = a_2(e)^{b2}$ (m/s)	a_2	1.0E-6	6.0E-7	2.0E-8	6.0E-9
	b_2	3.0892	2.172	4.0686	1.3754
Tensile strength, σ_t (kPa)		20	18	10	16
Fracture toughness, κ_c (kN/m$^{1.5}$)		3.5	3.25	2.75	3.3
Original solids contents, s_0 (%)		35	37	42	58
Potential evaporation rate, E_p (x 10^{-8}m/s)	Case 1	3.3	3.3	3.3	3.3
	Case 2	6.6	6.6	6.6	6.6

Table 7.4 Comparison between scheme 1 and scheme 2

Scheme Number	Items	Tailings Type			
		Copper	Gold	Coal	CT
	Deposited Thickness, H_ξ (m)	0.2	0.25	0.25	0.2
1	Recycle Water (%)	83	82	47	44
	Volume Reduction (%)	70	71	45	36
	Mini. Hydraulic Conductivity, k (m/s)	4.1E-7	3.5E-7	1.4E-8	3.8E-10
	Elapsed Time (Hours)	10	37	316	5895
	Mini. Degree of Saturation, S (%)	100	100	100	100
2	Recycle Water (%)	92	88	49	45
	Volume Reduction (%)	71	74	46	36
	Mini. Hydraulic Conductivity, k (m/s)	8.7E-4	1.6E-4	3.6E-3	5.5E-3
	Elapsed Time (Hours)	28	47	317	5898
	Mini. Degree of Saturation, S (%)	38	69	85	41

Note: $E_p = 3.3 \times 10^{-8}$ m/s for all cases; mini. means minimum.

Table 7.5 Comparison of modeling results for variation of a layer thickness

H_ξ (cm)	Crack Dimension	Tailings Type (Ep=3.3E-8 m/s)			
		Copper	Gold	Coal	CT
10	Crack Spacing, B (cm)	97.7	91.5	55.6	85.7
	Crack Depth, b (cm)	2.94	2.64	5.73	5.82
	Crack Width, υ (cm)	0.310	0.477	1.174	0.914
	Volume Remaining (%)	29.4	26.4	57.3	58.2
	Recyclable Water (%)	92.0	88.7	53.4	55.7
	Elapsed Time (Hour)	13	16	94	3414
15	Crack Spacing, B (cm)	121.8	114.6	80.6	89.1
	Crack Depth, b (cm)	4.44	4.02	8.24	9.38
	Crack Width, υ (cm)	0.240	0.280	0.829	0.405
	Volume Remaining (%)	29.6	26.8	54.9	62.5
	Recyclable Water (%)	92.4	89.3	53.0	46.7
	Elapsed Time (Hour)	16	19	142	4715
20	Crack Spacing, B (cm)	154.1	145.1	101.8	105.5
	Crack Depth, b (cm)	5.76	5.17	11.31	12.79
	Crack Width, υ (cm)	0.118	0.170	0.495	0.192
	Volume Remaining (%)	28.8	25.9	56.6	64.0
	Recyclable Water (%)	92.0	88.3	53.6	44.7
	Elapsed Time (Hour)	28	34	164	5897
25	Crack Spacing, B (cm)	162.0	158.6	141.0	151.4
	Crack Depth, b (cm)	7.19	6.61	13.58	15.92
	Crack Width, υ (cm)	0.046	0.068	0.183	0.091
	Volume Remaining (%)	28.8	26.4	54.3	63.7
	Recyclable Water (%)	92.1	88.2	48.9	45.1
	Elapsed Time (Hour)	32	47	317	7261

Table 7.6 Comparison of modeling results for different potential evaporation rate

E_p (m/s)	Crack Dimension	Tailings Type			
		Copper	Gold	Coal	CT
3.3E-8	Crack Spacing, B (cm)	98	92	56	86
	Crack Depth, b (cm)	2.94	2.64	5.73	5.82
	Crack Width, υ (cm)	0.31	0.48	1.17	0.91
	Accumulated Tailings Height (cm)	2.94	2.64	5.73	5.82
	Recyclable Water Available (%)	92	88	53	56
	Elapsed Time (hours)	13	16	94	3414
6.6E-8	Crack Spacing, B (cm)	93	84	41	68
	Crack Depth, b (cm)	2.93	2.64	5.65	6.21
	Crack Width, υ (cm)	0.32	0.50	1.87	1.17
	Accumulated Tailings Height (cm)	2.93	2.64	5.65	6.21
	Recyclable Water Available (%)	90	87	43	50
	Elapsed Time (hours)	12	16	87	3321

Note: $H_\xi = 0.1$m.

Table 7.7 D_{100} and predicted tensile crack dimensions and time of the tailings

Tailings Type	Copper	Gold	Coal	CT
Crack Spacing (cm)	98	92	56	86
Crack Depth (cm)	2.94	2.64	5.73	5.82
Crack Width (cm)	0.31	0.48	1.17	0.91
Elapsed Time (Hours)	13	16	94	3414
D_{100} (cm)	0.2	0.084	0.2	0.2

Note: E_p = 3.3 E-8 m/s, H_ξ = 0.1 m.

Table 7.8 Predicted final volume and recyclable water after cracking

Tailings Type	Copper	Gold	Coal	CT
Normalized Volume	0.29	0.26	0.57	0.58
Normalized Recyclable Water, Q_6/Q_1 (%)	92	89	53	56

Note: E_p = 3.3 E-8 m/s, H_ξ = 0.1 m.

Table 7.9 Predicted surface hydraulic conductivity before and after cracking

Tailings Type	Hydraulic Conductivity, (m/s) ($H_\xi = 0.1$ m)		Hydraulic Conductivity, (m/s) ($H_\xi = 0.2$ or0.25 m)*	
	Before Cracking	After Cracking	Before Cracking	After Cracking
Copper	7.57 E-7	1.24E-6 **	6.87E-7	8.73E-4
Gold	4.82E-7	5.99E-7 **	4.27E-7	1.63E-4
Coal	3.89E-7	4.06E-7 **	1.08E-7	3.55E-3
CT	3.82E-9	3.93E-9**	4.60E-9	5.45E-3

Note: $E_p = 3.3$ E-8 m/s; * $H_\xi = 0.2$ m for the copper tailings and CT, $H_\xi = 0.25$ m for the gold and coal tailings; **macro hydraulic conductivity in the filled cracked tailings due to $\upsilon > D_{100}$.

Table 7.10 Comparison of modeling results for multiple layer deposition

Deposition Sequence	Items	Tailings Type			
		Copper	Gold	Coal	CT
	Layer Thickness, H_ξ (m)	0.2	0.25	0.25	0.2
First Layer	Crack Spacing (cm)	154	159	141	106
	Crack Depth (cm)	5.76	6.61	13.58	12.79
	Crack Width (cm)	0.12	0.07	0.18	0.19
	Normalized Recyclable Water (%)	92	88	49	45
	Accumulated Tailings Height (cm)	5.76	6.61	13.58	12.79
	Total Elapsed Time (Hour)	28	47	317	5898
Second Layer	Crack Spacing (cm)	154	159	141	105
	Crack Depth (cm)	5.76	6.61	13.58	12.79
	Crack Width (cm)	0.14	0.08	0.19	0.2
	Normalized Recyclable Water (%)	92	88	51	45
	Accumulated tailings Height (cm)	11.52	13.22	27.16	25.58
	Total Elapsed Time (Hour)	51	94	633	11794
Third Layer	Crack Spacing (cm)	154	159	141	105
	Crack Depth (cm)	5.76	6.61	13.58	12.79
	Crack Width (cm)	0.14	0.08	0.19	0.2
	Normalized Recyclable Water (%)	92	88	51	45
	Accumulated tailings Height (cm)	17.28	19.83	40.74	38.37
	Total Elapsed Time (Hour)	74	141	950	17690

Note: $E_p = 3.3x10^{-8}$ m/s.

Table 7.11 Original conditions and existing deposition parameters

Items	Case 1	Case 2	Case 3
Bulk Density, ρ_0 (Mg/m^3)	1.29	1.44	1.29
Original Solids Content, s_0	0.35	0.49	0.35
Tailings Production Rate, P_t (t/d)	11430	2500	155000
Total Deposition Area, A_t (m^2)	331653	696355	23067900
Current Cell Number, N_c	6	2	N/A
Current Deposition Layer Thickness, H_ξ (m)	0.16 or 0.32	0.91	N/A
Current Cycle Time, T_c (day)	7 or 14	365	N/A
Average Potential Evaporation rate, E_p (m/s)	3.3E-8	3.3E-8	3.7E-8

Note: N/A means that the data are not available.

Table 7.12 Measured properties and in situ conditions of tailings for Case 1

Items	Values	
	Range	Average
Specific Gravity, Gs	2.6--2.8	2.75
Liquid Limit (%)	--	--
Plasticity Index (%)	--	--
Effective Shear Angle, ϕ' (°)	25-30	28
Effective Cohesion, C′ (kPa)	0	0
Degree of Saturation, S	0.73—0.95	0.84
Fines Content (<74 μm) (%)	18-50	34
D_{30} (mm)	0.074-0.143	0.1085
D_{50} (mm)	0.074-0.2047	0.1394
D_{60} (mm)	0.1053-0.2448	0.1751
D_{100} (mm)	2.0	2.0

Table 7.13 Regression parameters for case 1

$e = a_1(\sigma')^{b_1}$			$k = a_2(e)^{b_2}$ (m/s)			$e = a_3 \ln(\sigma') + b_3$		
a_1	b_1	R^2	a_2	b_2	R^2	a_3	b_3	R^2
0.9083	-0.0821	0.93	6.6E-8	2.45	0.97	-0.0559	0.893	0.98

Table 7.14 Basic properties of the tailings in case 2

Items	Values	
	Range	Average
Specific Gravity, Gs	2.68—2.77	2.71
Liquid Limit (%)	--	--
Plasticity Index (%)	--	--
Effective Shear Angle, ϕ' (°)	20—40	35
Effective Cohesion, C′ (kPa)	0	0
Clay Size Particles (<2μm) (%)	6—19.4	12.7
Sand content (>0.06mm) (%)	13.7—55	34.4
Fines Content (<74 μm) (%)	51.3—90.6	71.0
D_{10} (mm)	0.0011--0.007	0.004
D_{30} (mm)	0.0044—0.031	0.0177
D_{50} (mm)	0.013—0.07	0.0415
D_{60} (mm)	0.0189—0.0954	0.0572
D_{100} (mm)	0.84	0.84
Unified Soil Classification	ML—CL	

Table 7.15 Modeling results under optimum conditions

Layer Sequence	Items	Case 1	Case 2	Case 3
	Optimum Layer Thickness (cm)	15	25	17
First Layer	Crack Spacing (cm)	91	164	140
	Crack Depth (cm)	4.35	10.77	4.89
	Crack Width (cm)	0.19	0.06	0.16
	Normalized Recyclable Water (%)	79	70	92
	Accumulated Tailings Height (cm)	4.35	10.77	4.89
	Total Elapsed Time (Hour)	155	321	21
Second Layer	Crack Spacing (cm)	91	165	139
	Crack Depth (cm)	4.35	10.77	4.89
	Crack Width (cm)	0.2	0.08	0.18
	Normalized Recyclable Water (%)	79	70	92
	Accumulated tailings Height (cm)	8.70	21.54	9.78
	Total Elapsed Time (Hour)	310	659	40
Third Layer	Crack Spacing (cm)	91	165	139
	Crack Depth (cm)	4.35	10.77	4.89
	Crack Width (cm)	0.2	0.08	0.18
	Normalized Recyclable Water (%)	79	70	92
	Accumulated tailings Height (cm)	13.05	32.31	14.67
	Total Elapsed Time (Hour)	465	997	59

Table 7.16 Summary of the optimum depositional parameters

Parameters	Case 1	Case 2	Case3
Required Total Deposition Area, A_t (m^2)	457791	111458	824593
Depositional Cell Number, N_c	6	6	4
Deposition Layer thickness, H_ξ (m)	0.15	0.25	0.17
Discharge time, T_d (hour)	31	64	7
Drying Time, T_s (hour)	155	321	21
Cycle Time, T_c (hour)	186	385	28
Annual Full Cycle Number, M_c	47	23	313

Table 7.17 Modeling results for the existing operation in case history #1

Deposition Sequence	Items	Layer Thickness, H_ξ	
		0.16m	0.32m
First Layer	Crack Spacing (cm)	101	138
	Crack Depth (cm)	4.58	8.88
	Crack Width (cm)	0.18	0.07
	Normalized Recyclable Water (%)	79	78
	Accumulated Tailings Height (cm)	4.58	8.88
	Total Elapsed Time (Hour)	162	334
Second Layer	Crack Spacing (cm)	100	137
	Crack Depth (cm)	4.58	8.88
	Crack Width (cm)	0.19	0.1
	Normalized Recyclable Water (%)	78	78
	Accumulated tailings Height (cm)	9.16	17.76
	Total Elapsed Time (Hour)	339	679
Third Layer	Crack Spacing (cm)	100	137
	Crack Depth (cm)	4.58	8.88
	Crack Width (cm)	0.19	0.1
	Normalized Recyclable Water (%)	78	78
	Accumulated tailings Height (cm)	13.74	26.64
	Total Elapsed Time (Hour)	516	1024

Table 7.18 Modeling results for the existing operation in case history #2

At the time of cracking through the layer	Crack Spacing (cm)	88
	Crack Depth (cm)	38.0
	Crack Width (cm)	2.8
	Normalized Recyclable Water (%)	67
	Accumulated Tailings Height (cm)	38.0
	Total Elapsed Time (Hour)	2189
At the end of drying	Crack Spacing (cm)	88
	Crack Depth (cm)	38.0
	Crack Width (cm)	7.5
	Normalized Recyclable Water (%)	75
	Accumulated tailings Height (cm)	37.3
	Total Elapsed Time (Hour)	4383

Table 7.19 Comparison of the modeling results for case history #1

Items	State or Value at the end of the drying	
	One-Day Operation*	Optimum Operation
Cracking State	No Crack	Well-cracked ($\upsilon \leq D_{100}$)
Minimum Hydraulic Conductivity (m/s)	1.9E-8	5.7E-3
Recyclable water amount (%)	78	79
Tailings Volume Reduction (%)	70.9	71.0
Minimum Degree of Saturation (%)	85	71
Total Deposition Area (m^2)	331653	523256
Elapsed Time (hour)	144	155

Note: * drying time for the one-day operation is 6 days (144 hours).

Table 7.20 Comparison of the modeling results for case history #2

Items	State or Value at the end of the drying	
	Existing Operation	Optimum Operation
Cracking State	Well-cracked $(\upsilon > D_{100})$	Well-cracked $(\upsilon \leq D_{100})$
Minimum Hydraulic Conductivity (m/s)	7.5E-8 *	9.2E-5
Recyclable water amount (%)	75 (first layer)	70
Tailings Volume Reduction (%)	59 (first layer)	57
Minimum Degree of Saturation (%)	23	63
Total Deposition Area (m^2)	696355	111458
Elapsed Time (hour)	2289 (first layer)	321

* Note: this is the macro hydraulic conductivity with filled cracks

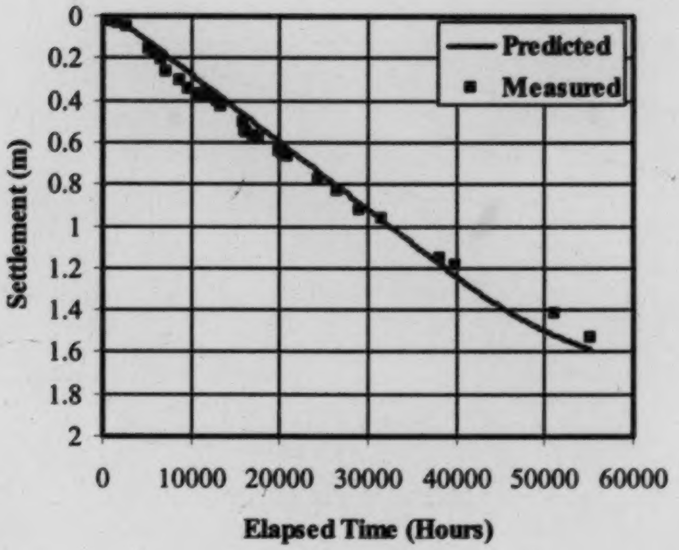

Figure 7.1 Measured and predicted settlement in a Ten Meter Standpipe

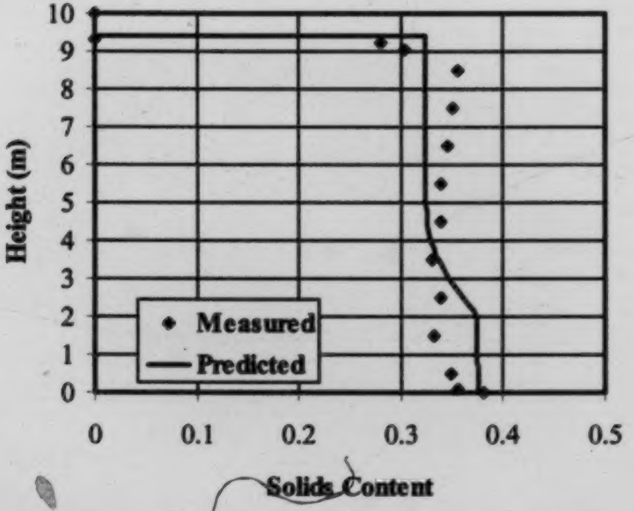

Figure 7.2 Measured and predicted solids content profile in a Ten Meter Standpipe after 20400 hours

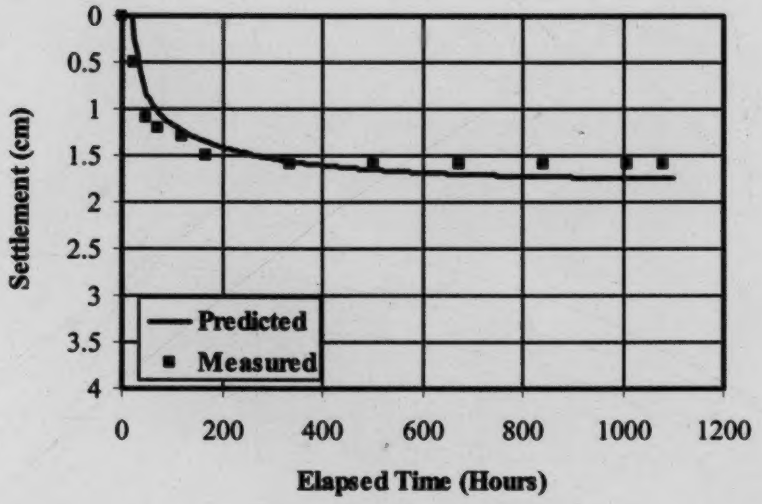

Figure 7.3 Measured and predicted settlement of copper tailings in drying test

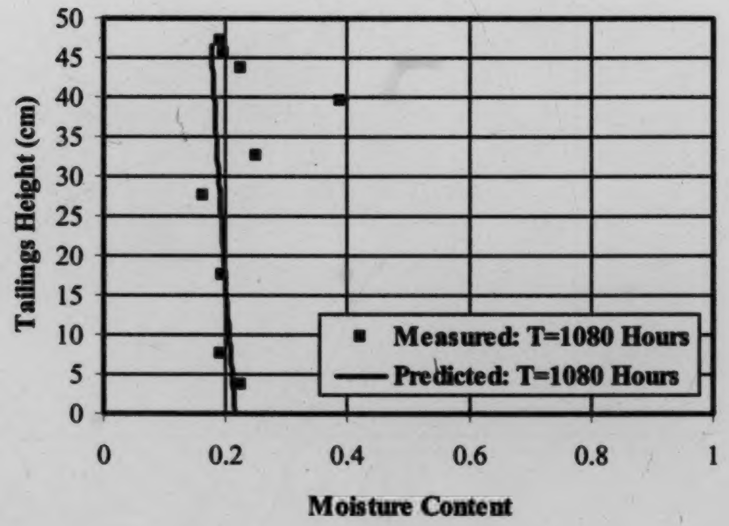

Figure 7.4 Measured and predicted moisture content profile of copper tailings in drying test

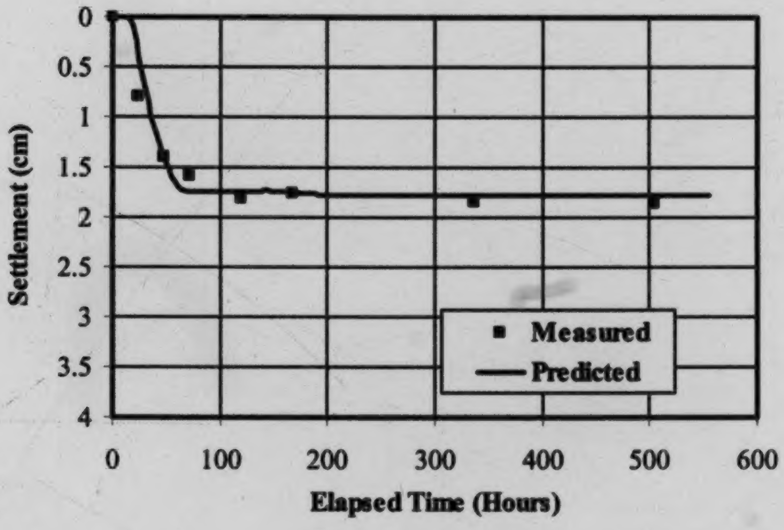

Figure 7.5 Measured and predicted settlement of gold tailings in drying test

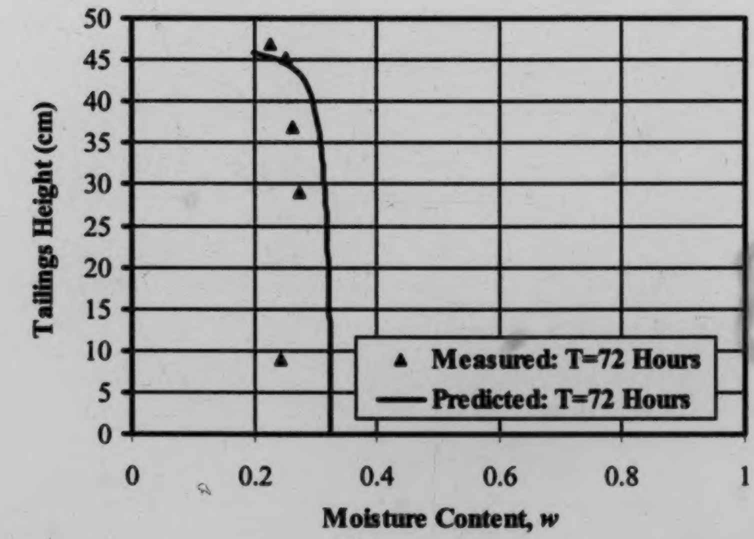

Figure 7.6 Measured and predicted moisture content profile of gold tailings in drying test

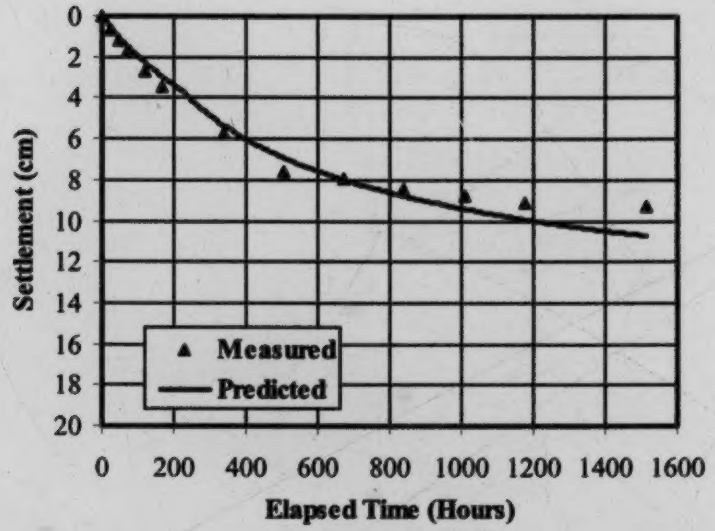

Figure 7.7 Measured and predicted settlement of coal tailings in drying test

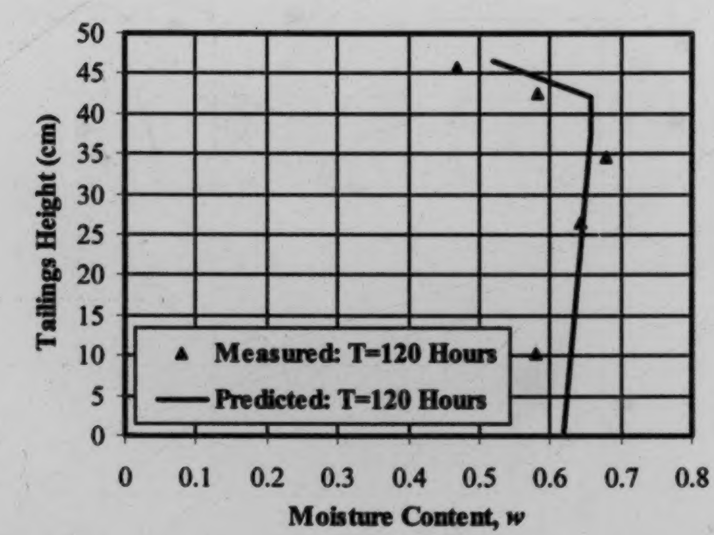

Figure 7.8 Measured and predicted moisture content profile of coal tailings in drying test

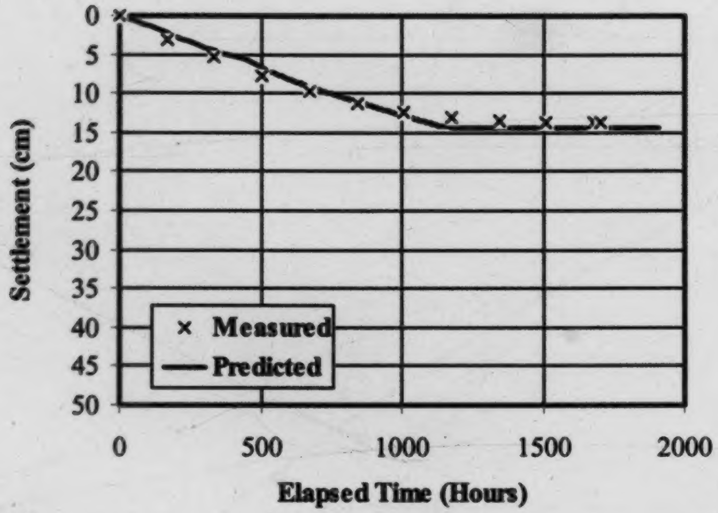

Figure 7.9 Measured and predicted settlement of CT in drying test

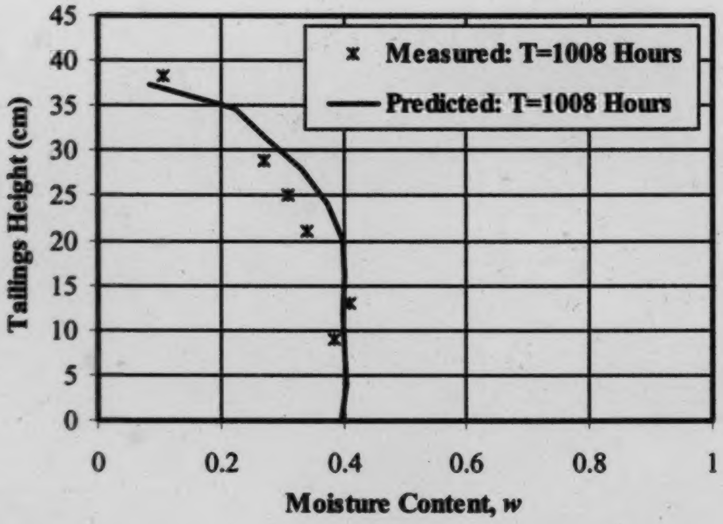

Figure 7.10 Measured and predicted moisture content profile of CT in drying test

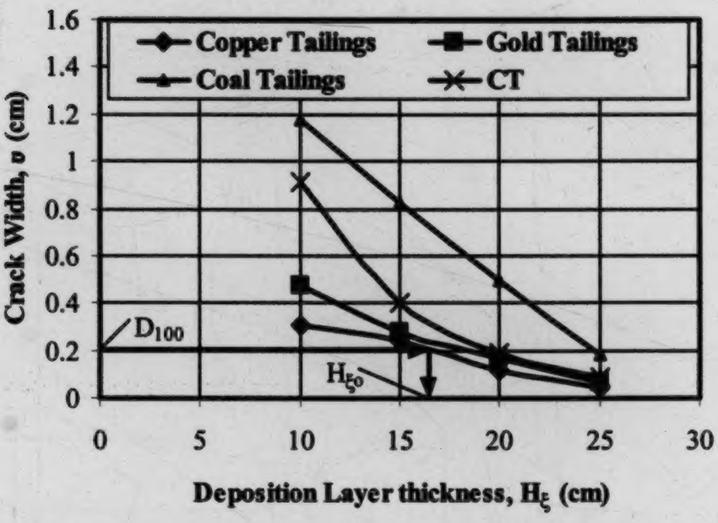

Figure 7.11 Relationship between crack width and layer thickness

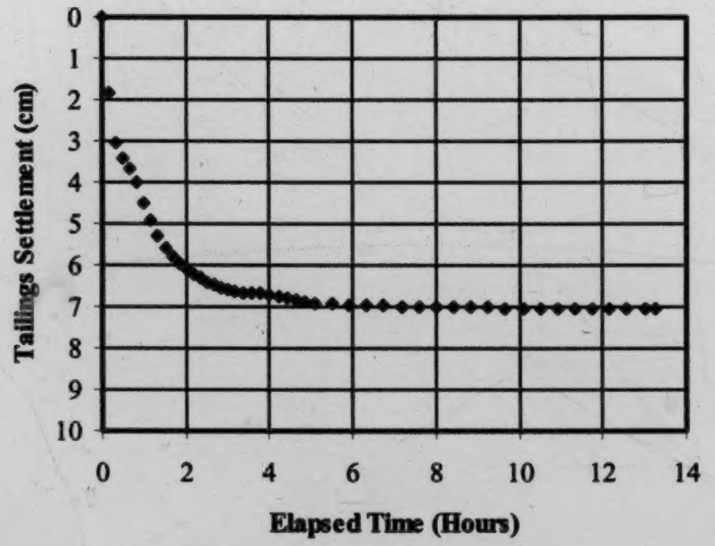

Figure 7.12 Predicted single layer settlement of the copper tailings at cracking

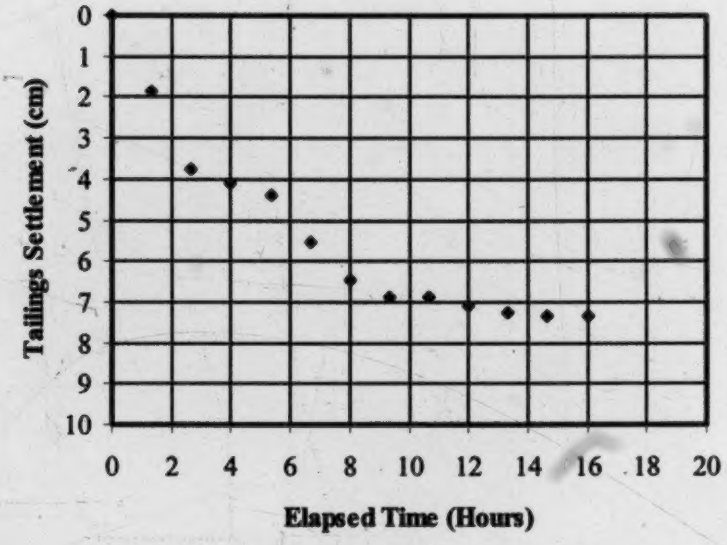

Figure 7.13 Predicted single layer settlement of the gold tailings at cracking

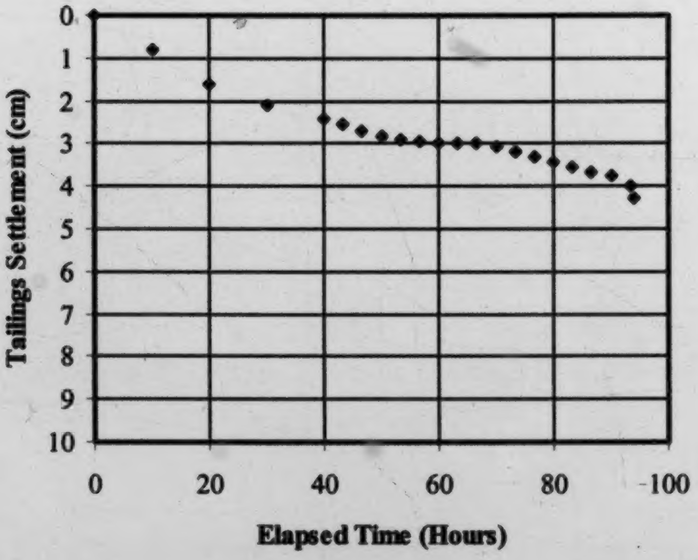

Figure 7.14 Predicted single layer settlement of the coal tailings at cracking

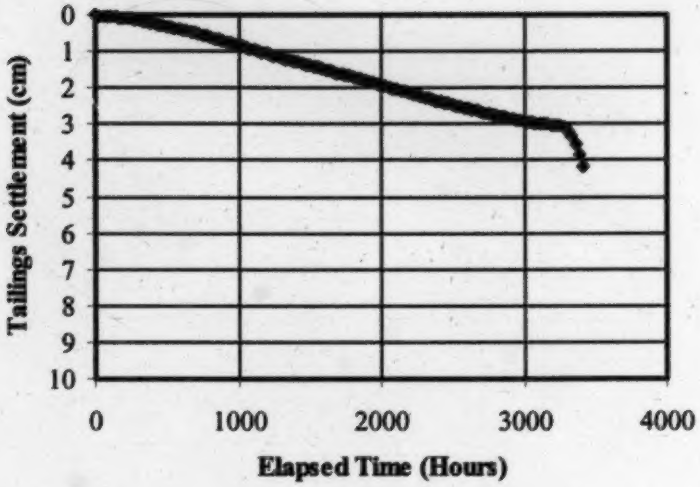

Figure 7.15 Predicted single layer settlement of CT at cracking

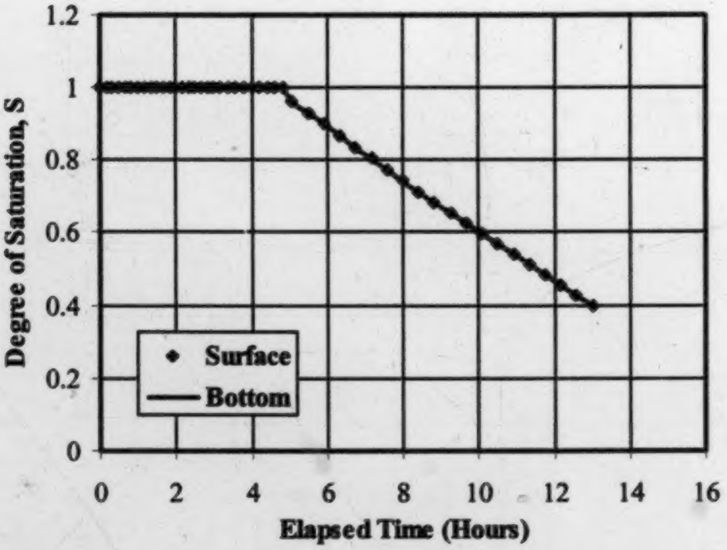

Figure 7.16 Degree of saturation change in copper tailings

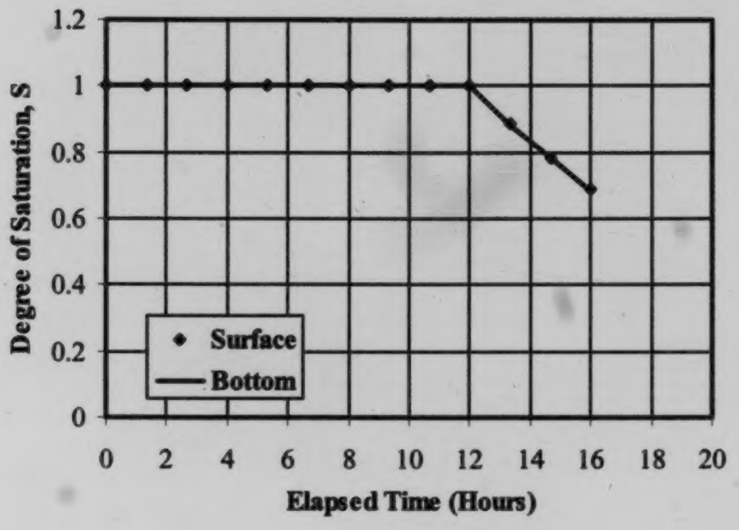

Figure 7.17 Degree of saturation change in gold tailings

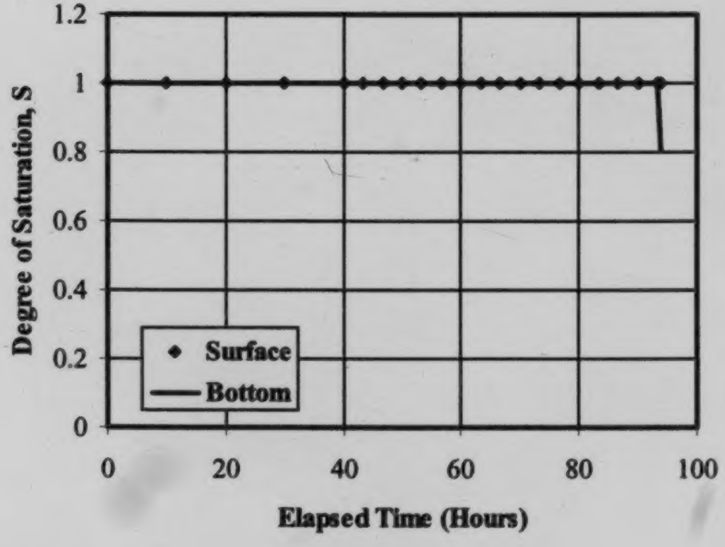

Figure 7.18 Degree of saturation change in coal tailings

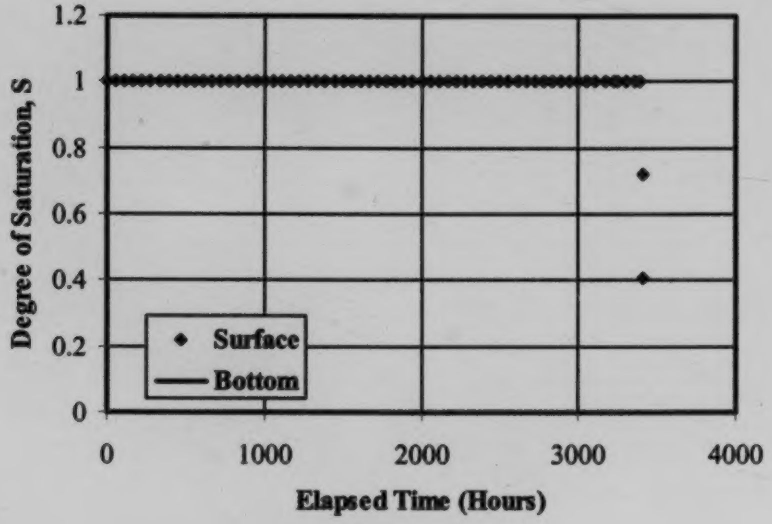

Figure 7.19 Degree of saturation change in CT

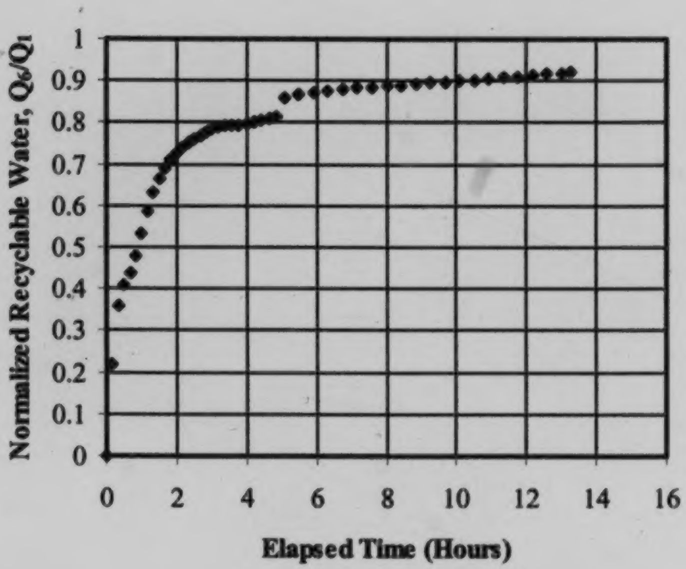

Figure 7.20 Normalized recyclable water in copper tailings

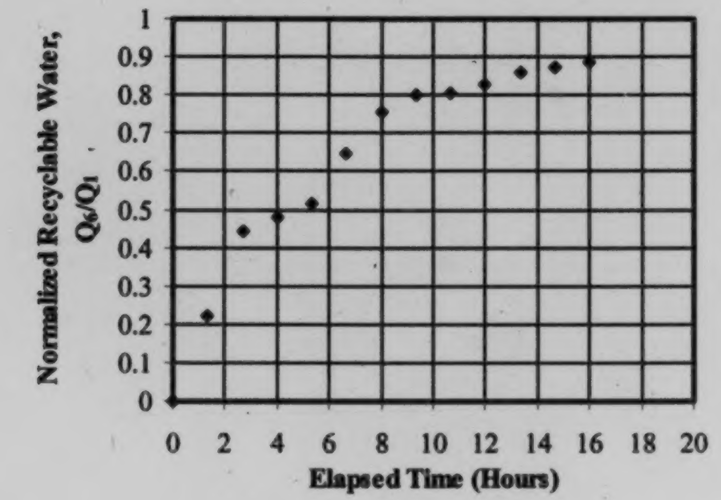

Figure 7.21 Normalized recyclable water in gold tailings

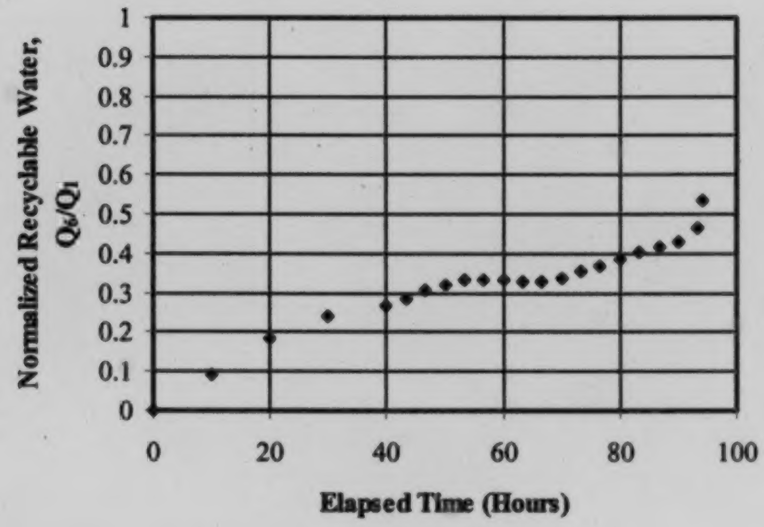

Figure 7.22 Normalized recyclable water in coal tailings

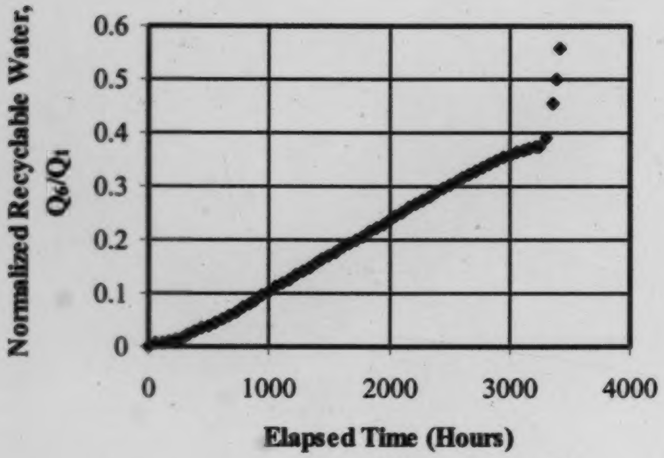

Figure 7.23 Normalized recyclable water in CT

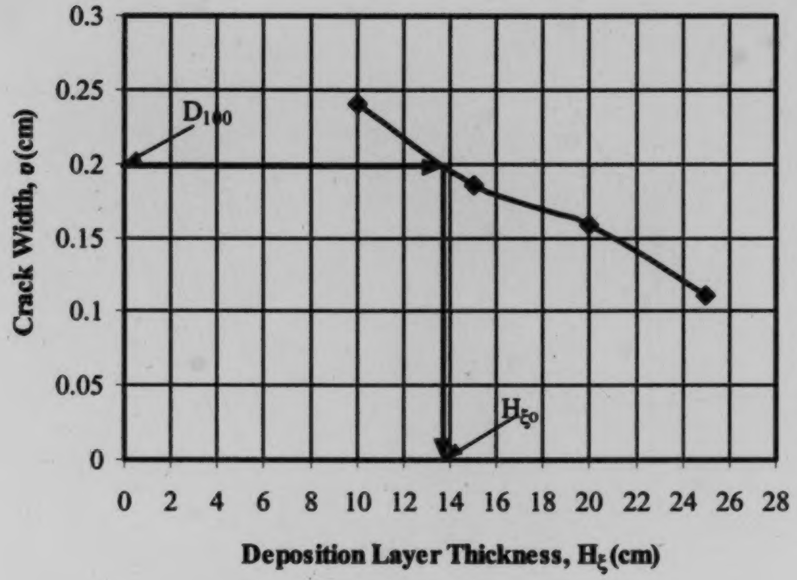

Figure 7.24 Optimum design curve for case history #1

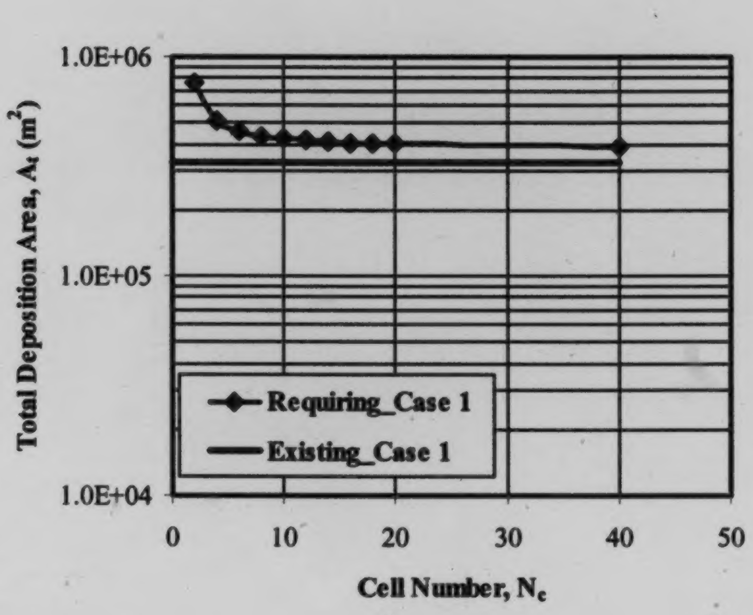

Figure 7.25 Deposition area versus cell number plot for case history #1

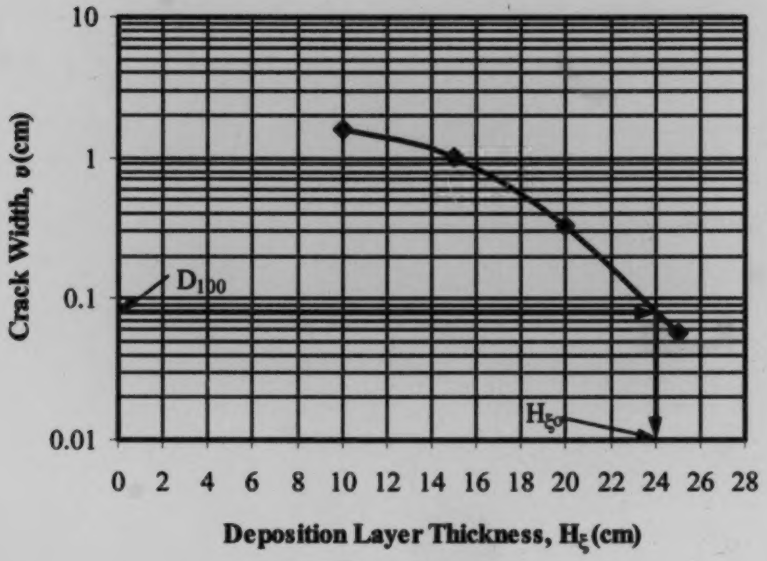

Figure 7.26 Optimum design curve for case history #2

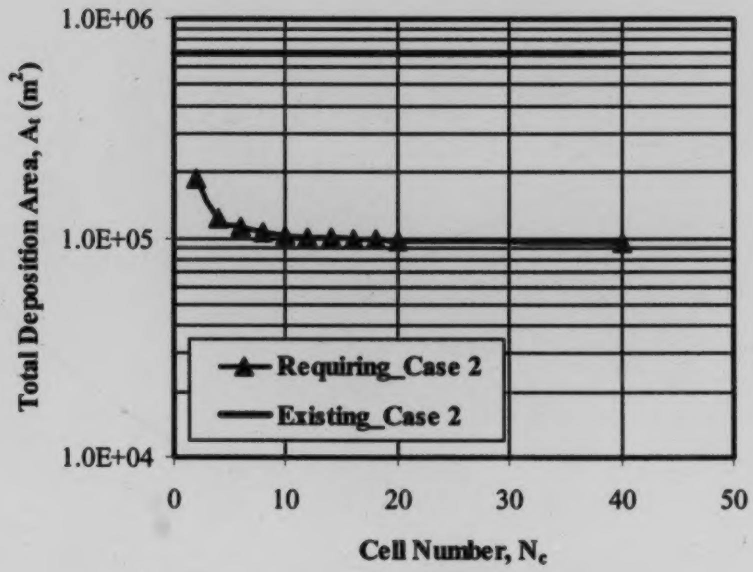

Figure 7.27 Deposition area versus cell number plot for case history #2

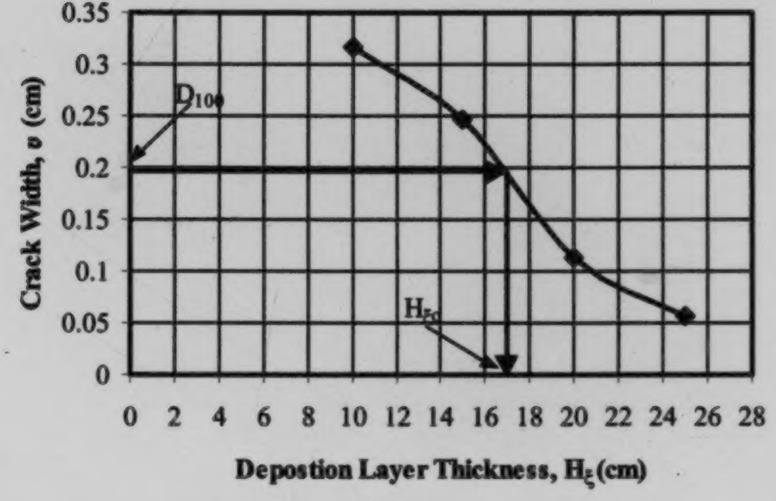

Figure 7.28 Optimum design curve for case history #3

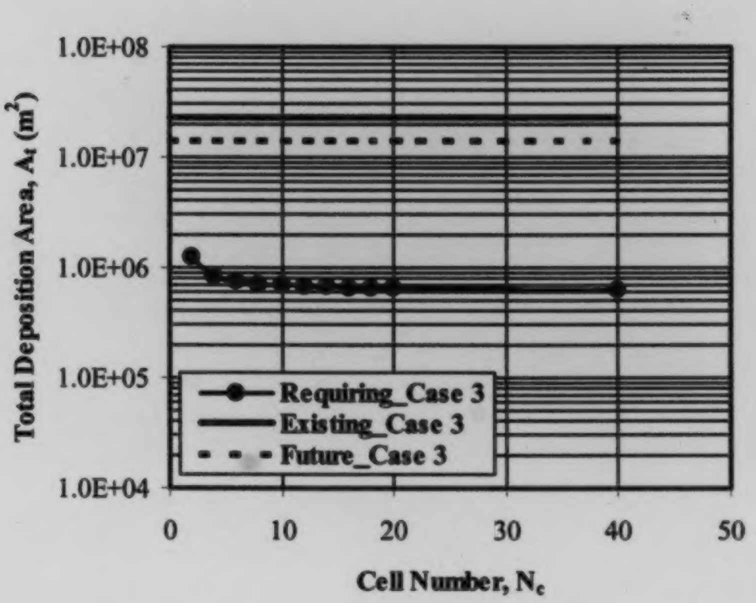

Figure 7.29 Deposition area versus cell number plot for case history #3

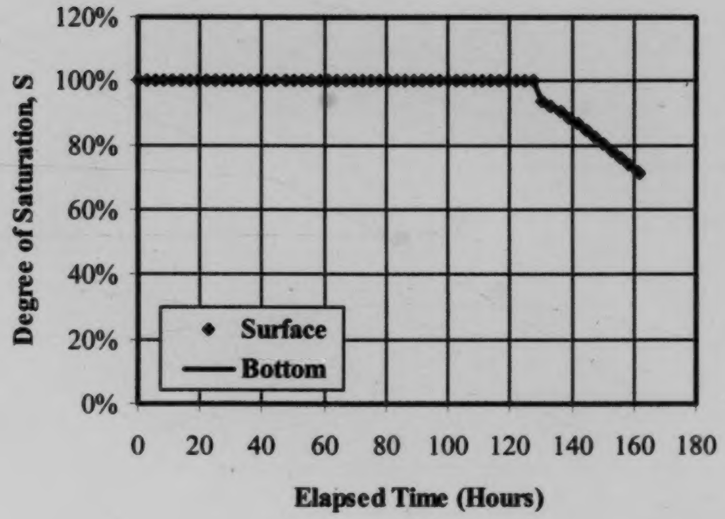

Figure 7.30 Degree of saturation in one-day operation for case history #1

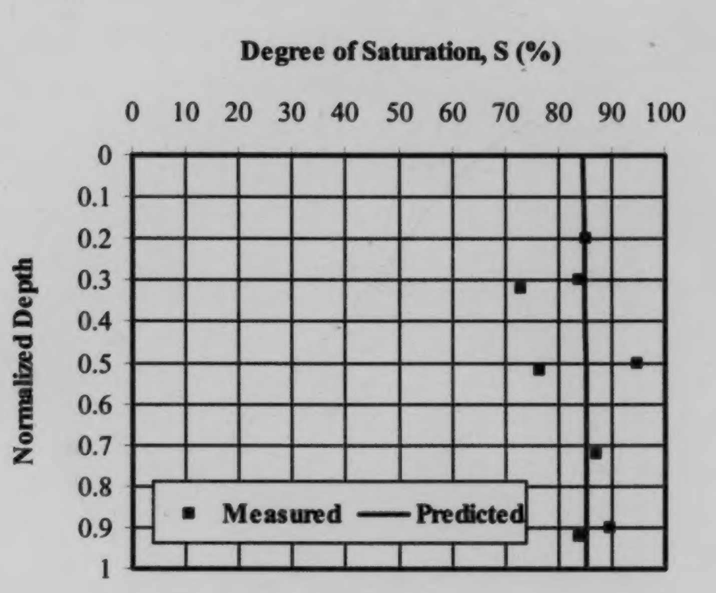

Figure 7.31 Measured and predicted degree of saturation in case history #1

Figure 7.32 Primary and secondary cracks within the tailings in the field for case history #2

CHAPTER 8 SUMMARY, CONCLUSIONS, AND RECOMMENDATIONS

8.1 SUMMARY AND CONCLUSIONS

The sub-aerial tailings deposition technique involves systematic deposition of tailings in a thin layer by discharging slurry from one or more points along the perimeter of the impoundment area. As slurry flows toward the low point in the impoundment, the tailings are allowed to settle, drain, and partially air dry, and as a result they increase in density in thin layers prior to covering them with the next layer. The free water released to the surface and the downward drainage are collected to be recycled into the processing system. Subsequent layers are then deposited, and the cycle is repeated.

To understand the tailings behavior and to further improve the efficiency of the disposal method, a series of laboratory tests were carried out and the engineering properties of the tailings studied in this project were investigated. The physical process of the sub-aerial tailings deposition technique was described. Then the factors affecting sub-aerial deposition were analyzed. A one-dimensional unified theory of sedimentation, consolidation, and desiccation that simulated the physical interaction of soil and fluid particles within the deformable soil skeleton has been described in this thesis. Then a design model for optimum sub-aerial tailings deposition in arid regions was established and presented. The model, referred to as DOSTAR, was coded in Visual Basic, and is capable of predicting sedimentation, consolidation, desiccation, crack initiation, crack propagation, crack dimensions (spacing, depth, and width), tailings volume, and water available for recycling. The design model was validated using results from both laboratory tests and field observations. Finally, the application of the model was demonstrated and some case studies were presented.

There were three phases in this research. Phase one involved theoretical background investigations. Phase two was to establish a unified theoretical framework. The final phase was to validate and apply the design model. The summary and conclusions drawn from this study are presented in the following sections.

8.1.1 Phase 1: theoretical background investigation

A literature review of previous work on sub-aerial tailings deposition, hydraulic fill, and modeling sedimentation, consolidation, and desiccation of soils was presented. A series of laboratory tests were carried out to identify the basic physical and engineering properties of tailings and their consolidation and desiccation behavior. The conclusions drawn from this phase of the research are the following:

1. The physical processes of the sub-aerial deposition technique are sedimentation, consolidation, and desiccation.
2. A comprehensive model for the evaluation of the design of an optimum deposition for the sub-aerial tailings disposal in arid regions with the intent of maximizing the amount of water available for recycling was not currently available.
3. An important property of the desiccated soil is the soil-water retention characteristics; any analysis of soil undergoing desiccation should consider this important characteristic.
4. Hydraulic conductivity is an important parameter in modeling the consolidation and desiccation of soils. The unsaturated hydraulic conductivity decreases dramatically with the increase in the matric suction.

5. A tension crack initiates when the total lateral tensile stress reaches the tensile strength of the soil. Linear elastic fracture mechanics is usually used to analyse crack propagation, and it is commonly proposed that the spacing of the cracks can be estimated from the theoretical stress relief field by assuming that another crack may exist at between 5% and 10% stress relief.
6. The copper, gold and oil sand CT tailings studied in this project are non-plastic cohesionless soils. They behave like sandy soils, except for the CT, which behaves unusually due to the presence of the bitumen. However, the coal wash tailings are plastic cohesive soils.
7. A near linear relationship exists between the void ratio and the logarithmic scale of the effective stress for these tailings. The compression indexes are 0.09, 0.16, 0.38, and 0.27 for copper, gold, coal, and CT tailings respectively.
8. The saturated hydraulic conductivity of the tailings is highly dependent on void ratio. The saturated hydraulic conductivity of the tailings is in a range of 2.7×10^{-5} to 9.8×10^{-5} cm/s for the copper and gold tailings with void ratios in a range of 0.7 to 1.0, of 4.0×10^{-7} to 1.1×10^{-5} cm/s for the coal tailings with void ratios in a range of 0.7 to 1.6, and of 2.2×10^{-7} to 6.3×10^{-7} cm/s for the CT with void ratios in a range of 0.5 to 1.1.
9. A shrinkage curve indicates the void ratio changes with moisture content. A non-linear relationship exists between the void ratio and moisture content.
10. The copper and gold tailings behave as strain softening soils in undrained loading, while the coal tailings and CT exhibit strain hardening behavior. The effective friction angles (ϕ') are 30°, 32°, 33°, and 34° for the CT, coal, gold, and copper tailings respectively. The effective cohesion is zero for the copper and gold tailings, 10 kPa for the coal tailings, and 3 kPa for the CT.

8.1.2 Phase 2: establishment of the unified theoretical framework

In this research phase, the water balance during the operation of the sub-aerial tailings deposition facility was analyzed. The factors affecting the sub-aerial technique were described. A one-dimensional theory of sedimentation, consolidation, and desiccation was presented. In addition, a design model capable of predicting sedimentation, consolidation and desiccation, crack initiation, crack propagation, crack dimensions (spacing, depth, and width), tailings volume, and the amount of recyclable water was established and coded in a modern computer language. The main conclusions drawn from this phase of the research are:

1. The physical processes of the sub-aerial tailings deposition technique can be modeled using a unified theory.
2. The numerical method, i.e. the Douglas-Jones method adapted here, can be used to solve the governing equations. Therefore, the processes of the sub-aerial tailings deposition can be modeled.
3. There are eight identifiable components of the water balance in sub-aerial tailings deposition.
4. The main factors that affect the sub-aerial deposition design for optimizing the release water for recycling are particle size of tailings, hydraulic conductivity, suction, drying time, evaporation, and layer thickness.
5. The design criterion for sub-aerial tailings deposition in arid regions is to maximize the amount of water available for recycling, to maximize tailings volume reduction, and to enhance the stability of the facility.
6. There are two optional design schemes for sub-aerial tailings deposition. One is to keep the tailings fully saturated to maintain the saturated hydraulic conductivity. The other is to allow them to desiccate and crack through the layer. Hence, the macro hydraulic conductivity due to the cracks dominates the hydraulic conductivity of the tailings deposit.
7. A design model named "DOSTAR" was established. It uses a unified sedimentation-unsaturated consolidation theory, coupled with the linear elastic fracture mechanics (LEFM) theory and semi-empirical desiccation deformation theory, to predict tailings behavior associated with the sub-aerial tailings disposal.

8.1.3 Phase 3: Validation and application of the model

In this phase, the validity of the model was tested by comparing the modeled results with the laboratory results. Ten meter high standpipe test results and column drying test results were used to test the various algorithms in "DOSTAR." Then the procedure of optimum deposition design using DOSTAR was described. Finally, three case studies were presented. The main conclusions from this phase are the following:

1. The numerical testing results show that the model "DOSTAR" can be used to model not only in situ sub-aerial tailings disposal, but also laboratory sedimentation, consolidation, and desiccation tests. It works well for both sandy and clayey tailings. The model has the ability to predict the initiation and propagation of a primary desiccation crack within a tailings deposit.
2. There are two optional deposition design schemes. Scheme 1 is to keep the layer fully saturated all the time. Scheme 2 is allowing deposits to dry and crack so that macro hydraulic conductivity can be offered by the tailings due to cracks. It was concluded that scheme 2 is the optimum one since it offers the following advantages over scheme 2: three to seven orders higher hydraulic conductivity; one to nine percentage greater amount of recyclable water; higher volume reduction; higher resistance against liquefaction potential.
3. Desaturation of the tailings can enhance their resistance to liquefaction. It is important to desaturate the sandy tailings to an 80% degree of saturation to minimize the potential risk of liquefaction failure. Since optimum sub-aerial tailings deposition offers a degree of saturation lower than 80%, these facilities may be considered as liquefaction resistance structures.
4. In sub-aerial tailings deposition, the important deposition parameters are layer thickness, crack dimensions, cycle time, total deposition area, and the number of deposition cells. The crack width should be no greater than the maximum particle size of the tailings to ensure that the macro hydraulic conductivity due to cracking is preserved.

5. The deposition layer thickness directly influences the quality of the deposition. The thicker the layer, the larger the crack spacing and the smaller the crack width.
6. The clay contents have a great effect on the parameter of the cracks. The higher the clay contents, the greater the crack width and the smaller the crack spacing.
7. The potential evaporation rate also directly affects the deposition. The higher the potential evaporation rate, the larger the crack width, the smaller the crack spacing, and the shorter the time to dry and for cracks to propagate through the layer.
8. When the potential evaporation rate is 3.3 x 10^{-8} m/s, the optimum deposition thickness is 17, 25, 25, and 20 cm for the copper, gold, coal and CT tailings studied in this project. The traditional deposition layer thickness range (10 to 15 cm) is not suitable for all these tailings.
9. Three case histories were investigated in this research. The existing depositional parameters in all cases are unreasonable in terms of the optimum design.
10. The optimum depositional parameters for the cases 1, 2, and 3 respectively are as follows: required total depositional areas are 457791, 111458, and 824593 m^2; the depositional cell numbers are 6, 6, and 4; the optimum deposition layer thicknesses are 0.15, 0.25, and 0.17 m; cycle times are 186, 385, and 28 hours.

8.2 RECOMMENDATIONS FOR FUTURE STUDIES

The recommended future research on the design of the optimum deposition for the sub-aerial tailings disposal in arid regions includes:

1. Field tests on sub-aerial tailings deposition would be helpful to provide more accurate knowledge of the tailings, in situ properties and desiccation behavior, hence improving the accuracy of the input parameters used in the model.

2. Laboratory measurements on the tensile strength of the tailings and the fracture toughness should result in more accurate knowledge of the basic properties of the tailings for use in the model.

3. Improvement of the laboratory column drying test, including suction profile measurement, should lead to more accurate input parameters.

4. Extending DOSTAR to two and three dimensions would allow the model to deal with practical problems such as segregation of the tailings during deposition.

REFERENCES

Abadjiev, C.B. 1976. Seepage through Mill Tailings Dams. XII Congress of ICOLD, Q. 44, R.18, pp.381-393.

Abadjiev, C.B. 1985. Estimation of physical characteristics of deposited tailings in the tailings dam of non ferrous metallurgy. Proceedings of 11th International Conference on Soil Mechanics and Foundation Engineering, **3**: 1231-1234.

Abu-Hejleh, A.N. 1993. Desiccation theory for soft cohesive soils. Ph.D. thesis, University of Colorado. Boulder, Colo.

Abu-Hejleh, A.N., and Znidarcic, D. 1995. Desiccation theory for soft cohesive soils. Journal of Geotechnical Engineering, ASCE, **121**(6): 493-502.

American Society for Testing and Materials. 1986. Standard test method for plane-strain fracture toughness of metallic materials. ASTM E399-83, American Society for Testing and Materials, Philadelphia, USA.

American Society for Testing and Materials. 1997. D 2325-68 (Reapproved 1994): Standard Test Method for Capillary-Moisture Relationships for Coarse- and Medium-Textured Soils by Porous-Plate Apparatus. In Annual Book of ASTM Standards, **04**(08): 195-201.

American Society for Testing and Materials. 1997. D 4767: Standard Test Method for Consolidated Undrained Triaxial Test for Cohesive Soils. In Annual Book of ASTM Standards, **04**(08): 856-865.

American Society for Testing and Materials. 1999. D 427-93 (Reapproved 1998): Standard test method for shrinkage factors of soils by the mercury method. In Annual Book of ASTM Standards, **04**(08): 22-25.

Aubertin, M., Bussière, B., and Chapuis, R. P. 1996. Hydraulic conductivity of homogenized tailings from hard rock mines. Canadian Geotechnical Journal, **33**: 470-482.

Aubertin, M., Richard J. and Chapuis, R.P. 1998. A predictive model for the water retention curve: application to tailings from hard-rock mines. Canadian Geotechnical Journal, **35**: 55-69.

Bates, D.M., and Watts, D.G., 1988. **Nonlinear regression analysis and its applications**. John Wiley & Sons, Inc., New York.

Bates, R.C. and Wayment, W.R. 1967. Laboratory study of factors influencing waterflow in mine backfill. U.S. Department of the Interior, Bureau of Mines, RI 7034.

Been, K. 1980. Stress strain behavior of a cohesive soil deposited under water. Ph.D. thesis, University of Oxford, Oxford, United Kingdom.

Been, K. and Sills, G. C. 1981. Self-Weight Consolidation of Soft Soils: An Experimental and Theoretical Study. Geotechnique, **31**: 519-535.

Biot, M. A. 1941. General theory of three-dimensional consolidation. Journal of Applied Physics. **12**(2): 155-164.

Bishop, A.W. 1960. The principle of effective stress. Norwegian Geotechnical Institute (NGI) Publication No. 32.

Bishop, A.W. and Henkel, D.J. 1957. **The Measurement of Soil Properties in the Triaxial Test**. Edward Arnold Publishers. 227p

Blight, G.E. 1987. The concept of the master profile for tailings dam beaches. *In* Prediction and performance in geotechnical engineering, Ed(s): Ramesh C. Joshi and Fred J. Griffiths, University of Calgary, pp. 361-365.

Blight, G.E. 1988. Some less familiar aspects of hydraulic fill structures. *In* Hydraulic Fill Structures, Ed(s): D.J. Van Zyl and S.G. Vick, American Society of Civil Engineers, Colorado State University, pp. 1000-1027.

Blight, G.E. 1996. Personal communications.

Blight, G.E. and Steffen, O.K.H. 1979. Geotechnics of Gold Mining Waste Disposal. In Current Geotechnical Practice in Mine Waste Disposal. American Society of Civil Engineering. pp.1-52.

Bronswijk, J.J.B. 1989. Prediction of actual cracking and subsidence in clay soils. Soil Science, **148**(2): 87-93.

Bronswijk, J.J.B. 1990. Shrinkage geometry of a heavy clay soil at various stresses. Soil Science Society of America Journal, **54**: 1500-1502.

Bronswijk, J.J.B. 1988. Modelling of water balance, cracking and subsidence of clay soils. Journal of Hydrology, **97**: 199-212.

Bronswijk, J.J.B. 1991. Drying, Cracking, and Subsidence of A Clay Soil in A Lysimeter. Soil Science, **152**(2): 92-99.

Brooks, R.H. and Corey, A.T. 1964. Hydraulic properties of porous medium. Colorado State University, Hydraulic paper No.3, 27p.

Burns, R., Cuddy, G. and Lahaie, R. 1993. Dewatering of Fine Tails By Natural Evaporation. In proceedings of Oil Sand--our Petroleum Future conference, F16.

Campbell, G.S. 1974. A simple method for determining unsaturated conductivity from moisture retention data. Soil Science **117**: 311-314.

Campbell, J.D. 1973. Pore pressures and volume changes in unsaturated soils. Ph.D. thesis, University of Illinois at Urbana-Champaign, Urbana-Champaign, U.S.A.

Cedergren, H. R. 1989. **Seepage, Drainage, and Flow Nets**. 3rd Edition. John Wiley & Sons, 465p.

Chan, C. and Masala. S. 1998. A Time Dependent Model for Sedimentation Analysis of Fine Grained Soils. Proceedings of 51st Canadian Geotechnical Conference. Edmonton, Alberta, October 4-7. pp. 599-606.

Chapuis, R.P., and Montur, I. 1992. Évaluation de l'équation de Kozeny-Carman pour prédire la conductivité hydraulique. Proceedings, 45th Canadian Geotechnical Conference, Toronto, pp. 78-1-78-10.

Childs, E.C., and Collis-George, G.N. 1950. The permeability of porous materials. Proceedings of the Royal Society of London, Series A, **201**: 392-405.

Chow, V. T., Maidment, D. R., and Mays, L. W. 1988. **APPLIED HYDROLOGY**. McGraw-Hill Book Company. 572p.

Chowdhury, R. N. 1978. **Slope Analysis**. Elsevier Scientific Publishing Company, 423p.

Craig, R.F. 1992. **Soil mechanics**. 5th ed., Chapman & Hall, London.

Darragh, R. D. Controlled water tests to preload tank foundations. Journal of the soil mechanics and Foundations Division, ASCE, **90**(SM5): 303-329.

Dasog, G. S. 1986. Properties, genesis and classification of clay soils in Saskatchewan. Unpublished Ph.D. thesis, Department. of Soil Science, University of Saskatchewan, Saskatoon, Canada.

Dawson, R. F. 1994. Mine Waste Geotechnics. Unpublished Ph.D. thesis, University of Alberta. Canada.

Douglas, J. and Jones, B.F. 1963. On predictor-corrector methods for nonlinear parabolic differential equations. Journal of Society, Industry and Applied Mathematics, **11**(1): 195-204.

Fisher, R.A. 1926. On the capillary forces in an ideal soil; correction of formulae given by W.B. Haines. Journal of Agriculture Science, **16**: 492-545.

Fredlund, D. G. 1985. Soil mechanics principles that embrace unsaturated soils. Proceedings of the 11th International Conference on Soil Mechanics and Foundation Engineering. (San Francisco), **2**: 465-472.

Fredlund, D. G., and Hasan, J. U. 1979. One-dimensional consolidation theory: unsaturated soils. Canadian Geotechnical Journal, **16**: 521-531.

Fredlund, D. G., and Rahardjo, H. 1993. **Soil mechanics for unsaturated soils**. John Willey & Sons, Inc. 517p.

Fredlund, D. G., Morgenstern, N. R., and Widger, R.A. 1978. The shear strength of unsaturated soils. Canadian Geotechnical Journal, **15**: 313-321.

Fredlund, D.G., and Xing, A. 1994. Equations for the soil-water characteristic curve. Canadian Geotechnical Journal, **31**: 521-532.

Fredlund, D.G., Xing, A. and Huang, S. 1994. Predicting the permeability function for unsaturated soils using the soil-water characteristic curve. Canadian Geotechnical Journal, **31**: 533-546.

Fredlund, D.G., Xing, A., Fredlund, M.D. and Barbour, S.L. 1995. The relationship of the unsaturated soil shear shrength to the soil-water characteristic curve. Canadian Geotechnical Journal, **32**: 440-448.

Geotechnical Laboratory. 1994. Consolidation and Hydraulic Conductivity Testing of Oil Sands Fine Tails.

Gibson, R.E. 1958. The progress of consolidation in a clay layer increasing in thickness with time. Geotechnique, **8**: 171-182.

Gibson, R.E., England, G.L., and Hussey, M.H.L. 1967. The theory of one-dimensional consolidation of saturated clays, I. finite nonlinear consolidation of thin homogeneous layers. Geotechnique, **17**(3): 261-273.

Gibson, R.E., Schiffman, R.L., and Cargill, K.W. 1981. The theory of one-dimensional consolidation of saturated clays, II. finite nonlinear consolidation of thick homogeneous layers. Canadian Geotechnical Journal, **18**: 280-293.

Gilding, B.H. 1983. The soil-moisture zone in a physically-based hydrologic model. Advances in Water Resources, **6**:36-43.

Grozic, J. L. H. 1999. The behavior of loose gassy sand and its susceptibility to liquefaction. Unpublished Ph.D. thesis. University of Alberta, Alberta, Canada, 344P.

Haine, W. B. 1923. The volume changes associated with variations of water content in soils. J. Agric. Sci. Camb. **13**: 296-311.

Hamouche, K. K., Leroueil, S., Roy, M., and Lutenegger, A. J. 1995. In situ evaluation of K_0 in eastern Canada clays. Canadian Geotechnical Journal, **32**: 677-688.

Head, K. H., 1992. **Manual of Soil Laboratory Testing**. Vol. 2, 2nd Ed. Pentech Press.

Hornberger, G. M. and Remson, I. 1970. A moving boundary model of a one-dimensional saturated-unsaturated, transient porous flow system. Water Resources Research, **6**(3): 898-905.

Imai, G. 1980. Settling behavior of clay suspension. Soils and Foundations, **20**(2): 61-77.

Imai, G. 1981. Experimental studies on sedimentation mechanism and sediment formation of clay materials. Soils and Foundations, **21**(1): 7-20

Irwin, G. R., 1958. Fracture. In Handbuch der physik, Flügge, S. edited. Spring-Verlag, Berlin, pp.551-590.

Jáky, C. 1944. The coefficient of earth pressure at-rest. Journal of the Society of Hungarian Architects and Engineers, **78**(22):355-358.

Jesen, D.T. 2000. Personal communication.

Keen, B. A. 1931. **The physical properties of the soil**. Longmans, Green & Co., London.

Knight, R.B. and Haile, J.P. 1983. Sub-aerial tailings deposition. Proc. 7th Pan-American Soil Mechanics Conference, Vol.2, Vancouver, Canada. Canadian Geotechnical Society, pp.627-639.

Konrad, J. -M. and Ayad, R. 1997. An idealized framework for the analysis of cohesive soils undergoing desiccation. Canadian Geotechnical Journal, **34**: 477- 488.

Kovacs, G. 1981. **Seepage hydraulics**. Elsevier Scientific Publication, Amsterdam.

Kunze, R.J., Uehara, G., and Graham, K. 1968. Factors important in the calculation of hydraulic conductivity. Soil Science Society of America, Proceedings, **32**: 760-765.

Küpper, A.A. 1991. Design of hydraulic fill. Ph.D. thesis, University of Alberta, Edmonton, Canada.

Küpper, A.A., Morgenstern, N.R. and Sego, D.C., 1992. Laboratory Tests to Study Hydraulic Fill. Canadian Geotechnical Journal, **29**: 405-417.

Kynch, G. J. 1952. A theory of sedimentation. Transactions of the Faraday Society, **48**: 166-176.

Lachenbruch, A.H. 1961. Depth and Spacing of Tension Cracks. Journal of Geophysical Research, **66**(12): 4273-4292.

Lachenbruch, A.H. 1962. Mechanics of thermal contraction cracks and ice-wedge polygons in permafrost. Geological Survey of America, Special Paper No. 70. 69p.

Lambe, T. W., and Whitman, R. V. 1968. **Soil Mechanics**. John Wiley & Sons, Inc. 553p.

Lau, J.T.K. 1987. Desiccation cracking of soils. Unpublished M.Sc. thesis, Department of Civil Engineering, University of Saskatchewan, Saskatoon, Canada.

Lawn, B.R., and Wilshaw, T.T. 1975. **Fracture of brittle solids**. Cambridge University Press, Cambridge. 204p.

Lee, F.H., Lo, K.W., and Lee, S.L. 1988. Tension crack development in soils. Journal of Geotechnical Engineering, ASCE, **114**(8): 915-929.

Lee, I.K., and Ingles, O.C. 1968. Strength and deformation of soil and rocks. *In* Soil mechanics, selected topics. Edited by I.K.Lee. Butterworths, Sydney, pp. 195-294.

Lee, I. K., White, W. and Ingles, O. G. 1983. **Geotechnical Engineering**. Pitman. 508P.

Liu, Y., Caughill, D., Scott, J.D. and Burn, R., 1994. Consolidation of Suncor nonsegregating tailings. Proceedings of 47th Canadian Geotechnical Conference. Halifax, Nova Scotia. September 21-23. pp. 504-523.

Marshall, T.J. 1958. A relation between permeability and size distribution of pores. Journal of Soil Science, **9**: 1-8.

McNabb, A. 1960. A mathematical treatment of one-dimensional soil consolidation. Quatery of Applied Mathematics. **17**(4): 337-347.

McRoberts, E. C. and Nixon, J. F. 1976. A theory of Soil Sedimentation. Canadian Geotechnical Journal, **13**: 294-310.

Meguid, S.A. 1989. **Engineering Fracture Mechanics**. Elsevier Science Publishers Ltd. 397p.

Mitchell, J.K. 1976. **Fundamentals of soil behavior.** 1st Ed. John Wiley & Sons, Inc.

Mittal, H. and Morgenstern, N.R. 1975. Parameters for the Design of Tailings Dams, Canadian Geotechnical Journal, 12: 235-261.

Morgenstern, N.R. and Küpper, A.A., 1988. Hydraulic fill structures-a perspective. In - Hydraulic Fill Structures, ASCE, Fort Collins, pp.1-31.

Morris, P.H., Graham, J., and Williams, D.J. 1992. Cracking in drying soils. Canadian Geotechnical Journal, **29**: 263-277.

Nearing, M. A., West, L. T., and Bradford, J. M. 1988. Consolidation of an unsaturated illitic clay soil. Soil Science Society of America Journal. **52**: 929-934.

Newson, T., Fujiyasu, Y., and Fahey, M. 1996. A field study of the consolidation behavior of saline gold tailings. In TAILINGS AND MINE WASTE' 96. A.A.BALKEMA. pp.179-188.

Pane, V., and Schiffman, R.L. 1985. A note on sedimentation and consolidation. Geotechnique, **35**: 69-72.

Penev, D., and Kawamura, M. 1993. Estimation of the spacing and the width of cracks caused by shrinkage in cement-treated slab under restraint. Cement And Concrete Reseach, **23**: 925-932.

Penman, H.L.1948. Natural evapotranspiration from open water, bare soil and grass. Royal Society of Agriculture Proceedings. **193**: 120-145.

Pettibone, H., and Kealy, C. 1971. Engineering properties of mine tailings. Journal of the soil mechanics and Foundations Division, ASCE, **97**(SM9): 1207-1225.

Pollock, G.W. 1988. Large strain consolidation of oil sand tailings sludge. Unpublished M.Sc. thesis, University of Alberta, Edmonton, Alberta, 276p.

Qiu, Y., and Sego, D. C. 1998a. Design of sub-aerial tailings deposition in arid regions. Proceedings of 51st Canadian Geotechnical Conference. Edmonton, Alberta, October 4-7. **2**: 615-622.

Qiu, Y. and Sego. D. C. 1998b. Laboratory test methods on mine tailings. Proceedings of 51st Canadian Geotechnical Conference. Edmonton, Alberta, October 4-7. **1**:155-162.

Qiu, Y. and Sego, D. C. 1998c. Engineering properties of mine tailings. Proceedings of 51st Canadian Geotechnical Conference. Edmonton, Canada, October 4-7. **1**: 149-154.

Qiu, Y., and Sego, D. C. 1999. Behavior of sub-aerial deposited tailings and design of sub-aerial deposition in arid regions. Proceedings of the Sixth International Conference on Tailings and Mine Waste'99, January 23-27, 1999. Fort Collins, USA. pp. 89-98.

Raats, P. A. C. 1984. Mechanics of cracking soils. *In* Proceedings of the ISSS symposium on water and solute movement in heavy clay soils (Edited by J. Bouma and P.A.C. Raats). Wageningen, Netherlands. pp. 23-38.

Remson, I., Hornberger, G. And Molz, F. 1971. **Numerical Methods in Subsurface Hydrology with an introduction to the finite element method**. Wiley-Interscience, 389p.

Ridlen, P.W., Davidson, R.R., Manka, D.L., Pilz, J. and Dunne, R.E. 1997. Geotechnical design of Kennecott Utah copper tailings. In TAILINGS AND MINE WASTE' 97. A.A.BALKEMA. pp. 741-752.

Ritcey, G.M., 1989, **Tailings Management**. Elsevier Publication.

Robinson, R. A. and Stokes, R. H. 1955. **Electrolyte solutions: The measurement and interpretation of conductance, chemical potential and diffusion in solutions of simple electrolytes**. Academic Press, New York.

Rosenberg, N.J., Blad, B.C., and Berma, S.B. 1983. **Microclimate, The Biological Environment**, John Wiley and Sons. Inc., pp. 209-287.

Schiffman, R. L., Chen, A.T-F., and Jordan, J. C. 1969. An analysis of consolidation theories. Journal of the Soil Mechanics and Foundation division, Proceedings of the American Society of Civil Engineers, **95** (SM1):285-312.

Schiffman, R.L., Pane, V., and Gibson, R.E. 1984. The theory of one-dimensional consolidation of saturated clays, IV. An overview of nonlinear finite strain sedimentation and consolidation. *In* Sedimentation/Consolidation Models, edited by R.N. Yong and F.C. Townsend, ASCE, pp. 1-29.

Schiffman, R.L., Vick, S.G. and Gibson, R.E. 1988. Behavior and properties of hydraulic fills. In Hydraulic Fill Structures, Ed(s): D.J. Van Zyl and S.G. Vick, American Society of Civil Engineers, Colorado State University, pp. 166-202.

Scott, J.D. 1995. Hydrometer Test Procedures for Tailings Materials. Unpublished paper. Department of Civil Engineering, University of Alberta.

Scott, J.D. and Miller, W.G. 1995. Procedures for Geotechnical Laboratory Testing of Syncrude Tailings Materials. Unpublished paper. Department of Civil Engineering, University of Alberta.

Sego, D.C., 1994. Factors affecting the hydraulic conductivity and volume change characteristics of oil sand fine tails (Draft). Submitted to Fine Tails Fundamentals Consortium, Nov., 1994.

Seneviratne, N.H., Fahey, M., Newson, T.A., and Fujiyasu, Y. 1996. Numerical modelling of consolidation and evaporation of slurried mine tailings. International Journal for Numerical and Analytical Methods in Geomechanics, **20**: 647-671.

Sherrard, J.L., Dunnigan, L.P., and Talbot, J.R. 1984. Basic properties of sand and gravel filters. Journal of Geotechnical Engineering, ASCE, **110**(6): 684-700.

Sih, G.C. 1973. **Handbook of stress-intensity factors: stress-intensity factor solutions and formulas for reference**. Bethlehem, Penn., Institute of Fracture and Solid Mechanics, Lehigh University.

Skempton, A. W., and Bjerrum, L. 1957. A contribution to settlement analysis of foundations on clay. Geotechnique, **7**: 168-178.

Snyder, V. A., and Miller, R. D. 1985. Tensile strength of unsaturated soils. Soil Science Society of America Journal. **49**: 58-65.

Somoyi, F. 1979. Analysis and prediction of phosphatic clay consolidation: implementation pakage. Technical Report, Florida, Florida phosphatic clay research project, Lakeland, Florida, USA.

Sridharan, A., Murthy, N. S. and Prakash, K. 1987. Rectangular hyperbola method of consolidation analysis. Géotechnique **37**: 355-368.

Suncor Ico. 1998. Quarterly results. Update. April 23. p2.

Suthaker, N. N. 1995. Geotechnics of oil sand fine tailings. Unpublished Ph.D. thesis, University of Alberta, Edmonton, Alberta, 233p.

Swarbrick, G.E. 1992. Transient unsaturated consolidation in desiccating mine tailings. Unpublished Ph.D. thesis, University of New South Wales, Australia.

Syncrude Canada Ltd. 1998. Sycrude Production To Date. Web online. May 20.

Terzaghi, K. 1936. The shear resistance of saturated soils. In Proc. 1st Int. conf. Soil Mech. Found. Eng. Vol. 1 pp. 54-56.

Terzaghi, K. 1923. Die Berechnung der Durchlassigkeitsziffer des Tone aus dem Verlaug der Hydro-dynamischen Spannungsercheinungen. Akademie der Wissenchaften in Wein, Sitzungsberichte. Mathematish Naturwissenschaftliche Klasse. Part Iia, **132**(3/4):125-138.

Terzaghi, K. 1943. **Theoretical Soil Mechanics**. New York: Wiley, 510p.

Ulrich, B. F. 1999. Personal communications.

Van Genuchten, M.T. 1980. A closed-form equation for predicting the hydraulic conductivity of unsaturated soils. Soil Science Society of America Journal, **44**: 892-898.

Van Zyl, Dirk, 1993. Mine waste disposal. In Daniel (ed.) Geotechnical Practice for Waste Disposal. Chapman & Hall. pp. 267-286.

Vanapalli, S.K., Fredlund, D.G., Putahl, D.E., and Clifton, A.W. 1996. Model for the prediction of shear strength with respect to soil suction, Canadian Geotechnical Journal, **33**: 379-392.

Vick, S.G. 1983. **Planning, Design and Analysis of Tailings Dams**. John Wiley and Sons, New York, 369p.

Volpe, R.L. 1979. Physical and Engineering Properties of Copper Tailings. In Current Geotechnical Practice in Mine Waste Disposal. American Society of Civil Engineering. pp. 242-260.

Von Rosenberg, D.U. 1969. **Methods for the numerical solution of partial differential equations**. American Elsevier Publishing Company, Inc. 128p.

Williams, D.J. and Morris, P.H. 1990. Engineering properties of Australian coal mine tailings relevant to their disposal and rehabilitation. Proceedings of the third international symposium on the Reclamation Treatment and Utilization of Coal Mining Wastes, Glasgow, United Kingdom, September 3-7. pp. 49-56.

Wilson, G. W., Fredlund, D. G. and Barbour, S. L. 1997. The Effect of Soil Suction on Evaporation Fluxes from Soil Surface. Canadian Geotechnical Journal. **34**: 145-155.

Wilson, G.W. 1997. Personal communications.

Wilson, G.W. 1990. Soil evaporative fluxes for geotechnical engineering problems. Ph.D. thesis, University of Saskatchewan, Saskatoon, Canada.

Yong, R. N. 1984. Particle interaction and stability of suspended solids. *In* Sedimentation/Consolidation Models, edited by R.N. Yong and F.C. Townsend, ASCE, pp. 30-59.

Young, J. F. 1967. Humidity Control in the Laboratory Using Salt Solutions--A Review. Journal of Applied Chemistry, **17**: 241-245.

Zein El Abedine, A. and Robinson, G. H. 1971. A study on cracking in some vertisols of the Sudan. Geoderma, **5**:229-241.

APPENDIX A ENGINEERING BEHAVIOR OF TAILINGS

The nature of tailings varies according to the ore being processed and the particular milling and mineral extraction operation. Pertinent index properties of the tailings are the grain size distribution, specific gravity, and plasticity.

The grain size distributions of some typical tailings are presented in Figure A.1 to A.8. The fines content, clay-sized particles content, specific gravity, and plasticity of different tailings are listed in table A.1.

A.1 DEPOSITIONAL CHARACTERISTICS

Tailings are generally deposited hydraulically, usually by some form of peripheral discharge method, either spigotting or rotating single-point discharge. The deposition method results in an above-water tailings beach with an average slope of 0.5 to 2.0% and a slime zone associated with the impounded water. Along the beach, tailings at different locations have different engineering behaviors.

The depositional process results in a highly heterogeneous beach deposit. Vertically, tailings beach deposits are frequently layered with the percentage of fines typically varying as much as 10%-20% over several inches in thickness (Vick 1983). Along the beach, coarser particles settle from the slurry, with the finer particles remaining suspended and settling only when the slurry reach the still water of the decant pond to form the slime zones. Various slimes have various sedimentation rates, as presented in Table A.2.

A.2 DENSITY AND RELATIVE DENSITY

In-place density is very important for tailings dam design. It can be expressed in terms of either dry density (ρ_d) or void ratio (e). Table A.3 shows typical values measured in actual impoundments for various types of deposited tailings.

Relative densities (D_r) of hydraulically deposited beach sands have important influences on dynamic strength behavior (Vick 1983). Mittal and Morgenstern (1975) and Pettibone and Kealy (1971) reported the minimum and maximum densities of tailings (Table A.4). The in-place relative density of sand tailings deposited hydraulically is summarized in Table A.5.

A.3 HYDRAULIC CONDUCTIVITY

Of the properties needed for evaluation of most geotechnical problems, none varies over so wide a range as hydraulic conductivity. Average hydraulic conductivity spans five or more orders of magnitude, from 10^{-2} cm/sec for clean, coarse sand tailings to as low as 10^{-7} cm/sec for well-consolidated slimes.

The hydraulic conductivity varies as a function of grain size and plasticity, depositional mode, and depth within the deposit. Mittal and Morgenstern (1975) proposed that average permeability for sand tailings is best predicted by the well-known Hazen formula:

$$[\text{A-1}] \quad k = C_1 D_{10}^{\ 2}$$

where k is the hydraulic conductivity in cm/s, D_{10} is the grain size in mm for which 10% of the particles pass by weight, C_1 is a material constant (C_1= 60-150, depending on grain-size distribution (Kovacs 1981); for homogeneous tailings, $C_1 \approx 100$ (Vick 1983; Craig 1992; Aubertin et al. 1996).

Aubertin et al. (1996) concluded that Hazen's formula appears to give a lower bound of the k value.

Sherard et al. (1984) proposed the following formula to calculate the hydraulic conductivity based on the distribution of particle size:

$$[\text{A-2}] \quad k=0.35(D_{15})^2$$

where k is in cm/s and D_{15} is in mm.

Hydraulic conductivity can also be expressed as functions of void ratio. One of the functions is the so-called the Kozeny-Carman equation (Chapuis and Montour 1992; Aubertin et al. 1996):

$$[\text{A-3}] \quad k=\frac{C_2 g}{\mu_w \rho_w D_r{}^2}\frac{1}{S^2}\frac{e^3}{1+e}$$

where k is hydraulic conductivity in cm/s, C_2 is a material parameter ($C_2 = 0.32$ (Chapuis et al. 1992)), e is void ratio, μ_w is the water viscosity at 20 °C (= 9.8x10-6 N.S/cm^2), ρ_w is the water density, g is the gravitational acceleration, and S is the specific surface.

The other function was specifically developed for tailings at the U.S. Bureau of Mines (Bates and Wayment, 1967):

$$[\text{A-4}] \quad k=\exp[x_1+x_2\ln(eD_{10})+x_3\ln(e)\ln(C_U)+x_4(eC_U)+x_5(D_{10}D_{50})]$$

where k is the hydraulic conductivity in inches per hour (1in/hr ≈7.055x10^{-4} cm/s), x_1 to x_5 are the constants ($x_1 = 11.02$, $x_2 = 2.912$, $x_3 = -0.085$, $x_4 = 0.194$ and $x_5 = -56.49$), D_{50} is the grain size for which 50% of the particles pass by weight (inch), and C_U is the uniformity coefficient.

Experimental results showed that the Kozeny-Carman equation (A.3) is usually the best of the three previous equations for estimating the hydraulic conductivity of the homogeneous tailings (Aubertin et al. 1996).

Aubertin et al. (1996) proposed a modified formulation:

$$[\text{A-5}] \quad k = C_3 \frac{\gamma_w}{\mu} D_{10}{}^2 C_U{}^{1/3} \frac{e^{3+x}}{1+e}$$

where C_3 is a coefficient ($C_3 = 0.004\text{-}0.02$ (Aubertin et al. 1996)), x is a material parameter (x = 2.16 for tailings), γ_w is the unit weight of the water (at room temperature, γ_w =9.79kN/m3), and μ is the fluid viscosity (at 20 °C, the water viscosity is 9.81x10^{-6} N.S/cm^2).

The equation [A-5] was shown to describe the measured results fairly well. This equation can be considered a useful tool for the estimation of the k values of homogenized tailings (Aubertin et al. 1996).

The hydraulic conductivity ranges of typical tailings are listed in Table A.6.

A.4 COMPRESSIBILITY AND CONSOLIDATION

Both compressibility and consolidation behavior are important for tailings impoundment disposal. Because of their loose depositional state, high angularity, and grading characteristics, both sands and slimes are more compressible than most natural soils. Typical values for the compression index, C_c, determined in one-dimensional compression tests are shown in Table A.7. Consolidation for sand tailings occurs very quickly, whereas for slime tailings it takes place very slowly. Typical values of the coefficient of consolidation, c_v, are listed in table A.8.

A.5 DRAINED AND UNDRAINED SHEAR STRENGTH

The drained shear strength of tailings, for both sands and slimes, is often higher than that for similar natural soils because of the high degree of particle angularity exhibited by most tailings. The drained shear strength is generally sensitive to the applied effective stress level.

Typical values of effective friction angles of tailings (ϕ') based on laboratory tests are shown in Table A.9.

Undrained shear strength implicitly accounts for the pore pressures generated by rapidly-applied shear stresses and is very important in evaluating the flow-like behavior exhibited by many tailings deposit failures, such as during liquefaction failure. Both initial density and testing procedures are important factors for undrained shear strength. The typical values of ϕ_T, C_T for various types of tailings are shown in Table A.10.

A.6 IN SITU DESICCATION CRACKS

Table A.11 shows the dimensions of the desiccation cracks of soils and solid wastes observed in the field.

Table A. 1 Specific gravity and plasticity of tailings (modified from Vick, 1983)

Type of Tailings	Specific Gravity, G_s	Liquid Limit (%)	Plastic Index (%)	Clay Size Contents (%)	Fines Contents (%)
Coal Refuse	1.5-1.8	35-50	0-13	22	93
	1.4-1.8	----	-----	--	50
	1.4-1.6	20-40	2-12	14	50
	1.7-2.4	30-60	3-30	15	71
	1.74	44	16	39*	
	1.86	74	46	57*	
Lead-Zinc	2.8-3.4		low		
	2.9			2	54
	3.3-3.6				
Gold-Silver	2.6-2.7		low to non		
				11	95
Copper	2.6-2.8	40	13		
	2.7-3.0	0-30	0-11		
Molybdenum	2.6-2.8				23
		30	non		
Taconite	3.0-3.4		non	13	92
	3.1			6	95
Phosphate	2.5-2.8	120-200	90-150	62	100
Gypsum	2.3-2.4		non		93
Bauxite	2.6-3.1	46	7-9	25(45)	76
	2.8-3.3			33(21)	83
	2.77	43	17	32*	
Uranium	2.6-2.7		non	15	
Trona	2.5-2.7		low-high	18	40
Iron	3.76	30	9	42*	29
	3.84	33	11	29*	
Nickel					55
Oil sands**		53.2	29.4	48.7*	95.5
		41.4	21.6	45-49*	100
		55	30	60*	100
		46.1	23.7	45*	92
	2.64				

Note: The content of clay-sized particles (<2 microns) and fines (<74 microns, except oil sand's <44 microns) are mainly obtained from the gradations; the data with * are clay mineral contents; ** oil sands data are from Sego (1994).

Table A. 2 Slime sedimentation rates (modified from Vick 1983)

Slime Type	Specific Gravity	Plasticity Index (%)	Sedimentation Rate, (m/hr)
Copper	2.7	10	0.095
	2.7	9	0.043
Phosphoric Clay	2.8	125	0.052 (field)
Copper-Zinc	2.9	0	0.116
	4.0	0	0.165

Table A. 3 Typical in-place density and void ratios (modified from Vick 1983)

Tailings Type	Specific Gravity, G_s	Void Ratio, e	Dry Density, γ_d (kN/m^3)
Fine coal refuse			
Eastern U.S.	1.5-1.8	0.8-1.1	7.1-8.6
Western U.S.	1.4-1.6	0.6-1.0	7.1-11
Great Britain	1.6-2.1	0.5-1.0	8.6-13.4
Oil sands			
Sands		0.9	13.7
Slimes		6-10	--
Lead-zinc			
Slimes	2.9-3.0	0.6-1.0	14.6-17.8
	2.6-2.9	0.8-1.1	12.6-16.2
Gold-silver			
Slimes		1.1-1.2	
Molybdenum			
Sands	2.7-2.8	0.7-0.9	14.5-15.6
Copper			
Sands	2.6-2.8	0.6-0.8	14.6-17.3
Slimes	2.6-2.8	0.9-1.4	11-14.1
Taconite			
Sands	3.0	0.7	17.3
Slimes	3.1	1.1	14.5
	3.1-3.3	0.9-1.2	15.2-16.5
Phosphate			
Slimes	2.5-2.8	11	2.2
Gypsum	2.4	0.7-1.5	9.4-14.1
Bauxite			
Slime	2.8-3.3	8	3.1
Trona			
Sands	2.4-2.5	0.7	14.5
Slimes	2.4-2.5	1.2	10.7

Table A. 4 Minimum and maximum densities of tailings (modified from Vick 1983)

γ_{min} (Mg/m^3)	γ_{max} (Mg/m^3)	e_{max}	e_{min}
1.2-1.52	1.59-1.79	0.72-1.23	0.51-0.68
1.36-1.59	1.68-2.07	0.99-1.32	0.51-0.67

Table A. 5 Average in-place relative density of tailings (modified from Vick 1983)

Type	Dr (%)
Tar sands	30-50
Molybdenum sands	31-55
Cycloned copper sands	33-54
Cycloned copper sands	45-68
Cycloned copper sands	10-55
Cycloned lead-zinc	30

Table A. 6 Typical hydraulic conductivity of tailings (modified from Vick 1983)

Type of Tailings	Average Hydraulic Conductivity (cm/sec)
Clean, coarse, or cycloned sands (fines<15%)	10^{-2} to 10^{-3}
Peripheral-discharged beach sands with up to 30% fines	10^{-3} to 5×10^{-4}
Non-plastic or low-plasticity slimes	10^{-5} to 5×10^{-7}
High-plasticity slimes	10^{-4} to 10^{-8}

Table A. 7 Typical values of compression index, C_c (modified from Vick 1983)

Material	Initial Void Ratio, e_0	Compression index, C_c	Stress Range (kPa)
Taconite, fine tailings	1.37	0.19	24-958
Copper slimes	1.3-1.5	0.2-0.27	1-958
		0.28	
Copper sands	1.1	0.05	10-96
(cycloned)	($D_r = 0$)	0.11	96-958
		0.09	
Tar sands	1.0 ($D_r = 0$)	0.06	10-958
Molybdenum, beach sands	0.72-0.84	0.05-0.13	24-958
Gold slimes	1.7	0.35	144-4788
Lead-zinc slimes	0.7-1.2	0.1-0.25	48-575
Fine coal refuse	0.6-1.0	0.06-0.27	
Phosphate slimes	>20	3.0	5-77
Bauxite slimes	1.6-1.8	0.26-0.38	48-958
Gypsum tailings	1.3	0.07	24-239
		0.28	239-958

Table A. 8 Typical values of coefficient of consolidation, c_v

Material type	c_v (cm^2/sec)
Copper beach sands	3.7×10^{-1}
Copper slimes	1.5×10^{-1}
Copper slimes	10^{-3}-10^{-1}
Molybdenum beach sands	10^{-2}
Gold slimes	6.3×10^{-2}
Lead-zinc slimes	10^{-2}-10^{-4}
Fine coal refuse	3×10^{-3}-10^{-2}
Bauxite slimes	10^{-3}-5×10^{-2}
Phosphate slimes	2×10^{-4}

Table A. 9 Typical values of drained friction angle ϕ' (modified from Vick 1983)

Material	ϕ' (degree)	Effective Stress Range (kPa)
Copper		
Sands	34	0-814
	33-37	0-670
slimes	33-37	0-670
Molybdenum beach sands	32-38	
Taconite		
Sands	34.5-36.5	
Slimes	33.5-35	
	27-32	
Lead-zinc-silver		
Sands	33.5-35	
Slimes	30-36	
Bauxite slimes	42	0-192
Gold slimes	28-40.5	0-958
Fine coal refuse	22-39	0-287
	22-35	0-1197
Gypsum tailings	32	0-479

Table A. 10 Typical total-stress strength parameters (modified from Vick 1983)

Material	Initial void ratio, e_0	Total Friction angle, ϕ_T (deg.)	Total Cohesion, c_T (kPa)
Fine coal refuse	0.5-0.8	16-24	29-72
Molybdenum sands	0.8	14	38
Copper all tailings		13-18	0-96
Copper beach sands	0.7	19-20	34-43
Copper slimes	0.6	14	62
	0.9-1.3	14-24	0-19
	1.1	14	0
Lead-zinc slimes	0.8-1	21	0
Gold slimes		28	0
Bauxite slimes		22	5

Table A. 11 Dimensions of in situ desiccation cracks

Soil Type	Crack Spacing (mm)	Crack Depth (mm)	Crack Width (mm)	Reference
Power-station flyash	100 – 300	100	1, 2, 3, 9, 20	Blight 1988
		200	5,10	
Coal Tailings, Australia	1000	500		Morris et al. 1992
Natural soils	300 -- 400	500, 6000, 1800 -- 3000	50	
Clay soil (Regina soil)	2100	381	17	Dasog 1986
	1900	449	19	
	1540	521	22	
	910	348	15	
	2500	521	18	
	3450	595	14	
Clay soil (Sceptre soil)	700	282	9	
	2100	291	9	
Caly soil (Sceptre soil)	1110	401	20	
	1200	417	22	
Clay soil (Tisdale soil)	1540	365	16	
Swelling clay, Sudan	280 -- 500	650 – 1350		Zein El Abedine and Robinson 1971

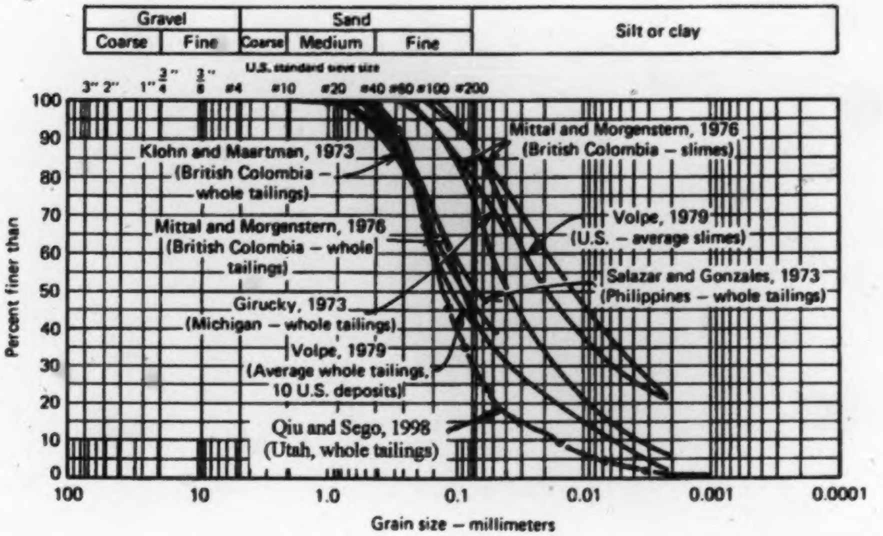

Figure A. 1 Grain size distribution of copper tailings (modified from Vick 1983)

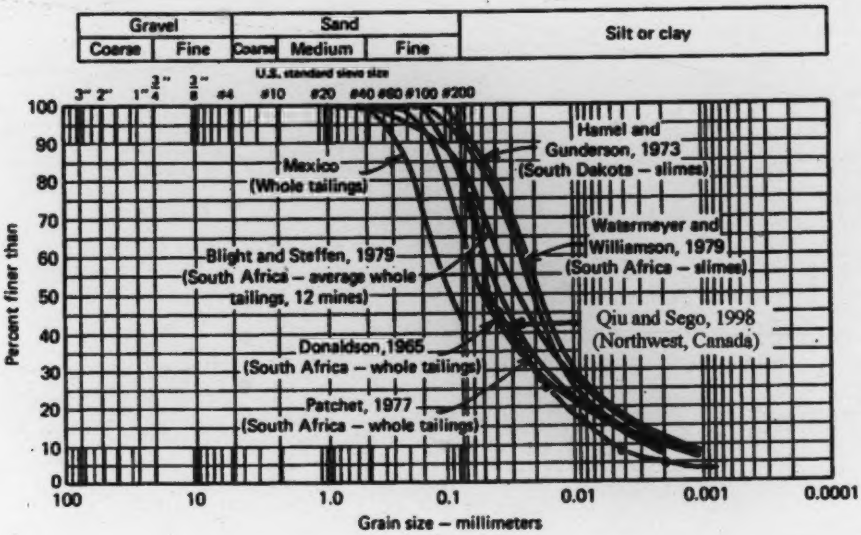

Figure A. 2 Grain size distribution of gold-silver tailings (modified from Vick 1983)

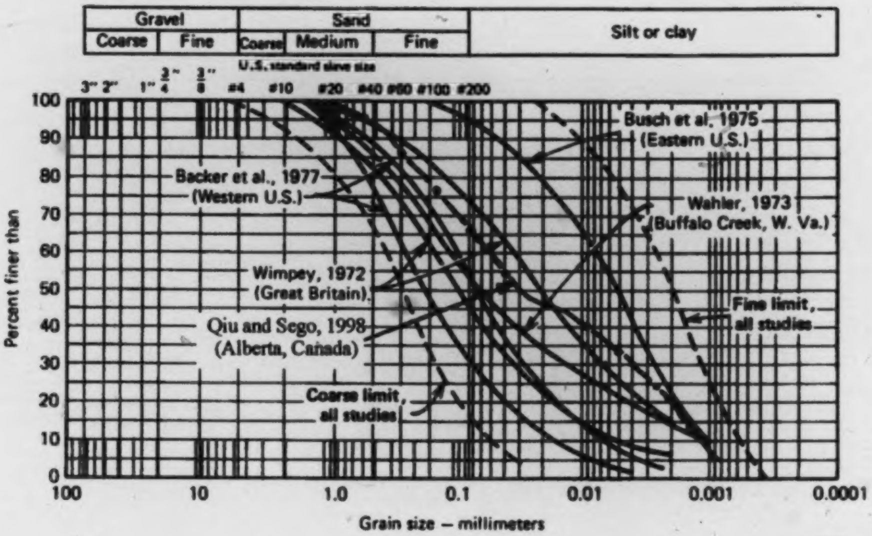

Figure A. 3 Grain size distribution of fine coal refuse (modified from Vick 1983)

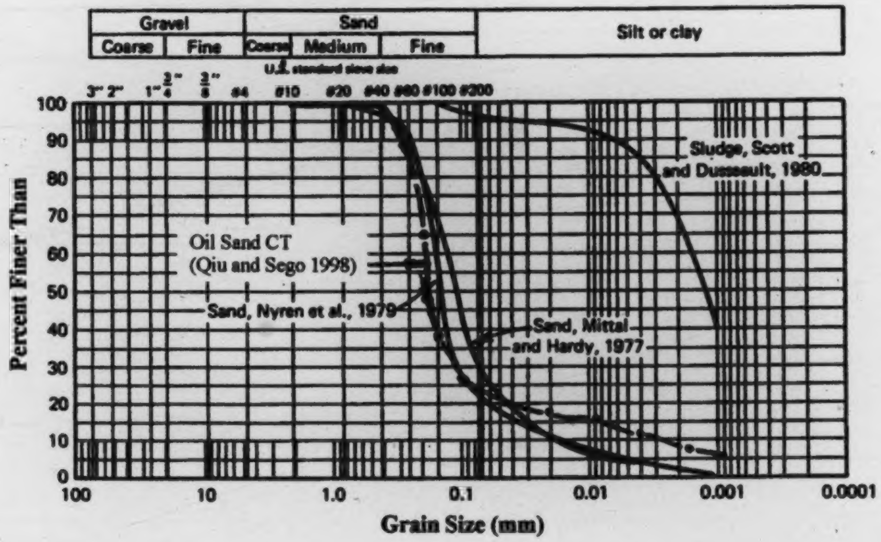

Figure A. 4 Grain size distribution of oil sand tailings (modified from Vick 1983)

APPENDIX B LABORATORY TEST RESULTS

B.1 CONSOLIDATON AND HYDRAULIC CONDUCTIVITY TESTS

Table B. 1 Consolidation and hydraulic conductivity test results for copper tailings

Sample No.	Items	Consolidation Stress σ' (kPa)							
		0	0.5	2	4	10	20	50	100
#1	e	0.84	0.84	0.78	0.76	0.74	0.73	0.7	0.67
	c_v			83.7	197.2	47.2	170.9	103.9	42.7
	m_v			20.18	4.96	1.92	0.93	0.57	0.34
	k ($\times 10^{-5}$)		5.7	5.9	6.1	5.2	5.0	8.8	2.8
#2	e	0.88	0.88	0.82	0.82	0.79	0.77	0.74	0.72
	c_v			77.5	110.2	56.9	165.4	46.6	74.9
	m_v			20.7	1.31	2.73	0.79	0.65	0.26
	k ($\times 10^{-5}$)		5.7	5.0	4.6	4.5	4.4	3.7	3.5
#3	e	0.96	0.95	0.89	0.86	0.83	0.81	0.77	0.72
	c_v			22.3	70	104.2	99.1	84.5	58
	m_v		18.55	19.76	6.43	2.86	1.24	0.68	0.63
	k ($\times 10^{-5}$)		9.8	8.9	8.6	7.2	6	5.3	4.5
#4	e	1.02	0.82	0.79	0.78	0.76	0.74	0.71	0.69
	c_v			41.7	63.5	89.8	136.3	56	41.4
	m_v		200.3	8.34	4.59	1.92	0.87	0.54	0.28
	k ($\times 10^{-5}$)		3.6	3	3	2.9	2.6	2.4	2.4

Note: c_v is in m^2/year, m_v is in m^2/MN and k is in cm/s.

Table B. 2 Consolidation and hydraulic conductivity test results for gold tailings

Sample No.	Items	Consolidation Stress σ′ (kPa)							
		0	0.5	2	4	10	20	50	100
#1	e	1.07	1.04	0.96	0.94	0.91	0.88	0.85	0.81
	c_v			34.4	38	69.6	31.3	61.1	41
	m_v		25.84	26.18	5.41	2.73	1.29	0.67	0.39
	k (x10^{-5})		6.7	5.7	5.4	5	4.7	4.2	3.6
#2	e	0.89	0.85	0.75	0.73	0.71	0.69	0.67	0.64
	c_v			8.3	22.2	38.7	26.9	28.3	24.7
	m_v		43.83	35.18	5.91	2.26	1	0.53	0.3
	k (x10^{-5})		2.2	3.6	3.5	3.4	3.2	3	2.8
#3	e	1.15	1.08	0.95	0.91	0.88	0.85	0.8	0.76
	c_v			10.5	28.8	59.6	36.9	51.1	42.8
	m_v		60.6	43.5	9.45	3.14	1.42	0.82	0.53
	k (x10^{-5})		4.8	5.1	5.1	4	2.8	2.7	2.5
#4	e	1.21	1.03	0.99	0.84	0.79	0.76	0.72	0.69
	c_v			80.1	13.6	43.3	33	49	45.4
	m_v		162.5	13.4	36.8	4.78	1.63	0.79	0.29
	k (x10^{-5})		6.7	5.5	4.1	3.5	3.3	2.9	2.7

Note: c_v is in m^2/year, m_v is in m^2/MN and k is in cm/s.

Table B. 3 Consolidation and hydraulic conductivity test results for coal tailings

Sample No.	Items	Consolidation Stress σ' (kPa)							
		0	0.5	2	4	10	20	50	100
#1	e	1.69	1.62	1.34	1.22	1.08	0.91	0.81	0.71
	c_v		0.76	2.16	2.98	12.1	7.8	15.4	13.1
	m_v		50.2	72	26.3	10.5	7.9	1.84	1.08
	k ($\times10^{-6}$)		14	4.8	4	2.4	1.1	0.78	0.58
#2	e	1.74	1.58	1.36	1.25	1.1	0.96	0.83	0.75
	c_v		2.19	2.42	3.85	8.46	8.6	24.3	16.5
	m_v		118	57.7	22.6	11	6.87	2.24	0.84
	k ($\times10^{-6}$)		9.5	6	4.4	1.5	1.6	1	0.36
#3	e	1.84	1.57	1.31	1.19	1.02	0.92	0.79	0.7
	c_v		1.48	3.1	4.47	5.44	9.2	10.9	17.3
	m_v		188	67.1	27.7	12.7	4.79	2.26	1.08
	k ($\times10^{-6}$)		11	5.3	3.4	1.9	1.2	0.74	0.42
#4	e	1.85	1.64	1.28	1.17	1	0.91	0.8	0.71
	c_v		1.35	2.32	3.46	6.02	7.57	12.1	17.4
	m_v		149	90.9	23.4	12.9	4.51	2.01	0.92
	k ($\times10^{-6}$)		13	4.9	3.7	2.2	1.3	0.84	0.23

Note: c_v is in m^2/year, m_v is in m^2/MN and k is in cm/s.

Table B. 4 Consolidation and hydraulic conductivity test results for oil sand CT

Sample No.	Items	Consolidation Stress σ' (kPa)							
		0	0.5	2	4	10	20	50	100
#1	e	1.64	1.21	0.84	0.74	0.67	0.6	0.53	0.49
	c_v			0.39	0.26	0.42	0.89	2.67	6.31
	m_v		326	111	26.7	7.48	3.74	1.45	0.58
	k ($x10^{-7}$)		7.7	4.8	3.4	2.8	2.5	1.8	1.7
#2	e	1.64	1.14	0.84	0.75	0.65	0.59	0.53	0.48
	c_v			0.5	0.31	0.62	0.77	4.58	8.46
	m_v		380	92.9	25.3	9.65	3.29	1.33	0.61
	k ($x10^{-7}$)		6.3	5	4.6	2.6	2.5	2.4	2.2
#3	e	1.69	1.23	0.75	0.68	0.61	0.55	0.5	0.45
	c_v			1.23	0.29	0.53	0.79	3.87	8.56
	m_v		340	144	20.8	7.16	3.22	1.21	0.66
	k ($x10^{-7}$)		8.4	6.3	5	2.9	2.2	1.4	1.3
#4	e	1.75	1.24	0.88	0.76	0.65	0.58	0.51	0.47
	c_v			4.42	0.26	0.44	1	16.4	6.18
	m_v		372	105	33.5	10.7	3.89	1.55	0.51
	k ($x10^{-7}$)		8.8	7.5	5.7	3.6	2.8	2.4	2.6

Note: c_v is in m^2/year, m_v is in m^2/MN and k is in cm/s.

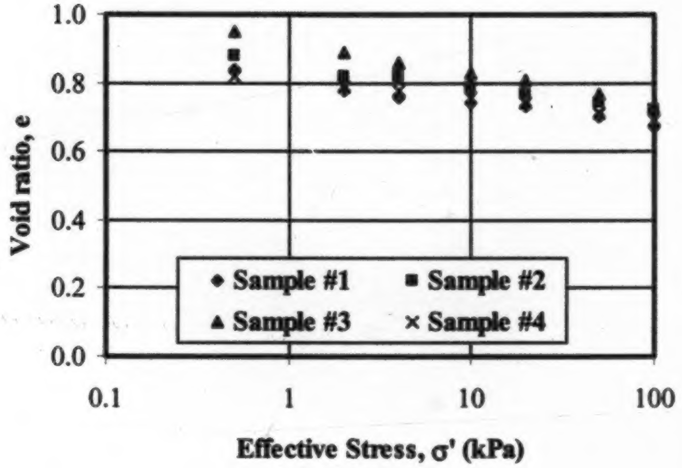

Figure B. 1 Compressibility of copper tailings

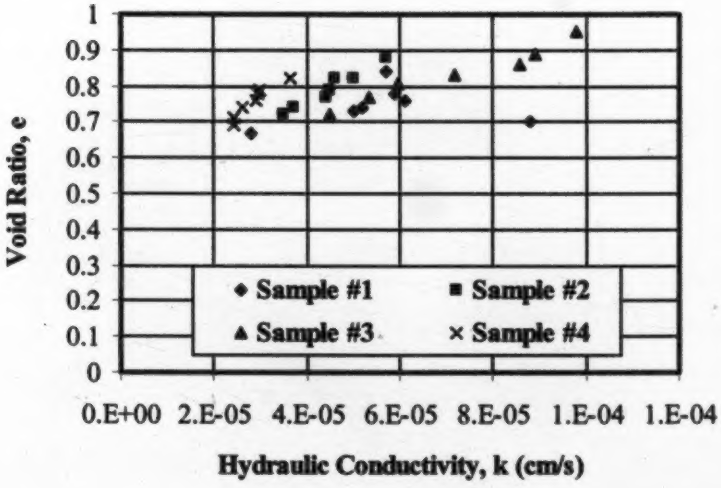

Figure B. 2 Void ratio versus hydraulic conductivity curve for copper tailings

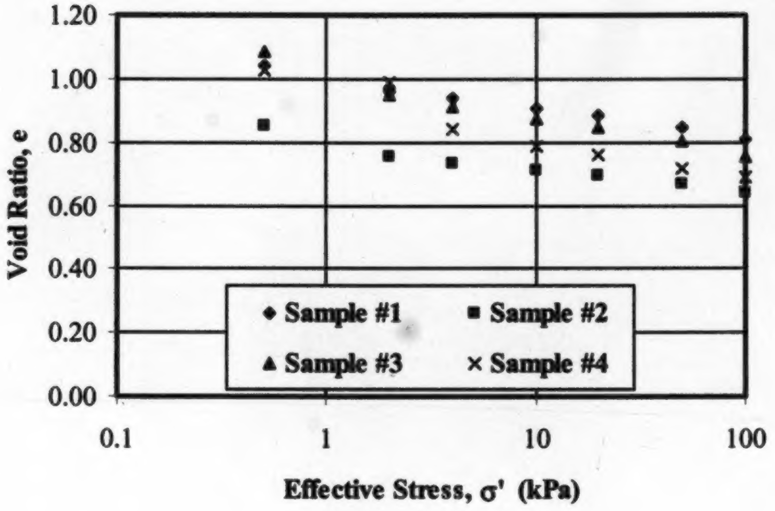

Figure B. 3 Compressibility of gold tailings

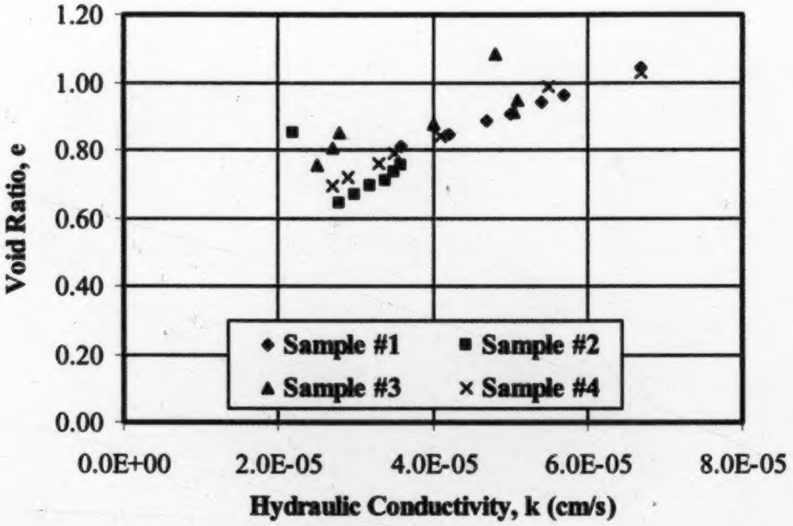

Figure B. 4 Void ratio versus hydraulic conductivity curve for gold tailings

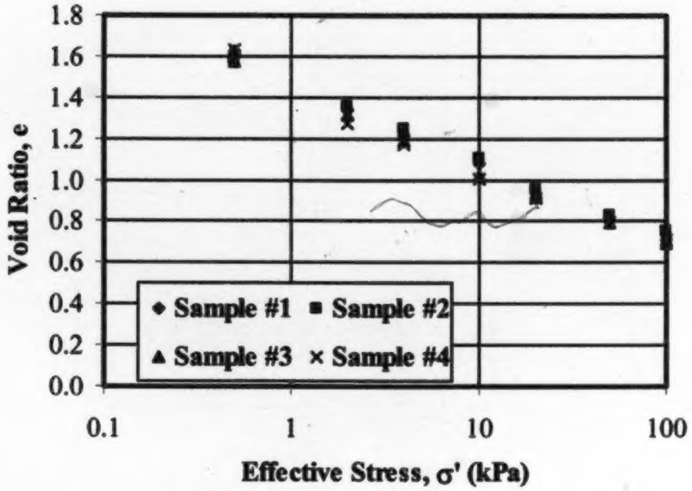

Figure B. 5 Compressibility of coal tailings

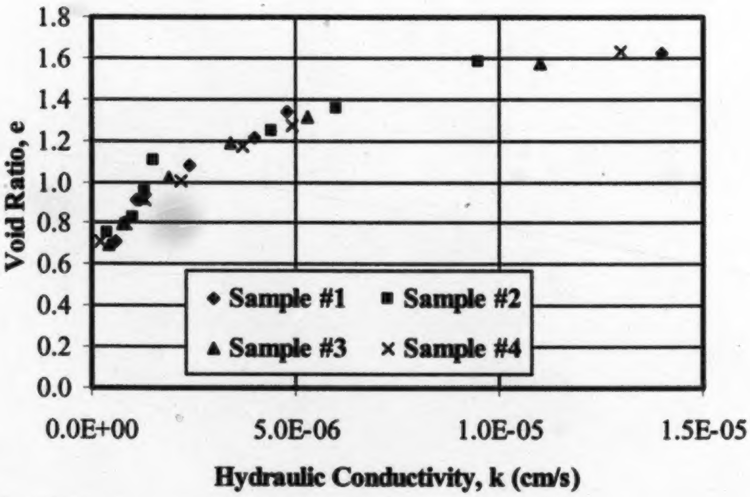

Figure B. 6 Void ratio versus hydraulic conductivity curve for coal tailings

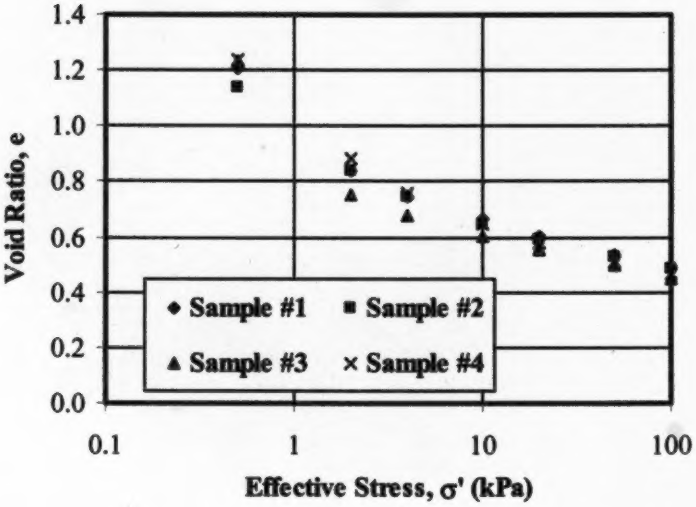

Figure B. 7 Compressibility of CT

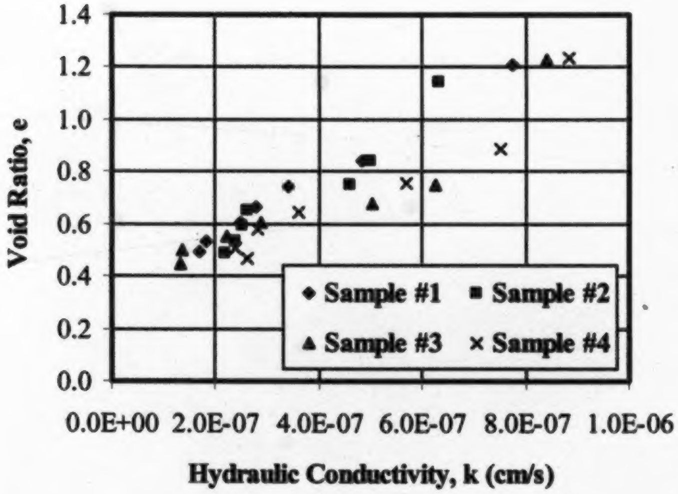

Figure B. 8 Void ratio versus hydraulic conductivity curve for oil sand CT

B.2 COLUMN DRYING TESTS

The specimen's height changes and evaporation changes in column drying tests are shown as following:

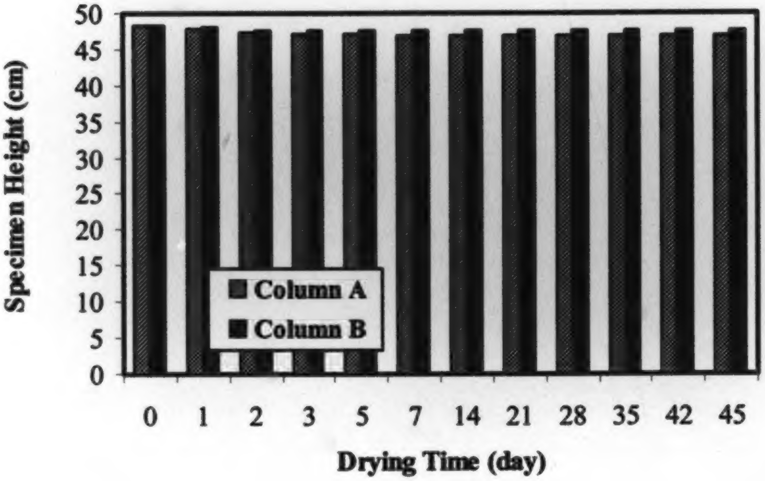

Figure B. 9 Specimen height changes in column drying test for copper tailings

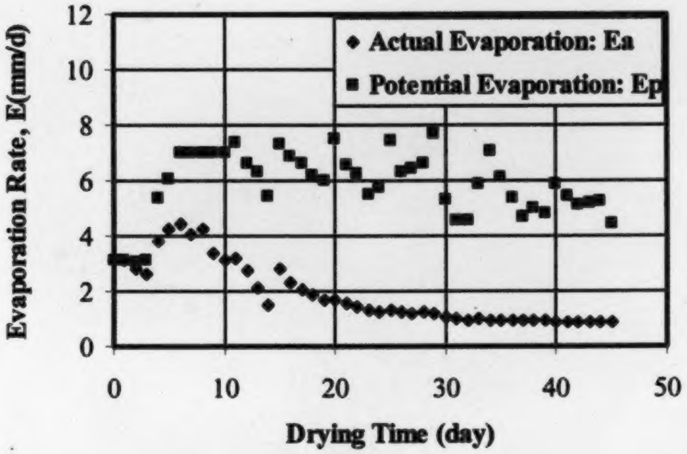

Figure B. 10 Evaporation changes in column drying tests for copper tailings

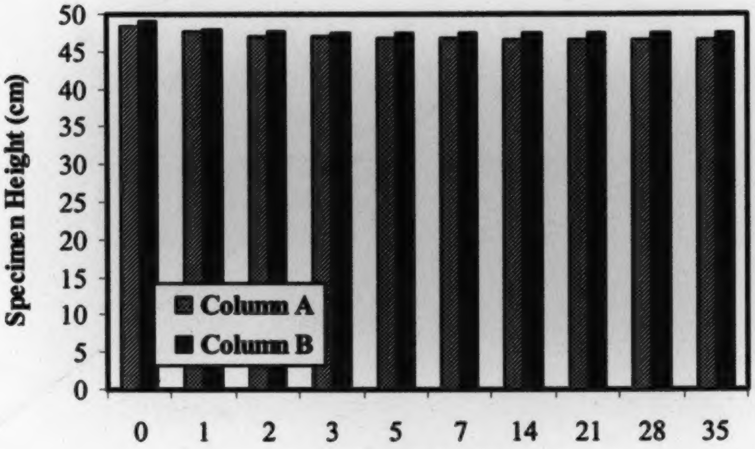

Figure B. 11 Specimen height changes in column drying tests for gold tailings

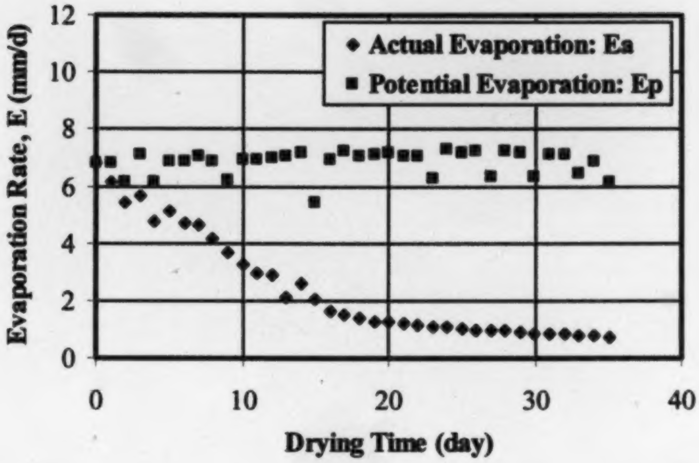

Figure B. 12 Evaporation changes in column drying tests for gold tailings

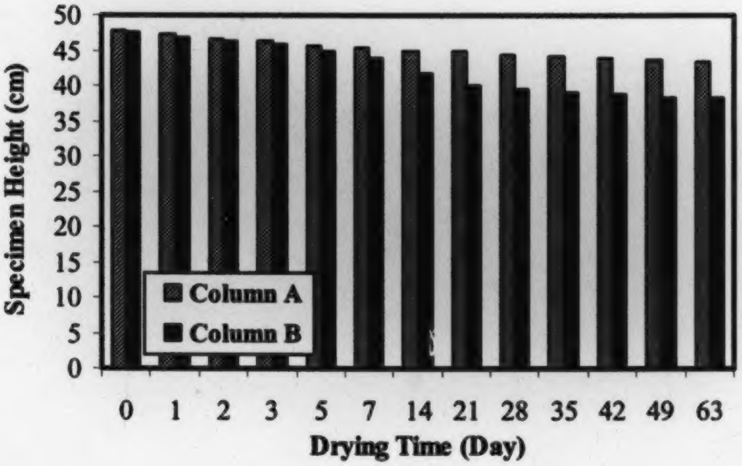

Figure B. 13 Specimen height changes in column drying tests for coal tailings

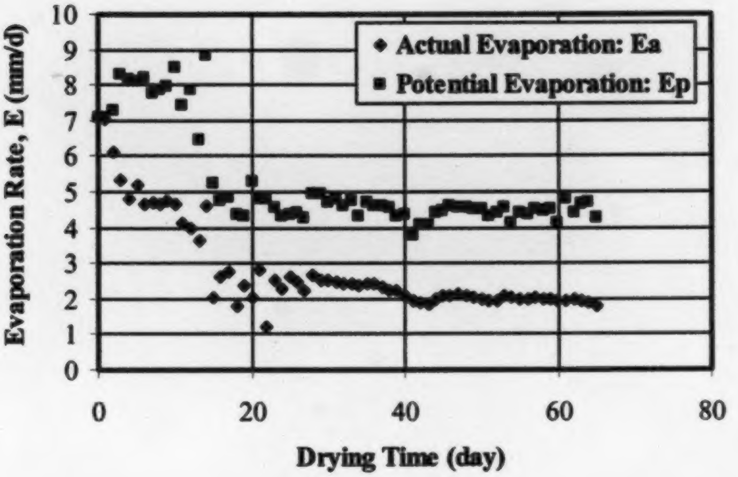

Figure B. 14 Evaporation changes in column drying tests for coal tailings

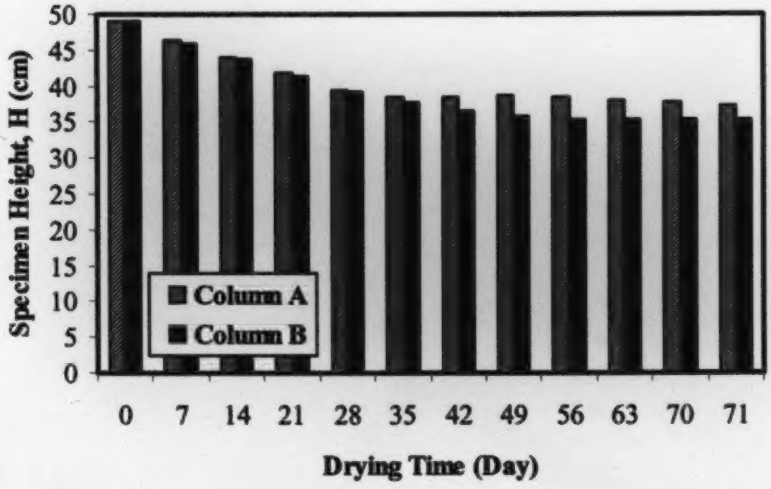

Figure B. 15 Specimen height changes in column drying tests for CT

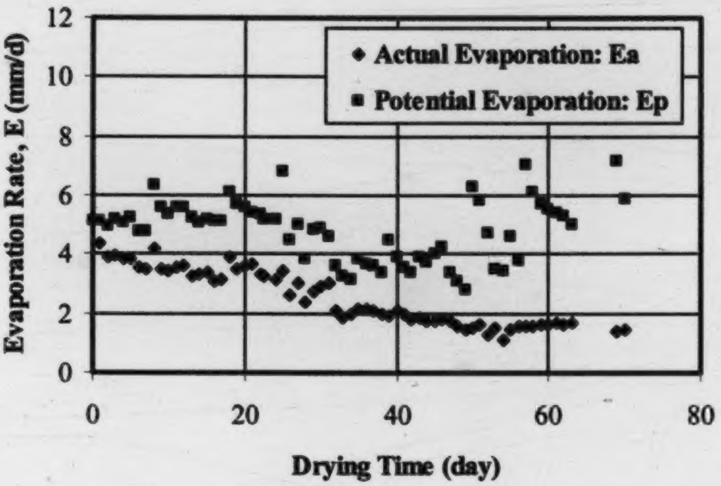

Figure B. 16 Evaporation changes in column drying tests for CT

B.3 SOIL-WATER RETENTION CURVE TESTS

The soil-water retention test results are shown as following:

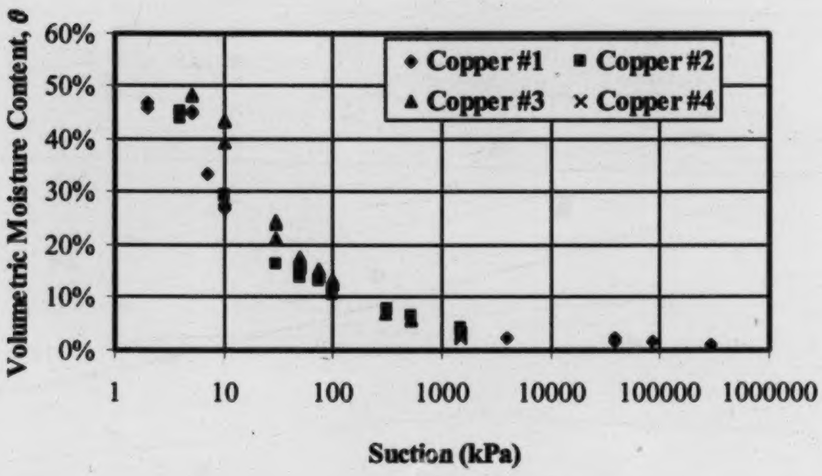

Figure B. 17 Soil-water retention curve test results for copper tailings

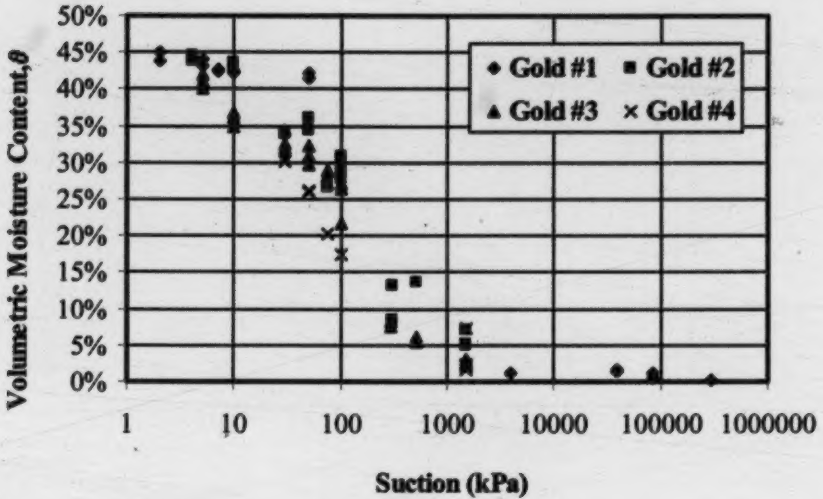

Figure B. 18 Soil-water retention curve test results for gold tailings

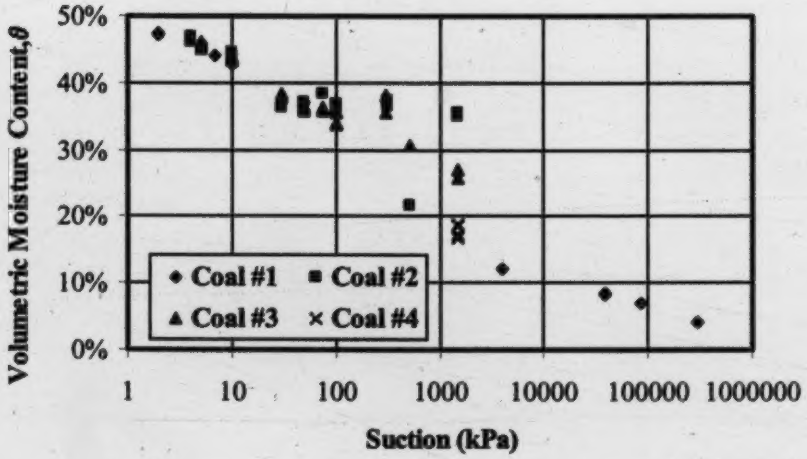

Figure B. 19 Soil-water retention curve test results for coal tailings

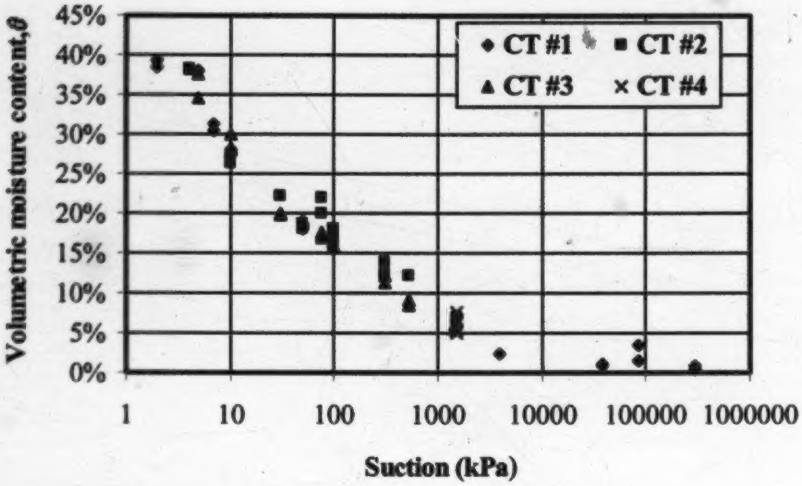

Figure B. 20 Soil-water retention curve test results for CT

B.4 TRIAXIAL TESTS

The triaxial test results for tailings are summarized as follows:

Table B. 5 Triaxial test results for tailings

Tailings Type	Sample No.	Peak Stress (kPa)		
		σ'_1	σ'_3	$(\sigma_1 - \sigma_3)$
Copper	1	89.2	55.3	33.9
	2	51.6	20.7	30.9
	3	35.6	18.8	16.8
	4	31.2	16.6	14.6
	5	46.8	29.3	17.5
	6	88.5	55.6	32.9
	7	82.0	27.7	54.3
	8	48.1	32.7	15.4
	9	108.6	66.7	41.9
Gold	1	93.4	33.2	60.2
	2	36.2	16.1	20.2
	3	35.2	15.7	19.5
	4	38.5	14.2	24.4
	5	111.7	57.6	54.1
	6	48.0	24.0	24.0
Coal	1	85.7	15	70.7
	2	113.7	22.5	91.2
	3	112.5	26.7	85.8
	4	206	41.5	164.5
	5	75.7	17.5	58.2
	6	101	24.7	76.3
CT	1	173	67	106
	2	246	66	180
	3	419	129	290
	4	74	49	25

B.5 SHRINKAGE TESTS

The shrinkage test results are summarized in the following tables.

Table B. 6 Shrinkage limits of tailings

Tailings Type	Sample No.	Shrinkage Limit	Shrinkage Ratio	Final Void Ratio
Copper	1	24.5%	1.64	0.67
	2	24.3%	1.65	0.67
	3	23.2%		
	4	25.1%		
Gold	1	21.8%	1.85	0.72
	2	21.3%	1.87	0.7
	3	21.1%		
	4	20.8%		
Coal	1	21.3%	1.31	0.48
	2	20.8%	1.33	0.46
	3	24%		
	4	25.8%		
CT	1	25.6%	1.58	0.65
	2	24.8%	1.58	0.64
	3	25.4%		
	4	25.5%		

Table B. 7 Shrinkage curve test results for copper tailings

Sample No.	Void Ratio, e	Moisture Content, w	Degree of Saturation, S
1	0.6666	0.02	0.08
2	0.6844	0.038	0.15
3	0.6786	0.018	0.07
4	0.702	0.017	0.07
5	0.671	0.015	0.06
6	0.6933	0.014	0.05
7	0.5921	0.1	0.53
8	0.7239	0	0.06
9	0.7921	0.1	0.29
10	0.6701	0.137	0.56
11	0.661	0.123	0.51
12	0.6646	0.12	0.49
13	0.6771	0.12	0.47

Table B. 8 Shrinkage curve test results for gold tailings

Sample No.	Void Ratio, e	Moisture Content, w	Degree of Saturation, S
1	0.6717	0.01	0.05
2	0.6769	0.015	0.07
3	0.6768	0.008	0.04
4	0.6823	0.009	0.04
5	0.6859	0.003	0.01
6	0.6771	0.009	0.04
7	0.7327	0.2	0.72
8	0.7311	0.2	0.71
9	0.7065	0.03	0.12
10	0.7621	0.1	0.26
11	0.7016	0.117	0.53
12	0.7164	0.114	0.51
13	0.6858	0.093	0.43
14	0.6863	0.096	0.44

Table B. 9 Shrinkage curve test results for coal tailings

Sample No.	Void Ratio, e	Moisture Content, w	Degree of Saturation, S
1	0.5328	0.117	0.43
2	0.5398	0.151	0.54
3	0.5167	0.079	0.30
4	0.5285	0.09	0.33
5	0.5197	0.08	0.30
6	0.529	0.097	0.36
7	0.5976	0.3	0.95
8	0.6181	0.3	0.96
9	0.5416	0.2	0.60
10	0.5474	0.2	0.87
11	0.5690	0.206	0.70
12	0.5613	0.137	0.47
13	0.5049	0.066	0.25
14	0.5435	0.080	0.29
15	0.5253	0.072	0.26
16	0.5349	0.075	0.27
17	0.5290	0.0397	0.15
18	0.5362	0.04288	0.16
19	0.5171	0.04038	0.15
20	0.5220	0.03949	0.15
21	0.604	0.275	0.88
22	0.592	0.273	0.89

Table B. 10 Shrinkage curve test results for CT

Sample No.	Void Ratio, e	Moisture Content, w	Degree of Saturation, S
1	0.5923	0.07	0.3
2	0.6507	0.092	0.4
3	0.6229	0.042	0.2
4	0.6299	0.059	0.2
5	0.6093	0.021	0.1
6	0.6318	0.024	0.1
7	0.6516	0.1	0.31
8	0.6542	0.1	0.35
9	0.6321	0.084	0.34
10	0.6395	0.150	0.61
11	0.6393	0.060	0.24
12	0.6332	0.042	0.17
13	0.6543	0.0106	0.04
14	0.6375	0.0108	0.04
15	0.6599	0.00235	0.01
16	0.6475	0.00304	0.01
17	0.6517	0.00152	0.01
18	0.6355	0.00391	0.02
19	0.640	0.195	0.79

APPENDIX C DERIVATION OF EQUATIONS

C.1 DERIVATION OF GOVERNING EQUATIONS

In the case of a tailings element with a unit area and a thickness of $\partial\xi$, as shown in Figure 5-3, under total stress condition in the Lagrangian system, the governing equations for sedimentation, consolidation, and desiccation can be derived through the equilibrium and continuity of the tailings element.

- **Equilibrium**

The mass of water in the element is

[C-1] $$\partial M_w = \theta\rho_w\partial v = \theta\rho_w\partial\xi$$

where ∂M_w is the mass of water in the element, θ is the volumetric water content in the element, ρ_w is the density of the water, and ∂v is the volume of the element.

The mass of solids in the element is

[C-2] $$\partial M_s = \rho_s\partial v_s = \rho_s\frac{\partial\xi}{1+e}$$

where ∂M_s is the mass of solids in the element, ρ_s is the density of the tailings particles, ∂v_s is the volume of the tailings solids particles in the element, and e is the void ratio.

Therefore, the total mass of the element (∂M) is

$$[\text{C-3}] \quad \partial M = \partial M_w + \partial M_s = \left[\theta\rho_w + \frac{\rho_s}{1+e}\right]\partial\xi$$

Then, the weight of the element (∂W) is

$$[\text{C-4}] \quad \partial W = \partial M \cdot g = \left[\theta\rho_w + \frac{\rho_s}{1+e}\right]\partial\xi \cdot g = \partial\xi\left[\theta\gamma_w + \frac{\gamma_s}{1+e}\right]$$

where ∂W is the weight of the element, g is the gravitational constant, and γ_w and γ_s are the unit weight of the water and tailings solids particles in the element respectively.

Considering vertical force equilibrium yields:

$$[\text{C-5}] \quad \sum F = 1 \cdot [\sigma(a,t) - \partial\sigma] - 1 \cdot [\sigma(a,t)] - \partial W = 0$$

where $\sigma(a,t)$ and $[\sigma(a,t)-\partial\sigma]$ are the normal stresses on the bottom face and upper face of the element respectively and $\partial\sigma$ is stress increment between the upper and bottom faces of the element ($\partial\sigma$ is assumed to be positive and the negative sign is due to the fact that the stress decreases as the Lagrangian coordinate a increases).

Substituting [C-4] into [C-5] gives

$$[\text{C-6}] \quad \partial\sigma + \partial\xi\left[\theta\gamma_w + \frac{\gamma_s}{1+e}\right] = 0$$

By dividing Equation [C-6] by ∂a on both sides and considering $\partial a \Rightarrow 0$, the following equation is obtained:

[C-7] $$\frac{\partial\sigma}{\partial a}+\frac{\partial\xi}{\partial a}\left[\theta\gamma_w+\frac{\gamma_s}{1+e}\right]=0$$

where ∂a is the increment of a in the Lagrangian system.

- **Continuity of the fluid phase**

The continuity of the fluid phase requires that the net rate at which fluid enters the element is equal to the time rate of change of mass of fluid in the element.

The velocity of the solid particles is denoted by v_s and that of the pore water is denoted by v_w (Gibson, et al. 1967). Then the rate of weight inflow of the pore water into the element is:

[C-8] $$\text{Rate of weight inflow} = \theta(v_w - v_s)\rho_w$$

while the rate of weight outflow of the pore water is

[C-9] $$\text{Rate of weight outflow} = \theta(v_w - v_s)\rho_w + \frac{\partial}{\partial a}[\theta(v_w - v_s)\rho_w]$$

Therefore, the net rate of inflow of the pore water is

[C-10] Net rate of inflow = Rate of inflow - Rate of outflow

$$= \theta(v_w - v_s)\rho_w - \left\{\theta(v_w - v_s)\rho_w + \frac{\partial}{\partial a}[\theta(v_w - v_s)\rho_w]\right\}$$

$$= -\frac{\partial}{\partial a}[\theta(v_w - v_s)\rho_w]$$

But the net rate of inflow must equal the time rate of change of weight of the pore water in the element, so that

$$\text{[C-11]} \quad -\frac{\partial}{\partial a}[\theta(v_w - v_s)\rho_w] = \frac{\partial}{\partial t}\left[\theta\rho_w \frac{\partial\xi}{\partial a}\right]$$

Rearranging and multiplying [C-11] by g gives

$$\text{[C-12]} \quad \frac{\partial}{\partial a}[\theta\gamma_w(v_w - v_s)] + \frac{\partial}{\partial t}\left[\theta\gamma_w \frac{\partial\xi}{\partial a}\right] = 0$$

- **Continuity of the solids phase**

Based on the definition of the Lagrangian coordinate system, the solids in the element remain constant. As shown in Figure 5-2, in the initial state (t=0), an element ∂a consists of solids (considered as a unit volume) and an initial void ratio e_0. At time t, the volume of solids is still a unit, but the void ratio has changed to e, which is different from e_0. Therefore, the following relation exists:

$$\text{[C-13]} \quad \frac{\partial\xi}{\partial a} = \frac{1+e}{1+e_0}$$

where e_0 is the initial void ratio at time equal to 0, and e is a function of a and t.

- **Darcy's Law**

Assuming that Darcy's Law is applicable in this case:

$$[C\text{-}14]\qquad \theta\left(v_w - v_s\right) = -k\frac{\partial \Psi}{\partial \xi}$$

where k is the hydraulic conductivity, Ψ is the total head,

$$[C\text{-}15]\qquad \Psi = h + \xi$$

where h is the pressure head and ξ is the elevation head from the datum plane (a = 0).

Substituting [C-15] into [C-14] gives

$$[C\text{-}16]\qquad \theta\left(v_w - v_s\right) = -k\left[\frac{\partial h}{\partial \xi} + 1\right]$$

Rewriting [C-7] gives

$$[C\text{-}17]\qquad \frac{\partial \sigma}{\partial z}\cdot\frac{dz}{da} + \frac{\partial \xi}{\partial a}\cdot\gamma_w\left[\frac{\theta(1+e)}{(1+e)} + \frac{\gamma_s}{\gamma_w(1+e)}\right] = 0$$

where z is the solids coordinate (refer to §5.2.1).

Substituting [C-13] and [5-2] into [C-17] gives

$$[C\text{-}18]\qquad \frac{\partial \sigma}{\partial z}\cdot\frac{1}{1+e_0} + \frac{1+e}{1+e_0}\cdot\gamma_w\left[\frac{\theta(1+e)}{(1+e)} + \frac{G_s}{(1+e)}\right] = 0$$

Multiplying [C-18] on both sides by (1+e_0) and rearranging yields

[C-19] $$\frac{\partial\sigma}{\partial z}+\gamma_w\left[\theta(1+e)+G_s\right]=0$$

Rewriting [C-12] gives

[C-20] $$\frac{dz}{da}\frac{\partial}{\partial z}\left[\theta\gamma_w\left(v_w-v_s\right)\right]+\frac{\partial}{\partial t}\left[\theta\gamma_w\frac{\partial\xi}{\partial a}\right]=0$$

Substituting [5-2], [C-16] and [C-13] into [C-20] yields

[C-21] $$\frac{1}{1+e_0}\frac{\partial}{\partial z}\left[-\gamma_w k\left(\frac{\partial h}{\partial\xi}+1\right)\right]+\frac{\partial}{\partial t}\left[\theta\gamma_w\frac{1+e}{1+e_0}\right]=0$$

Rewriting [C-21] gives

[C-22] $$\frac{\partial}{\partial z}\left\{k\left[\frac{\partial h}{\partial z}\cdot\frac{dz}{d\xi}+1\right]\right\}=\frac{\partial\left[\theta(1+e)\right]}{\partial t}$$

and substituting [5-4] into it gives

[C-23] $$\frac{\partial}{\partial z}\left\{k\left[\frac{\partial h}{\partial z}\cdot\frac{1}{1+e}+1\right]\right\}=\frac{\partial\left[\theta(1+e)\right]}{\partial t}$$

Rearranging [C-23] gives

[C-24] $$\frac{\partial}{\partial z}\left\{\frac{k}{1+e}\left[\frac{\partial h}{\partial z}+(1+e)\right]\right\}=\frac{\partial[\theta(1+e)]}{\partial t}$$

Therefore, the two governing equations finally become

[C-25] $$\frac{\partial\sigma}{\partial z}+\gamma_w[\theta(1+e)+G_s]=0$$

and

[C-26] $$\frac{\partial}{\partial z}\left\{\frac{k}{1+e}\left[\frac{\partial h}{\partial z}+(1+e)\right]\right\}=\frac{\partial[\theta(1+e)]}{\partial t}$$

C.2 NUMERICAL SOLUTION FOR THE DIFFERENTIAL EQUATIONS

C.2.1 Introduction to the Douglas-Johes (1963) predictor-corrector method

Considering a nonlinear parabolic differential equation

[C-27] $$\frac{\partial^2 u}{\partial x^2}=F\left(x,t,u,\frac{\partial u}{\partial x},\frac{\partial u}{\partial t}\right)$$

Its predictor is as

[C-28] $$\Delta_x^2 \omega_{i,n+\frac{1}{2}} = F\left(x_i, t_{n+\frac{1}{2}}, \omega_{in,} \delta_x \omega_{in}, \frac{\omega_{i,n+\frac{1}{2}} - \omega_{in}}{\frac{k}{2}} \right)$$

The corrector is as (I=1,2….N-1)

[C-29] $$\frac{1}{2}\Delta_x^2 \left(\omega_{i,n+1} + \omega_{in}\right) = F\left(x_i, t_{n+\frac{1}{2}}, \omega_{i,n+\frac{1}{2}}, \delta_x \omega_{i,n+\frac{1}{2}}, \frac{\omega_{i,n+1} - \omega_{in}}{k} \right)$$

where

$x_i = ih$, $t_n = nk$, $\omega_{in} = \omega(x_i,t_n)$

$\Delta_x{}^2\omega_{in} = h^{-2}(\omega_{i+1,n} - 2\omega_{in} + \omega_{i-1,n})$,

$\delta_x\omega_{in} = (2h)^{-1}(\omega_{i+1,n} - \omega_{i-1,n})$

C.2.2 Finite difference equations: Based on degree of saturation (S)

The original equations are

[5-38] $$f\frac{\partial h}{\partial t} = \frac{\partial g}{\partial z}\left\{\frac{\partial h}{\partial z} + (1+e)\right\} + g\left(\frac{\partial^2 h}{\partial z^2} + \frac{\partial e}{\partial z}\right)$$

where

[5-38a] $$f = f(h,e) = e\frac{dS}{dh} + S\frac{de}{dh}$$

and

[5-38b] $$g = g(h,e) = \frac{k(h,e)}{1+e}$$

The Douglas-Johes (1963) predictor-corrector method is used for Equation (5-38):

(1) Predictor for 2 ≤ i ≤ R-1

[C-30]

$$f_i^n \frac{h_i^{n+\frac{1}{2}} - h_i^n}{\frac{\Delta t}{2}} = \left[\frac{g_{i+1}^n - g_{i-1}^n}{2\Delta z}\right]\left\{\frac{h_{i+1}^n - h_{i-1}^n}{2\Delta z} + \left(1 + e_i^n\right)\right\} + g_i^n \left\{\frac{h_{i-1}^{n+\frac{1}{2}} - 2h_i^{n+\frac{1}{2}} + h_{i+1}^{n+\frac{1}{2}}}{(\Delta z)^2} + \frac{e_{i+1}^n - e_{i-1}^n}{2\Delta z}\right\}$$

Rearranging and multiplying by $4\Delta z^2 \Delta t$ on both sides gives:

[C-31] $A_i h_{i-1}^{n+\frac{1}{2}} + B_i h_i^{n+\frac{1}{2}} + C_i h_{i+1}^{n+\frac{1}{2}} = D_i$

where

$$A_i = C_i = 4 \cdot \Delta t \cdot g_i^n$$

$$B_i = -8\left[\Delta t \cdot g_i^n + (\Delta z)^2 \cdot f_i^n\right]$$

$$D_i = -8(\Delta z)^2 f_i^n h_i^n - 2\Delta t \cdot \Delta z \cdot g_i^n \left(e_{i+1}^n - e_{i-1}^n\right) - \Delta t\left(g_{i+1}^n - g_{i-1}^n\right)\left\{\left(h_{i+1}^n - h_{i-1}^n\right) + 2\Delta z\left(1 + e_i^n\right)\right\}$$

$$f_i^n = f\left(h_i^n, e_i^n\right)$$

$$g_i^n = g\left(h_i^n, e_i^n\right)$$

(2) Corrector for $2 \le i \le R\text{-}1$

$$[\text{C-32}] \qquad f_i^{n+\frac{1}{2}} \frac{h_i^{n+1} - h_i^n}{\Delta t} = \frac{g_{i+1}^{n+\frac{1}{2}} - g_{i-1}^{n+\frac{1}{2}}}{2\Delta z} \left\{ \frac{h_{i+1}^{n+\frac{1}{2}} - h_{i-1}^{n+\frac{1}{2}}}{2\Delta z} + \left(1 + e_i^{n+\frac{1}{2}} \right) \right\} +$$

$$+ g_i^{n+\frac{1}{2}} \left\{ \frac{1}{2} \left[\frac{h_{i+1}^{n+1} - 2h_i^{n+1} + h_{i-1}^{n+1}}{(\Delta z)^2} + \frac{h_{i+1}^n - 2h_i^n + h_{i-1}^n}{(\Delta z)^2} \right] + \frac{e_{i+1}^{n+\frac{1}{2}} - e_{i-1}^{n+\frac{1}{2}}}{2\Delta z} \right\}$$

Rearranging and multiplying by $4\Delta z^2 \Delta t$ on both sides gives

$$[\text{C-33}] \qquad a_i h_{i-1}^{n+1} + b_i h_i^{n+1} + c_i h_{i+1}^{n+1} = d_i$$

where

$$a_i = c_i = 2 \cdot \Delta t \cdot g_i^{n+\frac{1}{2}}$$

$$b_i = -4 \left[\Delta t \cdot g_i^{n+\frac{1}{2}} + (\Delta z)^2 f_i^{n+\frac{1}{2}} \right]$$

$$d_i = -4(\Delta z)^2 f_i^{n+\frac{1}{2}} h_i^n - \Delta t \left(g_{i+1}^{n+\frac{1}{2}} - g_{i-1}^{n+\frac{1}{2}} \right) \left\{ \left(h_{i+1}^{n+\frac{1}{2}} - h_{i-1}^{n+\frac{1}{2}} \right) + 2\Delta z \left(1 + e_i^{n+\frac{1}{2}} \right) \right\}$$

$$- 2\Delta t \cdot g_i^{n+\frac{1}{2}} \left[h_{i-1}^n - 2h_i^n + h_{i+1}^n + \Delta z \left(e_{i+1}^{n+\frac{1}{2}} - e_{i-1}^{n+\frac{1}{2}} \right) \right]$$

$$f_i^{n+\frac{1}{2}} = f\left(h_i^{n+\frac{1}{2}}, e_i^{n+\frac{1}{2}} \right)$$

$$g_i^{n+\frac{1}{2}} = g\left(h_i^{n+\frac{1}{2}}, e_i^{n+\frac{1}{2}}\right)$$

$$e_i^{n+\frac{1}{2}} = e_i^n + \left(h_i^{n+\frac{1}{2}} - h_i^n\right) \cdot f_e\left(h_i^n, e_i^n\right)$$

C.2.3 Boundary Conditions

Bottom boundary conditions are introduced to eliminate all values of fictitious points.

(1) Lower Boundary (i.e. i=1)

The boundary conditions of the sub-aerial tailings deposition are shown in Figure 5-10.

(a) Permeable boundary

When the lower boundary is permeable, i.e. free drainage is applied, the bottom boundary condition can be expressed as (see equation [5-60]):

[C-34] $$\left.\frac{\partial h}{\partial z}\right|_{z=0} = 0$$

Using the backward difference equation in Equation [C-35] gives

[C-35] $$\left.\frac{h_i - h_{i-1}}{\Delta z}\right|_{z=0} = 0$$

so

[C-36] $h_{i-1} = h_i$

Applying the above equation to n, n + ½ and n + 1 time levels at i = 1 gives

[C-37] $$\begin{cases} h_0^n = h_1^n \\ h_0^{n+\frac{1}{2}} = h_1^{n+\frac{1}{2}} \\ h_0^{n+1} = h_1^{n+1} \end{cases}$$

For i = 1, predictor can be expressed as:

[C-38]

$$f_1^n \frac{h_1^{n+\frac{1}{2}} - h_1^n}{\frac{\Delta t}{2}} = \left[\frac{g_2^n - g_1^n}{\Delta z}\right]\left\{\frac{h_2^n - h_0^n}{2\Delta z} + \left(1 + e_1^n\right)\right\} + g_1^n \left\{\frac{h_0^{n+\frac{1}{2}} - 2h_1^{n+\frac{1}{2}} + h_2^{n+\frac{1}{2}}}{(\Delta z)^2} + \frac{e_2^n - e_1^n}{\Delta z}\right\}$$

Substituting Equation [3-37] into [C-38] gives

[C-39]

$$f_1^n \frac{h_1^{n+\frac{1}{2}} - h_1^n}{\frac{\Delta t}{2}} = \left[\frac{g_2^n - g_1^n}{\Delta z}\right]\left\{\frac{h_2^n - h_1^n}{2\Delta z} + \left(1 + e_1^n\right)\right\} + g_1^n \left\{\frac{h_1^{n+\frac{1}{2}} - 2h_1^{n+\frac{1}{2}} + h_2^{n+\frac{1}{2}}}{(\Delta z)^2} + \frac{e_2^n - e_1^n}{\Delta z}\right\}$$

and rearranging gives

[C-40] $B_1 h_1^{n+\frac{1}{2}} + C_1 h_2^{n+\frac{1}{2}} = D_1$

where

[C-40a] $B_1 = 2\left(\Delta t \cdot g_1^n + 2\Delta z^2 \cdot f_1^n\right)$

[C-40b] $C_1 = -2\Delta t \cdot g_1^n$

[C-40c] $D_1 = 4\Delta z^2 \cdot f_1^n \cdot h_1^n + 2\Delta t \cdot \Delta z \cdot g_1^n\left(e_2^n - e_1^n\right) + \Delta t\left(g_2^n - g_1^n\right)\left\{\left(h_2^n - h_1^n\right) + 2\Delta z\left(1 + e_1^n\right)\right\}$

For i = 1, the corrector can be expressed as:

[C-41]
$$f_1^{n+\frac{1}{2}}\frac{h_1^{n+1} - h_1^n}{\Delta t} = \frac{g_2^{n+\frac{1}{2}} - g_1^{n+\frac{1}{2}}}{\Delta z}\left\{\frac{h_2^{n+\frac{1}{2}} - h_0^{n+\frac{1}{2}}}{2\Delta z} + \left(1 + e_1^{n+\frac{1}{2}}\right)\right\} +$$
$$+ g_1^{n+\frac{1}{2}}\left\{\frac{1}{2}\left[\frac{h_0^{n+1} - 2h_1^{n+1} + h_2^{n+1}}{(\Delta z)^2} + \frac{h_0^n - 2h_1^n + h_2^n}{(\Delta z)^2}\right] + \frac{e_2^{n+\frac{1}{2}} - e_1^{n+\frac{1}{2}}}{\Delta z}\right\}$$

Substituting [C-37] into [C-41] gives

[C-42]
$$f_1^{n+\frac{1}{2}}\frac{h_1^{n+1} - h_1^n}{\Delta t} = \frac{g_2^{n+\frac{1}{2}} - g_1^{n+\frac{1}{2}}}{\Delta z}\left\{\frac{h_2^{n+\frac{1}{2}} - h_1^{n+\frac{1}{2}}}{2\Delta z} + \left(1 + e_1^{n+\frac{1}{2}}\right)\right\} +$$
$$+ g_1^{n+\frac{1}{2}}\left\{\frac{1}{2}\left[\frac{h_1^{n+1} - 2h_1^{n+1} + h_2^{n+1}}{(\Delta z)^2} + \frac{h_1^n - 2h_1^n + h_2^n}{(\Delta z)^2}\right] + \frac{e_2^{n+\frac{1}{2}} - e_1^{n+\frac{1}{2}}}{\Delta z}\right\}$$

and rearranging gives

[C-43] $b_1 h_1^{n+1} + c_1 h_2^{n+1} = d_1$

where

$$[\text{C-43a}]\quad b_1 = \Delta t \cdot g_1^{n+\frac{1}{2}} + 2\Delta z^2 \cdot f_1^{n+\frac{1}{2}}$$

$$[\text{C-43b}]\quad c_1 = -\Delta t \cdot g_1^{n+\frac{1}{2}}$$

$$[\text{C-43c}]\quad d_1 = 2\Delta z^2 \cdot f_1^{n+\frac{1}{2}} \cdot h_1^n + \Delta t\left(g_2^{n+\frac{1}{2}} - g_1^{n+\frac{1}{2}}\right)\left\{\left(h_2^{n+\frac{1}{2}} - h_1^{n+\frac{1}{2}}\right) + 2\Delta z\left(1 + e_1^{n+\frac{1}{2}}\right)\right\}$$

$$+ \Delta t \cdot g_1^{n+\frac{1}{2}}\left[-h_1^n + h_2^n + 2\Delta z\left(e_2^{n+\frac{1}{2}} - e_1^{n+\frac{1}{2}}\right)\right]$$

where

$$[\text{C-43d}]\quad f_1^{n+\frac{1}{2}} = f\left(h_1^{n+\frac{1}{2}}, e_1^{n+\frac{1}{2}}\right)$$

$$[\text{C-43e}]\quad g_1^{n+\frac{1}{2}} = g\left(h_1^{n+\frac{1}{2}}, e_1^{n+\frac{1}{2}}\right)$$

$$[\text{C-43f}]\quad g_2^{n+\frac{1}{2}} = g\left(h_2^{n+\frac{1}{2}}, e_2^{n+\frac{1}{2}}\right)$$

$$[\text{C-43g}]\quad e_1^{n+\frac{1}{2}} = e_1^n + \left(h_1^{n+\frac{1}{2}} - h_1^n\right) \cdot f_e\left(h_1^n, e_1^n\right)$$

$$[\text{C-43h}]\quad e_2^{n+\frac{1}{2}} = e_2^n + \left(h_2^{n+\frac{1}{2}} - h_2^n\right) \cdot f_e\left(h_2^n, e_2^n\right)$$

(b) Impermeable boundary

When the lower boundary is impermeable, based on equation [5- 58], we have

[C-44] $$\left.\frac{\partial h}{\partial z}\right|_{z=0} = -(1+e)$$

Using the backward difference equation in [C-44] gives

[C-45] $$\left.\frac{h_i - h_{i-1}}{\Delta z}\right|_{z=0} = -(1+e_i)$$

Rearranging [C-45] and applying to i =1 gives

[C-46] $$h_0 = h_1 + \Delta z(1+e_1)$$

Applying [C-46] to n, n+1/2 and n+1 time levels gives

[C-47]

$$\begin{cases} h_0^n = h_1^n + \Delta z(1+e_1^n) \\ h_0^{n+\frac{1}{2}} = h_1^{n+\frac{1}{2}} + \Delta z\left(1+e_1^{n+\frac{1}{2}}\right) = \left[1+\Delta z\cdot f_e(h_1^n, e_1^n)\right]\cdot h_1^{n+\frac{1}{2}} + \Delta z\left[1+e_1^n - h_1^n\cdot f_e(h_1^n, e_1^n)\right] \\ h_0^{n+1} = h_1^{n+1} + \Delta z(1+e_1^{n+1}) = \left[1+\Delta z f_e\left(h_1^{n+\frac{1}{2}}, e_1^{n+\frac{1}{2}}\right)\right] h_1^{n+1} + \Delta z\left[1+e_1^{n+\frac{1}{2}} - h_1^{n+\frac{1}{2}} f_e\left(h_1^{n+\frac{1}{2}}, e_1^{n+\frac{1}{2}}\right)\right] \end{cases}$$

For predictor at i =1 in the impermeable lower boundary:

Substituting [C-47] into [C-38] and rearranging gives

[C-48] $B_1 h_1^{n+\frac{1}{2}} + C_1 h_2^{n+\frac{1}{2}} = D_1$ (for the impermeable lower boundary)

where

[C-48a] $B_1 = 4\Delta z^2 \cdot f_1^n - 2\Delta t \cdot g_1^n \left[\Delta z \cdot f_e\left(h_1^n, e_1^n\right) - 1\right]$

[C-48b] $C_1 = -2\Delta t \cdot g_1^n$

[C-48c]
$D_1 = 4\Delta z^2 f_1^n h_1^n + 2\Delta t \Delta z g_1^n \left[1 + e_2^n - h_1^n f_e\left(h_1^n, e_1^n\right)\right] + \Delta t\left(g_2^n - g_1^n\right)\left[h_2^n - h_1^n + \Delta z\left(1 + e_1^n\right)\right]$

For corrector at i =1 in the impermeable lower boundary:

Substituting [C-47] into [C-41] and rearranging gives

[C-49] $b_1 h_1^{n+1} + c_1 h_2^{n+1} = d_1$

where

[C-49a] $b_1 = \Delta t \cdot g_1^{n+\frac{1}{2}} \left[1 - \Delta z f_e\left(h_1^{n+\frac{1}{2}}, e_1^{n+\frac{1}{2}}\right)\right] + 2\Delta z^2 \cdot f_1^{n+\frac{1}{2}}$

[C-49b] $c_1 = -\Delta t \cdot g_1^{n+\frac{1}{2}}$

$$\text{[C-49c]}\quad d_1 = 2\Delta z^2 \cdot f_1^{n+\frac{1}{2}} \cdot h_1^n + \Delta t\left(g_2^{n+\frac{1}{2}} - g_1^{n+\frac{1}{2}}\right)\left[h_2^{n+\frac{1}{2}} - h_1^{n+\frac{1}{2}} + \Delta z\left(1 + e_1^{n+\frac{1}{2}}\right)\right]$$

$$+ \Delta t \cdot g_1^{n+\frac{1}{2}}\left\{-h_1^n + h_2^n + \Delta z\left(1 + e_1^n\right) + \Delta z\left[1 + 2e_2^{n+\frac{1}{2}} - e_1^{n+\frac{1}{2}} - h_1^{n+\frac{1}{2}} f_e\left(h_1^{n+\frac{1}{2}}, e_1^{n+\frac{1}{2}}\right)\right]\right\}$$

(2) Upper boundary (i = R)

The upper boundary flux condition can be expressed as:

$$\text{[C-50]}\quad E = -\frac{k}{1+e}\left\{\frac{\partial h}{\partial z} + (1+e)\right\}\Bigg|_{z=H_z}$$

where E is the upper flux rate from the tailings, ($E = q_{z=Hz} = E_p$ during the sedimentation, $E = E_a$ after sedimentation), and E_a is the actual evaporation rate on the tailings surface.

Equation [C-50] can be expressed in form of a difference equation:

(i) For the predictor, the following form is used:

$$\text{[C-51]}\quad E_R^{n+\frac{1}{2}} = -g_R^n\left\{\frac{h_{R+1}^{n+\frac{1}{2}} - h_{R-1}^{n+\frac{1}{2}}}{2 \cdot \Delta z} + 1 + e_R^n\right\}$$

$$\text{[C-51a]}\quad E_R^n = -g_R^n\left\{\frac{h_{R+1}^n - h_{R-1}^n}{2 \cdot \Delta z} + 1 + e_R^n\right\}$$

(ii) For the corrector, the following form is used:

[C-52] $$\mathrm{E}_{\mathrm{R}}^{\mathrm{n+1}} = -\mathrm{g}_{\mathrm{R}}^{\mathrm{n}+\frac{1}{2}}\left\{\frac{\mathrm{h}_{\mathrm{R+1}}^{\mathrm{n+1}} - \mathrm{h}_{\mathrm{R-1}}^{\mathrm{n+1}}}{2\cdot\Delta \mathrm{z}} + 1 + \mathrm{e}_{\mathrm{R}}^{\mathrm{n}+\frac{1}{2}}\right\}$$

[C-52a] $$\mathrm{E}_{\mathrm{R}}^{\mathrm{n+1}} = -\mathrm{g}_{\mathrm{R}}^{\mathrm{n}+\frac{1}{2}}\left\{\frac{\mathrm{h}_{\mathrm{R+1}}^{\mathrm{n}+\frac{1}{2}} - \mathrm{h}_{\mathrm{R-1}}^{\mathrm{n}+\frac{1}{2}}}{2\cdot\Delta \mathrm{z}} + 1 + \mathrm{e}_{\mathrm{R}}^{\mathrm{n}+\frac{1}{2}}\right\}$$

For i = R, the predictor becomes

[C-53]

$$\mathrm{f}_{\mathrm{R}}^{\mathrm{n}}\frac{\mathrm{h}_{\mathrm{R}}^{\mathrm{n}+\frac{1}{2}} - \mathrm{h}_{\mathrm{R}}^{\mathrm{n}}}{\frac{\Delta \mathrm{t}}{2}} = \left[\frac{\mathrm{g}_{\mathrm{R}}^{\mathrm{n}} - \mathrm{g}_{\mathrm{R-1}}^{\mathrm{n}}}{\Delta \mathrm{z}}\right]\left\{\frac{\mathrm{h}_{\mathrm{R+1}}^{\mathrm{n}} - \mathrm{h}_{\mathrm{R-1}}^{\mathrm{n}}}{2\Delta \mathrm{z}} + \left(1 + \mathrm{e}_{\mathrm{R}}^{\mathrm{n}}\right)\right\} + \mathrm{g}_{\mathrm{R}}^{\mathrm{n}}\left\{\frac{\mathrm{h}_{\mathrm{R-1}}^{\mathrm{n}+\frac{1}{2}} - 2\mathrm{h}_{\mathrm{R}}^{\mathrm{n}+\frac{1}{2}} + \mathrm{h}_{\mathrm{R+1}}^{\mathrm{n}+\frac{1}{2}}}{(\Delta \mathrm{z})^2} + \frac{\mathrm{e}_{\mathrm{R}}^{\mathrm{n}} - \mathrm{e}_{\mathrm{R-1}}^{\mathrm{n}}}{\Delta \mathrm{z}}\right\}$$

Substituting boundary condition equation [C-51] and [C-52] into the predictor equation gives

[C-54]

$$\mathrm{f}_{\mathrm{R}}^{\mathrm{n}}\frac{\mathrm{h}_{\mathrm{R}}^{\mathrm{n}+\frac{1}{2}} - \mathrm{h}_{\mathrm{R}}^{\mathrm{n}}}{\frac{\Delta \mathrm{t}}{2}} = \left[\frac{\mathrm{g}_{\mathrm{R}}^{\mathrm{n}} - \mathrm{g}_{\mathrm{R-1}}^{\mathrm{n}}}{\Delta \mathrm{z}}\right]\left\{-\frac{\mathrm{E}_{\mathrm{R}}^{\mathrm{n}}}{\mathrm{g}_{\mathrm{R}}^{\mathrm{n}}}\right\}$$

$$+ 2\mathrm{g}_{\mathrm{R}}^{\mathrm{n}}\left\{\frac{\mathrm{h}_{\mathrm{R-1}}^{\mathrm{n}+\frac{1}{2}} - \mathrm{h}_{\mathrm{R}}^{\mathrm{n}+\frac{1}{2}} - \Delta \mathrm{z}\left(1 + \mathrm{e}_{\mathrm{R}}^{\mathrm{n}}\right) - \Delta \mathrm{z}\,\mathrm{E}_{\mathrm{R}}^{\mathrm{n}+\frac{1}{2}} \big/ \mathrm{g}_{\mathrm{R}}^{\mathrm{n}}}{(\Delta \mathrm{z})^2} + \frac{\mathrm{e}_{\mathrm{R}}^{\mathrm{n}} - \mathrm{e}_{\mathrm{R-1}}^{\mathrm{n}}}{2\Delta \mathrm{z}}\right\}$$

Rearranging gives

[C-55] $$A_R h_{R-1}^{n+\frac{1}{2}} + B_R h_R^{n+\frac{1}{2}} = D_R$$

where

[C-55a] $A_R = 2\Delta t \cdot g_R^n$

[C-55b] $B_R = -2\left(\Delta t \cdot g_R^n + \Delta z^2 f_R^n\right)$

[C-55c]

$$D_R = 2\Delta z^2 f_R^n h_R^n + \Delta t \cdot \Delta z \frac{E_R^n\left(g_R^n - g_{R-1}^n\right)}{g_R^n} + \Delta t \cdot g_R^n \left\{ 2\Delta z \left[1 + e_R^n + E_R^{n+\frac{1}{2}} \Big/ g_R^n \right] - e_R^n + e_{R-1}^n \right\}$$

[C-55d] $E_R^n = E_p \left\{ A_r \left[\frac{1}{1+\left(\alpha(T-\Delta t)\right)^p} \right]^q + B_r \right\}$ (Previous time step value = EA)

[C-55e] $E_R^{n+\frac{1}{2}} = E_p \left\{ A_r \left[\frac{1}{1+\left(\alpha(T-\Delta t/2)\right)^p} \right]^q + B_r \right\}$ (Half time step value)

For i = R, the corrector becomes

$$\text{[C-56]} \quad f_R^{n+\frac{1}{2}} \frac{h_R^{n+1} - h_R^n}{\Delta t} = \frac{g_R^{n+\frac{1}{2}} - g_{R-1}^{n+\frac{1}{2}}}{\Delta z} \left\{ \frac{h_{R+1}^{n+\frac{1}{2}} - h_{R-1}^{n+\frac{1}{2}}}{2\Delta z} + \left(1 + e_R^{n+\frac{1}{2}} \right) \right\} +$$

$$+ g_R^{n+\frac{1}{2}} \left\{ \frac{1}{2} \left[\frac{h_{R+1}^{n+1} - 2h_R^{n+1} + h_{R-1}^{n+1}}{(\Delta z)^2} + \frac{h_{R+1}^n - 2h_R^n + h_{R-1}^n}{(\Delta z)^2} \right] + \frac{e_R^{n+\frac{1}{2}} - e_{R-1}^{n+\frac{1}{2}}}{\Delta z} \right\}$$

and substituting [C-52] and [C-52a] into [C-56] gives

[C-57]

$$f_R^{n+\frac{1}{2}}\frac{h_R^{n+1}-h_R^n}{\Delta t}=\frac{g_R^{n+\frac{1}{2}}-g_{R-1}^{n+\frac{1}{2}}}{\Delta z}\left\{-\frac{E_R^{n+1}}{g_R^{n+\frac{1}{2}}}\right\}+g_R^{n+\frac{1}{2}}\cdot\frac{-h_R^{n+1}+h_{R-1}^{n+1}-\Delta z\left(1+e_R^{n+\frac{1}{2}}\right)-\frac{\Delta zE_R^{n+1}}{g_R^{n+\frac{1}{2}}}}{(\Delta z)^2}$$

$$+g_R^{n+\frac{1}{2}}\cdot\frac{-h_R^n+h_{R-1}^n-\Delta z\left(1+e_R^{n+\frac{1}{2}}\right)-\frac{\Delta zE_R^{n+1}}{g_R^{n+\frac{1}{2}}}}{(\Delta z)^2}+g_R^{n+\frac{1}{2}}\cdot\frac{e_R^{n+\frac{1}{2}}-e_{R-1}^{n+\frac{1}{2}}}{\Delta z}$$

Rearranging gives

[C-58] $a_R h_{R-1}^{n+1}+b_R h_R^{n+1}=d_R$

where

[C-58a] $a_R=\Delta t\cdot g_R^{n+\frac{1}{2}}$

[C-58b] $b_R=-\Delta t\cdot g_R^{n+\frac{1}{2}}-\Delta z^2 f_R^{n+\frac{1}{2}}$

[C-58c]

$$d_R=\Delta t\cdot\Delta z\left(g_R^{n+\frac{1}{2}}-g_{R-1}^{n+\frac{1}{2}}\right)\cdot\frac{E_R^{n+1}}{g_R^{n+\frac{1}{2}}}-\Delta z^2\cdot f_R^{n+\frac{1}{2}}\cdot h_R^n-\Delta t\cdot\Delta z\cdot g_R^{n+\frac{1}{2}}\left(e_R^{n+\frac{1}{2}}-e_{R-1}^{n+\frac{1}{2}}\right)$$

$$+\Delta t\cdot\Delta z\cdot g_R^{n+\frac{1}{2}}\left(1+e_R^{n+\frac{1}{2}}+\frac{E_R^{n+1}}{g_R^{n+\frac{1}{2}}}\right)+\Delta t\cdot g_R^{n+\frac{1}{2}}\left\{h_R^n-h_{R-1}^n+\Delta z\left(1+e_R^{n+\frac{1}{2}}\right)+\frac{\Delta z\cdot E_R^{n+1}}{g_R^{n+\frac{1}{2}}}\right\}$$

where

[C-58d] $f_R^{n+\frac{1}{2}} = f(h_R^{n+\frac{1}{2}}, e_R^{n+\frac{1}{2}})$

[C-58e] $g_R^{n+\frac{1}{2}} = g(h_R^{n+\frac{1}{2}}, e_R^{n+\frac{1}{2}})$

[C-58f] $g_{R-1}^{n+\frac{1}{2}} = g(h_{R-1}^{n+\frac{1}{2}}, e_{R-1}^{n+\frac{1}{2}})$

[C-58g] $\mathrm{e}_\mathrm{R}^{n+\frac{1}{2}} = \mathrm{e}_\mathrm{R}^n + \left[\mathrm{h}_\mathrm{R}^{n+1} - \mathrm{h}_\mathrm{R}^n\right] \cdot \mathrm{f}_1\left(\mathrm{h}_\mathrm{R}^n, \mathrm{e}_\mathrm{R}^n\right)$

[C-58h] $\mathrm{e}_{\mathrm{R}-1}^{n+\frac{1}{2}} = \mathrm{e}_{\mathrm{R}-1}^n + \left[\mathrm{h}_{\mathrm{R}-1}^{n+1} - \mathrm{h}_{\mathrm{R}-1}^n\right] \cdot \mathrm{f}_1\left(\mathrm{h}_{\mathrm{R}-1}^n, \mathrm{e}_{\mathrm{R}-1}^n\right)$

[C-58i] $\mathrm{E}_\mathrm{R}^{n+1} = \mathrm{E}_\mathrm{p}\left\{\mathrm{A}_\mathrm{r}\left[\frac{1}{1+(\alpha\mathrm{T})^p}\right]^q + \mathrm{B}_\mathrm{r}\right\}$ (Current time step value)